Linköping Studies in Science and Technology
Dissertations, No. 1612

Dry Clutch Modeling, Estimation, and Control

Andreas Myklebust

Linköping University
INSTITUTE OF TECHNOLOGY

Department of Electrical Engineering
Linköping University
SE-581 83 Linköping, Sweden

Linköping 2014

Linköping Studies in Science and Technology
Dissertations, No. 1612

This is a Swedish Doctoral Dissertation.
A Doctor's degree comprises 240 ECTS credits (4 years of full-time postgraduate studies), of which at least 120 ECTS credits constitute a doctoral dissertation.

Andreas Myklebust
andreas.myklebust@liu.se
www.vehicular.isy.liu.se
Division of Vehicular Systems
Department of Electrical Engineering
Linköping University
SE–581 83 Linköping, Sweden

Myklebust, Andreas
Dry Clutch Modeling,
Estimation, and Control
ISBN 978-91-7519-261-1
ISSN 0345-7524

The graph on the **cover** is based on data from Figure 4 in Paper D. Actuator position, time, and clutch torque are on the axes and the coloring depends on the clutch disc temperature. The details are left as an exercise to the reader. The drawing in the background pictures a clutch disc.

Typeset with LaTeX 2ε
Printed by LiU-Tryck, Linköping, Sweden 2014

"*A mathematical model does not have to be exact; it just has to be close enough to provide better results than can be obtained by common sense.*"

— Herbert A. Simon

Abstract

Increasing demands on comfort, performance, and fuel efficiency in vehicles lead to more complex transmission solutions. One such solution is the Automated Manual Transmission (AMT). It works just like an ordinary manual transmission but the clutch and the gear selection are computer controlled. In this way high efficiency can be accomplished with increased comfort and performance. To be able to control and fully utilize an AMT, it is of great importance to have knowledge about how torque is transmitted in the clutch. The transmitted torque in a slipping dry clutch is therefore studied in a series of experiments with Heavy Duty Trucks (HDT). It is shown that material expansion with temperature can explain torque variations up to 900 Nm for the same clutch actuator position. A dynamic clutch temperature model that can describe the torque variations is developed. The dynamic model is validated in experiments, and shown to reduce the error in transmitted torque from 7 % to 3 % of the maximum engine torque compared to a static model. Since all modeling, parameter estimation, and validation are performed with production HDTs, i.e. production sensors only, it is straightforward to implement the model in a production HDT following the presented methodology.

The clutch model is extended with lock-up/break-a-part dynamics and an extra state describing wear. The former is done using a state machine and the latter uses a slow random walk for a parameter corresponding to the thickness of the clutch disc. Two observability analyses are made: one with production sensors, and one with a torque sensor in addition to the production sensors. The analyses show that, in both cases, the temperature states and the wear state are observable both during slipping of the clutch and when it is fully closed. The latter is possible since a sensor measures the actuator position. The unknown offset in the torque sensor is possible to observe (at all times) if the model is further augmented with engine inertia dynamics. An Extended Kalman Filter (EKF) is developed and evaluated on measurement data for both cases. The estimated states converge from poor initial values, enabling prediction of the translation of the torque transmissibility curve and sensor offset. The computational complexity of the EKF is low and it is thus suitable for real-time applications.

The clutch model is also integrated into a driveline model capable of capturing vehicle shuffle (longitudinal speed oscillations) and engine torque fluctuations. Parameters are estimated to fit an HDT and the complete model shows good agreement with data. It is used to show that the effect of thermal expansion, even for moderate temperatures, is significant in clutch control applications. One such application is micro-slip control. A control structure has been made and the basic components are a reference-slip calculator, an LQ controller and an EKF that can compensate for the thermal dynamics of the clutch. The controller isolates the driveline from the engine oscillations without dissipating more heat than the clutch can handle. An analysis shows a noticeable fuel consumption increase. Nonetheless, the real benefits of micro-slip control will only be evident when combined with other cost-reducing changes in the powertrain. The feasibility of a micro-slip control system for a dry clutch HDT has been proven.

Populärvetenskaplig Sammanfattning

Ökande krav på komfort, prestanda och bränsleeffektivitet i fordon leder till mer komplexa växellådslösningar. En möjlig lösning är en så kallad automatiserad manuell växellåda, även kallad robotväxellåda. En sådan fungerar precis som en vanlig manuell växellåda fast kopplingen och växelväljaren styrs automatiskt av en dator. Denna lösning ger samma höga effektivitet i växellådan som en vanlig manuell växellåda men med ökad komfort och prestanda, förutsatt att växellådan styrs på ett bra sätt. För att kunna programmera styrdatorn så att den presterar bättre än en mänsklig förare är det viktigt att känna till hur kopplingen överför vridmoment från motor till växellåda. Därför har det överförda vridmomentet studerats i tunga lastbilar försedda med automatiska torrkopplingar. Mätningar har visat att vridmomentet kan variera med upp till 900 Nm för en given position på kopplingens ställdon. Momentvariationen har visats bero på materialexpansion på grund av värmeutvecklingen som sker när kopplingen slirar. För att kunna förutse materialexpansionen har en modell utvecklats över hur kopplingen värms upp och expanderar. Alla experiment som behövts för att utveckla modellen samt validera den har utförts på produktionslastbilar och det är därför rättframt att anpassa modellen till önskvärt fordon genom att följa den metodik som presenteras i avhandlingen.

Om simuleringen av modellen startas ifrån ett felaktigt tillstånd och/eller modellen inte är helt exakt kommer simuleringen att resultera i ett felaktigt värde. För att motverka detta kan en observatör användas. En observatör justerar simuleringen så att felet mellan mätsignal och modellerat värde blir så litet som möjligt. På detta sätt kan styrsystemet, med hjälp av modellen, beräkna värdet på variabler som inte är direkt mätbara. I detta fall rör det sig om temperaturerna i kopplingen samt kopplingslamellens tjocklek. Det senare är viktigt då slitage minskar lamellens tjocklek. En observatör har designats och testats framgångsrikt på data. Detta betyder att med observatören är det möjligt att förutse, i växellådans styrenhet, hur kopplingens vridmoment varierar med temperatur och slitage.

Kopplingsmodellen har även integrerats i en större fordonsmodell som beskriver hur en lastbil beter sig i längdled. Fordonsmodellen har använts för att påvisa vikten av att kompensera kopplingsstyrningen för värmeeffekterna vid en start. Fordonsmodellen har sedan vidareutvecklats med en modell för det pulserande vridmoment en förbränningsmotor producerar. Dessa pulsationer ger upphov till oscillationer i motorhastigheten och är viktiga att beakta när slirhastigheten i kopplingen är av motsvarande storlek. En styralgoritm som klarar av att kontinuerligt hålla kopplingens slirhastighet låg utan att låsa upp kopplingen, en så kallad mikroslip-regulator, har utvecklats med hjälp av fordonsmodellen. Fördelen med mikroslip-regulatorn är att växellådan, och i förlängningen drivhjulen, isoleras från motorns pulserande vridmoment eftersom kopplingen överför moment genom friktion och inte genom pulserande förbränningar. Nackdelen är att mekanisk energi omvandlas till värme i kopplingen vilket leder till ökad bränsleförbrukningen samt högre temperaturer, som kan vara skadliga för kopplingen. Temperaturerna i kopplingen visas vara hanterbara medan bränsleförbrukningen måste vägas mot andra kostnadsbesparande åtgärder som möjliggörs i drivlinan. Hursomhelst är mikroslip-reglering är en möjlig strategi för tunga lastbilar.

Acknowledgments

I would like to thank my supervisor Lars "Lasse" Eriksson for showing me, and walking me through the very curvy path of PhD-studies. I would also like to thank Lars Nielsen for valuable feedback as my stand-in supervisor during the last two months of work (i.e. during June). Additional appreciation goes to Torkel Glad for proofreading the last article, and to David Mattsson and Neda Nickmehr for proofreading the thesis.

A dissertation is not formed by writing alone (at least not in this field), thoughtful experiments and conclusions are also necessary. For aid in these matters I would like to thank some people at Scania CV AB: Foremost Karl Redbrandt (during the first years) and Anders Larsson (during the last year) for help with setting up the experiments as well as interesting discussions. Also Jörgen Hansson is acknowledged for some early experiments, and Kristian Hellgren is acknowledged for some valuable clutch[1] conversations.

And at last, I would like to thank Elin Julin for help with the cover design, endless moral support, and for doing roughly 80-90 % of all household work during the last two months of work. I hope we can continue with this division of labor, even though I now will have time for some vacation...

[1] The word clutch is used 933 times in this thesis, including the cover.

Contents

Chapter 1

Introduction

In order to propel a vehicle the engine must be connected to the wheels somehow, and different driveline solutions are available to create this connection. In a common rear-wheel-drive setup, see Figure 1.1, the tractive wheels are connected to a drive shaft each. These drive shafts are, through a final drive (a differential), driven by a propeller shaft that is connected to the transmission. The transmission consists of two parts: First, the actual transmission part where torque and speed is changed by a gear ratio. Second, a connection between the Internal Combustion Engine (ICE) and transmission that is capable of decoupling the speeds between the engine and transmission. Historically comfort was best accomplished with a classical Automatic Transmission (AT) and high efficiency with a Manual Transmission (MT).

An AT actuates different gear ratios through clutches and brakes that locks different parts of planetary gear sets. The coupling between engine and transmission is handled by a torque converter. These two technologies put together, enable seamless gear shifts that can be controlled through simple hydraulics; the AT was put in production as early as 1939 (Nunney, 1998). The drawbacks are lower efficiency, mainly due to pumping of oil in the torque converter, and the increased complexity and cost, compared to an MT.

The MT is coupled to the engine via a clutch that is operated by the driver via the clutch pedal. A simple explanation of the clutch is that it consists of two rotating plates that can be pressed together. When pressed together, friction will arise and transmit a torque between the plates, which acts to reduce the speed difference. See Chapter 2 for a more detailed explanation. Gear selection is realized using two shafts, both with a set of cog wheels, that mesh together. One pair of cog wheels, corresponding to a certain gear, can be engaged by a mechanical linkage connected to the gear lever. This type of transmission has a high efficiency and a simple construction, but requires the clutch to be disengaged during shifting (torque interrupt) and manual input from the driver. For more details on possible transmission constructions see Newton et al. (1996) or Nunney (1998).

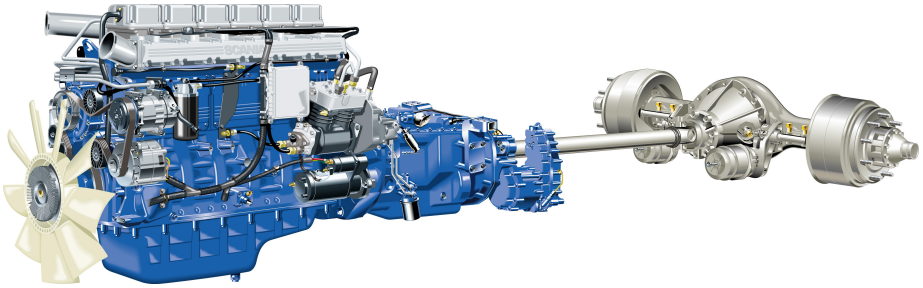

Figure 1.1: A rear-wheel-drive driveline from a Scania truck. The engine, transmission, propeller shaft, differential (final drive), and drive shafts can be seen.

AMT

Increasing demands on comfort, performance, and fuel efficiency in vehicles lead to more complex transmission solutions. The Automated Manual Transmission (AMT) is one way to combine the best from two worlds. It has the same components and basic operation as an MT but the gear selection and clutch operation have been made automatic. This has become possible thanks to technological advances within actuators and computer controllers. The AMT has the benefits of the MT but without the need of driver attention. However, it still has the drawback of torque interrupt during gear changes. Another option, capable of removing the torque interrupt, is the Dual Clutch Transmission (DCT). The DCT further improves comfort and performance with the drawbacks of increased complexity and cost.

Potential Problems

An important part in both an AMT and a DCT is clutch control, which has a profound effect on vehicle performance. A poorly controlled clutch can make starts, stops, and gearshifts slow, rough on the hardware, or uncomfortable. An example can be seen in Figure 1.2. In this case driveline oscillations, which cause discomfort, are induced by too rapid disengagement/engagement of the clutch. The driveline oscillations can be seen in both the speed graphs and in the acceleration graphs. This type of oscillations can be clearly felt by the driver and passengers.

Focus of the Thesis

To be able to control the clutch in a fast and comfortable manner without causing excessive wear, it is important to know the torque transmitted in the clutch with high precision. Moreover, the clutch torque is of great interest if the clutch is to be integrated in a powertrain control scheme that is of the common torque

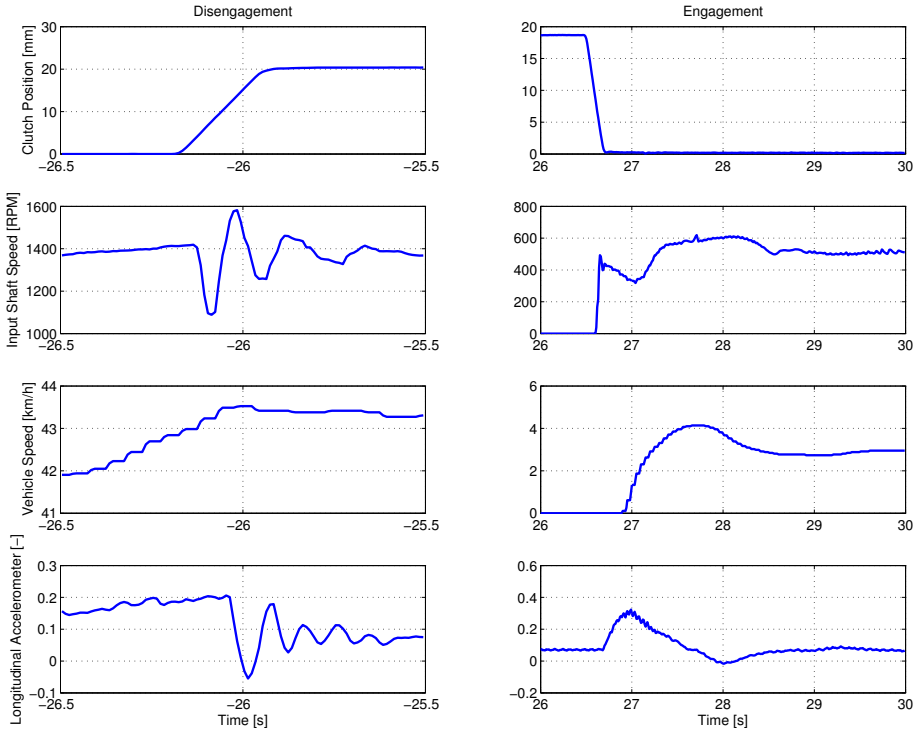

Figure 1.2: The left graphs show measurements of driveline oscillations due to (too) rapid disengagement of the clutch; a scenario possible during gear shifting. The right graphs show the same measurements but in the case of rapid engagement from standstill, which could be the case if the driver wants a quick launch. In both cases the oscillations could clearly be felt by the driver and passenger.

based structure (Eriksson and Nielsen, 2014). Models have come to play an important role in estimation and control of the transmitted torque, since torque sensors still are expensive. Therefore modeling and observation of the clutch torque are main topics here. Since the purpose is to improve clutch control, the resulting model and observer are required to be of low enough complexity to run in real time. Previous experimental investigations of the clutch characteristics (Velardocchia et al., 1999; Moon et al., 2004; Vasca et al., 2011) and (Deur et al., 2012), have been carried out in test rigs equipped with various sensors. Here the experimental platform is limited to production vehicles without additional sensors. On the one hand, this choice imposes certain difficulties in setting up useful experiments. On the other hand, the resulting model and observer can be directly applied to the intended vehicle, in or after production. The goal has been to have a platform for control, and the achievement of this goal is demonstrated through micro-slip control.

1.1 Contributions

A set of experiments for determining significant effects in the clutch and their characteristics has been performed, and has led to a proposed methodology. Since the experimental platforms used here are production vehicles, the proposed methodology can easily be applied to new platforms without the use of additional test equipment. Moreover, the clutch is put in its true thermal environment, between a transmission and a warm combustion engine, which affects the temperature dynamics. The attached papers A-F continue upon the experiments and conclusions of Chapter 3 as well as upon each other in the order they are presented here. The exception is Paper F that is included more as an appendix over the driveline model, although it has its own contributions. The main contributions from each paper are summarized below.

Paper A

The main contribution of Paper A is a novel clutch model that includes the temperature dynamics and thermal effects on the transmitted torque during slipping. The model is developed using a method that utilizes production sensors only. The resulting model is simple enough to run in real time.

Paper B

Paper B integrates the clutch model of Paper A into the complete driveline model of Paper F and models clutch lock-up/break-a-part with a simple approach. The complete model is validated against data of vehicle launches. The main contribution is the demonstration of the importance of considering the thermal dynamics during vehicle launch.

Paper C

Paper C extends the clutch model of Paper A with a wear parameter corresponding to thinning of the clutch disc. The main contributions are an observability analysis and an observer design for the augmented model. The observability of the augmented model is found to be dependent on the mode of the system. An Extended Kalman Filter (EKF) that can observe the temperatures and the wear parameter is designed and tested on data from production vehicles.

Paper D

When a torque sensor with an unknown offset is introduced in the powertrain the work from Paper C needs to be revised. The model of Paper C is augmented with a sensor bias and engine inertia dynamics. The main contribution is the revision of the observability analysis and the observer design. The sensor offset is observable at all time while the observability of the other states are unchanged. The EKF is tested on data from an experiment vehicle equipped with a torque sensor.

Paper E

Paper E uses the driveline model of Paper B and augments it with a model for oscillating ICE torque in order to study micro-slip control. The main contributions are the design of a controller structure, including reference slip calculations, and analyses of the temperature and fuel consumption increases. The fuel consumption increase is noticeable but micro-slip control is a possible strategy for a heavy duty truck.

Paper F

A driveline model is presented in Paper F and shown to be appropriate for vehicle longitudinal shuffle simulation. The main contribution is an investigation, using the model, of how and why a discretized slope signal needs to be filtered.

Errata

In Paper C there is an error in (33). The element on the second row, fourth column should be -1. With the correct equation, the state x_4 is observable when the clutch is slipping. This error has been corrected in Paper D.

1.2 Outlook

Significant temperature effects in the clutch torque have been observed in experiments. A model that explains these effects and an EKF based thereupon has been developed. The EKF is of sufficiently low complexity to be implemented for online use in a vehicle. A case study of micro-slip control has been performed and the EKF was utilized for accurate torque control. This usage of the EKF naturally extends to other areas of clutch control, e.g. launch control and gear changing. Moreover the experimental procedure is general and can be used to modify the model parameterization to suit different setups, e.g. a double clutch.

1.3 Publications

The following papers are included in the thesis.

Journals

- Andreas Myklebust and Lars Eriksson. Modeling, observability and estimation of thermal effects and aging on transmitted torque in a heavy duty truck with a dry clutch. *IEEE/ASME Transactions on Mechatronics* PP(99):1-12, February 2014. **(Paper C)**

Conference papers

- Andreas Myklebust and Lars Eriksson. Torque model with fast and slow temperature dynamics of a slipping dry clutch. In *2012 IEEE Vehicle Power and Propulsion Conference*. October 2012. **(Paper A)**

- Andreas Myklebust and Lars Eriksson. The effect of thermal expansion in a dry clutch on launch control. In *7th IFAC Symposium on Advances in Automotive Control*. September 2013. **(Paper B)**

- Andreas Myklebust and Lars Eriksson. Road slope analysis and filtering for driveline shuffle simulation. In *2012 IFAC Workshop on Engine and Powertrain Control, Simulation and Modeling*. October 2012. **(Paper F)**

Submitted

- Andreas Myklebust and Lars Eriksson. Thermal clutch model observability and observer effects of a torque sensor in the powertrain. Submitted to *IEEE/ASME Transactions on Mechatronics*. **(Paper D)**

- Andreas Myklebust and Lars Eriksson. Dry clutch micro-slip control and temperature considerations. Submitted to *IEEE/ASME Transactions on Mechatronics*. **(Paper E)**

Chapter 2

Introduction to Clutch and Driveline

This chapter gives some background to Chapter 3 and the papers. First, the basic operation of a clutch is explained. Second, the concept of micro slip, an application studied in Paper E, (Myklebust and Eriksson, 2014c), is explained. Third, introductory literature reviews are given on the subjects of driveline modeling, clutch modeling, and micro-slip control. More details from the literature are given in Chapter 3 and the papers.

2.1 Clutch Operation

A schematic of the dry clutch and actuator studied in this thesis is found in Figure 2.1. It has an electro-hydraulic actuator and the clutch construction is typical for a dry clutch. Double clutches have slightly altered constructions but the main principle is the same.

The electric motor rotates a worm gear that pushes into the hydraulic fluid; in an MT the clutch pedal would do this. When the opening to the reservoir is passed the hydraulic fluid pushes on a piston that through a lever pulls the throw-out bearing away from the clutch; the depicted clutch is hence called a pull-type clutch.

The throw-out bearing pulls on the fingers of the diaphragm (also called belleville, washer, slotted disc) spring. This spring is radially pivoted and angularly fixed to the clutch cover that is bolted to the flywheel. The bolting of the clutch cover pre-loads the diaphragm spring so that it exerts a force on the pressure (or push) plate and thus clamps the clutch disc between the pressure plate and the flywheel. The pressure plate is angularly fixed to the clutch cover and thereby to the flywheel as well. When the throw-out bearing is pulling the fingers of the diaphragm spring, load is taken off the pressure plate. As the pressure plate exerts less clamp load, the cushion (or flat) spring inside the

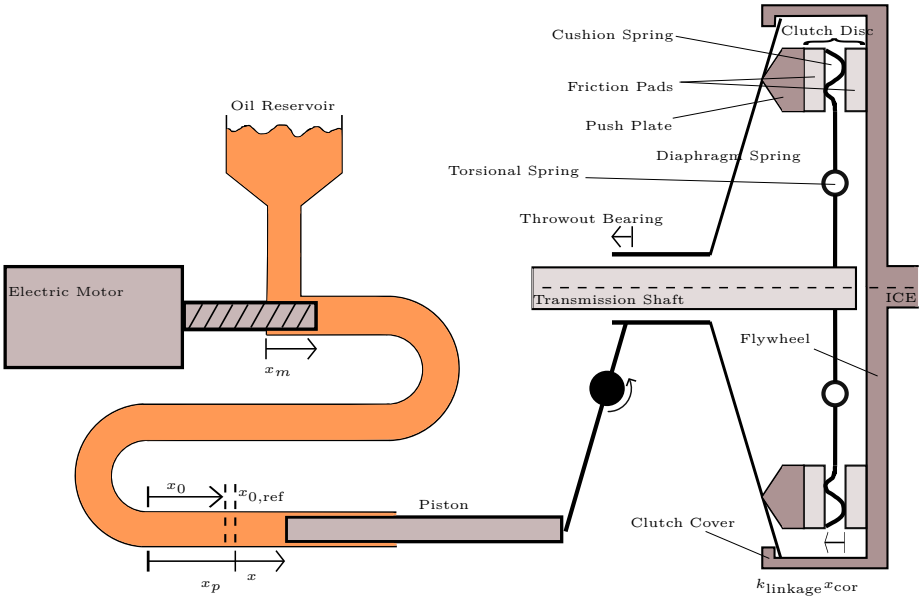

Figure 2.1: A schematic over the actuator and the dry single-plate pull-type clutch studied here. k_{linkage} is the combined ratio of all levers between the piston and the push plate. Sometimes the measurement x is used instead of x_p as a wear compensated piston position that is in the same range as x_m.

clutch disc expands leading to a new equilibrium position for the clutch linkage. The connection between positions, spring characteristics, and bearing force can be seen in Figure 2.2. Through this arrangement a certain actuator position will correspond to a certain clamp load, which facilitates control, especially in the manual case.

The clutch disc is angularly fixed to the transmission input shaft and can therefore rotate with a different speed than the engine and flywheel. When the clamp load becomes greater than zero a friction force will arise if there is a speed difference. This force will result in a torque around the crank shaft and input shaft working to reduce the speed difference. With a larger normal force a larger torque will be transmitted and if the speed difference gets reduced to zero the clutch will lock up, i.e. static friction will take place. When locked up, the clutch acts as a solid unit and transmits the engine torque as long as it does not exceed the stiction torque. For more detailed descriptions of how a clutch works see Mashadi and Crolla (2012); Newton et al. (1996); Dolcini et al. (2010) or Vasca et al. (2011).

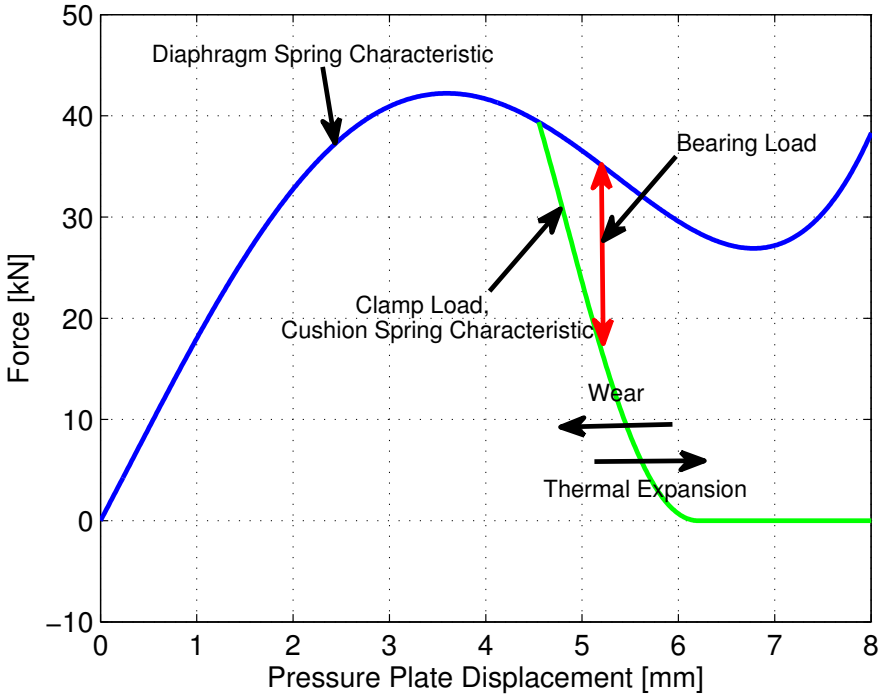

Figure 2.2: Illustration of how the two spring forces in the clutch and the throw-out bearing force interact. The diaphragm spring characteristic is the spring torque at the pivot point divided by the length of the lever between the pivot and the pressure plate. The throw-out bearing force is multiplied with the length of the lever between the bearing and the pivot and then divided with the length of the lever between the pivot and the pressure plate.

2.2 The Idea of Micro Slip Control

Unlike the slipping friction torque in the clutch, the engine torque is oscillatory, which can be seen in Figure 2.3. The ICE torque needs to be damped both for comfort reasons as well as for reducing the stress on driveline components (Reik et al., 1998). The classic solution to the damping problem is to put torsional springs, see Figure 2.1, and friction rings in either the clutch disc or a dual-mass flywheel. A new possibility, when the powertrain is equipped with an automatic clutch, is to damp the oscillations by continuously slipping the clutch. However, when slipping the clutch it will wear and energy is dissipated into the clutch, increasing the fuel consumption and possibly leading to clutch failure due to overheating. Therefore it is of great importance to keep the slip as low as possible, to have a "micro-slip". More background about micro-slip control is found in Section 2.4.

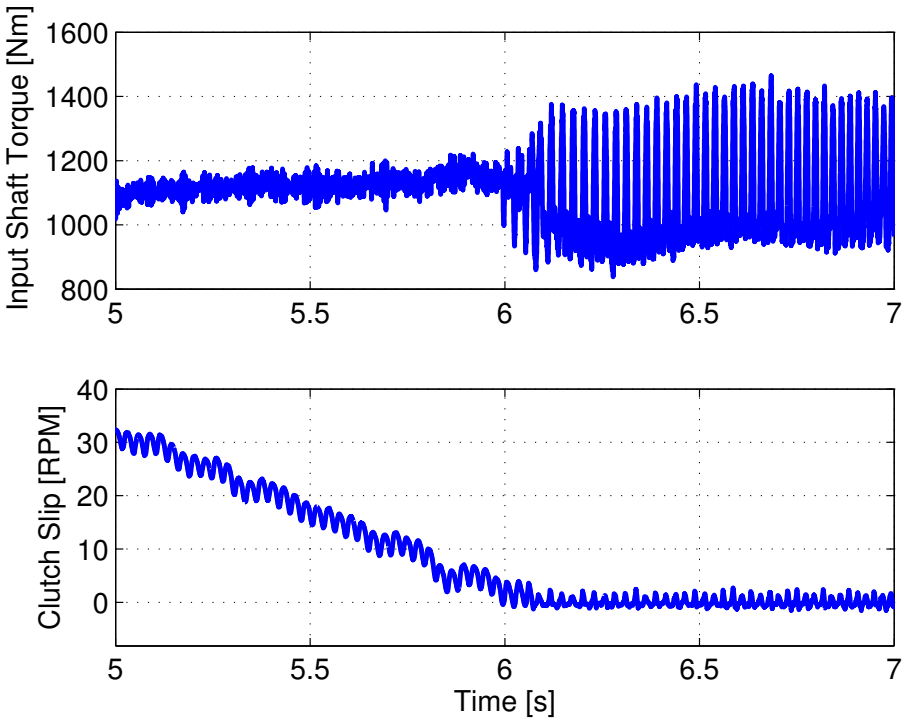

Figure 2.3: High resolution measurement of the clutch slip and a transmission input shaft torque sensor. The oscillations in the input shaft torque become significantly higher when the clutch locks up (zero slip speed) right after 6 s.

2.3 Review of Clutch and Driveline Models

When modeling for control purposes not every detail has to be captured. It is sufficient if significant dynamics are captured and preferable if the model complexity can be kept low (Ljung, 1999). In the case of the clutch the transmitted torque is an important quantity to model. However, the importance of clutch torque control becomes clearer if it is put into the wider context of driveline control. For advanced driveline control, a driveline model is useful, either for simulation during development or for model based control. The model should capture the dynamics in the driveline, such as shunt and shuffle, that affects the comfort of the driver (and the passengers) (Eriksson and Nielsen, 2014).

2.3.1 Driveline Models

When modeling for control purposes it is common in the literature to include one or more flexibilities. In Pettersson (1997); Eriksson and Nielsen (2014);

and Pettersson and Nielsen (2003) active shuffle damping and clutch-less gear-shift control is studied. There the model includes flexibilities in the clutch, propeller shaft and drive shafts. The clutch torsion springs are modeled both in a linear and a piece-wise linear fashion. Also Fredriksson and Egardt (2003) and Pettersson and Nielsen (2000) looks at clutch-less gear-shift control, but this time only the drive-shaft flexibility is modeled. Garofalo et al. (2002) and Dolcini et al. (2008) study optimal control of clutch engagement. The former models two flexibilities in the driveline, one before the transmission and one after. Whereas, the latter models only the flexibility after the gearbox. A clutch-by-wire system is built in Moon et al. (2004), there a non-linear clutch and drive-shaft flexibilities are used. Clutch judder is examined in Crowther et al. (2004) using a driveline model with two flexibilities. A paper about AMT modeling in general (Lucente et al., 2007), states that three flexibilities are useful, one in the engine, one before the transmission, and one after.

2.3.2 Clutch Models

A wide range of models have been proposed in the literature. The most simple models have a clutch torque that is assumed to be a controllable input, see for example Dolcini et al. (2008) or Garofalo et al. (2002). These models rely on the assumption that there is perfect knowledge of how the clutch behaves. More advanced models include submodels for slipping and sticking torques. For example a LuGre model is used in Dolcini et al. (2005) and a Karnopp model in Bataus et al. (2011). The former is a one-state model that captures stick-slip behavior, varying break-away force, Stribeck effect, and viscous friction. The latter includes a dead-zone around zero speed to ease the simulation of stick-slip behavior. The clutch torque during slipping is commonly modeled using a function with the following structure

$$M_{\text{trans,k}} = \operatorname{sgn}(\Delta\omega)\, n\, \mu\, R_e\, F_N \tag{2.1}$$

where $\Delta\omega$ is the clutch slip (speed), n the number of friction surfaces, μ the friction coefficient, R_e the effective radius and F_N the clamping (normal) force. In these models F_N is often either given as input or a static nonlinear function of clutch position, x, i.e. $F_N = F_N(x)$, see for example Vasca et al. (2011) or Glielmo and Vasca (2000). In particular Dolcini et al. (2010) mentions that a third-order polynomial is suitable to describe the connection between throwout-bearing position and clutch transmitted torque, mainly governed by the cushion spring characteristic. In Deur et al. (2012) μ is fitted to the following regression curve

$$\begin{aligned}\mu = {} & a_0 + a_1 \left(e^{-a_2 \Delta\omega} - 1\right) T_b + \left(a_3 - a_4 \ln(\Delta\omega)\right) T_b^2 \\ & + \left(a_5 - a_6 \Delta\omega\right) F_N + a_7 T_b F_N\end{aligned} \tag{2.2}$$

where T_b is the temperature of the clutch body and assumed to be an input signal. $a_0 - a_7$ are curve parameters. F_N is mapped against actuator position

and T_b in Deur et al. (2012). More advanced FEM models of the clutch are also found in the literature. To name some: Nam et al. (2000) investigates the stresses in the diaphragm spring; Sfarni et al. (2008) has studied how the clutch-disc characteristics change with wear; and Cappetti et al. (2012b) examines the temperature effect on the cushion spring. Especially temperature distributions are popular to investigate using FEM. Both in clutch parts: Abdullah and Schlattmann (2012a) examines temperature distributions in clutch discs with different grooves; and Lee et al. (2007) investigates the temperature distribution in the pressure plate; and in the clutch as a whole: Abdullah and Schlattmann (2012b) and Sun et al. (2013). These FEM models point out interesting effects but are of little use here as the computational complexity is too high for control purposes.

In Velardocchia et al. (2000) and Wikdahl and Ågren (1999) simpler temperature models are established. However, these two models do not include the effect of the temperature on $M_{\text{trans,k}}$. The models in Velardocchia et al. (2000) and Wikdahl and Ågren (1999) could be combined with the model presented in Deur et al. (2012), where the clutch temperature is an input, in order to give the clutch torque. Although that approach requires a map of the normal force as function of actuator position and temperature, whereas the approach in Paper A, (Myklebust and Eriksson, 2012b), is completely model based. Furthermore, the clamping load and temperatures, which are not available in production vehicles, need to be measured during the parameter estimation procedure. In Paper A, (Myklebust and Eriksson, 2012b), only sensors available in production vehicles are used.

2.4 Introduction to Micro-Slip Control

The idea of micro-slip control in AMTs has been around for over 20 years (Albers, 1990), but the amount of literature on the subject is limited. In Albers (1990) a slip control system and its capability of isolating the driveline from engine oscillations are demonstrated. It is also concluded that the increase in clutch wear is not a problem as long as excessive temperatures are avoided. Furthermore it is seen that above a certain engine speed the vibration isolation is sufficient without micro-slip and slip control can therefore be turned off at high engine speeds. This functionality is confirmed to exist in a production solution in Audi of America (2001). Further confirmation is found in Fischer and Berger (1998) where excitation and resonance frequencies are studied. It is concluded that locking the clutch is not only sufficient for vibration oscillation at higher engine speeds, but also necessary. A further conclusion is that the hardware in the driveline's torsion damper can be simplified without sacrifice of comfort if micro-slip is used. Tests in passenger vehicles have been performed in Küpper et al. (2002) and the vibration isolation performance of a single-mass-flywheel slip-controlled vehicle is equal to that of a dual-mass flywheel equipped vehicle without slip control. Only a slight increase in wear was detected and fuel

consumption was unchanged. The latter was possible since the smaller inertia of the single-mass flywheel contributed to a lower fuel consumption.

Slip control is also of interest for ATs. To improve the efficiencies of ATs a lock-up clutch (or Torque Converter Clutch (TCC)) is employed, inside the Torque Converter (TC), that is capable of locking the pump to the turbine and thereby reducing the slip losses. Micro-slip is used for the TCC as well to allow a larger lock-up range and thereby improved fuel efficiency (Hiramatsu et al., 1985; Otanez et al., 2008). Both advanced control strategies, e.g. Higashimata et al. (2004), and more straight forward strategies, e.g. Hebbale et al. (2011), have been implemented and tested in passenger vehicles. In Higashimata et al. (2004) the TC is modeled as a linear parameter varying system and a feedforward link together with a μ-synthesis feedback link is used to control the slip speed of the TCC. The controller is further developed using gain scheduling in Kaneko et al. (2009) and coasting capabilities are introduced in Katsumata et al. (2008). In Hebbale et al. (2011) model-based feedforward and slip-references-signal smoothing are used in order to get smooth slip control. Although there are similarities between slip control in an AT and an AMT the two are quite different. In an AT there is a second path for the torque, through the nonlinear TC, which is not present in an AMT. Moreover, the actuators are different and AMTs have less heat capacity.

Chapter 3

Experimental Observations and Model Structure

This chapter presents a chain of experiments, considerations, and literature comparisons leading to the model structure used in the thesis.

3.1 Experimental Platform

As seen in Chapter 2, there are different ways to model the clutch. In order to choose a suitable model structure an experimental platform and data are required. Here Scania Heavy Duty Trucks (HDTs) with standard production sensors are used. A variety of trucks have been used but the two most used are Ara and Ernfrid. Both are equipped with a 14-speed AMT and a 16.4 liter V8 capable of producing 3500 Nm. Ara weighs 105 tonnes and Ernfrid 21 tonnes. The clutch was described in Chapter 2. A list of the measurement signals used can be found in Table 3.1 and their respective location in the driveline can be seen in Figure 3.1. The special case of a torque sensor in the powertrain is

Table 3.1: A list over the different measurements used in the HDTs

Notation	Explanation
ω_e	Engine speed
ω_t	Transmission input-shaft speed
ω_p	Transmission output-shaft speed
ω_w	Tractive-wheel speed
v	Vehicle speed, actually speed of the free rolling (front) wheels
T_{coolant}	Engine coolant temperature
T_{amb}	Ambient temperature
x_m	Clutch actuator motor position
x_p	Clutch actuator piston position
M_e	Engine torque, reported from ECU

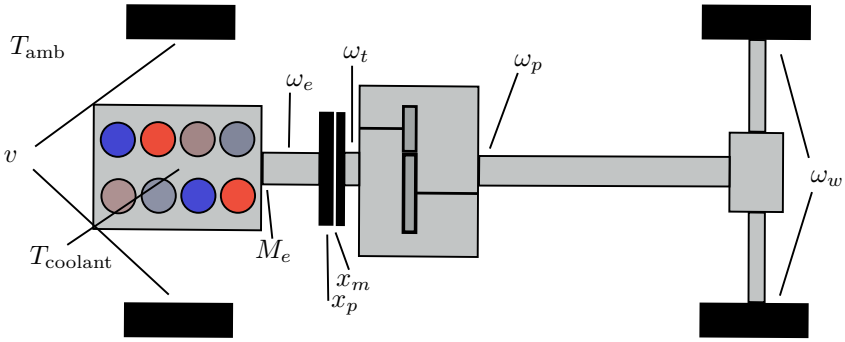

Figure 3.1: Sketch of a typical HDT driveline and where the sensors are located. See Table 3.1 for an explanation of the notation.

only studied in Paper D, (Myklebust and Eriksson, 2014b). So in order to get a measurement of the clutch torque, the reported engine torque is used with added compensation for inertia effects of the engine and flywheel.

The main benefit of this setup, with only production sensors, is that the resulting model and observer are directly applicable on a production HDT. Furthermore, the developed procedure for experiments, model building, model validation, and observer evaluation can easily be performed on other vehicles equipped with a dry clutch. On the other hand, the drawback, compared to a test stand, e.g. Velardocchia et al. (1999); Moon et al. (2004) or Deur et al. (2012), is fewer and less precise sensors. All the cited test stands consist of a stand-alone dry clutch that is cooled towards the stagnated room-temperature air. In a truck there might be an airflow, the clutch is installed below the truck floor, bolted to the transmission, and especially the flywheel is bolted to a 1 tonne, ~ 90 °C warm engine. Naturally all this leads to different temperature dynamics.

3.2 Motivating Experiment

As a first investigation of the clutch characteristics the actuator position has been ramped back and forth several times while the clutch torque has been measured. Every second ramp pair the actuator has moved a shorter path. This is performed in order to study possible hysteresis effects. The results from such an experiment is presented in Figure 3.2. There the ramps are seen to follow a curve that can be fitted to a third order polynomial (Dolcini et al., 2010; Myklebust and Eriksson, 2012b). However, the polynomial is different for each ramp; there is clearly some dynamics present.

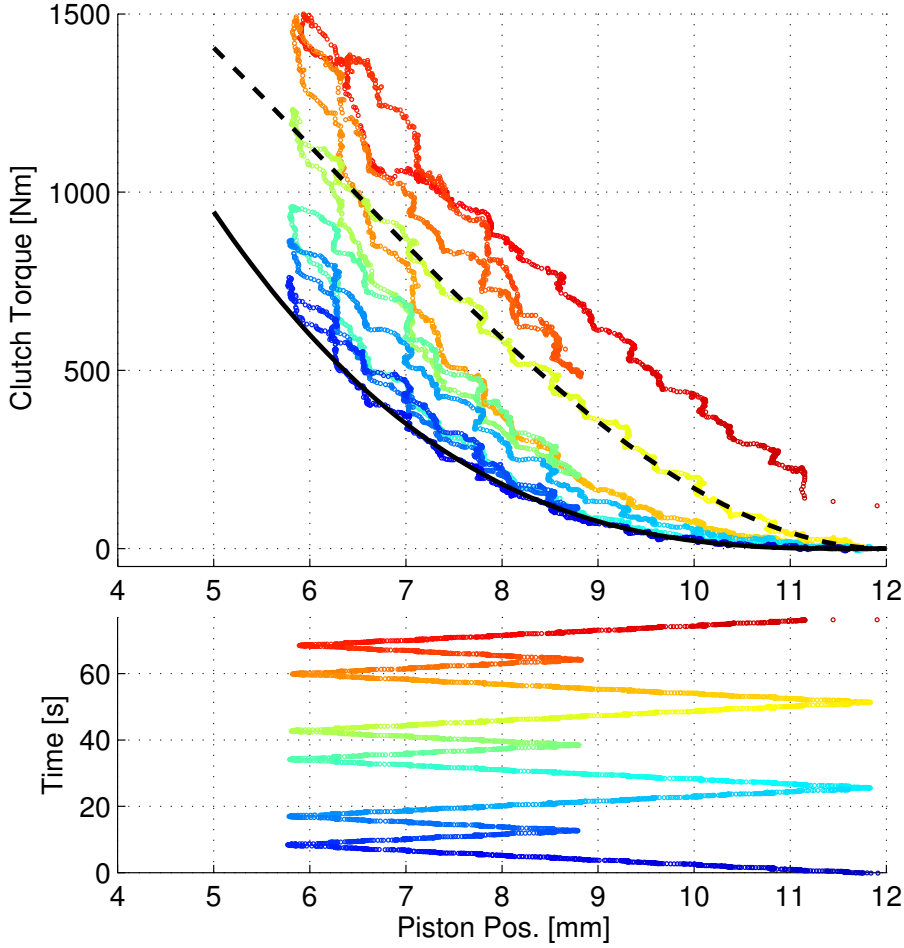

Figure 3.2: The clutch position, x, has been ramped back and forth while the clutch torque has been measured, top plot. The transmitted torque clearly depends on something more than the clutch position, in particular there is a drift with time. The time scale can be viewed by following the position into the lower plot. The time scale is also color coded: blue=0 s and red=75 s. The torque difference between the first and last ramp is up to 900 Nm. The two black lines represent two possible parameterizations of a third order polynomial.

3.3 Actuator Dynamics

The clutch actuator has a built-in position controller. This has the benefit that effects causing hysteresis in the actuator force, e.g. friction or the diaphragm spring, will not affect the actuator output/clutch torque relation (Deur et al., 2012). Furthermore, a position measurement of the piston effectively makes

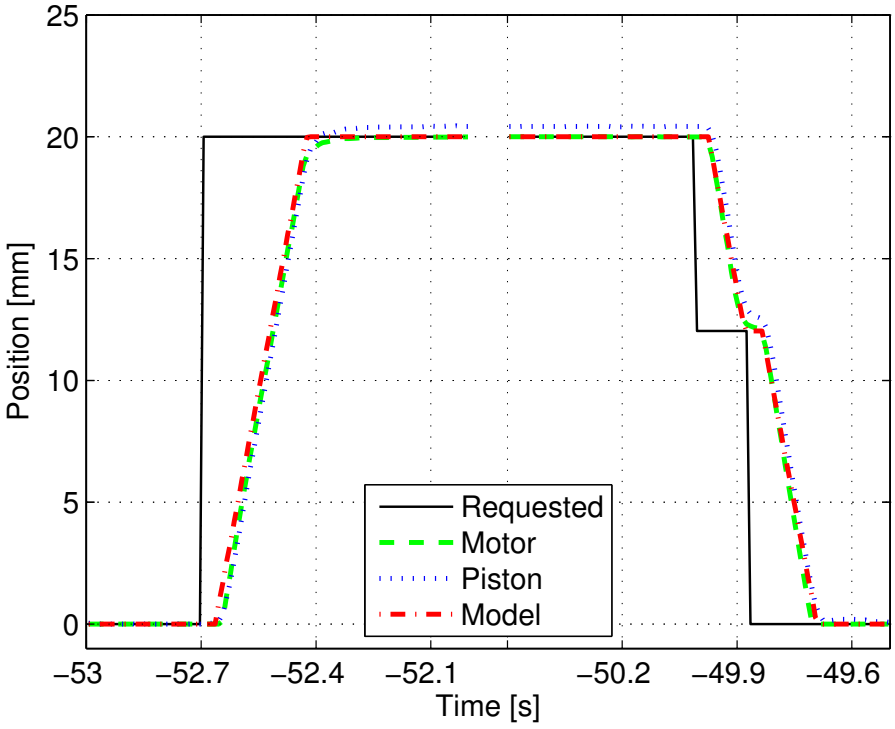

Figure 3.3: A step change in actuator (motor) position has been demanded. The corresponding response in both motor and piston position can be seen. The actuator is fast and can be modeled as a rate limiter of 84 mm/s and a time delay of 0.03 s.

the piston position the output of the actuator. Since the actuator output is known the clutch torque can be modeled without knowing the actuator dynamics. However, for control applications the limitations of the actuator need to be considered. Conveniently the motor in the actuator is both accurate and fast, see Figure 3.3. The motor position can therefore be modeled as the requested position rate limited to 84 mm/s and delayed 0.03 s.

Some dynamics exists in the hydraulics of the actuator but the piston still moves at approximately the same rate as the motor, so control of the piston position has similar performance. During intense use of the clutch the hydraulic oil can be heated and thereby expand. This will cause a change in the relation between the motor and piston position. However, since the piston position is measured and controlled, this is of small concern. It should be noted that the clutch is located inside the bell housing (the housing surrounding the clutch) whereas the actuator is outside the bell housing. The temperature dynamics of the actuator has therefore little to do with the temperature dynamics of the clutch discussed in Section 3.8.

3.4 Clutch Variables

Several factors could be the reason for the dynamics seen in Figure 3.2. First lets recall (2.1) from the previous chapter

$$M_{\text{trans,k}} = \text{sgn}(\Delta\omega)\, n\, \mu\, R_e\, F_N \tag{3.1}$$

Looking at (3.1) one factor that directly affects the clutch torque is the clamp load. The clamp load is dependent on the actuator position but also on other factors, mainly the cushion spring characteristic. This characteristic is reported to have a decreasing slope with temperature in Cappetti et al. (2012a). However, in Cappetti et al. (2012b) thermal expansion in the axial direction of the spring is shown to be a more significant effect. Sfarni et al. (2008) reports about steeper cushion spring characteristic with wear. From a graph in Hong et al. (2012) the normal force can be seen to be speed dependent. The speed dependency is said to be due to centrifugal forces acting on the diaphragm spring in Dolcini et al. (2010). The works Mashadi and Crolla (2012); Moon et al. (2004); and Szimandl and Németh (2012) report of hysteresis in the diaphragm spring, which could lead to hysteresis in the normal force. A decrease in diaphragm spring force with temperature is reported in Sun et al. (2013). The decrease is especially pronounced for temperatures above 200 °C. In Mattiazzo et al. (2002) a temperature and wear dependency of the normal force/bearing position characteristics is shown. The wear is reported to affect the characteristics both through thinning of the disc, as in Figure 2.2, and through fatigue of the diaphragm spring. In Mattiazzo et al. (2002) the normal force decreases with temperature. In Deur et al. (2012); Cappetti et al. (2012b); and Hoic et al. (2013) the change in normal force/bearing position characteristics is explained by thermal expansion of clutch parts. The normal force is increasing with temperature, although with an exception for low forces in Hoic et al. (2013). There the normal force is decreasing with temperature due to the expansion of a return spring, which is not present in the more common setup studied here.

However, the normal force is not the only component of (3.1) that varies. It is generally recognized that μ can depend on temperature, slip speed, and wear while R_e can depend on temperature and wear as well (Velardocchia et al., 1999; Sun et al., 2013). Sun et al. (2013) has data showing an increase of μ with temperature up to 200 °C, after that μ decreases. In Vasca et al. (2011) a slip speed dependency of μR_e is shown, this was especially pronounced for slip speeds below ∼100 RPM. R_e has been assumed constant in Deur et al. (2012), and there μ decreases with temperature and increases with slip for a low to medium normal force but for a high normal force no clear trend is seen. The result is explained using (2.2).

It can be difficult to separate which parameter in (3.1) that is the reason for a change in $M_{\text{trans,k}}$. The clutch torque is therefore often studied as a lumped model. In Velardocchia et al. (1999) $M_{\text{trans,k}}$ is seen to decrease with temperature and $\Delta\omega$. However, there are large variations with wear. In Ercole et al. (2000) $M_{\text{trans,k}}$ initially decreases with temperature for low temperatures and then

increases for medium and high temperatures. Similarly there are variations with wear, and in addition, temperature-torque hysteresis are reported.

A summary of the effects and dependencies above is to express (3.1) as

$$M_{\text{trans,k}} = \text{sgn}(\Delta\omega)\, n\, \mu(\Delta\omega, T, t)\, R_e(T, t)\, F_N(x, T, \omega_e, t) \tag{3.2}$$

where T is the temperature(s) and t represents wear (with time). Since production trucks are used as experimental platforms, the number of sensors is limited. This reduces the possibilities to separate the effects in (3.2). Therefore a lumped model has been studied here

$$M_{\text{trans,k}} = M_{\text{trans,k}}(\Delta\omega, \omega_e, T, t, x) \tag{3.3}$$

However, the more general model (3.2) gives some insight that can be used for setting up experiments and selecting the internal structure of the model (3.3). In the following sections, experiments useful for investigation of the clutch torque are described together with their results. The experiments have been designed to isolate different effects from each other and to step through the dependencies of (3.3).

3.5 Wear

Investigations of wear require a lot of time consuming measurements. Luckily wear is usually a slow process that is not noticeable in single experiments. Wear is therefore omitted from the model structure

$$M_{\text{trans,k}} = M_{\text{trans,k}}(\Delta\omega, \omega_e, T, x) \tag{3.4}$$

However, in a production application wear has to be dealt with through e.g. adaptation. The only wear effect that has been observed throughout this thesis is thinning of the clutch disc. A method for adapting the disc thickness is proposed in Paper C, (Myklebust and Eriksson, 2014a).

3.6 Slip

In order to investigate the slip-speed dependency experiments have been carried out as follows. A truck has been driven to an uphill and has been kept stationary by slipping the clutch at a constant position. This way the vehicle will accelerate forwards if more torque is transmitted and backwards if less torque is transmitted. Furthermore, it is easy, at least initially, to keep the input-shaft speed stationary this way, and by doing so the engine speed can be used to control the slip speed. The change in slip speed will of course have a corresponding change in dissipated power and hence the temperature rate. In order to isolate the slip dependency from temperature dynamics a fast change in slip speed is desirable. Slip-speed steps are therefore made and an abrupt change in torque/input-shaft

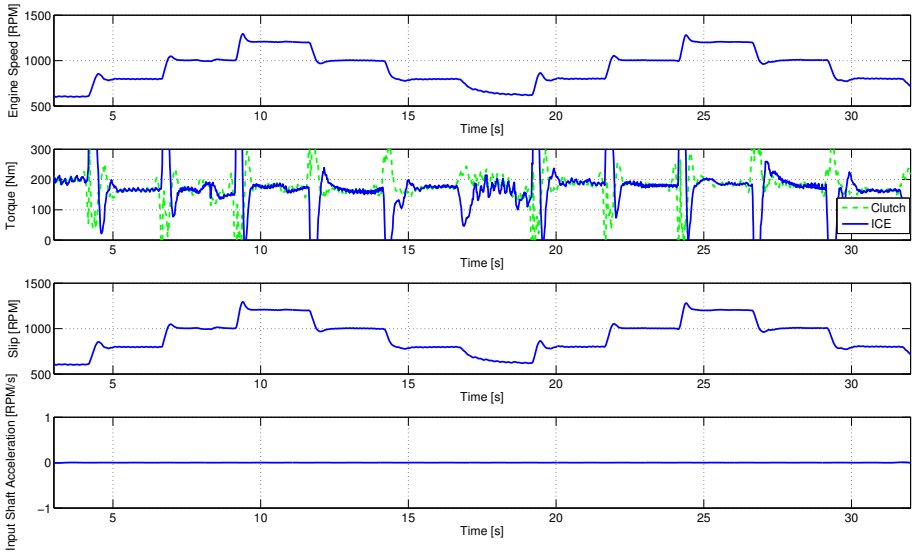

Figure 3.4: Slip steps are made through engine-speed control when the truck is held stationary in a slight uphill using a constant clutch position. No reaction is seen in neither clutch torque nor input shaft acceleration.

acceleration should be seen if there is a slip-speed dependency, see Figure 3.4. Note that the engine torque has a transient during the edges of a step, due to the acceleration of the engine. A smaller transient is present in the clutch torque signal due to imperfections in the compensation for the acceleration. No significant change is seen in the input-shaft acceleration and no correlation between steady-state clutch torque and slip speed is seen neither, see Figure 3.5. Based on this experiment (3.4) can be reduced to

$$M_{\text{trans,k}} = M_{\text{trans,k}}(\omega_e, T, x) \tag{3.5}$$

This is somewhat in contrast to the data in Velardocchia et al. (1999) where a slip dependency is shown. The slip has only been investigated at relatively large speeds and does therefore not contrast the data in Vasca et al. (2011) where the slip dependency only is present below 100 RPM.

3.7 Rotational Speed

Centrifugal effects in the diaphragm spring can be studied with the same experiment as in Section 3.6 since the engine speed (and thereby diaphragm spring speed) is varied whereas the other parameters of (3.5) are kept constant. Hence no effects are seen in the torque in Figure 3.4, no speed dependency is

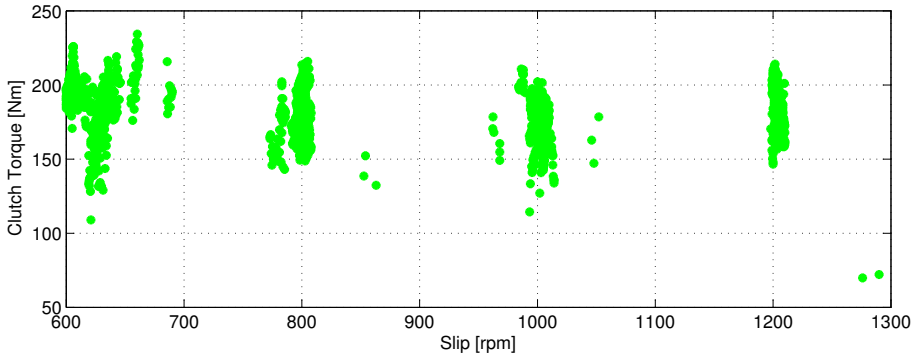

Figure 3.5: The data points from Figure 3.4 when the engine speed is constant. No correlation is seen between clutch torque and slip speed.

present either. The model can be further simplified into

$$M_{\text{trans,k}} = M_{\text{trans,k}}(T, x) \tag{3.6}$$

There is a risk that an effect of ω_e is present but canceled by an effect of $\Delta\omega$. In order to fully investigate this the experiment of Section 3.6 would need to be repeated with different input-shaft speeds, which would give different combinations of slip speed and engine speed. This kind of experiment has not been performed due to practical difficulties with controlling the input-shaft speed to a constant non-zero value.

3.8 Temperature

A variation of the experiment of Section 3.6 can be used to isolate the thermal effect. The truck is placed in an uphill and the clutch is controlled to a point where it can keep the truck stationary. Movement of the truck is not desirable as it can make the clutch lock up (and the slip to vary). The dissipated power will heat the clutch and if that affects the transmitted torque the truck will start to move unless the clutch position is controlled to maintain a constant torque. Therefore the clutch torque is put under feedback and the clutch position is measured. In Figure 3.6 the position is seen to increase as more energy is dissipated into the clutch. There is clearly some temperature dynamics present.

When performing experiments for identifying the thermal dynamics the cool down process is also of interest. However, a position that transmits a slipping torque can not be measured if the clutch is to cool down. One possibility then is to investigate how the kiss point, where pressure plate and clutch disc first meet, changes with cooling. This feels intuitive as the kiss point is an important parameter in clutch control. However, due to inexactness in the torque measurement and the cushion spring characteristic of the clutch

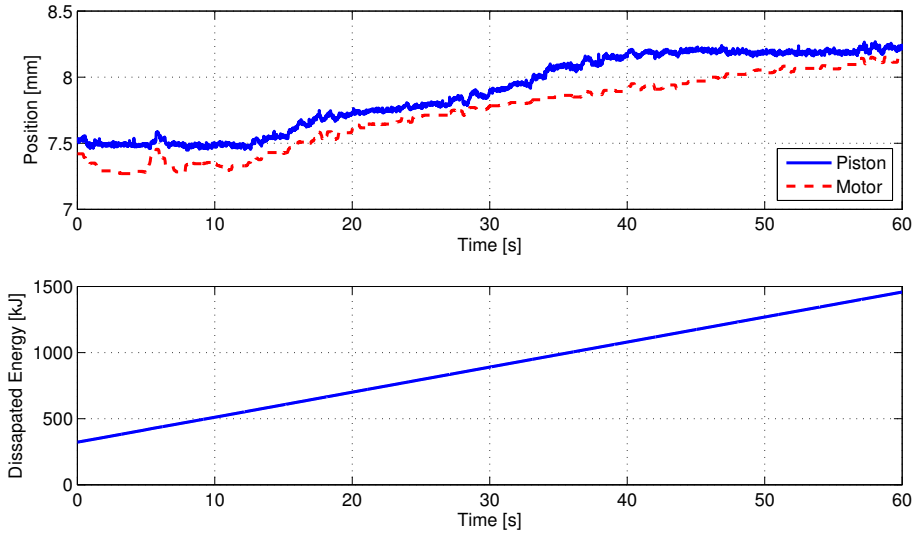

Figure 3.6: Slip and torque through the clutch have been held constant. To keep them constant the clutch position has to be varied. The motor position and piston position vary differently. The position increases with dissipated energy.

transmissibility curve around zero torque, the exact position of the kiss point is hard to detect. One way to ease the detection is to engage the clutch when neutral gear is engaged. This way the input-shaft speed will respond to the transmitted torque quickly. Experiments of this type have shown that the kiss point varies sporadically, see Figure 3.7. This is thought to be because the clutch disc can slide axially along the transmission input-shaft and stop in an arbitrary position in the gap between pressure plate and flywheel. The friction along the shaft can provide a sufficient clamp load to transfer enough torque to spin the input shaft when in neutral gear, but not enough to transmit any significant torque for the truck dynamics. Therefore the exact value of the kiss point is not of great concern, instead the point where clutch torque gets significant is of greater concern.

An alternative measure is the position where the clutch is fully closed, here called the zero position. This point is easy to determine, when the actuator motor is fully backed out (motor position zero, hence the name zero position) the clutch will, due to the diaphragm spring, be fully closed. If the clutch is closed when neutral gear is engaged, no significant energy is dissipated into the clutch. The zero position does therefore give a more stable measurement, see Figure 3.7. The zero position increases when heat is dissipated into the clutch and it decreases exponentially when no heat is dissipated. A hypothesis is that thermal expansion of the clutch is the reason for the change in zero position. Therefore a rough estimate of the thermal expansion has been made as follows:

The clutch mass is estimated as the flywheel and pressure plate, $m_c = m_{fw} + m_{pp} = 47 + 34 = 81$ kg. They are made out of cast iron, and according to Nording and Österman (1999) the expansion coefficient is $e_{ci} = 11 \cdot 10^{-6}$ 1/K, and the specific heat capacity is, $c_p = 500$ J/(kg K). If 4 MJ of energy is dissipated into the clutch through slipping, as in Figure 3.7, the clutch will heat up with approximately 98 K and expand by 0.11 %. The clutch is about 100 mm thick, which means it will expand by 0.11 mm. At the actuator this is seen as 0.96 mm (ratio of 8.8 measured in drawings). When comparing this number with the change in the zero position seen in Figure 3.7, the numbers are in the same order of magnitude. During the warm up the zero position increases with ~ 1.2 mm and during cool down it decreases ~ 0.8 mm asymptotically. This gives further support for the hypothesis that this effect is due to the thermal expansion of the clutch.

In order to observe the zero position, not only when the clutch is cooling but also when the clutch is heated, the following procedure has been used. The clutch has been slipped for a short time while the truck has been in gear and kept stationary by the parking brake. After the slipping phase the clutch has been closed in neutral gear so that the zero position can be measured. The slipping phase and the measurement phase are alternated like this for an extended period of time. The result of such an experiment can be seen in Figure 3.8. A two-state temperature model can be fitted to this data, see Paper A, (Myklebust and Eriksson, 2012b), or Paper C, (Myklebust and Eriksson, 2014a), for details.

However, if the dynamics seen in Figure 3.8 is compared to those seen in Figure 3.6 two things can be noticed: First, the change in position is much larger in Figure 3.6. Second, the time constant in Figure 3.6 is much smaller. This smaller time constant could correspond to a smaller thermal mass, e.g. the clutch disc. The thermal behavior of the cushion spring inside the clutch disc is investigated in Cappetti et al. (2012b) and could explain the faster dynamics seen here. A third temperature state with faster dynamics is useful in order to explain the clutch thermal dynamics, again see Paper A, (Myklebust and Eriksson, 2012b), or Paper C, (Myklebust and Eriksson, 2014a), for details.

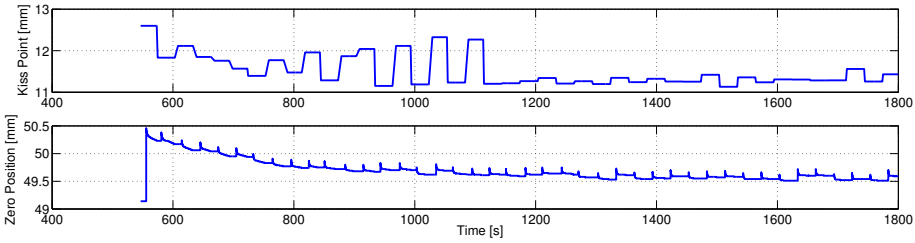

Figure 3.7: About 4 MJ of energy has been dissipated in the clutch. Afterwards the truck has been standing still with neutral gear engaged while the kiss point and zero position have been monitored.

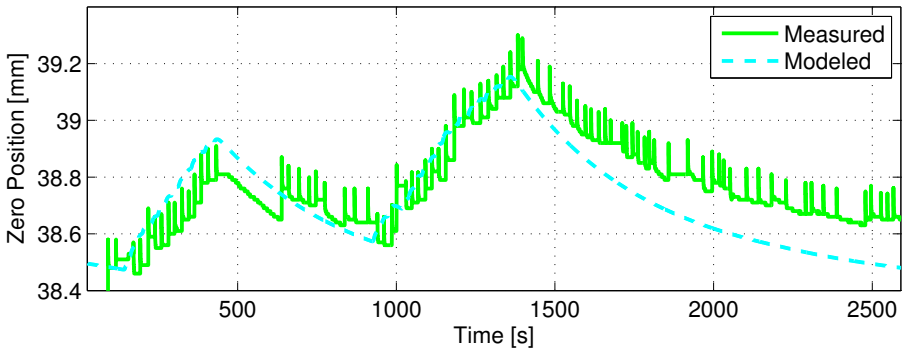

Figure 3.8: The clutch has been heated through slipping and then left to cool down. The zero position has been recorded as a measure of the expansion. A two-state temperature model can explain the data.

The temperature dynamics consists of three temperatures and in common for all of them is that energy is gained through the power dissipated in the clutch

$$P = M_{\text{trans,k}}\, \Delta\omega \tag{3.7}$$

and energy is dissipated to the ambient air and to the ICE, but not so much to the transmission (Wikdahl and Ågren, 1999). Since the truck is moving and the clutch is spinning there will be forced convection. Therefore the vehicle and clutch speed are also possible variables

$$\dot{T} = f\left(T, P, T_{\text{ICE}}, T_{\text{amb}}, \omega_e, v\right) \tag{3.8}$$

where T is a temperature vector, T_{ICE} is the coolant temperature of the ICE, T_{amb} is the ambient temperature and the engine speed is used as clutch speed.

3.8.1 Vehicle Speed Dependency

The speed of the truck directly affects the speed by which air is flowing past the bell housing. This forced convection will naturally increase the cooling of the clutch. In most experiments performed here, the truck has been held stationary in order to keep the clutch from locking up. Although, this should be of smaller concern when using the observer of Paper C, (Myklebust and Eriksson, 2014a), since the bell housing temperature only affects the clutch torque indirectly through the ambient conditions of the flywheel and pressure plate. Equation (3.8) can be reduced to

$$\dot{T} = f\left(T, P, T_{\text{ICE}}, T_{\text{amb}}, \omega_e\right) \tag{3.9}$$

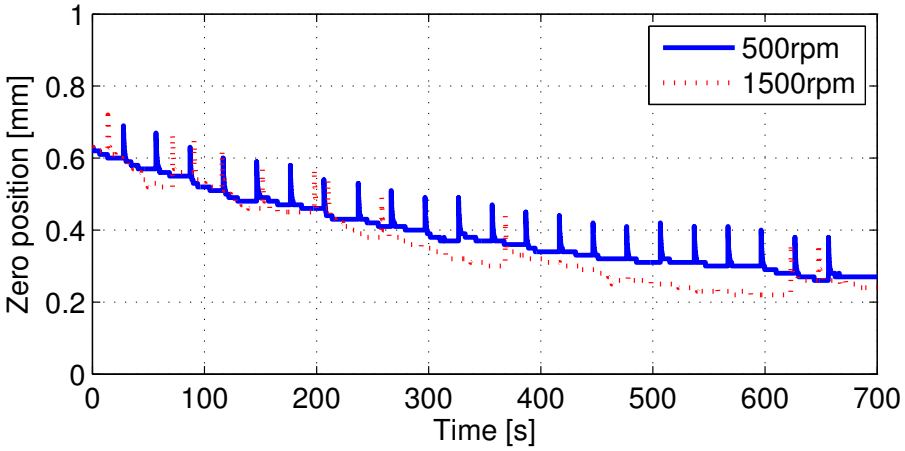

Figure 3.9: Zero position measurements when the clutch is cooling down. In one case the engine speed has been 500 RPM and the coolant temperature has been 77 °C. In the other case the engine speed has been 1500 RPM and the coolant temperature has been 82 °C. The two trajectories are similar. The zero position has been adjusted with an offset to compensate for different wear levels in the two experiments.

3.8.2 Engine Speed Dependency

If the clutch is spinning at a higher speed there should be more forced convection and the clutch body should cool faster towards clutch housing temperatures. Experiments have therefore been carried out where the zero position has been measured during cooling of the clutch with two different engine speeds, and hence two different clutch body speeds. Looking at the data in Figure 3.9 there is no significant difference in the curve shapes indicating that the clutch speed has no significant effect on the clutch temperature. Therefore (3.8) can be further reduced to

$$\dot{T} = f\left(T, P, T_{\mathrm{ICE}}, T_{\mathrm{amb}}\right) \tag{3.10}$$

Using the observer from Paper C, (Myklebust and Eriksson, 2014a), it can be verified that both measurements start at the same temperature level. For the 500 RPM case and the 1500 RPM case the clutch body temperature is 109 °C and 107 °C, respectively and the clutch housing temperature is 83 °C and 85 °C, respectively. The engine coolant temperature was measured to 77 °C and 82 °C, respectively.

3.9 Model Summary and Usage in Papers

In this and the previous chapter a literature survey of dry-clutch models and experiments is summarized into the model structure (3.3). Thereafter a set of experiments is designed to investigate which variables in (3.3) that are significant. All experiments have been performed on production trucks driven on roads. Therefore this set of experiments can easily be adapted to new platforms. After performing the experiments the model structure is

$$\begin{aligned} \dot{T} &= f\left(T, P, T_{\text{ICE}}, T_{\text{amb}}\right) \\ M_{\text{trans,k}} &= M_{\text{trans,k}}\left(T, x\right) \end{aligned} \tag{3.11}$$

This model structure is developed and parameterized in Paper A, (Myklebust and Eriksson, 2012b), using the experiments described in this chapter. The model that results from Paper A, (Myklebust and Eriksson, 2012b), is the foundation for Paper B, (Myklebust and Eriksson, 2013), and Paper C, (Myklebust and Eriksson, 2014a). In Paper B, (Myklebust and Eriksson, 2013), simulations of the clutch model and the driveline model from Paper F, (Myklebust and Eriksson, 2012a), are used to demonstrate the importance of considering the thermal dynamics in clutch control applications. One way to do that is to build an observer using the model. This is done in Paper C, (Myklebust and Eriksson, 2014a), and Paper D, (Myklebust and Eriksson, 2014b), where a clutch torque and temperature observer is designed. In the latter paper the special case when a torque sensor is available in the driveline is studied. The observer from Paper C, (Myklebust and Eriksson, 2014a), is put to use in a micro-slip controller in Paper E, (Myklebust and Eriksson, 2014c).

References

Oday I. Abdullah and Josef Schlattmann. Finite element analysis for grooved dry friction clutch. *Advances in Mechanical Engineering and its Applications*, 2(1):2167–6380, 2012a.

O.I. Abdullah and J. Schlattmann. Finite element analysis of temperature field in automotive dry friction clutch. *Tribology in Industry*, 34(4):206–216, 2012b.

Albert Albers. Torque control isolation (TCI) the smart clutch. In *4th LuK Symposium*, 1990.

Inc. Audi of America. Variable automatic transmission multitronic 01j, August 2001. Self-Study Program Course Number 951103.

Marius Bataus, Andrei Maciac, Mircea Oprean, and Nicolae Vasiliu. Automotive clutch models for real time simulation. *Proceedings of the Romanian Academy, Series A*, 12(2):109–116, 2011.

Nicola Cappetti, Mario Pisaturo, and Adolfo Senatore. Modelling the cushion spring characteristic to enhance the automated dry-clutch performance: The temperature effect. *Proc IMechE, Part D: Journal of Automobile Engineering*, 226(11):1472–1482, 2012a.

Nicola Cappetti, Mario Pisaturo, and Adolfo Senatore. Cushion spring sensitivity to the temperature rise in automotive dry clutch and effects on the frictional torque characteristic. *Mechanical Testing and Diagnosis*, 3(2):28–38, 2012b.

A. Crowther, N. Zhang, D.K. Liu, and J.K. Jeyakumaran. Analysis and simulation of clutch engagement judder and stick-slip in automotive powertrain systems. *Proc IMechE, Part D: Journal of Automobile Engineering*, 218(12): 1427–1446, December 2004.

Josko Deur, Vladmir Ivanovic, Zvonko Herold, and Milan Kostelac. Dry clutch control based on electromechanical actuator position feedback loop. *International Journal of Vehicle Design*, 60(3-4):305–326, 2012.

Pietro Dolcini, Carlos Canudas de Wit, and Hubert Béchart. Improved optimal control of dry clutch engagement. *Proceedings of the 16th IFAC World Congress*, 16(1), 2005.

Pietro Dolcini, Carlos Canudas de Wit, and Hubert Béchart. Lurch avoidance strategy and its implementation in AMT vehicles. *Mechatronics*, 18(1):289–300, May 2008.

Pietro J. Dolcini, Carlos Canudas de Wit, and Hubert Béchart. *Dry Clutch Control for Automotive Applications*. Advances in Industrial Control. Springer-Verlag London, 2010.

G. Ercole, G. Mattiazzo, S. Mauro, M. Velardocchia, F. Amisano, and G. Serra. Experimental methodologies to determine diaphragm spring clutch characteristics. In *SAE Technical Paper: 2000-01-1151*, March 2000.

Lars Eriksson and Lars Nielsen. *Modeling and Control of Engines and Drivelines*. John Wiley & Sons, 2014.

Robert Fischer and Reinhard Berger. Automation of manual transmissions. In *6th LuK Symposium*, 1998.

Jonas Fredriksson and Bo Egardt. Active engine control for gear shifting in automated manual transmissions. *International Journal of Vehicle Design*, 32 (3-4):216–230, 2003.

Franco Garofalo, Luigi Glielmo, Luigi Iannelli, and Francesco Vasca. Optimal tracking for automotive dry clutch engagement. In *2002 IFAC, 15th Triennial World Congress*, 2002.

Luigi Glielmo and Francesco Vasca. Optimal control of dry clutch engagement. In *SAE Technical Paper: 2000-01-0837*, March 2000.

Kumaraswamy Hebbale, Chunhao Lee, Farzad Samie, Chi-Kuan Kao, Xu Chen, Jeremy Horgan, and Scott Hearld. Model based torque converter clutch slip control. In *SAE Technical Paper: 2011-01-0396*, April 2011.

Akira Higashimata, Kazutaka Adachi, Satoshi Segawa, Nobuo Kurogo, and Hironobu Waki. Development of a slip control system for a lock-up clutch. In *SAE Technical Paper: 2004-01-1227*, April 2004.

Takeo Hiramatsu, Takao Akagi, and Haruaki Voneda. Control technology of minimal slip-type torque converter clutch. In *SAE Technical Paper: 850460*, February 1985.

Matija Hoic, Zvonko Herold, Nenad Kranjcevic, Josko Deur, and Vladimir Ivanovic. Experimental characterization and modeling of dry dual clutch thermal expansion effects. In *SAE Technical Paper: 2013-01-0818*, April 2013.

Sungwha Hong, Sunghyun Ahn, Beakyou Kim, Heera Lee, and Hyunsoo Kim. Shift control of a 2-speed dual clutch transmission for electric vehicle. In *2012 IEEE Vehicle Power and Propulsion Conference*, October 2012.

Yutaka Kaneko, Kazutaka Adachi, Fumiyo Iino, and Mitsuo Hirata. Development of a slip speed control system for a lock-up clutch (part iii). In *SAE Technical Paper: 2009-01-0955*, April 2009.

Yuji Katsumata, Satoshi Segawa, Kazutaka Adachi, and Akira Higashimata. Development of a slip speed control system for a lock-up clutch (part ii). In *SAE Technical Paper: 2008-01-0001*, April 2008.

Klas Küpper, Roland Seebacher, and Olaf Werner. Think systems - software by LuK. In *7th LuK Symposium*, 2002.

Choon Yeol Lee, Ilsup Chung, and Young Suck Chai. Finite element analysis of an automobile clutch system. *Key Engineering Materials*, 353-358(1):2707–2711, September 2007.

Lennart Ljung. *System Identification Theory for the user*. Prentice Hall Information ans System Sciences Series. Prentice-Hall, Inc, 2nd edition, 1999.

Gianluca Lucente, Marcello Montanari, and Carlo Rossi. Modelling of an automated manual transmission system. *Mechatronics*, 17(1):73–91, November 2007.

Behrooz Mashadi and David Crolla. *Vehicle Powertrain Systems*. John Wiley & Sons Ltd, first edition, 2012.

G. Mattiazzo, S. Mauro, M. Velardocchia, F. Amisano, G. Serra, and G. Ercole. Measurement of torque transmissibility in diaphragm spring clutch. In *SAE Technical Paper: 2002-01-0934*, March 2002.

S.E. Moon, M.S. Kim, H. Yeo, H.S Kim, and S.H Hwang. Design and implementation of clutch-by-wire system for automated manual transmissions. *International Journal Vehicle Design*, 36(1):83–100, 2004.

Andreas Myklebust and Lars Eriksson. Road slope analysis and filtering for driveline shuffle simulation. In *2012 IFAC Workshop on Engine and Powertrain Control, Simulation and Modeling*, October 2012a.

Andreas Myklebust and Lars Eriksson. Torque model with fast and slow temperature dynamics of a slipping dry clutch. In *2012 IEEE Vehicle Power and Propulsion Conference*, October 2012b.

Andreas Myklebust and Lars Eriksson. The effect of thermal expansion in a dry clutch on launch control. In *7th IFAC Symposium on Advances in Automotive Control*, September 2013.

Andreas Myklebust and Lars Eriksson. Modeling, observability, and estimation of thermal effects and aging on transmitted torque in a heavy duty truck with a dry clutch. *IEEE/ASME Transactions on Mechatronics*, PP(99):1–12, 2014a.

Andreas Myklebust and Lars Eriksson. Thermal clutch model observability and observer effects of a torque sensor in the powertrain. Submitted to IEEE/ASME Transactions on Mechatronics, 2014b.

Andreas Myklebust and Lars Eriksson. Dry clutch micro-slip control and temperature considerations. Submitted to IEEE/ASME Transactions on Mechatronics, 2014c.

Wook-Hee Nam, Choon-Yeol Lee, Young S. Chai, and Jae-Do Kwon. Finite element analysis and optimal design of automobile clutch diaphragm spring. In *Seoul 2000 FISITA World Automotive Congress*, June 2000.

K. Newton, W. Steeds, and T K Garrett. *The Motor Vehicle*. Butterworth-Heinemann, 1996.

Carl Nording and Jonny Österman. *Physics Handbook*. Studentlitteratur, 1999.

M.J. Nunney. *Automotive Technology*. Butterworth-Heinemann, third edition, 1998.

Paul Otanez, Farzad Samie, Chunhao Joseph Lee, and Chi-Kuan Kao. Aggressive torque converter clutch slip control and driveline torsional velocity measurements. In *SAE Technical Paper: 2008-01-1584*, April 2008.

Magnus Pettersson. *Driveline Modeling and Control*. PhD thesis, Linköpings Universitet, May 1997.

Magnus Pettersson and Lars Nielsen. Gear shifting by engine control. *IEEE Transactions Control Systems Technology*, 8(3):495–507, May 2000.

Magnus Pettersson and Lars Nielsen. Diesel engine speed control with handling of driveline resonances. *Control Engineering Practice*, 11(3):319–328, March 2003.

Wolfgang Reik, Roland Seebacher, and Ad Kooy. Dual mass flywheel. In *6th LuK Symposium*, 1998.

Samir Sfarni, Emmanuel Bellenger, Jérome Fortin, and Matthieu Malley. Numerical modeling of automotive riveted clutch disc for contact pressure verification. In *49th Scandinavian Conference on Simulation and Modeling*, October 2008.

Shaohua Sun, Yulong Lei, Yao Fu, Cheng Yang, and ShunBo Li. Analysis of thermal load for dry clutch under the frequent launching condition. In *SAE Technical Paper: 2013-01-0814*, April 2013.

Barna Szimandl and Huba Németh. Dynamic hybrid model of an electropneumatic clutch system. *Mechatronics*, 23(1):21–36, 2012.

Francesco Vasca, Luigi Iannelli, Adolfo Senatore, and Gabriella Reale. Torque transmissibility assessment for automotive dry-clutch engagement. *IEEE/ASME transactions on Mechatronics*, 16(3):564–573, June 2011.

M. Velardocchia, G. Ercole, G. Mattiazzo, S. Mauro, and F. Amisano. Diaphragm spring clutch dynamic characteristic test bench. In *SAE Technical Paper: 1999-01-0737*, March 1999.

M. Velardocchia, F. Amisano, and R. Flora. A linear thermal model for an automotive clutch. In *SAE Technical Paper: 2000-01-0834*, March 2000.

Anna Wikdahl and Åsa Ågren. Temperature distribution in a clutch. Master's thesis, Linköping University, 1999.

Publications

Paper A

Torque Model with Fast and Slow Temperature Dynamics of a Slipping Dry Clutch*

A

*Published in *The 8th IEEE Vehicle Power and Propulsion Conference.*

Torque Model with Fast and Slow Temperature Dynamics of a Slipping Dry Clutch

Andreas Myklebust and Lars Eriksson

Vehicular Systems, Department of Electrical Engineering, Linköping University, SE-581 83 Linköping, Sweden

Abstract

The transmitted torque in a slipping dry clutch is studied in experiments with a heavy duty truck. It is shown that the torque characteristic has little or no dependence on slip speed, but that there are two dynamic effects that make the torque vary up to 900 Nm for the same clutch actuator position. Material expansion with temperature can explain both phenomena and a dynamic clutch temperature model with two different time constants is developed. The dynamic model is validated in experiments, with an error of only 3 % of the maximum engine torque, and is shown to improve the behavior significantly compared to a static model.

1 Introduction

Increasing demands on comfort, performance, and fuel efficiency in vehicles lead to more complex transmission solutions. Historically high efficiency was best met with a classical Manual Transmission and comfort with a classical Automatic Transmission. The Automated Manual Transmission (AMT) is one way to combine the best from two worlds. An important part in an AMT is clutch control that has a profound effect on vehicle performance. Therefore it is of importance to know the torque transmitted in the clutch with high precision. Models have come to play an important role in estimation and control of the transmitted torque, since torque sensors are expensive.

A sketch of a dry single-plate clutch is found in Figure 1, while in-depth explanations are found in for example Mashadi and Crolla (2012) and Vasca et al. (2011). In clutch-modeling literature a wide range of models are proposed. The most simple models have a clutch torque that is assumed to be a controllable input, see for example Dolcini et al. (2008); Garofalo et al. (2002). These models rely on the assumption that there is perfect knowledge of how the clutch behaves. More advanced models include submodels for slipping and sticking torques. For example a LuGre model is used in Dolcini et al. (2005) and a Karnopp model in Bataus et al. (2011). The former is a one-state model that captures stick-slip behavior, varying break-away force, Stribeck effect, and viscous friction. The latter simply applies a dead-zone around zero speed to ease the simulation of stick-slip behavior.

Models for the clutch torque during slipping commonly use a function with the following structure,

$$M_c = \operatorname{sgn}(\Delta\omega)\, \mu\, R_e\, F_N \tag{1}$$

where $\Delta\omega$ is the clutch slip (speed), μ the friction coefficient, R_e the effective radius and F_N the clamping (normal) force. In these models F_N is often either given as input or a static nonlinear function of clutch position, x, i.e. $F_N = F_N(x)$, see for example Vasca et al. (2011); Glielmo and Vasca (2000). In particular Dolcini et al. (2010) mentions that a third-order polynomial is suitable to describe the connection between throwout-bearing position and clutch transmitted torque, mainly governed by the flat (cushion) spring characteristics. Furthermore a slight speed dependency of the normal force is hinted in Dolcini et al. (2010), centrifugal forces acting on the springs in the clutch. Mashadi and Crolla (2012) reports of hysteresis in the diaphragm spring, that could lead to hysteresis in the normal force. In Mattiazzo et al. (2002) a temperature and wear dependency of the normal force/bearing position characteristics is shown.

Concerning the other model components it is generally recognized that μ can depend on temperature, slip speed, and wear and that R_e can depend on temperature and wear as well, see Velardocchia et al. (1999). In Vasca et al. (2011) a slip speed dependency of μR_e is shown, this was especially pronounced for slip speeds below $\sim$100 RPM.

It can be difficult to separate which parameter in (1) that is the reason for a change in M_c. Therefore the clutch torque is often studied as a lumped model. In Velardocchia et al. (1999) M_c is seen to decrease with temperature and $\Delta\omega$. However there are large variations with wear. In Ercole et al. (2000) M_c initially decreases with temperature for low temperatures and then increases for medium and high temperatures. Similarly there are variations with wear and in addition temperature-torque hysteresis are reported. In Velardocchia et al. (2000) and Wikdahl and Ågren (1999) temperature models are established, but no work seems to include the temperature effect on M_c. In view of this the main contribution in this paper is the analysis and model of a clutch that includes temperature dynamics and the corresponding effects on the transmitted torque.

The clutch model presented here is built solely from the observation made on the data presented in this paper. No slip dependency is seen and the torque is increasing with temperature. A limitation of the problem statement is that the clutch is only studied when it is slipping.

2 Experimental Setup

The AMT clutch in a Heavy Duty Truck (HDT) is studied. The clutch, that is in focus here, is a dry single-plate pull-type normally closed clutch. A schematic is seen in Figure 1. The clutch is actuated by an electric motor that through a worm gear moves a hydraulic master cylinder that in turn moves a slave piston and via a lever pulls the throwout bearing. Both motor position, x_m, and slave position, x, are measured.

The truck used here is only equipped with production sensors, engine speed, idle shaft speed and slave position. Hence no exact torque measurement, is available. In order to get a measurement of the clutch torque the reported engine torque has been compensated for inertia effects of the engine and flywheel. The limited amount of sensors add to the difficulty in making a clutch model and validating it.

3 Modeling Outline

As mentioned in Section 1, M_c depends on several factors such as, actuator position, temperatures, rotational speeds and wear. In Figure 2 it is seen how the transmitted torque varies with up to 900 Nm for a given position. Furthermore components are non-linear e.g. spring characteristics, hysteresis, etc. However during experiments no clear hysteresis have been detected and therefore not modeled. Due to the difficulties involved in measuring wear, especially when access to test equipment is limited and non-exclusive, wear has been assumed slow enough to not have a significant effect in the experiments. The only exception is the parameter $x_{0,\mathrm{ref}}$ of Section 5, which is directly affected by the thickness of the friction pads. $x_{0,\mathrm{ref}}$ had to be parameterized to each measurement session

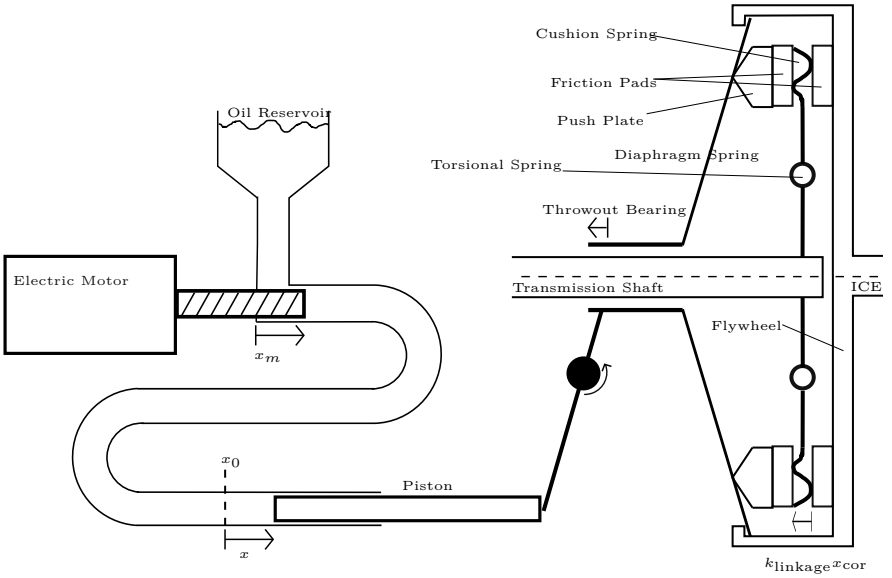

Figure 1: A schematic over the actuator and the dry single-plate pull-type clutch studied here. k_{linkage} is the combined ratio of all levers between the piston and the push plate.

(months apart). In an on-line application of the model, such as an observer or controller, more parameters would probably need to be adapted continuously.

In the collected measurement $\Delta\omega > 0$ has always hold, hence the sgn-function from (1) has not been considered. And since the clutch is only considered during slipping no advanced friction model, e.g. LuGre, is needed as they tend to be focused around lock up. All these simplifications leave the model structure at

$$M_c = \mu(\Delta\omega, T)\, R_e(T)\, F_N(x, T, \Delta\omega) \tag{2}$$

In Section 5 the temperature effect will be explained by a changing F_N, at least for medium temperatures of the clutch. Nevertheless with the available sensors there is no way to truly separate the effects between the parameters. Therefore the model structure will be,

$$M_c = M_c(x, T, \Delta\omega) \tag{3}$$

In the next section the slip dependency will be investigated and in the subsequent section the position and temperature dependency will be handled.

4 Slip dependency

Slip speed, $\Delta\omega$, dependency is recognized in the literature, (Vasca et al., 2011), (Velardocchia et al., 1999). Therefore experiments have been carried out to

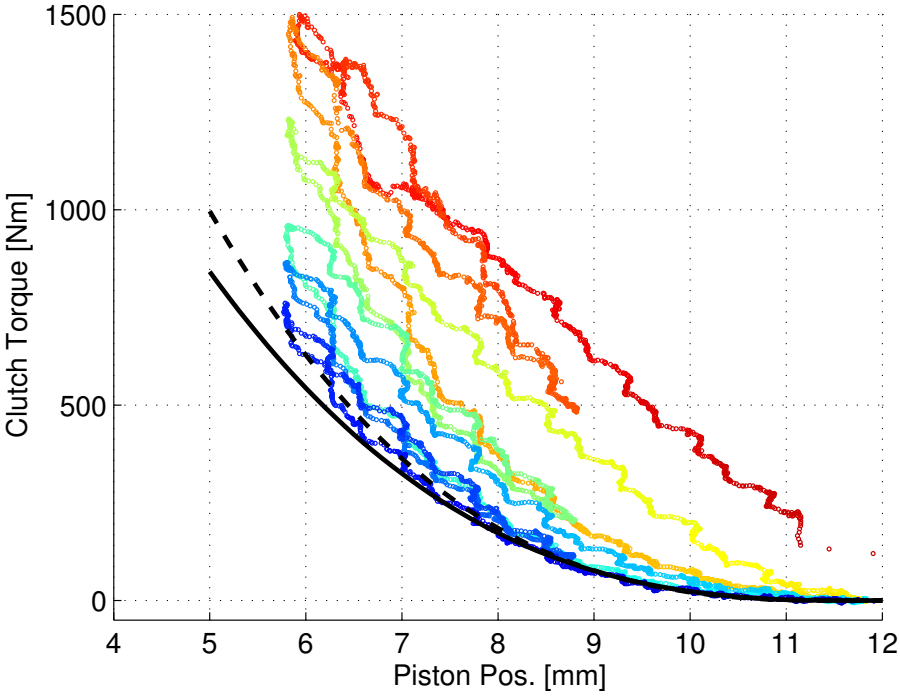

Figure 2: The clutch position has been ramped back and forth while the clutch torque has been measured. The transmitted torque clearly depends on something more than the clutch position, in particular there is a drift with time (the color changes with time, blue=0 s and red=75 s). The torque difference between the first and last ramp is up to 900 Nm. The black lines are two parameterizations of (5).

investigate this. Remember that since this work is limited to when the clutch is slipping, slip speeds have been relatively large. There has been no investigation of what happens when the clutch approaches lock up.

The experiments have been carried out as follows. The truck has been driven to an uphill and has been kept stationary by slipping the clutch at a constant position. This way the vehicle will accelerate forwards if more torque is transmitted and backwards if less torque is transmitted. Furthermore it is easy to initially keep the input shaft speed stationary this way, and by doing so the engine speed can be used to control the slip speed. Slip-speed steps are made and an abrupt change in torque/input shaft acceleration should be seen if there is a slip-speed dependency, Figure 3. Note that the engine torque will see a transient during the flank of a step due to the acceleration of the engine. A smaller transient is present in the clutch torque signal due to imperfections in the compensation for the acceleration. No significant change is seen in the

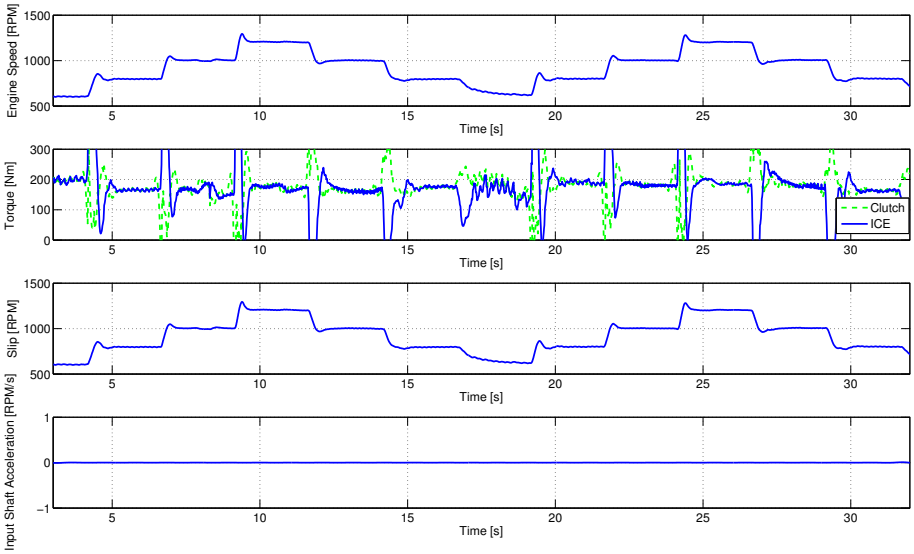

Figure 3: Slip steps are made through engine-speed control when the truck is held stationary in a slight uphill using a constant clutch position. No reaction is seen in neither clutch torque or input shaft acceleration.

input shaft acceleration and no correlation between steady-state clutch torque and slip speed is seen neither, Fig 4. Therefore it is assumed that there is no slip dependency at the slip speeds of interest in this paper. Equation (3) can be reduced to

$$M_c = M_c(x, T) \tag{4}$$

This is somewhat in contrast to the data in Velardocchia et al. (1999) where a slip dependency is shown. The slip has only been investigated at relatively large speeds and does therefore not contrast the data in Vasca et al. (2011).

5 Temperature Effects and Models

The shape of the torque transmissibility curve is mainly due to the cushion spring characteristics. Dolcini et al. (2010) mentions that this curve can be described by a third order polynomial,

$$M_{\text{ref}}(x_{\text{ref}}) = \begin{cases} a(x_{\text{ref}} - x_{\text{ref,ISP}})^3 + \\ +b(x_{\text{ref}} - x_{\text{ref,ISP}})^2 & \text{if } x_{\text{ref}} < x_{\text{ref,ISP}} \\ 0 & \text{if } x_{\text{ref}} \geq x_{\text{ref,ISP}} \end{cases} \tag{5}$$

where x_{ISP} (Incipient Sliding Point) is the kiss point, where the push plate and clutch disc first meet and torque can start to transfer. There is no first or

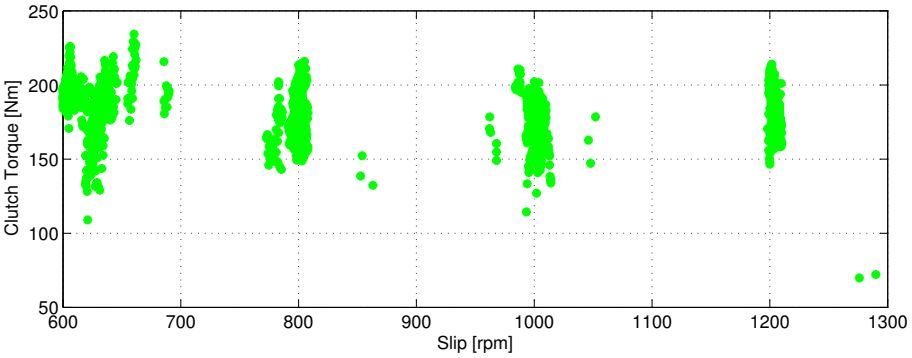

Figure 4: The data points from Figure 3 when the engine speed is constant. No correlation is seen between clutch torque and slip speed.

zeroth order term in the equation since it is desired to have zero torque and derivative at $x_{\text{ref,ISP}}$. The exact value of x_{ISP} can be difficult to find since the transmissibility curve is very flat around x_{ISP}. However it is only important to find a x_{ISP} that gives a good curve fit, as errors will be small near x_{ISP}. A suggestion in Mattiazzo et al. (2002) is to define x_{ISP} as the point that transmits a certain small torque. That method should give sufficient estimates of x_{ISP} for the application described here.

Experimental data confirms (5) to be a good approximation for a given temperature, T_{ref}, see Figure 2. However during slipping of the clutch, heat is dissipated from the friction surface into the cast iron parts of the clutch that naturally will expand. When the actuator motor is fully retracted (position=0) the expansion can be measured through the position sensor on the slave. This slave position is called the zero position, x_0, see Figure 1.

A set of experiments has been performed to investigate the dynamics of the clutch expansion. In order to be able to measure the zero position during heating, the clutch has been alternating between closed and slipping with short time intervals. After some time of heating the clutch has been held closed for a prolonged time while the zero position has been constantly monitored as the clutch cools down. The measurement results are found in Figure 5. The zero position increases in a repeatable way with dissipated energy in the clutch and decays in an exponential manner with time. This supports the hypothesis that temperature is causing the change in zero position.

5.1 Material Expansion Analysis

In order to see that the change in zero position is due to material expansion, the temperature increase is calculated in two ways. During the first heating period of Figure 5, 1.5 MJ of energy is dissipated. The pressure plate and flywheel have a combined mass of 81 kg and are made of cast iron that has a specific

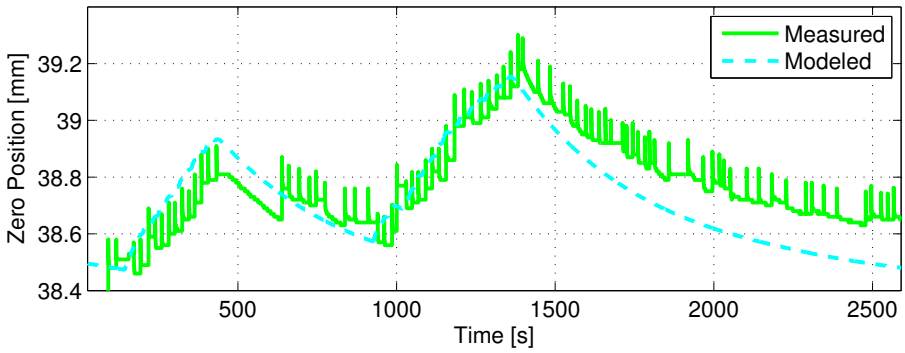

Figure 5: The clutch has been heated through slipping and then left to cool down. The zero position has been recorded as a measure of the expansion. The temperature model (6)-(9) shows good agreement with the measurement. Parameters have been fitted to a separate set of data.

heat of 0.5 kJ/(kg K), (Nording and Österman, 1999). If cooling of the clutch is neglected a slightly high estimation of the temperature increase is obtained.

$$\frac{1.5 \cdot 10^6}{500 \cdot 81} = 37 \text{ K}$$

The measured expansion of the clutch during the same period is 0.3 mm at the piston. With a linkage ratio of 8.8, a 100 mm thick clutch and an expansion coefficient for cast iron of $11 \cdot 10^{-6}$ K^{-1}, (Nording and Österman, 1999), this corresponds to a temperature increase of,

$$\frac{0.3}{8.8 \cdot 100 \cdot 11 \cdot 10^{-6}} = 30 \text{ K}$$

The two temperature estimates are practically the same. Therefore the measured expansion can be said to depend on temperature.

5.2 Expansion Model

In order to model the expansion a temperature model is required. In Velardocchia et al. (2000) a linear model with one thermal mass in the pressure plate and one in the flywheel is proposed. All parts of the clutch are cooled towards the air in the clutch housing. Here the model is extended to capture the changes in the housing temperature, T_h. In contrast to Velardocchia et al. (2000) the clutch studied here is mounted in a vehicle, therefore the clutch is, in addition, thermally connected to both the ICE and transmission. However only a few percent of the dissipated power, P, goes into the transmission, Wikdahl and Ågren (1999). Therefore the heat flow to the transmission has been neglected.

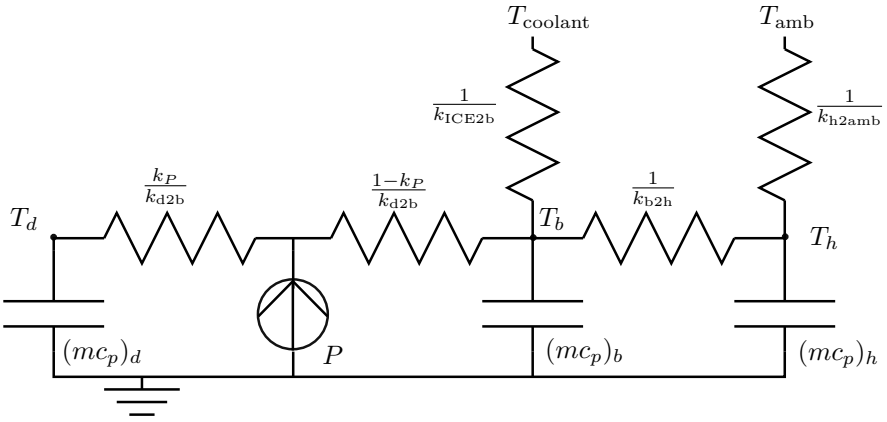

Figure 6: An electrical analogy of the temperature model (12)-(14). If $(mc_p)_d = 0$ the model can also be described by (6)-(7).

Moreover it has been found that the thermal masses of the flywheel and pressure plate can be taken as one mass, $(mc_p)_b$, for the clutch body, without loosing accuracy with respect to the expansion. For an electrical analogy of the model see Figure 6. The corresponding equations are:

$$(mc_p)_b \dot{T}_b = k_{\text{ICE2b}}(T_{\text{coolant}} - T_b) + k_{\text{b2h}}(T_h - T_b) + P \tag{6}$$

$$(mc_p)_h \dot{T}_h = k_{\text{b2h}}(T_b - T_h) + k_{\text{h2amb}}(T_{\text{amb}} - T_h) \tag{7}$$

where,

$$P = M_c \, \Delta\omega \tag{8}$$

In order to connect the temperature model with the change in zero position, the levers and the expansion of the clutch body as function of temperature are assumed linear.

$$x_0 = k_{\text{exp},1} \, (T_b - T_{\text{ref}}) + x_{0,\text{ref}} \tag{9}$$

The eight parameters in the equations have been fitted against measured data and the validation results, on a different set of data, can be seen in Figure 5. Using these results the piston position can be corrected for the expansion effect to correspond to the actual compression of the flat spring, see Figure 1.

$$\Delta x_0 = x_0 - x_{0,ref} \tag{10}$$

$$x_{\text{cor}} = x - \Delta x_0 \tag{11}$$

Nevertheless the expansion model does not explain the torque drift, see Figure 7. The time scale in Figure 2 is significantly smaller than that of Figure 5. The torque drift is also much larger than what is explained by the expansion.

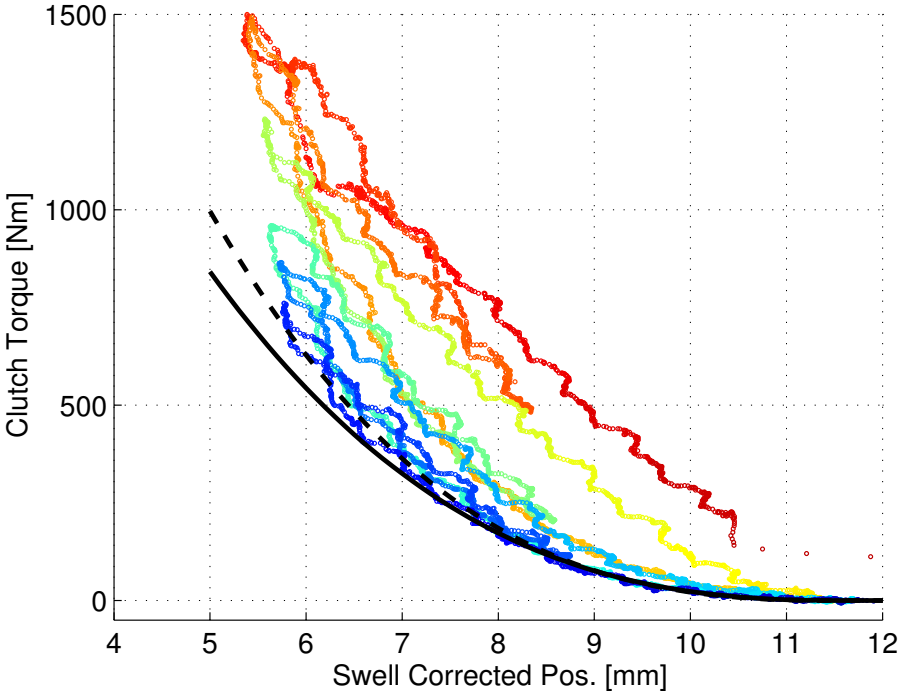

Figure 7: The data from Figure 2 has been corrected for swelling of the clutch body using (11). The correction is not sufficient to explain the torque drift.

This has led to the hypothesis that the clutch disc is also expanding with heat. In particular the clutch disc has a much smaller (thermal) mass, which could correspond to the faster time constant phenomenon seen in the data.

5.3 Including Fast Dynamics

The clutch disc temperature, T_d, has been modeled in a similar fashion, see Figure 6 for an electrical analogy and below for equations.

$$(mc_p)_b\dot{T}_b = k_{\mathrm{ICE2b}}(T_{\mathrm{coolant}} - T_b) + k_{\mathrm{b2h}}(T_h - T_b) + \\ + k_{\mathrm{d2b}}(T_d - T_b) + k_P P \tag{12}$$

$$(mc_p)_h\dot{T}_h = k_{\mathrm{b2h}}(T_b - T_h) + k_{\mathrm{h2amb}}(T_{\mathrm{amb}} - T_h) \tag{13}$$

$$(mc_p)_d\dot{T}_d = k_{\mathrm{d2b}}(T_b - T_d) + (1 - k_P)P \tag{14}$$

A new situation with this extended model is that the dissipated energy has to be split between the clutch disc and the body. In the model it is split by the parameter k_P, which is 1 if all energy goes to the body and 0 if all goes to the disc. However the model is not sensitive to k_P due to two facts. Firstly the vast

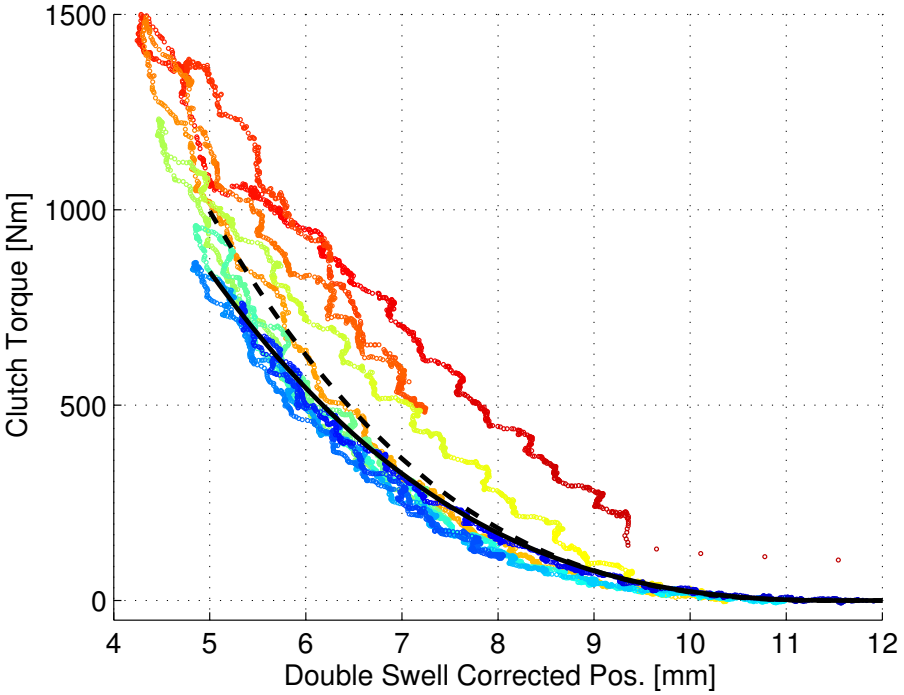

Figure 8: The data from Figure 2 has been corrected for swelling of the clutch body using (11) and (15). The correction explains the torque drift until the temperatures get too high (somewhere when state T_d becomes greater than 200 °C).

difference in time constants, a factor of ∼50, between the disc and the body decouples (12) from (14), i.e. $k_{\mathrm{d2b}}(T_d - T_b) + k_P P \approx (1 - k_P)P + k_P P = P$, leaving the dynamics of T_b almost unchanged. Secondly the parameters are fitted to data, i.e. if k_P is 0 instead of 0.5 the value of $(mc_p)_d$ and k_{d2b} will double, leaving the dynamics of T_d almost unchanged. In the data the expansion has been seen to lag the dissipated power. The lag is maximized by $k_P = 0$ this is thus the choice of k_P.

The expansion of the clutch disc is modeled by extending (9) with an extra term

$$\begin{aligned}\Delta x_0 &= k_{\mathrm{exp}}\left(T_b - T_{\mathrm{ref}}\right) + k_{\mathrm{exp},2}\left(T_d - T_{\mathrm{ref}}\right) = \\ &= k_{\mathrm{exp}}\left(T_b - T_{\mathrm{ref}}\right) + k_{\mathrm{exp},2}\left(\left(T_d - T_b\right) + \left(T_b - T_{\mathrm{ref}}\right)\right) = \\ &= \underbrace{\left(k_{\mathrm{exp}} + k_{\mathrm{exp},2}\right)}_{k_{\mathrm{exp},1}}\left(T_b - T_{\mathrm{ref}}\right) + k_{\mathrm{exp},2}\left(T_d - T_b\right) \end{aligned} \tag{15}$$

where the second term was practically zero during the zero-position measurements

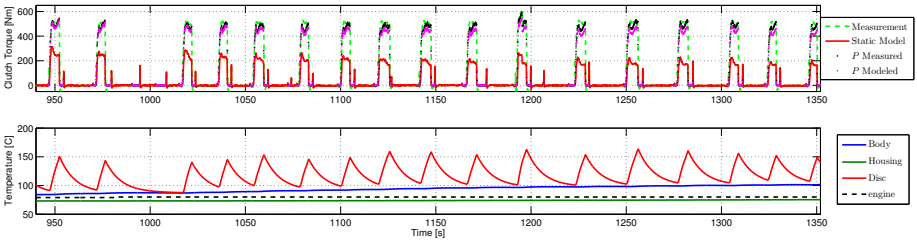

Figure 9: The dynamic torque model shows good agreement with measurements in a validation data set. There is a slight decay in torque when P is modeled instead of measured. However both implementations are significant improvements compared the static model, $M_c = M_{\text{ref}}(x)$. The open-loop simulation started at 0 seconds. In the lower plot P is measured.

due to the fast dynamics of T_d. Therefore the new parameters can be estimated separately from the old parameters. After estimation of the new parameters the position can be corrected with (12)-(15) and Figure 8 is obtained.

The model works well until the temperatures become too high (state T_d reaches more than 200 °C). It has been found empirically that saturating the term $(T_d - T_b)$ at 110 °C improves the model at higher temperatures. One should note that values of the temperature states have not been validated against any measurement but they have reasonable magnitudes.

The transmitted torque can now be calculated as,

$$M_c = M_{\text{ref}}(x_{\text{cor}}) \tag{16}$$

Note that x_{cor} increases with temperature which in turn makes M_c increase with temperature. This is in contrast with the data in Velardocchia et al. (1999) where the torque is decreasing with temperature. Although in the experiments performed here the clutch mostly has a medium to high temperature and could comply with the data in Ercole et al. (2000).

In summary, the model is a three state model with one static non-linearity. All calculations are simple and therefore the model is suitable for running in real time, for example in a clutch-control application.

6 Model Validation

The model has been validated on several data sets separate from those used for parameter identification. One of these validations is shown in Figure 9. The model can be said to agree well with data. If the dissipated power is calculated from the measured torque the model agrees very well, but it still simulates a slightly low clutch torque. If instead the dissipated power is calculated from the simulated torque the torque error makes the simulated power dissipation too low

and therefore the temperature states get lower. In turn this will lead to even lower simulated torque in the next torque pulse. This is the explanation for the decay in the simulated torque. In spite of this it still models the torque better than the more common static model. On one hand, calculating the power from the measured torque gives a better estimate of the current transmissibility curve, which could be used for feed forward in control applications. On the other hand the measured torque is not always available, e.g. some special driving scenarios, when evaluating new controllers through simulation, or in the prediction made by a model-based controller.

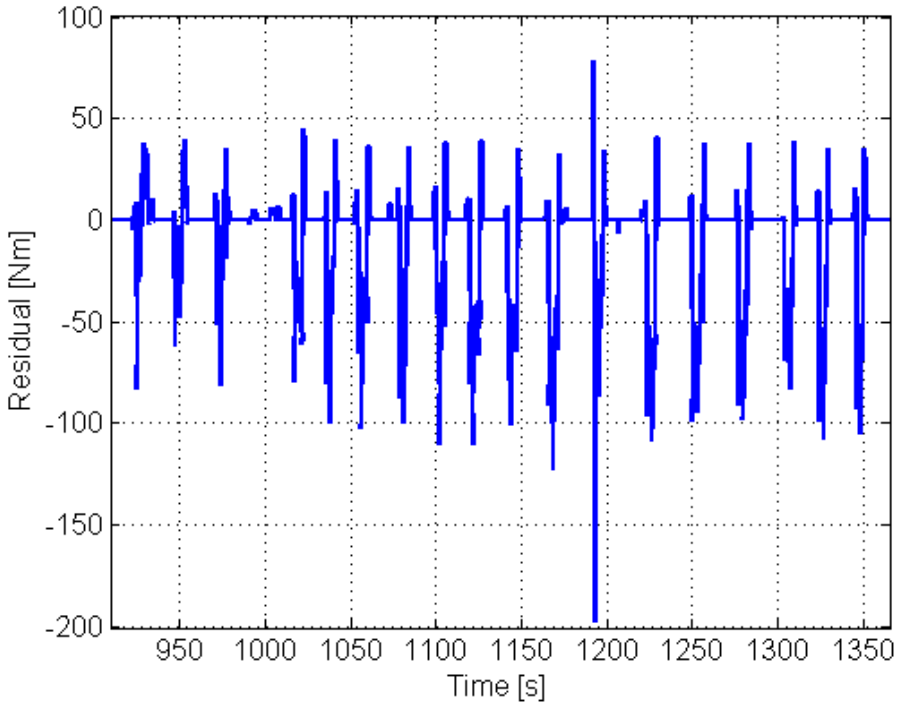

Figure 10: The residuals between the model and data presented in Figure 9. The residuals are less than 200 Nm and most of the time less than 100 Nm. Or in other words, most of the time less than 3% of maximum ICE torque.

At the end of the torque pulses, the modeled torque drops faster than the measured torque, when the clutch is fully opened in 0.3 s. This is however believed to be due to delays in the computation of the engine torque, sensors and other data processing. Therefore the residuals have been filtered using a moving median of five samples (10 Hz). The result is presented in Figure 10. The residuals are less than 200 Nm and most of the time less than 100 Nm. Considering that 100 Nm is less than 3% of maximum engine torque, the model works well. In fact the engine estimated torque can have errors of similar

magnitude.

A validation of a launch is shown in Figure 11. The static and dynamic models are compared to measurement data. The dynamic model has a small error that is always less than 104 Nm, and has better performance than the static model.

In other data sets it has been seen that somewhere when T_d is greater than 200 °C the model deteriorates. This however is of small concern since these temperatures are only reached during extreme driving. The accuracy of the model has also been seen to be less good when the truck is cold.

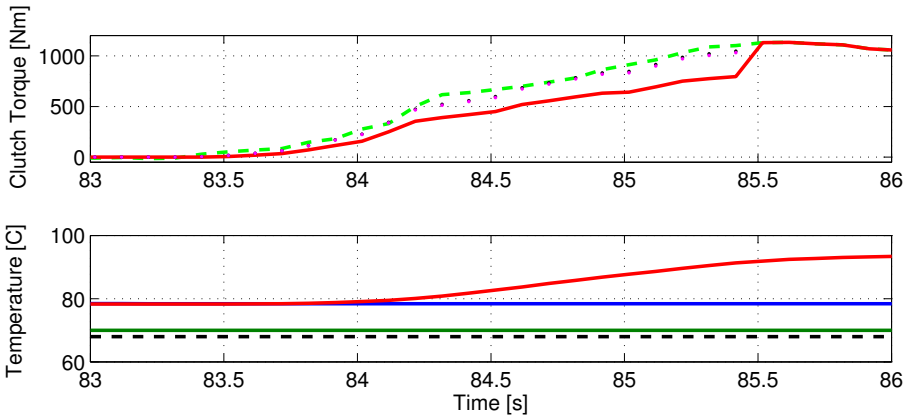

Figure 11: The dynamic torque model shows good agreement with measurement data of a start. The open-loop simulation started at 0 seconds. Line colors and styles are the same as in Figure 9. The clutch is locked up when there are no black or magenta dots. In the lower plot P is measured.

The clutch temperatures could not be quantitatively validated as no temperature measurements were available. Therefore only a qualitative validation is performed, showing that the magnitudes of the temperature states are reasonable for an HDT clutch, see Figure 9 and 11.

7 Conclusion

The transmitted torque in an heavy-duty truck dry clutch at slipping conditions has been studied. Experiments showed no direct slip-speed dependency at the levels of slip investigated here, instead dynamic effects were clearly visible. In particular the measurements showed that the transmitted torque can vary with up to 900 Nm for a given position. To capture the dynamic behavior, a model with three temperature states was built. The model was developed and validated on a production HDT, were no temperature measurements were available. Therefore

only a qualitative validation of the temperatures was performed, showing that they had reasonable magnitudes.

The temperature dynamics have two vastly different time constants, a factor of ∼50 apart, and the slow part could be physically explained to affect the transmitted torque through expansion of clutch parts. Due to the vast difference in the two time constants the model shows little sensitivity to how the dissipated heat enters the model.

In validations, on driving sequences with intense use of the clutch, the open-loop simulation error was kept under 200 Nm and most of the time under 100 Nm, which is less than 3% of maximum engine torque and comparable to the accuracy of the engine torque estimate. The dynamic model was shown to give a significant improvment compared to a static model.

Finally, the model is simple and suitable for running in real time applications, such as a clutch controller or a torque observer.

Acknowledgment

Vinnova industrial excellence center LINK-SIC and Scania CV have supported this work. Special thanks to Karl Redbrandt at Scania for conducting the experiments.

References

Marius Bataus, Andrei Maciac, Mircea Oprean, and Nicolae Vasiliu. Automotive clutch models for real time simulation. *Proceedings of the Romanian Academy, Series A*, 12(2):109–116, 2011.

Pietro Dolcini, Carlos Canudas de Wit, and Hubert Béchart. Improved optimal control of dry clutch engagement. *Proceedings of the 16th IFAC World Congress*, 16(1), 2005.

Pietro Dolcini, Carlos Canudas de Wit, and Hubert Béchart. Lurch avoidance strategy and its implementation in AMT vehicles. *Mechatronics*, 18(1):289–300, May 2008.

Pietro J. Dolcini, Carlos Canudas de Wit, and Hubert Béchart. *Dry Clutch Control for Automotive Applications*. Advances in Industrial Control. Springer-Verlag London, 2010.

G. Ercole, G. Mattiazzo, S. Mauro, M. Velardocchia, F. Amisano, and G. Serra. Experimental methodologies to determine diaphragm spring clutch characteristics. In *SAE Technical Paper: 2000-01-1151*, March 2000.

Franco Garofalo, Luigi Glielmo, Luigi Iannelli, and Francesco Vasca. Optimal tracking for automotive dry clutch engagement. In *2002 IFAC, 15th Triennial World Congress*, 2002.

Luigi Glielmo and Francesco Vasca. Optimal control of dry clutch engagement. In *SAE Technical Paper: 2000-01-0837*, March 2000.

Behrooz Mashadi and David Crolla. *Vehicle Powertrain Systems*. John Wiley & Sons Ltd, first edition, 2012.

G. Mattiazzo, S. Mauro, M. Velardocchia, F. Amisano, G. Serra, and G. Ercole. Measurement of torque transmissibility in diaphragm spring clutch. In *SAE Technical Paper: 2002-01-0934*, March 2002.

Carl Nording and Jonny Österman. *Physics Handbook*. Studentlitteratur, 1999.

Francesco Vasca, Luigi Iannelli, Adolfo Senatore, and Gabriella Reale. Torque transmissibility assessment for automotive dry-clutch engagement. *IEEE/ASME transactions on Mechatronics*, 16(3):564–573, June 2011.

M. Velardocchia, G. Ercole, G. Mattiazzo, S. Mauro, and F. Amisano. Diaphragm spring clutch dynamic characteristic test bench. In *SAE Technical Paper: 1999-01-0737*, March 1999.

M. Velardocchia, F. Amisano, and R. Flora. A linear thermal model for an automotive clutch. In *SAE Technical Paper: 2000-01-0834*, March 2000.

Anna Wikdahl and Åsa Ågren. Temperature distribution in a clutch. Master's thesis, Linköping University, 1999.

Paper B

The Effect of Thermal Expansion in a Dry Clutch on Launch Control*

B

*Published in *7th IFAC Symposium on Advances in Automotive Control.*

The Effect of Thermal Expansion in a Dry Clutch on Launch Control

Andreas Myklebust and Lars Eriksson

Vehicular Systems, Department of Electrical Engineering, Linköping University, SE-581 83 Linköping, Sweden

Abstract

A dry clutch model with thermal dynamics is added to a driveline model of a heavy-duty truck equipped with an automated manual transmission. The model captures driveline oscillations and can be used to simulate how different clutch-control strategies affect vehicle performance, drivability and comfort. Parameters are estimated to fit a heavy-duty truck and the complete model is validated with respect to shuffle, speed trajectory, clutch torque and clutch lock-up/break-apart behavior. The model shows good agreement with data. Furthermore the model is used to study the effect of thermal expansion in the clutch on launch control. It is shown that the effect of thermal expansion, even for moderate temperatures, is significant in launch control applications.

1 Introduction

Increasing demands on comfort, performance, and fuel efficiency in vehicles lead to more complex transmission solutions. Historically high efficiency was best met with a classical Manual Transmission and comfort with a classical Automatic Transmission. The Automated Manual Transmission (AMT) is one way to combine the best from two worlds. An important part in an AMT is clutch control that has a profound effect on vehicle performance. Therefore it is of importance to know the torque transmitted in the clutch with high precision. Models have come to play an important role in estimation and control of the transmitted torque, since torque sensors are expensive.

A sketch of a dry single-plate clutch is found in Figure 1, while in-depth explanations are found in for example Mashadi and Crolla (2012) and Vasca et al. (2011). In clutch-modeling literature a wide range of models are proposed. The most simple models have a clutch torque that is assumed to be a controllable input, see for example Dolcini et al. (2008); Garofalo et al. (2002). These models rely on the assumption that there is perfect knowledge of how the clutch behaves. More advanced models include submodels for slipping and sticking torques. For example a LuGre model is used in Dolcini et al. (2005) and a Karnopp model in Bataus et al. (2011). The former is a one-state model that captures stick-slip behavior, varying break-away force, Stribeck effect, and viscous friction. The latter simply applies a dead-zone around zero speed to ease the simulation of stick-slip behavior.

Models for the transmittable clutch torque during slipping commonly use a function with the following structure,

$$M_{\text{trans,k}} = \operatorname{sgn}(\Delta\omega)\, \mu\, R_e\, F_N \tag{1}$$

where $\Delta\omega$ is the clutch slip (speed), μ the friction coefficient, R_e the effective radius and F_N the clamping (normal) force. In these models F_N is often either given as input or a static nonlinear function of clutch position, x, i.e. $F_N = F_N(x)$, see for example Vasca et al. (2011); Glielmo and Vasca (2000). Furthermore a graph with speed dependency of the normal force is shown in Hong et al. (2012). In Dolcini et al. (2010) that speed dependency is said to be due to centrifugal forces acting on the springs in the clutch. Mashadi and Crolla (2012); Moon et al. (2004) reports of hysteresis in the diaphragm spring, that could lead to hysteresis in the normal force. In Mattiazzo et al. (2002) a temperature and wear dependency of the normal force/bearing position characteristics is shown.

Concerning the other model components it is generally recognized that μ can depend on temperature, slip speed, and wear and that R_e can depend on temperature and wear as well, see Velardocchia et al. (1999). In Vasca et al. (2011) a slip speed dependency of μR_e is shown, this was especially pronounced for slip speeds below $\sim$100 RPM.

It can be difficult to separate which parameter in (1) that is the reason for a change in $M_{\text{trans,k}}$. Therefore the clutch torque is often studied as a

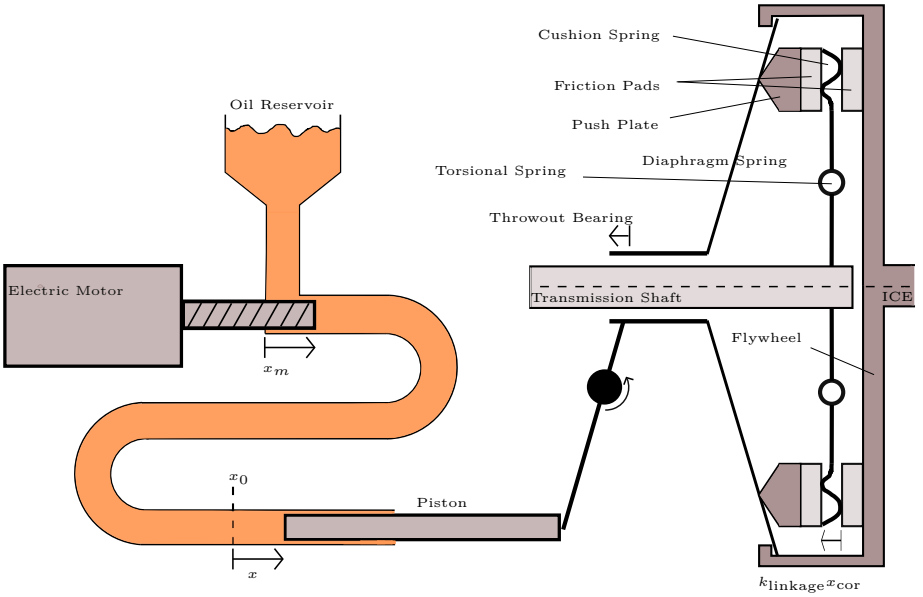

Figure 1: A sketch over the actuator and dry single-plate pull-type clutch installed in the experiment vehicle.

lumped model. In Velardocchia et al. (1999) $M_{\text{trans,k}}$ is seen to decrease with temperature and $\Delta\omega$. However there are large variations with wear. In Ercole et al. (2000) $M_{\text{trans,k}}$ initially decreases with temperature for low temperatures and then increases for medium and high temperatures. Similarly there are variations with wear and in addition temperature-torque hysteresis are reported. In Velardocchia et al. (2000), Wikdahl and Ågren (1999) and Myklebust and Eriksson (2012b) temperature models are established, but only Myklebust and Eriksson (2012b) includes the effect of the temperature on M_{trans}.

When modeling the rest of the driveline for (clutch) control purposes it is common to include one or more flexibilities, (Pettersson, 1997; Garofalo et al., 2002; Fredriksson and Egardt, 2003; Moon et al., 2004; Crowther et al., 2004; Lucente et al., 2007; Dolcini et al., 2008)

Here yet another driveline model with focus on the clutch and the control of it is presented and validated. The contribution lies in that here the thermal dynamics of the clutch are included in the model. Particularly the significance to launch performance of including the thermal part is shown.

2 Driveline Model

In order to evaluate the quality of a certain launch control, a longitudinal model of the heavy-duty truck in question is required. The model has to capture

important dynamics in the driveline and how they make the truck shuffle. One such model is found in Myklebust and Eriksson (2012a). It is used here with one modification, the clutch model is replaced with the more advanced model from Myklebust and Eriksson (2012b).

An overview of the model is seen in Figure 2. There the different parts of the model, Internal Combustion Engine (ICE), clutch, gearbox, propeller shaft, final drive, drive shafts and vehicle dynamics, can be seen as well as where the flexibilities are located. Next, a quick review of the model equations are given.

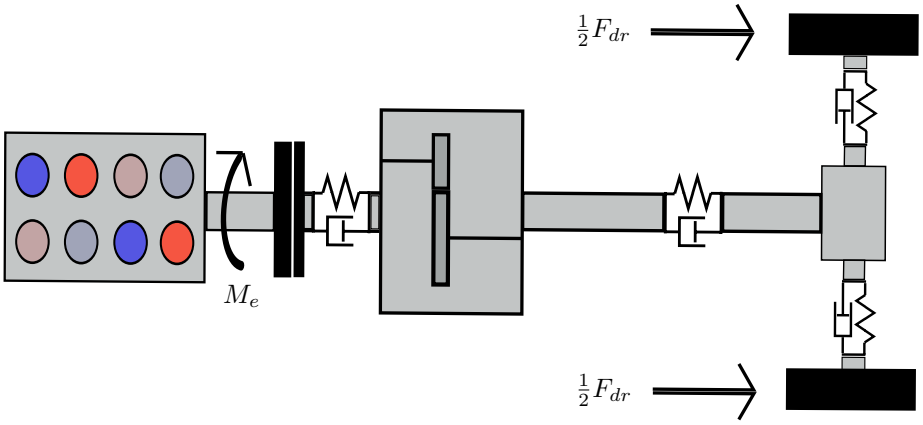

Figure 2: Sketch of the driveline model. Modeled parts and locations of flexibilities are visible.

If not otherwise stated the nomenclature follows this system: θ=angle, $\omega = \dot{\theta}$, v=velocity, r=radius, T=temperature, M=torque, F=force, P=power, c=damping or vehicle dynamics coefficient, k=spring coefficient, b=viscous friction coefficient, J=inertia, i=gear ratio, and x=clutch piston position. These quantities are often equipped with subscripts, e=engine, fw=flywheel, c=clutch transmission side, t=transmission, p=propeller shaft, f=final drive, d=drive shaft, w=wheel, i=gear number, and amb=ambient.

2.1 Internal Combustion Engine

The ICE produces the engine torque, M_e, that is given as model input. Note that this is the net (brake) torque of the ICE, e.g. $M_e = 0$ with open clutch will keep the engine speed constant.

2.2 Clutch

The explanation of the clutch model is split into three parts, the friction and temperature dynamics, the mode changes between locked and slipping, and the torsional springs. An overview of the studied clutch is seen in Figure 1.

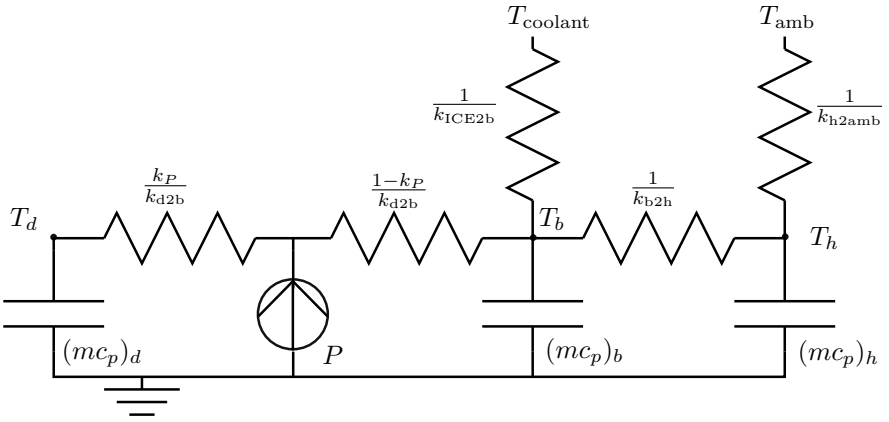

Figure 3: An electrical analogy of the temperature model (3)-(5).

Clutch Friction

The natural output from the actuator is the clamping force, F_N. However F_N is not measurable, therefore it is directly recalculated into a transmittable torque, $M_{\text{trans}} = k\mu F_N$, that is used as actuator output. The shape of the torque transmissibility curve is described by a third order polynomial, (Dolcini et al., 2010; Myklebust and Eriksson, 2012b)

$$M_{\text{ref}}(x_{\text{ref}}) = \begin{cases} a(x_{\text{ref}} - x_{\text{ref,ISP}})^3 + \\ +b(x_{\text{ref}} - x_{\text{ref,ISP}})^2, & \text{if } x_{\text{ref}} < x_{\text{ref,ISP}} \\ 0, & \text{if } x_{\text{ref}} \geq x_{\text{ref,ISP}} \end{cases} \tag{2}$$

where x_{ISP} (Incipient Sliding Point) is the kiss point. The exact value of x_{ISP} can be difficult to find since the transmissibility curve is very flat around x_{ISP}. However it is only important to find a x_{ISP} that gives a good curve fit, for a certain temperature, T_{ref}, as errors will be small near x_{ISP}.

The clutch disc temperature, T_d, clutch body (flywheel and pressure plate) temperature, T_b, and the clutch housing temperature, T_h, have been modeled in order to explain the torque drift, see Figure 5, due to temperature. An electrical analogy of the model is found in Figure 3 and below are the equations.

$$\begin{aligned} (mc_p)_b\dot{T}_b = {} & k_{\text{ICE2b}}(T_{\text{coolant}} - T_b) + k_{\text{b2h}}(T_h - T_b) + \\ & + k_{\text{d2b}}(T_d - T_b) + k_P P \end{aligned} \tag{3}$$

$$(mc_p)_h\dot{T}_h = k_{\text{b2h}}(T_b - T_h) + k_{\text{h2amb}}(T_{\text{amb}} - T_h) \tag{4}$$

$$(mc_p)_d\dot{T}_d = k_{\text{d2b}}(T_b - T_d) + (1 - k_P)P \tag{5}$$

where,

$$P = M_{\text{trans},k}\,\Delta\omega = M_{\text{trans},k}\,(\omega_e - \omega_c) \tag{6}$$

The temperature model is connected to the transmitted torque through a change of the position x_{cor}, see Figure 1, corresponding to the expansion of parts in the clutch. The expansion of the clutch body and disc as a function of temperatures is assumed linear.

$$\Delta x_0 = (k_{\text{exp},1} + k_{\text{exp},2})(T_b - T_{\text{ref}}) + k_{\text{exp},2}(T_d - T_b) \tag{7}$$

$$x_{\text{cor}} = x - \Delta x_0 \tag{8}$$

The transmitted torque can now be calculated as,

$$M_{\text{trans},k} = M_{\text{ref}}(x_{\text{cor}}) \tag{9}$$

Note that x_{cor} increases with temperature which in turn makes $M_{\text{trans},k}$ increase with temperature. The k in the subscript stands for kinetic because the friction is modeled as coulomb friction with stick-slip behavior. Define k_μ as the ratio of the static friction coefficient over the kinetic. Then the maximum transmittable torque when sticking is:

$$M_{\text{trans},s} = k_\mu M_{\text{trans},k} \tag{10}$$

Lock-Up/Break-Apart Logic

The clutch model has two modes, locked and slipping mode. While in locked mode, the clutch behaves as one rigid body, whereas during slipping the clutch consists of two bodies where each one has an angular velocity and position. The equations are:

Conditions for switching from slipping to locked mode:

$$\dot{\theta}_e = \dot{\theta}_c \tag{11}$$

$$M_{\text{trans}} \leq M_{\text{trans,s}} \tag{12}$$

Conditions for switching from locked to slipping mode:

$$M_{\text{trans}} \geq M_{\text{trans,s}} \tag{13}$$

Equations specific for the clutch in locked mode:

$$M_e - M_c = (J_e + J_{\text{fw}} + J_c)\,\ddot{\theta}_e \tag{14}$$

$$\dot{\theta}_c = \dot{\theta}_e \tag{15}$$

$$M_{\text{trans}} = \frac{M_e J_c + M_c (J_e + J_{\text{fw}})}{J_e + J_{\text{fw}} + J_c} \tag{16}$$

Equations specific to the clutch in slipping mode:

$$M_{\text{trans}} = \text{sgn}\left(\dot{\theta}_e - \dot{\theta}_c\right) M_{\text{trans,k}} \tag{17}$$

$$M_e - M_{\text{trans}} = (J_e + J_{\text{fw}})\,\ddot{\theta}_e \tag{18}$$

$$M_{\text{trans}} - M_c = J_c \ddot{\theta}_c \tag{19}$$

Torsional Part

The main flexibility of the clutch is in the torsion springs in the clutch disc. They are located on the vehicle side of the friction surfaces and can be modeled as a separate part.

The clutch torsional part is modeled as a torsional spring and damper.

$$M_c = c_c(\dot{\theta}_c - \dot{\theta}_t) + k_c(\theta_c - \theta_t) \tag{20}$$

2.3 Transmission

The transmission consists of some inertia, viscous friction and a gear ratio. Note that no synchronizers are modeled and the model can not engage neutral gear. Therefore gear shifting will be instantaneous. This is an acceptable approximation when the clutch is disengaged, since the transmission input side has low inertia compared to the rest of the vehicle.

With the states $\dot{\theta}_p$, θ_p, and θ_t the equations become:

$$M_t = M_c\, i_{t,i} \tag{21}$$

$$(J_{t,i} + J_p)\,\ddot{\theta}_p = M_t - b_t\dot{\theta}_p - M_p \tag{22}$$

$$\dot{\theta}_t = \dot{\theta}_p i_{t,i} \tag{23}$$

2.4 Propeller Shaft

The flexible propeller shaft is modeled in the same way as the clutch flexibility, (20). The propeller-shaft equation is:

$$M_p = c_p(\dot{\theta}_p - \dot{\theta}_f) + k_p(\theta_p - \theta_f) \tag{24}$$

2.5 Final Drive

The final drive with differential is assumed to act symmetrically on the drive shafts. Therefore it can be modeled as the transmission but with fixed gear ratio, i_f, and inertia, J_f. With the states $\dot{\theta}_d$, θ_d the equations become:

$$\left(J_p i_f^2 + J_f + J_d\right)\ddot{\theta}_d = M_p i_f - b_f\dot{\theta}_d - M_d \tag{25}$$

$$\dot{\theta}_f = \dot{\theta}_d i_f \tag{26}$$

2.6 Drive Shafts

The driveline's main flexibility is in the drive shafts, which can, with a symmetrical differential, be modeled as the clutch flexibility, (20). The drive shaft equation is:

$$M_d = c_d(\dot{\theta}_f - \dot{\theta}_w) + k_d(\theta_f - \theta_w) \tag{27}$$

2.7 Vehicle Dynamics

The wheels and non-driveline parts that affect the longitudinal dynamics are modeled in this section. Tire dynamics are neglected and rolling condition is assumed. The wheels simply consists of a radius, r_w, an inertia, J_w and a rolling resistance force, F_r. F_r is multiplied with a smoothing function in order to improve performance of the simulation, (Myklebust and Eriksson, 2012a).

Model inputs that directly affect the vehicle dynamics are braking force and road-slope angle, α (in radians). The road-slope angle is used to calculate the gradient force that is added with the braking force, rolling resistance and aerodynamic drag.

With the states v ($\dot{v} = a$) and θ_w the equations become:

$$F_a = \frac{1}{2}\rho_a c_w A_f v^2, \quad F_g = mg\sin(\alpha) \tag{28}$$

$$F_r = f(v)(c_{r1} + c_{r2}|v|)mg, \quad \dot{\theta}_w = v/r_w \tag{29}$$

$$\begin{aligned} \frac{M_d}{r_w} - \operatorname{sgn}(v)(F_r + F_a + F_b) - F_g = \\ = \frac{M_d}{r_w} - F_{dr} = \left(m + \frac{J_w + J_d}{r_w^2}\right) a \end{aligned} \tag{30}$$

Let torsions replace the states corresponding to angles, then the state vector is reduce to: ω_e, ω_c, $\theta_c - \theta_t$, ω_p, $\theta_p - \theta_f$, ω_d, $\theta_d - \theta_w$, ω_w, T_b, T_h, and T_d. When the clutch is locked one state disappears, $\omega_e = \omega_c$

3 Parameter Estimation

The driveline model and the clutch model have both been validated separately in their respective paper. However they have not been validated when put together and the lock-up/break-a-part detection has not been validated before. In order to do that a number of launches have been recorded. However these experiments have been carried out in a different truck than those used in the previous papers. Therefore the parameters have to be estimated. The driveline parameters have been estimated using a launch where the clutch has been closed rapidly (clutch is slipping less than 0.1 s). This gives negligible clutch dynamics and large shuffle oscillations, which is appropriate when estimating the flexibilities and damping coefficients. The result can be seen in Figure 4. Since it is difficult to do open-loop simulation of a system under feedback, the model also utilizes feedback. In the experiments the combustion engine is under speed control, therefore also the modeled engine is put under speed control. A PI-controller with feedforward of the measured engine torque is used. However since the engine model is simply an inertia, the PI-controller performs better than the real controller. Therefore the measured engine speed has been used as reference,

in order to capture the imperfections in the speed control and the inherent shuffle. The other driveline speeds follow the measurements well. The model is leading somewhat in the start due to sensor dynamics. There is some difference in the engine reported torque and the modeled engine torque, although it is hard to draw any conclusions from this, since the torque signal is inexact during transients. The parameterization seems good.

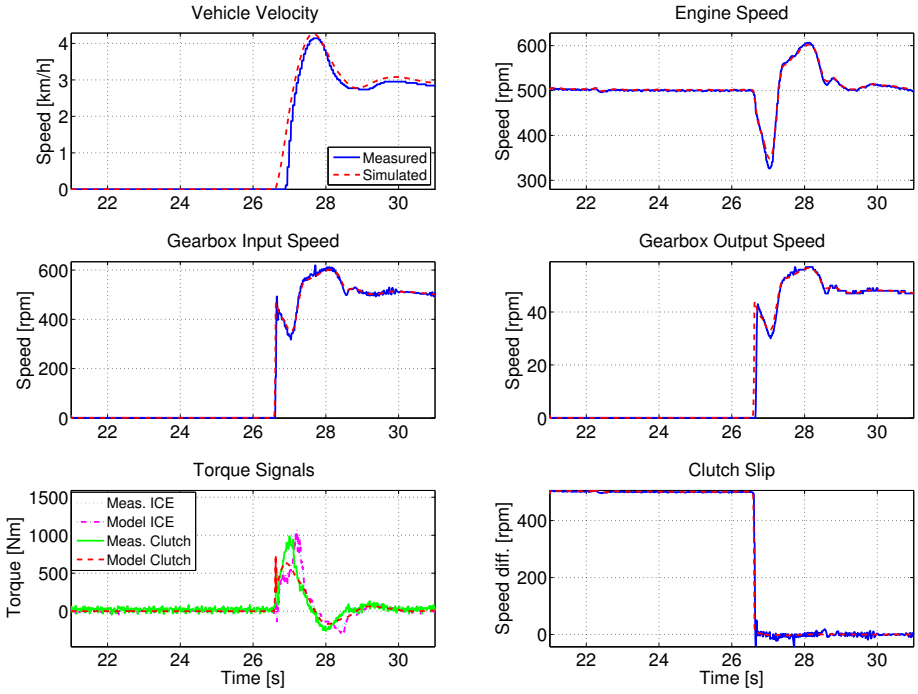

Figure 4: A quick launch (clutch locks-up in less than 0.1 s) with large oscillations was used to parameterize the driveline model. Both the real and modeled engines were under speed control. The measured output-shaft speed is lagging the model due to sensor dynamics.

Next the clutch model needs to be parameterized. The experiment conducted to do this has consisted of ramping the clutch position back and forth while the truck has been kept stationary using the parking brake. The resulting data can be seen in Figure 5. The torque drift due to temperature can clearly be seen. By applying (3)-(8) to the data, using the same parameters as in Myklebust and Eriksson (2012b), Figure 6 is attained. There the ramps have converged to one curve and consequently these parameters work here too. The 3rd degree polynomial, (2), has been fitted to this curve using the least square method.

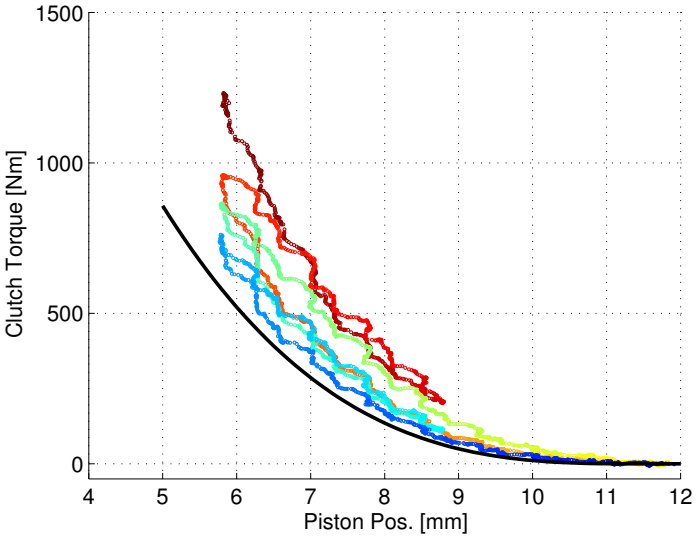

Figure 5: The data used for parameterizing the clutch model. The torque drift with temperature can be clearly seen. The color indicates time (blue=0 s, red=45 s).

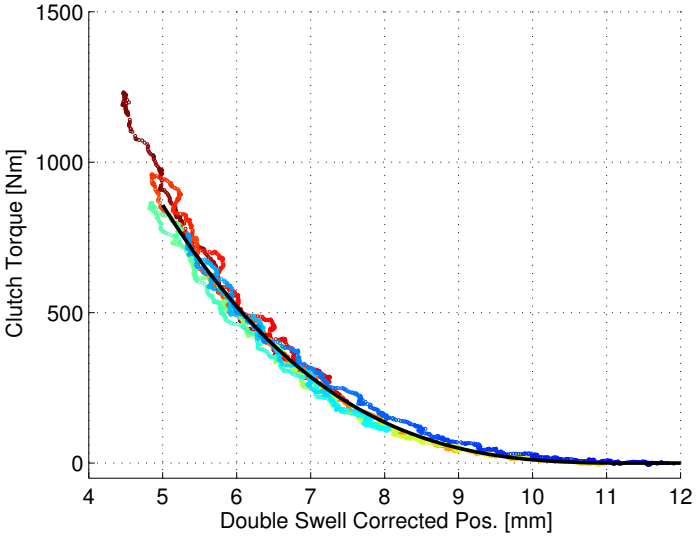

Figure 6: Same as Figure 5 but the position has been corrected for the thermal expansion using (8). All lines converge. The black line is the least square fit of the 3rd degree polynomial, (2).

4 Model Validation

A number of launches have been performed in different gears in order to validate the complete model. Here two launches are shown, one in third gear, Figure 7, and one in sixth gear, Figure 8. In third gear there is some drift in vehicle speed with the consequence that the clutch locks up earlier in the model compared to the measurement. During the slipping phase the clutch torque has been modeled correctly, however after lock up the torque decreases due to the engine speed controller. When the engine speed reaches a set value the controller is switched off and torque is used as model input, since then the measurement is no longer under feedback. When the controller is switched off the drift naturally returns. Nevertheless the oscillations in the driveline are captured with respect to amplitude and frequency, although the attenuation in the model is a bit too high. In sixth gear the driveline speeds and clutch torque matches the measurement very well. As a result it is easy to see that the lock-up/break-apart logic makes mode switches at the correct time points. This is a further addition to the base-line model in Myklebust and Eriksson (2012a). However when the clutch torque goes from positive to negative and vice versa there is some oscillations seen in the measurement due to backlash. These oscillation are naturally not captured in the model since the backlash is not modeled.

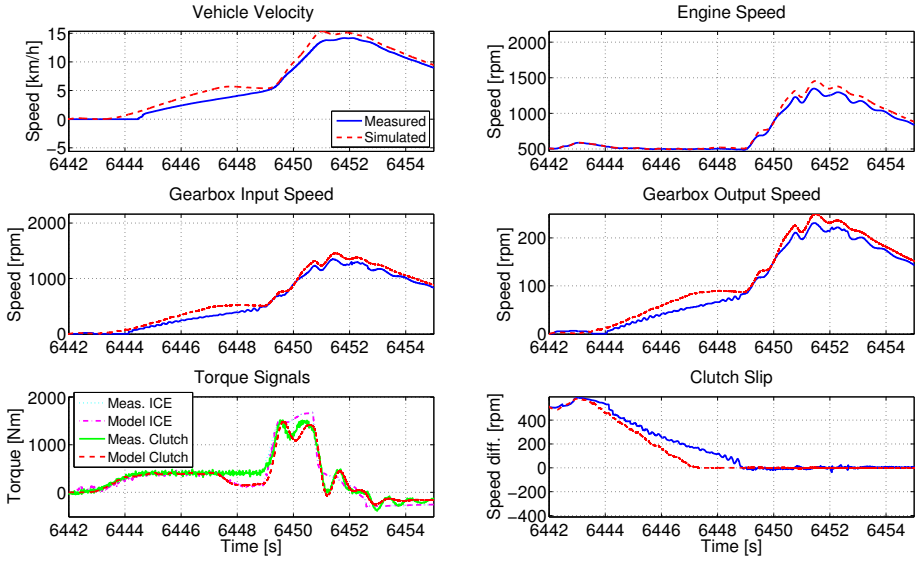

Figure 7: Validation of the complete model in 3rd gear. Vehicle oscillations are captured and the clutch torque is correct (while slipping). The engine is under speed control when the speed is close to 500 RPM and using torque as input otherwise.

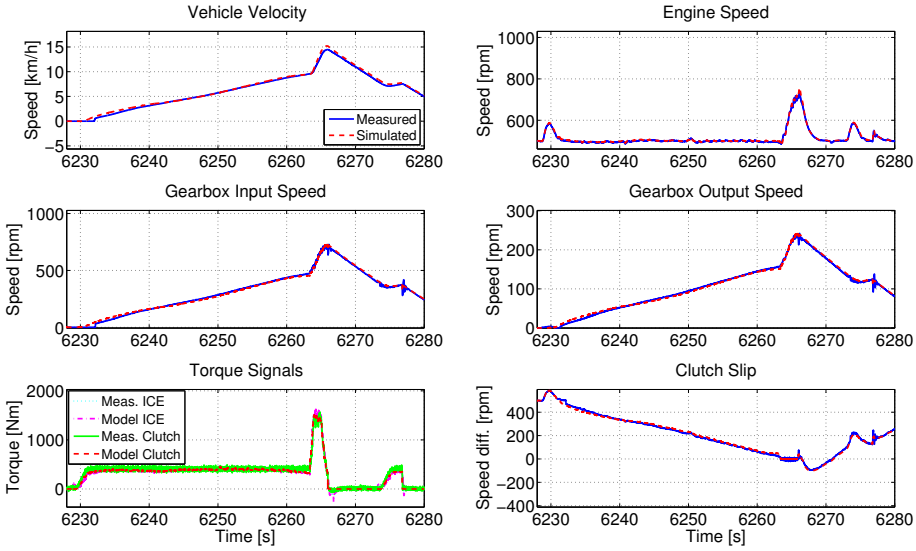

Figure 8: Validation of the complete model in 6th gear. Vehicle motion and the clutch torque are modeled with high accuracy. The lock-up/break-apart logic can be seen to work as intended at 6263/6266 s. When the torque transferred in the clutch changes between positive and negative some oscillations are seen in the measurement due to unmodeled backlash. The engine is under speed control.

In conclusion both validations look fine and the model is suitable for investigating different clutch control strategies during launch and their effect on vehicle shuffle and performance.

5 Thermal Effect on Launching

This section highlights possible problems that can arise in clutch control during launch when not considering the thermal effects. Here two controllers taking requested torque as input are studied. This is a natural choice of input since it is common to use torque based driveline control, (Heintz et al., 2001). When so the driver intention over time can be interpreted as a reference torque trajectory. The first controller is the simplest possible, an open-loop controller consisting of an inversion of (2), the torque transmissibility curve at 60 °C. The second controller uses the first controller as a feedforward part but in addition it has a PI-controller in order to utilize the engine torque for feedback. For both controllers the clutch is fully open when the torque request is zero and fully closed when there is no slip in the clutch. The clutch actuator is fast and exact

and therefore it is modeled with a rate limiter of 82 mm/s on x. The ICE directly gives the requested torque and has in addition a PI idle-speed controller in order to not stall the engine if the requested torque is too low. The simulations will be evaluated mainly from a comfort perspective and a measurement relating to comfort is jerk (time derivative of the vehicle acceleration). According to Zeng et al. (2013) the maximum jerk and minimum (negative) jerk are important comfort measures.

A requested torque trajectory has been chosen as follows; starts out at zero torque until 1.5 s where it is ramped up to 3 % of maximum torque at 2.5 s. It is

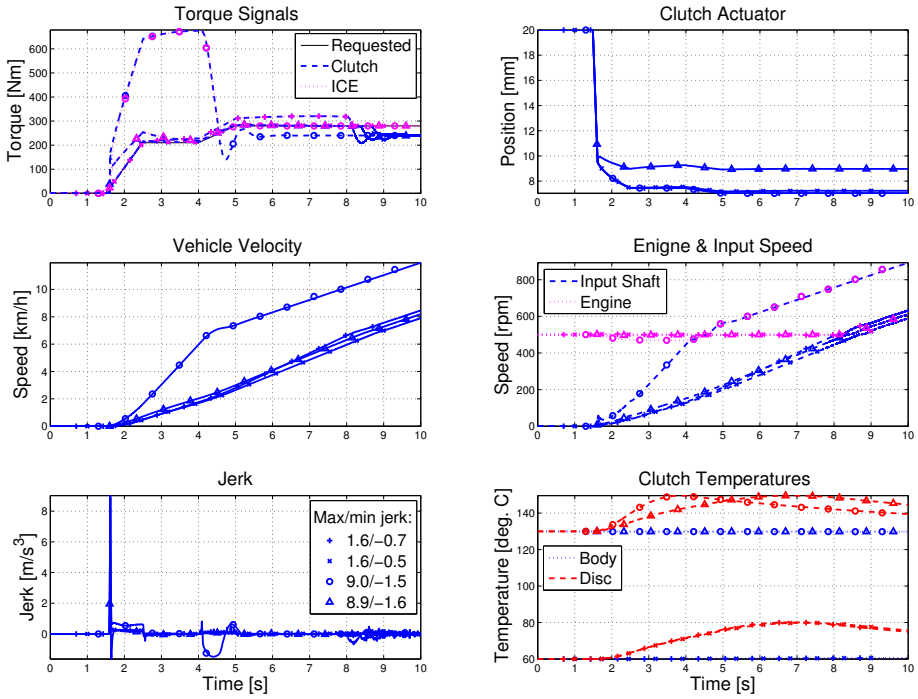

Figure 9: A simulated launch in fourth gear for four different cases, cold clutch with open loop control marked with plus signs, cold clutch with closed loop control marked with crosses, warm clutch with open loop control marked with circles and warm clutch with closed loop control marked with triangles. Cold clutch means $[T_b, T_h, T_d] = [60, 50, 60]$°C and warm means $[T_b, T_h, T_d] = [130, 120, 130]$°C. The cold closed loop case follows the reference torque closely whereas the cold open loop case has a slight drift due to heating of the clutch. The warm open loop case has a completely different speed trajectory that should correspond to a different accelerator input and, as in both warm cases, jerk levels are about five times higher.

kept there until 4 s when it is ramped further up to 4 % at 5 s and kept there for the rest of the simulation. This trajectory is used as input to the simulation model together with no braking, no slope, fourth gear and 500 RPM as idle speed. Simulations are run for both controllers in cold, $\begin{bmatrix} T_b, & T_h, & T_d \end{bmatrix} = \begin{bmatrix} 60, & 50, & 60 \end{bmatrix}$°C, and warm, $\begin{bmatrix} T_b, & T_h, & T_d \end{bmatrix} = \begin{bmatrix} 120, & 110, & 120 \end{bmatrix}$°C, conditions, four cases in total. The results are seen in Figure 9. The maximum jerk levels can be seen to rise more than a factor of five when the clutch is warm. This is due to that the clutch controller overshoots the kiss point at 1.5 s. The feedback controller also get a large negative jerk when it tries to compensate for the excessive torque due to incorrect kiss point. In the open loop case no such compensation is present and naturally the truck recieves a completly different speed trajectory although the driver input is the same. Furthermore the jerk is larger when the clutch locks-up in this case. The open-loop controller for the cold case has a drift in torque due to heating of the clutch. Only the closed-loop controller for the cold case manages to follow the desired trajectory.

Even though the example in Figure 9 utilizes simple clutch-control algorithms it highlights a problem that will be present in any controller that does not compensate for the thermal dynamics. In order to give a quick response to driver request the clutch needs to quickly move to the kiss point. If the kiss point is overshot large discomfort can arise, as seen in Figure 9. An additional problem is that the large change in the torque transmissibility curve can put the controller in a situation it has not been tuned for, as demonstrated by the negative peak in the jerk for the closed loop controller in the warm case. Moreover it should be mentioned that the temperatures used in this example are normal, temperatures can even go above 200°C.

A remedy for this problem is to estimate the temperature and compensate the clutch piston position for the expansion using the model in Myklebust and Eriksson (2012b).

6 Conclusion

A driveline model for vehicle shuffle and a clutch model including thermal effects have been merged together in order to simulate how different clutch-control strategies affect vehicle shuffle and performance. Parameters have been estimated to fit a heavy-duty truck and the complete model has been successfully validated, including the lock-up/break-apart logic. The complete driveline model has been used to show the profound effect of thermal phenomenon in the clutch on launch control, even for moderate temperatures. The launch control example showcases the importance of incorporating a thermal model of the clutch in launch control applications.

References

M. Bataus, A. Maciac, M. Oprean, and N. Vasiliu. Automotive clutch models for real time simulation. *Proc. of the Romanian Academy, Series A*, 12(2): 109–116, 2011.

A Crowther, N Zhang, D K Liu, and J K Jeyakumaran. Analysis and simulation of clutch engagement judder and stick-slip in automotive powertrain systems. *Proc IMechE„ Part D: J. of Automobile Engineering*, 218(12):1427–1446, December 2004.

P. Dolcini, C. Canudas de Wit, and H. Béchart. Improved optimal control of dry clutch engagement. *Proc. of the 16th IFAC World Congress*, 16(1), 2005.

P. Dolcini, C. Canudas de Wit, and H. Béchart. Lurch avoidance strategy and its implementation in AMT vehicles. *Mechatronics*, 18(1):289–300, May 2008.

P. J. Dolcini, C. Canudas de Wit, and H. Béchart. *Dry Clutch Control for Automotive Applications*. Advances in Industrial Control. Springer-Verlag London, 2010.

G. Ercole, G. Mattiazzo, S. Mauro, M. Velardocchia, F. Amisano, and G. Serra. Experimental methodologies to determine diaphragm spring clutch characteristics. In *SAE Technical Paper: 2000-01-1151*, March 2000.

J. Fredriksson and B. Egardt. Active engine control for gear shifting in automated manual transmissions. *Int. J. of Vehicle Design*, 32(3-4):216–230, 2003.

F. Garofalo, L. Glielmo, L. Iannelli, and F. Vasca. Optimal tracking for automotive dry clutch engagement. In *2002 IFAC, 15th Triennial World Congress*, 2002.

L. Glielmo and F. Vasca. Optimal control of dry clutch engagement. In *SAE Paper: 2000-01-0837*, March 2000.

N. Heintz, M. Mews, G. Stier, A. J. Beaumont, and A. D. Noble. An approach to torque-based engine management systems. In *SAE Technical Paper: 2001-01-0269*, March 2001.

S. Hong, S. Ahn, B. Kim, H. Lee, and H. Kim. Shift control of a 2-speed dual clutch transmission for electric vehicle. In *2012 IEEE Vehicle Power and Propulsion Conference*, October 2012.

G. Lucente, M. Montanari, and C. Rossi. Modelling of an automated manual transmission system. *Mechatronics*, 17(1):73–91, November 2007.

B. Mashadi and D. Crolla. *Vehicle Powertrain Systems*. John Wiley & Sons Ltd, first edition, 2012.

G. Mattiazzo, S. Mauro, M. Velardocchia, F. Amisano, G. Serra, and G. Ercole. Measurement of torque transmissibility in diaphragm spring clutch. In *SAE Technical Paper: 2002-01-0934*, March 2002.

S.E. Moon, M.S. Kim, H. Yeo, H.S Kim, and S.H Hwang. Design and implementation of clutch-by-wire system for automated manual transmissions. *Int. J. Vehicle Design*, 36(1):83–100, 2004.

A. Myklebust and L. Eriksson. Road slope analysis and filtering for driveline shuffle simulation. In *2012 IFAC Workshop on Engine and Powertrain Control, Simulation and Modeling*, October 2012a.

A. Myklebust and L. Eriksson. Torque model with fast and slow temperature dynamics of a slipping dry clutch. In *2012 IEEE VPPC*, October 2012b.

M. Pettersson. *Driveline Modeling and Control*. PhD thesis, Linköpings Universitet, May 1997.

F. Vasca, L. Iannelli, A. Senatore, and G. Reale. Torque transmissibility assessment for automotive dry-clutch engagement. *IEEE/ASME transactions on Mechatronics*, 16(3):564–573, June 2011.

M. Velardocchia, G. Ercole, G. Mattiazzo, S. Mauro, and F. Amisano. Diaphragm spring clutch dynamic characteristic test bench. In *SAE Technical Paper: 1999-01-0737*, March 1999.

M. Velardocchia, F. Amisano, and R. Flora. A linear thermal model for an automotive clutch. In *SAE Technical Paper: 2000-01-0834*, March 2000.

A. Wikdahl and Å. Ågren. Temperature distribution in a clutch. Master's thesis, Linköping University, 1999.

H. Zeng, Y. Lei, Y. Fu, Y. Li, and W. Ye. Analysis of a shift quality metric for a dual clutch transmission. In *SAE Technical Paper: 2013-01-0825*, April 2013.

Paper C

Modeling, Observability, and Estimation of Thermal Effects and Aging on Transmitted Torque in a Heavy Duty Truck with a Dry Clutch*

C

*Published in *IEEE/ASME Transactions on Mechatronics*, PP(99):1-12, 2014.

Modeling, Observability, and Estimation of Thermal Effects and Aging on Transmitted Torque in a Heavy Duty Truck with a Dry Clutch

Andreas Myklebust and Lars Eriksson
Vehicular Systems, Department of Electrical Engineering, Linköping University, SE-581 83 Linköping, Sweden

Abstract

A transmission with both high comfort and high efficiency is the Automated Manual Transmission (AMT). To be able to control and fully utilize this type of transmission it is of great importance to have knowledge about the torque transmissibility curve of the clutch. The transmitted torque in a slipping dry clutch is therefore studied in experiments with a heavy duty truck (HDT). It is shown that the torque characteristic has little or no dependence on slip speed, but that there are two dynamic effects that make the torque vary up to 900 Nm for the same clutch actuator position. Material expansion with temperature can explain both phenomena and a dynamic clutch temperature model that can describe the dynamic torque variations is used. The dynamic model is validated in experiments, and it is shown to reduce the error in transmitted torque from 7 % to 3 % of the maximum engine torque compared to a static model. Clutch wear is also a dynamic phenomenon that is of interest to track and compensate for, and therefore the model is augmented with an extra state describing wear. An observability analysis is performed showing that the augmented model is fully or partially observable depending on the mode of operation. In particular, by measuring the actuator position the temperature states are observable, both during slipping of the clutch and when it is fully closed. An Extended Kalman Filter (EKF), which observes the temperature states, was developed since it is straight forward to incorporate different modes of operation. The EKF was evaluated on measurement data and the estimated states converged from poor initial values, enabling prediction of the translation of the torque transmissibility curve. The computational complexity of the EKF is low and thus it is suitable for real-time applications. Modeling, parameter estimation, observer design and validation are all carried out using production sensors only and therefore it is straight forward to implement the observer in a production HDT following the presented methodology.

1 Introduction

Increasing demands on comfort, performance, and fuel efficiency in vehicles lead to more complex transmission solutions. Historically high efficiency was best accomplished with a classical Manual Transmission and comfort with a classical Automatic Transmission. The Automated Manual Transmission (AMT) is one way to combine the best from two worlds. An important part in an AMT is clutch control that has a profound effect on vehicle performance. In clutch control it is of importance to know the torque transmitted in the clutch. Models have come to play an important role in estimation and control of the transmitted torque, since torque sensors are expensive.

The most common clutch type in AMTs is the dry single-plate clutch, which has been studied here. A sketch of the studied clutch is found in Figure 1, while in-depth explanations are found in for example Mashadi and Crolla (2012) and Vasca et al. (2011).

1.1 Outline

After a short survey of related work the contributions of the paper are discussed. Section 2 gives a brief description of the experimental platform that has been used to parameterize the thermal clutch model used. The clutch model is an extension of Myklebust and Eriksson (2012) and it is described and discussed in Section 3. In Myklebust and Eriksson (2013) the thermal effects in the clutch are shown to have a significant effect on launch control and therefore a temperature state observer is built in Section 4. However before the observer is built an observability analysis of the model is performed and the results are used in the design. The observer is evaluated on experimental data in Section 5.

1.2 Survey of Clutch Models

In clutch-modeling literature a wide range of models have been proposed. The most simple models have a clutch torque that is assumed to be a controllable input, see for example Dolcini et al. (2008) or Garofalo et al. (2002). These models rely on the assumption that there is perfect knowledge of how the clutch behaves. More advanced models include submodels for slipping and sticking torques. For example a LuGre model is used in Dolcini et al. (2005b) and a Karnopp model in Bataus et al. (2011). The former is a one-state model that captures stick-slip behavior, varying break-away force, Stribeck effect, and viscous friction. The latter includes a dead-zone around zero speed to ease the simulation of stick-slip behavior.

Models for the clutch torque during slipping commonly use a function with the following structure,

$$M_{\text{trans,k}} = \operatorname{sgn}(\Delta\omega)\, n\, \mu\, R_e\, F_N \tag{1}$$

where $\Delta\omega$ is the clutch slip (speed), n the number of friction surfaces, μ the friction coefficient, R_e the effective radius and F_N the clamping (normal) force. In these models F_N is often either given as input or a static nonlinear function of clutch position, x, i.e. $F_N = F_N(x)$, see for example Vasca et al. (2011) or Glielmo and Vasca (2000). In particular Dolcini et al. (2010) mentions that a third-order polynomial is suitable to describe the connection between throwout-bearing position and clutch transmitted torque, mainly governed by the flat (cushion) spring characteristics. These characteristics are reported to have a decreasing slope with temperature in Cappetti et al. (2012a). However in Cappetti et al. (2012b) thermal expansion in the axial direction of the spring is shown to be a more significant effect. From a graph in Hong et al. (2012) the normal force can be seen to be speed dependent. In Dolcini et al. (2010) that speed dependency is said to be due to centrifugal forces acting on the springs in the clutch. The papers Mashadi and Crolla (2012); Moon et al. (2004) and Szimandl and Németh (2012) report of hysteresis in the diaphragm spring, that could lead to hysteresis in the normal force. In Mattiazzo et al. (2002) a temperature and wear dependency of the normal force/bearing position characteristics is shown. There it decreases with temperature. In Myklebust and Eriksson (2012); Deur et al. (2012); Cappetti et al. (2012b) and Hoic et al. (2013) the change in normal force/bearing position characteristics is explained by thermal expansion of clutch parts and the normal force is increasing with temperature. However with an exception for low forces in Hoic et al. (2013). There the normal force is decreasing with temperature due to the expansion of a return spring, which is not present in the more common setup studied here.

When studying the components of (1) besides the normal force, it is generally recognized that μ can depend on temperature, slip speed, and wear while R_e can depend on temperature and wear as well, (Velardocchia et al., 1999). In Vasca et al. (2011) a slip speed dependency of μR_e is shown, this was especially pronounced for slip speeds below ∼100 RPM. In Deur et al. (2012) R_e is assumed constant and μ is fitted to the following regression curve:

$$\begin{aligned}\mu = {} & a_0 + a_1\left(e^{-a_2\Delta\omega} - 1\right)T_b + \left(a_3 - a_4\ln(\Delta\omega)\right)T_b^2 \\ & + \left(a_5 - a_6\Delta\omega\right)F_N + a_7 T_b F_N \end{aligned} \tag{2}$$

where T_b is the temperature of the clutch body and $a_0 - a_7$ are curve parameters.

It can be difficult to separate which parameter in (1) is the reason for a change in $M_{\text{trans,k}}$. Therefore the clutch torque is often studied as a lumped model. In Velardocchia et al. (1999) $M_{\text{trans,k}}$ is seen to decrease with temperature and $\Delta\omega$. However there are large variations with wear. In Ercole et al. (2000) $M_{\text{trans,k}}$ initially decreases with temperature for low temperatures and then increases for medium and high temperatures. Similarly there are variations with wear and in addition temperature-torque hysteresis is reported. In Velardocchia et al. (2000), Wikdahl and Ågren (1999) and Myklebust and Eriksson (2012) temperature models are established, but only Myklebust and Eriksson (2012) includes the effect of the temperature on $M_{\text{trans,k}}$. The models in Velardocchia

et al. (2000) and Wikdahl and Ågren (1999) could be complemented with (1) and (2) in order to give the clutch torque. However that approach requires more parameters to be estimated compared to the model in Myklebust and Eriksson (2012). Furthermore the clamping load needs to be measured, which is not available in production vehicles. In Myklebust and Eriksson (2012) only sensors available in production vehicles are used. Furthermore the clutch is only modeled during slipping, there is no slip-speed dependency and torque is increasing with temperature, in accordance with the observations made there. It is also computationally simple enough to be used in control applications.

1.3 Contributions

For the reasons given in the previous section the clutch model in Myklebust and Eriksson (2012) is built upon. The first contribution is that a wear parameter is added to the clutch model and the observability of this new model is investigated. The observability varies with the mode of operation and subsequently an observer must be able to handle different modes of operation. Therefore an EKF is built using the clutch model to allow for compensation of the thermal dynamics and wear. Clutch torque observers have been built before, e.g. Dolcini et al. (2005a, 2010); Kim and Choi (2010); Gao et al. (2012) and the contribution here lies in that the thermal effects have been observed. This makes it possible to not only know the current torque, but also the translation of the torque transmissibility curve. As a result not only feedback control but also feedforward is supported. In particular, the model makes it possible to use measurements of the actuator position when the clutch is fully closed to estimate the temperatures. The observer utilizes production sensors only and in fact, the entire synthesis process, from model building to observer validation, is performed using the production sensors. All in all this gives an observer that is light weight and implementable in production trucks.

2 Experimental Setup

Two rear-wheel drive Heavy Duty Trucks (HDT), called Ara and Ernfrid, have been used for experiments. Both are equipped with a 14-speed AMT and a 16.4 liter V8 capable of producing 3500 Nm. Ara weighs 105 tonnes and Ernfrid 21 tonnes. The clutch, that is in focus here, is a dry single-plate pull-type normally closed clutch. A schematic is seen in Figure 1. The clutch is actuated by an electric motor that through a worm gear moves a hydraulic master cylinder that in turn moves a slave piston and via a lever pulls the throwout bearing. Both motor position, x_m, and slave piston position, x_p, are measured. In order to bring x_p to the same range as x_m and make data sets with different amount of wear comparable to each other the signal $x = x_p - x_{0,\text{ref}}$ is used for the slave position, see Figure 1.

The trucks used here are only equipped with production sensors, namely:

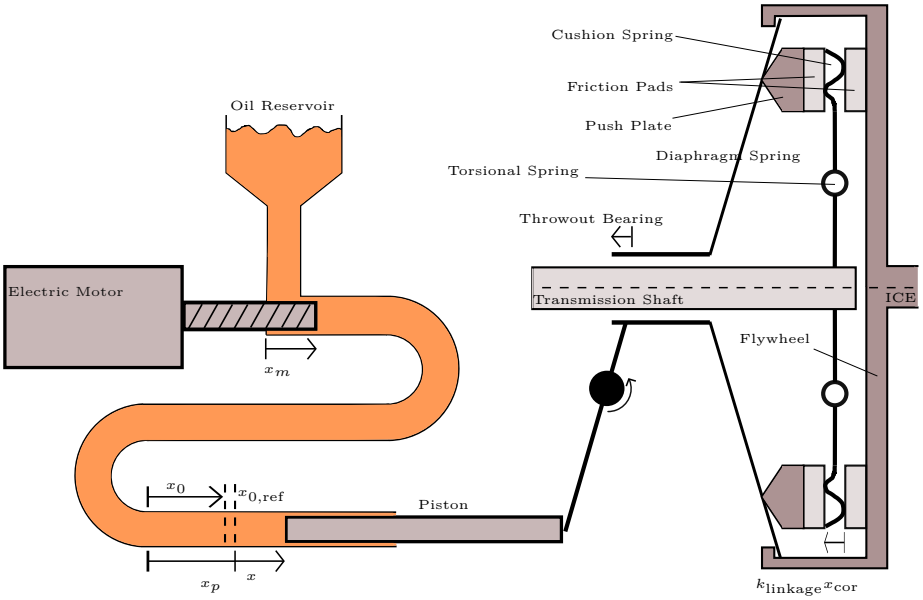

Figure 1: A schematic over the actuator and the dry single-plate pull-type clutch studied here. k_{linkage} is the combined ratio of all levers between the piston and the push plate.

engine speed, input shaft speed, coolant temperature, motor position and slave position. The engine speed and coolant temperature is measured by the Engine Control Unit (ECU) and sent via CAN to the Transmission Control Unit (TCU) that samples the other sensors. The TCU is capable of receiving CAN messages, sampling and actuating at 100 Hz. With this setup no torque sensor is available. In order to get a measurement of the clutch torque the reported engine torque is compensated for inertia effects of the engine and flywheel. The accuracy of this signal is around 100 Nm when the engine is warm. The exact properties when cold is not known. The engine torque signal is also known to be less exact during transients.

The main benefit of this setup, with only production sensors, is that the resulting model and observer is directly applicable on a production truck. Furthermore the procedure for experiments, model building, model validation, and observer evaluation can easily be performed on other vehicles equipped with a dry clutch. On the other hand, the drawback, compared to a test stand, e.g. Velardocchia et al. (1999); Moon et al. (2004) or Deur et al. (2012), is fewer and less precise sensors. All these mentioned test stands consists of a stand-alone dry clutch that is cooled towards the stagnated room-temperature air. In a truck there might be an airflow, the clutch is installed below to the truck floor, bolted to the transmission, and especially the flywheel is bolted to a 1 tonne, ~ 90 °C warm engine. Naturally all this leads to different temperature dynamics.

3 Clutch Model

The modeled clutch is a single-plate dry clutch with two contact surfaces, see Figure 1 for an overview. Torque is transferred between the flywheel and the clutch disc through friction. The friction is modeled as coulomb friction with stick-slip behavior. This is simply modeled with two friction coefficients, one static, μ_s, and one dynamic, μ_k. By defining the ratio of the friction coefficients, $k_\mu = \frac{\mu_s}{\mu_k}$ the equation for the transmittable torque during sticking (the stiction torque) becomes:

$$M_{\text{trans},s} = k_\mu M_{\text{trans},k} \tag{3}$$

where $M_{\text{trans},k}$ is given by (27). The modeling of the two modes, slipping and locked-up, is done by a state machine, described in Section 3.1. Nevertheless here the focus is upon the clutch when it is slipping and it is the equations for the clutch in slipping mode that is used by the observer in Section 4. Nevertheless it is useful to discuss some aspects of the mode switching to better understand the different modes introduced in Section 4.1.

3.1 Lock-Up/Break-Apart Logic

The clutch model has two modes, locked and slipping mode. While in locked mode, the clutch behaves as one rigid body, whereas during slipping the clutch consists of two bodies where each one has an angular velocity and position. Torque from the ICE, M_e, and transmission, M_t, are inputs and angular velocity on both sides, ω_e and ω_t, respectively, are states. The equations are:

Conditions for switching from slipping to locked mode:

$$\omega_e = \omega_t \tag{4}$$
$$|M_{\text{trans}}| \leq M_{\text{trans,s}} \tag{5}$$

Equations for the clutch in locked mode:

$$M_e - M_t = (J_e + J_{\text{fw}} + J_c)\,\dot{\omega}_e \tag{6}$$
$$\omega_c = \omega_e \tag{7}$$
$$M_{\text{trans}} = \frac{M_e J_c + M_t\,(J_e + J_{\text{fw}})}{J_e + J_{\text{fw}} + J_c} \tag{8}$$

Conditions for switching from locked to slipping mode:

$$|M_{\text{trans}}| \geq M_{\text{trans,s}} \tag{9}$$

Equations specific to the clutch in slipping mode:

$$M_{\text{trans}} = \text{sgn}(\underbrace{\omega_e - \omega_t}_{\Delta\omega}) M_{\text{trans,k}} \tag{10}$$

$$M_e - M_{\text{trans}} = (J_e + J_{\text{fw}})\,\dot{\omega}_e \tag{11}$$

$$M_{\text{trans}} - M_t = J_c \dot{\omega}_t \tag{12}$$

The state machine is validated in Myklebust and Eriksson (2013).

3.2 Slipping Torque Model Structure

The rest of Section 3 discusses how to model the clutch during slipping, or more precise, how to model $M_{\text{trans,k}}$. This discussion is an extension of the one in Myklebust and Eriksson (2012). As mentioned in Section 1.2, $M_{\text{trans,k}}$ depends on several factors such as, actuator position, temperatures, rotational speeds and wear. In Figure 2 it is seen how the transmitted torque varies up to 900 Nm for a given position. Furthermore components are non-linear e.g. spring characteristics, hysteresis, etc. During experiments no clear hysteresis have been detected and therefore not modeled. At a quick glance of Figure 2 it might look like some hysteresis is present. Nonetheless this is only because a third dimension, temperature, has been projected into the 2D-plot. This will become more clear as the temperature modeling progress and finally result in Figure 8. Due to the difficulties involved in measuring wear, especially when access to test equipment is limited and non-exclusive, wear has been assumed slow enough to not have a significant effect in experiments performed during a single day. The only wear effect that has been observed between measurement sessions (months apart) is the parameter $x_{0,\text{ref}}$ of (20), which is directly affected by the thickness of the friction pads. $x_{0,\text{ref}}$ had to be parameterized to each measurement session. A continuous adaptation of $x_{0,\text{ref}}$ suitable for an online application is proposed in Section 4. During the life time of an HDT more parameters would probably need to be adapted continuously. However more prolonged testing is required to reach any conclusion. With the above assumptions and the addition of $n = 2$ it is possible to write (1) as:

$$M_{\text{trans,k}} = 2\mu(\Delta\omega, T)\, R_e(T)\, F_N(x, T, \omega_e) \tag{13}$$

In Section 3.4 the temperature effect will be explained by a changing F_N, at least for medium temperatures of the clutch. Nevertheless with the available sensors there is no way to truly separate the effects between the parameters. Therefore the model structure will be,

$$M_{\text{trans,k}} = M_{\text{trans,k}}(x, T, \Delta\omega) \tag{14}$$

In the next section the slip dependency will be investigated and in the subsequent section the position and temperature dependency will be handled.

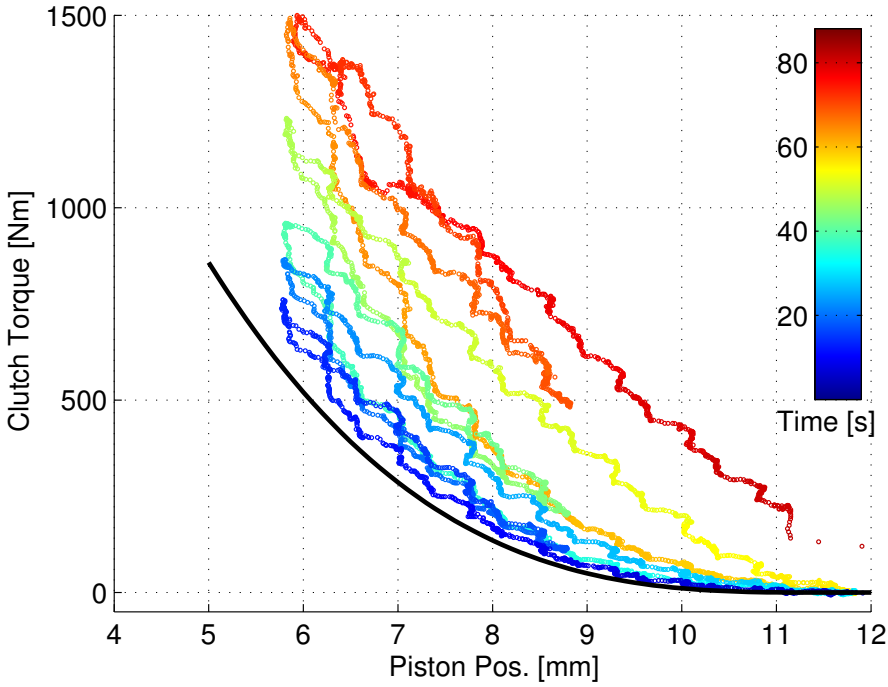

Figure 2: The clutch position, x, has been ramped back and forth while the clutch torque has been measured. During this experiment the truck was held stationary using the parking brake in order to avoid lock-up of the clutch. The transmitted torque clearly depends on something more than the clutch position, in particular there is a drift with time. The torque difference between the first and last ramp is up to 900 Nm. The black line is a parameterization of (16).

3.3 Slip dependency

Slip speed, $\Delta\omega$, dependency is recognized in the literature, (Vasca et al., 2011), (Velardocchia et al., 1999), this is therefore further investigated here. Experiments have been carried out as follows. A truck has been driven to an uphill and has been kept stationary by slipping the clutch at a constant position. This way the vehicle will accelerate forwards if more torque is transmitted and backwards if less torque is transmitted. Furthermore it is easy to initially keep the input shaft speed stationary this way, and by doing so the engine speed can be used to control the slip speed. Slip-speed steps are made and an abrupt change in torque/input shaft acceleration should be seen if there is a slip-speed dependency, Figure 3. Note that the engine torque will see a transient during the edges of a step due to the acceleration of the engine. A smaller transient is present in the clutch torque signal due to imperfections in the compensation for the

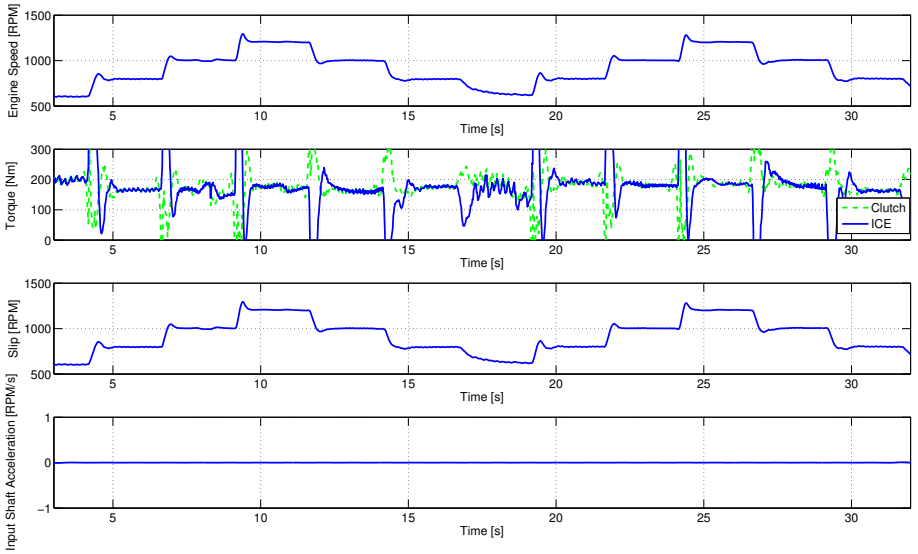

Figure 3: Slip steps are made through engine-speed control when the truck is held stationary in a slight uphill using a constant clutch position. No reaction is seen in neither clutch torque nor input shaft acceleration.

acceleration. No significant change is seen in the input shaft acceleration and no correlation between steady-state clutch torque and slip speed is seen either, Fig 4. Therefore (14) can be reduced to

$$M_{\text{trans,k}} = M_{\text{trans,k}}(x, T) \tag{15}$$

This is somewhat in contrast to the data in Velardocchia et al. (1999) where a slip dependency is shown. The slip has only been investigated at relatively large speeds, $\Delta\omega > 100$ RPM, as a slipping clutch is in focus here and does therefore not contrast the data in Vasca et al. (2011).

3.4 Temperature Effects and Models

The shape of the torque transmissibility curve is mainly due to the cushion spring characteristics. In Dolcini et al. (2010) it is mentioned that this curve can be described by a third order polynomial,

$$M_{\text{ref}}(x_{\text{ref}}) = \begin{cases} a(x_{\text{ref}} - x_{\text{ref,ISP}})^3 \\ +b(x_{\text{ref}} - x_{\text{ref,ISP}})^2 & \text{if } x_{\text{ref}} < x_{\text{ref,ISP}} \\ 0 & \text{if } x_{\text{ref}} \geq x_{\text{ref,ISP}} \end{cases} \tag{16}$$

where x_{ISP} (Incipient Sliding Point) is the kiss point, where the push plate and clutch disc first meet and torque can start to transfer. There is no first or

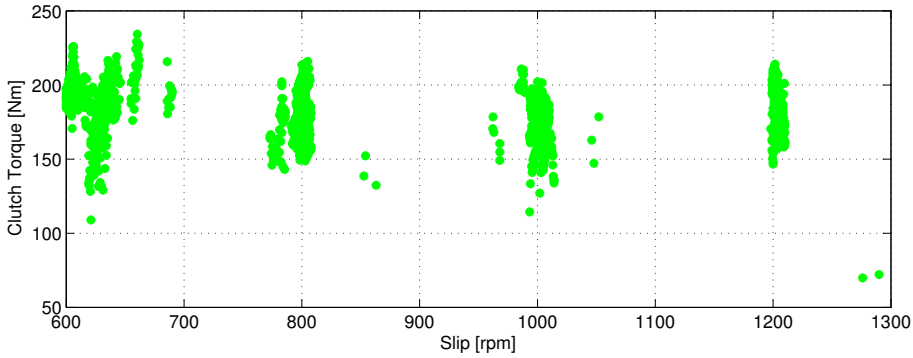

Figure 4: The data points from Figure 3 when the engine speed is constant. No correlation is seen between clutch torque and slip speed.

zeroth order term in the equation since it is desired to have zero torque and derivative at $x_{\text{ref,ISP}}$. The exact value of x_{ISP} can be difficult to find since the transmissibility curve is very flat around x_{ISP}. However it is only important to find an x_{ISP} that gives a good curve fit, as errors will be small near x_{ISP}. A suggestion in Mattiazzo et al. (2002) is to define x_{ISP} as the point that transmits a certain small torque. That method should give sufficient estimates of x_{ISP} for the application described here.

Experimental data confirms that (16) is a good approximation for a given temperature, T_{ref}, see Figure 2. However during slipping of the clutch, heat is dissipated from the friction surface into the cast iron parts of the clutch that naturally will expand. When the actuator motor is fully retracted (position=0) the expansion can be measured through the position sensor on the slave. This slave position is called the zero position, x_0, see Figure 1.

A set of experiments has been performed to investigate the dynamics of the clutch expansion. In order to be able to measure the zero position during heating, the clutch has been alternating between closed and slipping with short time intervals. During the slipping periods the truck was held stationary using the parking brake in order to avoid lock-up of the clutch. After some time of heating the clutch has been held closed for a prolonged time while the zero position has been constantly monitored as the clutch cools down. The measurement results are found in Figure 5. The zero position increases in a repeatable way with dissipated energy in the clutch and decays in an exponential manner with time. This supports the hypothesis that temperature is causing the change in zero position.

Material Expansion Analysis

In order to see that the change in zero position is due to material expansion, the temperature increase is calculated in two ways. During the first heating period

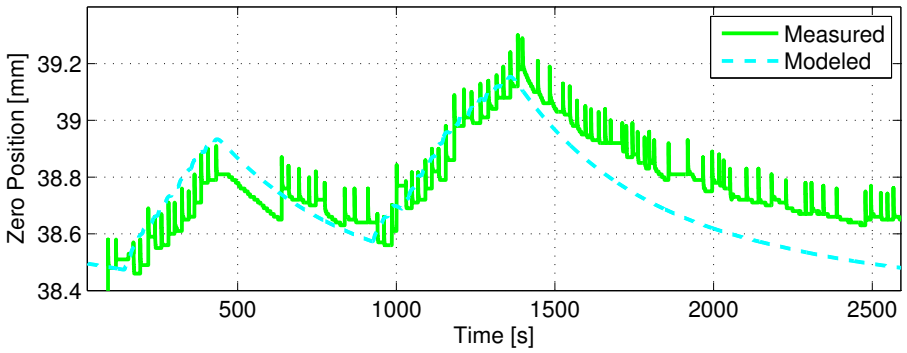

Figure 5: The clutch has been heated through slipping and then left to cool down. The zero position has been recorded as a measure of the expansion. The spikes in the data indicate when the clutch has been closed. The temperature model (17)-(20) shows good agreement with the measurement. Parameters have been fitted to a separate set of data.

of Figure 5, 1.5 MJ of energy is dissipated. The pressure plate and flywheel have a combined mass of 81 kg and are made of cast iron that has a specific heat of 0.5 kJ/(kg K), (Nording and Österman, 1999). If cooling of the clutch is neglected a slightly high estimation of the temperature increase is obtained.

$$\frac{1.5 \cdot 10^6}{500 \cdot 81} = 37 \text{ K}$$

The measured expansion of the clutch during the same period is 0.3 mm at the piston. With a linkage ratio of 8.8, a 100 mm thick clutch and an expansion coefficient for cast iron of $11 \cdot 10^{-6}$ K^{-1}, (Nording and Österman, 1999), this corresponds to a temperature increase of,

$$\frac{0.3}{8.8 \cdot 100 \cdot 11 \cdot 10^{-6}} = 30 \text{ K}$$

The two temperature estimates are practically the same, which indicates that the measured expansion depends on temperature.

Expansion Model

In order to model the expansion a temperature model is required. In Velardocchia et al. (2000) a linear model with one thermal mass in the pressure plate and one in the flywheel is proposed. All parts of the clutch are cooled towards the air in the clutch housing. In Myklebust and Eriksson (2012) the model is extended to capture the changes in the housing temperature, T_h. In contrast to Velardocchia et al. (2000) the clutch studied here is mounted in a vehicle, therefore the clutch is, in addition, thermally connected to both the ICE and

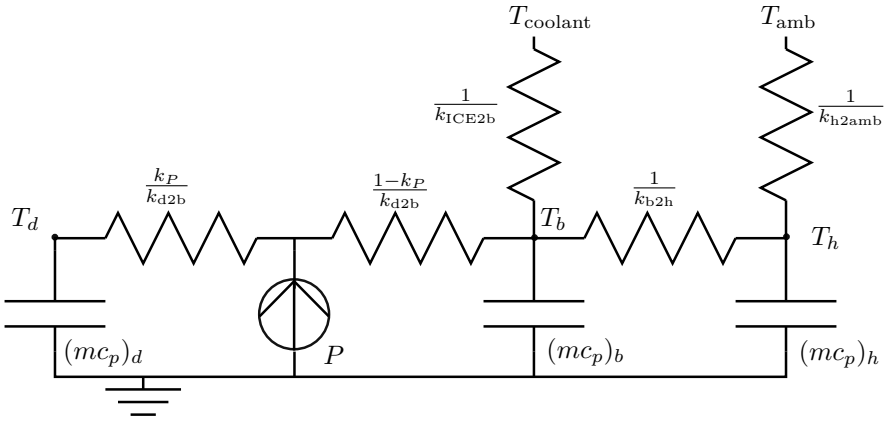

Figure 6: An electrical analogy of the temperature model (23)-(25). If $(mc_p)_d = 0$ the model can also be described by (17)-(18).

transmission. However only a few percent of the dissipated power, P, goes into the transmission, (Wikdahl and Ågren, 1999). Therefore the heat flow to the transmission has been neglected. Moreover it has been found that the thermal masses of the flywheel and pressure plate can be taken as one mass, $(mc_p)_b$, for the clutch body, without loosing accuracy with respect to the expansion. For an electrical analogy of the model see Figure 6. The corresponding equations are:

$$(mc_p)_b\dot{T}_b = k_{\text{ICE2b}}(T_{\text{coolant}} - T_b) + k_{\text{b2h}}(T_h - T_b) + P \tag{17}$$

$$(mc_p)_h\dot{T}_h = k_{\text{b2h}}(T_b - T_h) + k_{\text{h2amb}}(T_{\text{amb}} - T_h) \tag{18}$$

where,

$$P = M_{\text{trans,k}}\,\Delta\omega \tag{19}$$

In order to connect the temperature model with the change in zero position, the levers and the expansion of the clutch body as function of temperature are assumed linear.

$$x_0 = k_{\text{exp,1}}\,(T_b - T_{\text{ref}}) + x_{0,\text{ref}} \tag{20}$$

The $x_{0,\text{ref}}$ parameter corresponds to x_0 when the temperature is T_{ref}. $x_{0,\text{ref}}$ will naturally decrease with wear as the friction pads get thinner, see Figure 1. However the thinning of the pads is a slow process compared to the thermal dynamics and does therefore not need to be modeled at this stage. However it is an inevitable process and will need to be dealt with during the life time of an HDT. Therefore $x_{0,\text{ref}}$ is modeled in Section 4.

The eight parameters in the equations have been fitted against measured data and the validation results, on a different set of data, can be seen in Figure 5. The two integrations in the open-loop simulation give a slow drift. In online

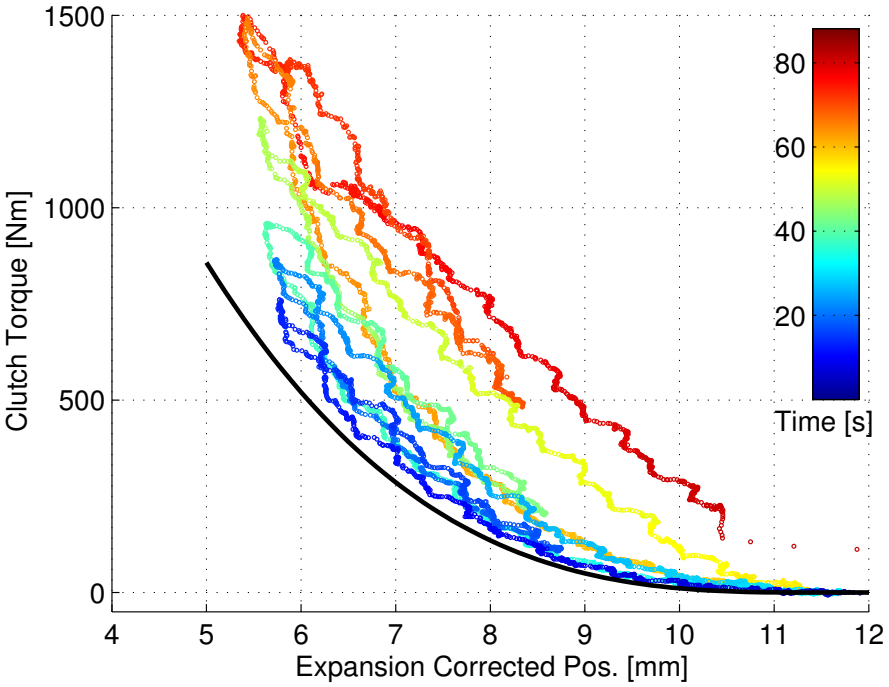

Figure 7: The data from Figure 2 has been corrected for expansion of the clutch body using (20)-(22). The correction is not sufficient to explain the torque drift.

applications this drift can be compensated for using an observer, as in Section 4. In order to model the change in torque the zero-position model, (17)-(20), can be used to correct the piston position for the expansion effect to correspond to the actual compression of the flat spring, see Figure 1.

$$\Delta x_0 = x_0 - x_{0,ref} \tag{21}$$

$$x_{\text{cor}} = x - \Delta x_0 \tag{22}$$

Nevertheless the expansion model does not fully explain the torque drift, see Figure 7. The time scale in Figure 2 is significantly smaller than that of Figure 5. The torque drift is also much larger than what is explained by the modeled expansion. In fact the remaining relative torque drift is of the same magnitude as that reported in Cappetti et al. (2012b) due to flat spring axial expansion. This has led to the hypothesis that the clutch disc, or at least the flat spring, is also expanding with heat. In particular the clutch disc/flat spring has a much smaller (thermal) mass, which could correspond to the faster time constant phenomenon seen in the data.

Including Fast Dynamics

The clutch disc temperature, T_d, has been modeled in a similar fashion, see Figure 6 for an electrical analogy and below for equations.

$$\begin{aligned}(mc_p)_b\dot{T}_b &= k_{\mathrm{ICE2b}}(T_{\mathrm{coolant}} - T_b) + k_{\mathrm{b2h}}(T_h - T_b) \\ &\quad + k_{\mathrm{d2b}}(T_d - T_b) + k_P P \qquad (23)\\ (mc_p)_h\dot{T}_h &= k_{\mathrm{b2h}}(T_b - T_h) + k_{\mathrm{h2amb}}(T_{\mathrm{amb}} - T_h) \qquad (24)\\ (mc_p)_d\dot{T}_d &= k_{\mathrm{d2b}}(T_b - T_d) + (1 - k_P)P \qquad (25)\end{aligned}$$

A new situation with this extended model is that the dissipated energy has to be split between the clutch disc and the body. In the model it is split by the parameter k_P, which is 1 if all energy goes to the body and 0 if all goes to the disc. However the model is not sensitive to k_P due to two facts. First the vast difference in time constants, a factor of ∼30, between the disc time-constant[1], $\tau_{T_d} = 8.3$ s, and the body time-constant[1], $\tau_{T_b} = 3.7$ min, decouples (23) from (25), i.e. $k_{\mathrm{d2b}}(T_d - T_b) + k_P P \approx (1 - k_P)P + k_P P = P$, leaving the dynamics of T_b almost unchanged. Second the parameters are fitted to data, i.e. if k_P is 0 instead of 0.5 the value of $(mc_p)_d$ and k_{d2b} will double, leaving the dynamics of T_d almost unchanged. In the data the expansion has been seen to lag the dissipated power. The lag is maximized by $k_P = 0$ this is thus the choice of k_P.

The expansion of the clutch disc is modeled by extending (21) with an extra term

$$\begin{aligned}\Delta x_0 &= k_{\mathrm{exp}}\left(T_b - T_{\mathrm{ref}}\right) + k_{\mathrm{exp},2}\left(T_d - T_{\mathrm{ref}}\right) = \\ &= k_{\mathrm{exp}}\left(T_b - T_{\mathrm{ref}}\right) + k_{\mathrm{exp},2}\left(\left(T_d - T_b\right) + \left(T_b - T_{\mathrm{ref}}\right)\right) = \\ &= \underbrace{\left(k_{\mathrm{exp}} + k_{\mathrm{exp},2}\right)}_{k_{\mathrm{exp},1}}\left(T_b - T_{\mathrm{ref}}\right) + k_{\mathrm{exp},2}\left(T_d - T_b\right) \qquad (26)\end{aligned}$$

where the second term was practically zero during the zero-position measurements due to the fast dynamics of T_d. Therefore the new parameters can be estimated separately from the old parameters. After estimation of the new parameters the position can be corrected with (23)-(26) and Figure 8 is obtained.

The model works well with some deterioration for the later, and thereby hotter, ramps. One should note that values of the temperature states have not been validated against any measurement but they have reasonable magnitudes.

The transmitted torque can now be calculated as,

$$M_{\mathrm{trans,k}} = M_{\mathrm{ref}}(x_{\mathrm{cor}}) \qquad (27)$$

Note that x_{cor} increases with temperature which in turn makes $M_{\mathrm{trans,k}}$ increase with temperature. This is in contrast with the data in Velardocchia et al. (1999)

[1]The technical term 'time constant' is only well defined for LTI SISO first-order systems. Here $\tau_{T_d} = (mc_p)_d/k_{\mathrm{d2b}}$ and $\tau_{T_b} = (mc_p)_b/\left(k_{\mathrm{ICE2b}} + k_{\mathrm{b2h}} + k_{\mathrm{d2b}}\right)$ are used, which gives similar information regarding the speed of the dynamics

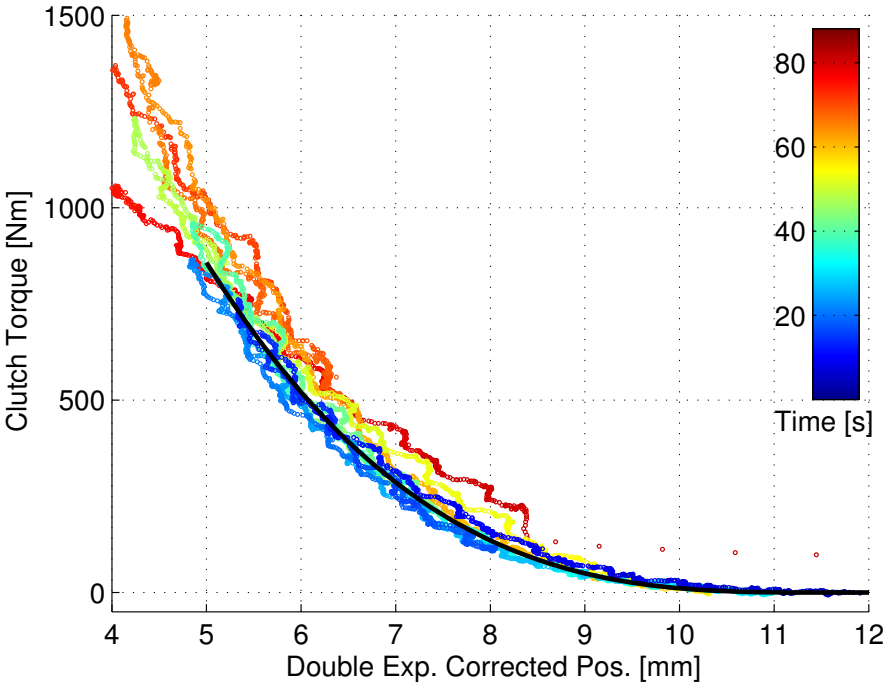

Figure 8: The data from Figure 2 has been corrected for expansion of the clutch body using (22) and (26). The correction explains the torque drift.

where the torque is decreasing with temperature. However in the experiments performed here the clutch mostly has a medium to high temperature and could comply with the data in Ercole et al. (2000).

Power as Input?

It can be discussed whether the dissipated power, P, should be considered an input signal since it is calculated using (19). On one hand, calculating the power from the measured torque gives a better power signal that in turn gives a better estimate of the current transmissibility curve, which could be used for feedforward in control applications. On the other hand the measured torque is not always available, e.g. some special driving scenarios, when evaluating new controllers through simulation, or in the prediction made by a model-based controller. Then P has to be calculated using the modeled torque. In Section 3.7 the model will be evaluated using both a measured P and a modeled P.

3.5 Tuning Methodology

In order to use the presented model in a new application the model tuning might need to be repeated. A simple approach is to follow the same outline as the presentation of the model. Start with fitting the slow dynamics, (17)-(20), to data from an experiment of the type seen in Figure 5. Since the model is semi-physical a good start is to find approximate physical values for the parameters. Simple optimization methods tend to get stuck in local minima and therefore manual tuning has been used here. T_{ref} is preferably chosen as the initial temperature if the vehicle is in steady-state at the start of the measurements. When the slow dynamics are satisfactory it is time for the fast dynamics. The new parameters in (23)-(26) are fitted to make the data from Figure 7 converge into one single curve. This curve is described by (16) and those parameters can be fitted using a least-squares method.

3.6 Model Summary

In summary, the model is a three state model with one static non-linearity. The model parameterization and estimation can be performed using a production vehicle by following the methodology of Section 3.5. All calculations are simple and therefore the model is suitable for running in real time, for example in a clutch-control application.

3.7 Clutch Model Validation

The model has been validated on several data sets, separate from those used for parameter identification, and one of these, which is similar to the data in Figure 5, is shown in Figure 10. At the end of the torque pulses, the modeled torque drops faster than the measured torque, when the clutch is fully opened in 0.3 s. This is however believed to be due to delays in the computation of the engine torque, sensors and other data processing since the model only leads the measurement in really fast transients. Furthermore when the clutch is opened quickly the engine flywheel inertia will be accelerated. When the engine torque is compensated for the inertia in order to give the clutch torque, a lag will naturally arise from the low-pass filtering of the engine speed. Comparing the observed lag and the trajectory of the engine speed, the low-pass filtering could very well be the explanation. Therefore the residuals, $M_{\text{sim}} - M_{\text{meas}}$, have been filtered using a moving median of five samples (10 Hz). The result is presented in Figure 9. The residuals are less than 100 Nm. Considering that 100 Nm is less than 3 % of maximum engine torque and that the mean absolute relative error during slipping is a mere 0.3 %, the model works sufficiently well for control purposes. In fact the estimated engine torque can have errors of similar magnitude, which naturally limits the possible accuracy of a model developed using this experimental platform.

Note that when the dissipated power is measured the simulation shows a

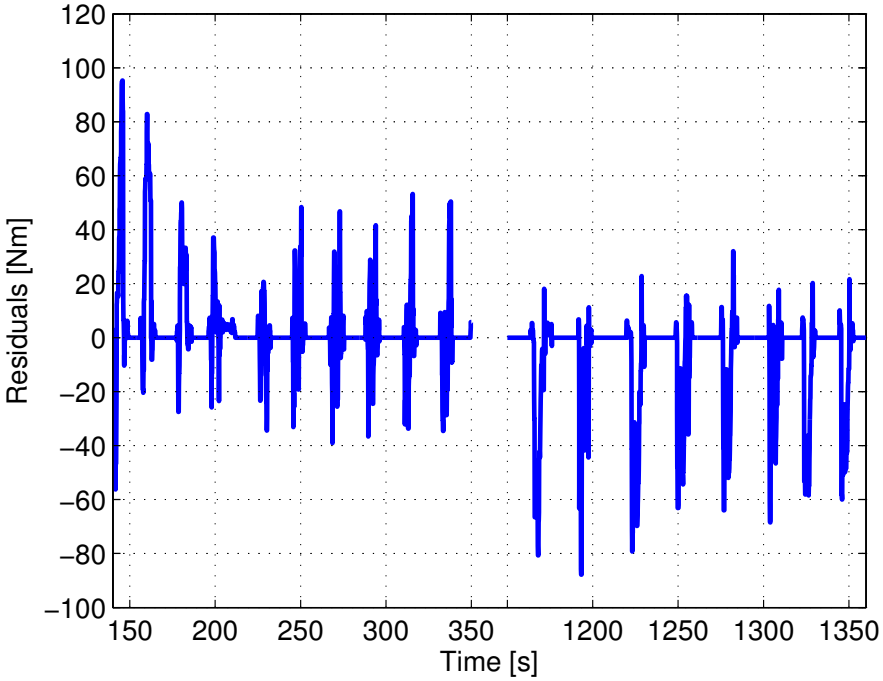

Figure 9: The residuals between the model and data presented in Figure 10. The residuals are less than 100 Nm. Or in other words, less than 3 % of maximum ICE torque. The mean absolute relative error is a mere 0.3 %

slightly low clutch torque. If instead the dissipated power is calculated from the simulated torque the torque error makes the simulated power dissipation too low and therefore the temperature states get lower. In turn this will lead to even lower simulated torque in the next torque pulse. This is the explanation for the decay in the simulated torque when also the power is simulated. In spite of this it still models the torque better than the more common static model.

A validation of a launch is shown in Figure 11. The static and dynamic models are compared to measurement data. The dynamic model has a small error that is always less than 100 Nm, and has better performance than the static model.

In some data sets it has been seen that when T_d is greater than 200 °C the model deteriorates, although not in the data set of Figure 8. This could be due to μ-fading or other effects coming into play. However it is of small concern that the model deteriorates above 200 °C since these temperatures are only reached during extreme driving, where other measures can be taken. The accuracy of the model has also been seen to be less good when the truck is cold. Cold starting has not been thoroughly investigated since measurements are very

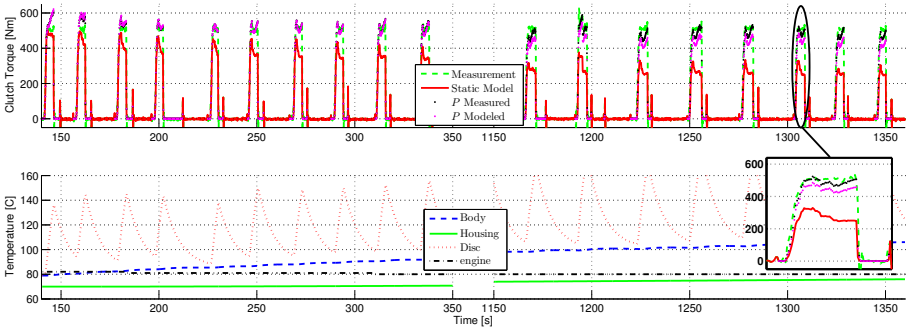

Figure 10: The dynamic torque model shows good agreement with measurements in a validation data set. There is a slight decay in torque when P is modeled instead of measured. However both implementations are significant improvements compared the static model, $M_{\text{trans}} = M_{\text{ref}}(x)$, with parameters fitted to the rising edge of the first torque pulse (at 142 s). The open-loop simulation started at 0 seconds. In the lower plot P is measured.

time consuming. The truck heats up relatively quick but takes a long time to cool down again. Moreover the engine reported torque is less reliable when the engine is cold. In both the warm and the cold case the model error can become a couple of hundred newton meters.

The clutch temperatures can not be quantitatively validated as no temperature measurements are available. Therefore only a qualitative validation is performed, showing that the magnitudes of the temperature states are reasonable for an HDT clutch, see Figure 10 and 11.

4 Observer

As shown in Myklebust and Eriksson (2013) the thermal effects in a dry clutch can have a significant effect on launch control of a vehicle. Controllers that assume the clutch torque to be an controllable input signal, e.g. Dolcini et al. (2008) and Garofalo et al. (2002), would need an underlying compensation of the thermal effect. This could be done like in Deur et al. (2012), although there measurements of the temperature is used. Due to the difficulties involved in measuring the temperatures of rotating bodies, this is not a feasible solution for production vehicles. Instead the model of Section 3 can be used to estimate the temperatures. With the help of an observer the model can be made insensitive to poor initial values and wear (here only considered as a change in $x_{0,\text{ref}}$). The latter is taken care of by adding a fourth equation to the state space (23)-(25).

$$\dot{x}_{0,\text{ref}} = 0 \tag{28}$$

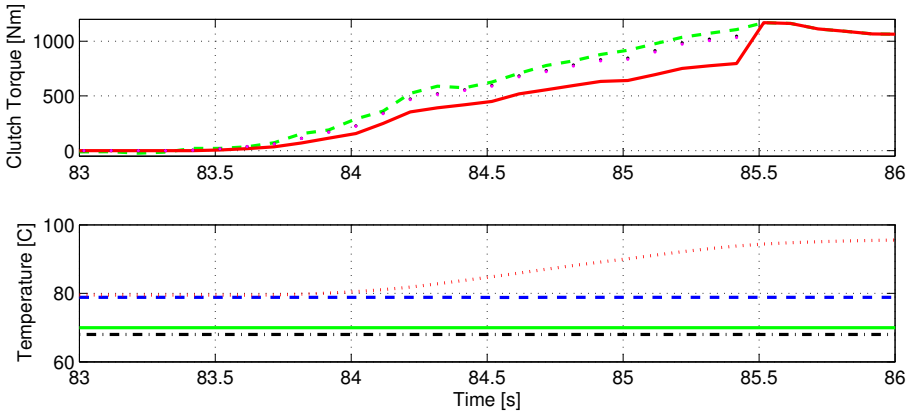

Figure 11: The dynamic torque model shows good agreement with measurement data of a launch. The open-loop simulation started at 0 seconds. Line colors and styles are the same as in Figure 10. The clutch is locked up when there are no black or magenta dots. In the lower plot P is measured.

The following definitions are made: state vector $X = \left[T_b,\, T_h,\, T_d,\, x_{0,\mathrm{ref}}\right]^T$, input vector $U = \left[x,\, P,\, T_{\mathrm{coolant}},\, T_{\mathrm{amb}}\right]^T$ and intermediate output variable $\tilde{y} = \left[x_0,\, x_{\mathrm{cor}}\right]^T$. Now, with (26), (21), (22), (27) and (16) the model can be expressed as:

$$\dot{X} = AX + BU \tag{29}$$

$$\tilde{y} = CX + DU + \begin{bmatrix} -1 \\ 1 \end{bmatrix} k_{\mathrm{exp},1} T_{\mathrm{ref}} \tag{30}$$

where,

$$A = \begin{pmatrix} -\frac{k_{\mathrm{b2h}}+k_{\mathrm{ICE2b}}+k_{\mathrm{d2b}}}{(mc_p)_b} & \frac{k_{\mathrm{b2h}}}{(mc_p)_b} & \frac{k_{\mathrm{d2b}}}{(mc_p)_b} & 0 \\ \frac{k_{\mathrm{b2h}}}{(mc_p)_h} & -\frac{k_{\mathrm{b2h}}+k_{\mathrm{h2amb}}}{(mc_p)_h} & 0 & 0 \\ \frac{k_{\mathrm{s2b}}}{(mc_p)_d} & 0 & -\frac{k_{\mathrm{s2b}}}{(mc_p)_d} & 0 \\ 0 & 0 & 0 & 0 \end{pmatrix} \tag{31}$$

$$B = \begin{pmatrix} 0 & 0 & \frac{k_{\mathrm{ICE2b}}}{(mc_p)_b} & 0 \\ 0 & 0 & 0 & \frac{k_{\mathrm{h2amb}}}{(mc_p)_h} \\ 0 & \frac{1}{(mc_p)_d} & 0 & 0 \\ 0 & 0 & 0 & 0 \end{pmatrix} \tag{32}$$

$$C = \begin{pmatrix} C_1 \\ C_2 \end{pmatrix} = \begin{pmatrix} k_{\mathrm{exp},1} - k_{\mathrm{exp},2} & 0 & k_{\mathrm{exp},2} & 1 \\ -k_{\mathrm{exp},1} + k_{\mathrm{exp},2} & 0 & -k_{\mathrm{exp},2} & 0 \end{pmatrix} \tag{33}$$

$$D = \begin{pmatrix} D_1 \\ D_2 \end{pmatrix} = \begin{pmatrix} 0 & 0 & 0 & 0 \\ 1 & 0 & 0 & 0 \end{pmatrix} \tag{34}$$

and the measurable model outputs are,

$$y = \begin{bmatrix} x_0 \\ M_{\text{trans,k}} \end{bmatrix} = \begin{bmatrix} \tilde{y}_1 \\ M_{\text{ref}}(\tilde{y}_2) \end{bmatrix} \tag{35}$$

However all measurements are not always available. The zero position is only available when the clutch is fully closed and slipping torque only when the clutch is slipping. This naturally affects observability and observer design, and is therefore analyzed below.

4.1 Observability

When studying the observability of a system the structure of the output function (35) is important. Due to the varying nature of that structure in this application it is natural to break down the problem into different cases: fully closed, engaged and locked-up, engaged and slipping, and open clutch.

Fully Closed Clutch

When the clutch is fully closed it is not restrictive to assume that the clutch is locked up. Then the clutch torque is a direct response of the engine torque and not temperature or clamp load dependent. Therefore the transmitted torque does not contribute with information regarding the states, but the zero position does and can be measured so in this mode the output is:

$$y = C_1 X - k_{\text{exp},1} T_{\text{ref}} \tag{36}$$

This subsystem, (29) together with (36), is locally observable according to linear theory, (Rugh, 1996).

Engaged and Locked-Up Clutch

The clutch does not need to be fully closed in order to be locked-up. If the clutch is not fully closed the piston position does not contain any information about the thermal expansion since an expansion does not alter the piston position, instead it compresses the cushion spring. Furthermore the transmitted torque only gives a lower bound of the stiction torque and therefore the states can be bounded, but not observed.

Engaged and Slipping Clutch

When the clutch is slipping the output is given by:

$$y = M_{\text{ref}} \left(C_2 X + D_2 U + k_{\text{exp},1} T_{\text{ref}} \right) \tag{37}$$

This subsystem is structured as a linear state space and a non-linearity on the output. The non-linearity, i.e. the torque transmissibility curve, is invertible

in the range where the clutch is engaged. Therefore the nonlinearity does not affect the observability of this mode.

When looking at the structure of the rest of the subsystem, (29) together with the second row of (30), it can be seen that $x_{0,\text{ref}}$ does not enter y nor any of its time derivatives. Therefore $x_{0,\text{ref}}$ is not observable in this mode. If this state is removed the observability matrix receives full rank. In conclusion the temperature states are locally observable whereas $x_{0,\text{ref}}$ is not observable

Open Clutch

When the clutch is open the transmitted torque is simply zero. This gives a bound on the kiss point and thereby a bound on the states but no observability.

Complete System

The complete system with all four different modes is a non-linear system. With non-linear systems the observability can depend on the input signal, (Hermann and Krener, 1977). There exists input-signal trajectories that control the system into the observable mode and therefore the complete system is observable. To obtain observability in practice the system needs to visit the observable mode, i.e. fully closed clutch. Conveniently enough this mode is frequently visited during normal operation. In addition the partially observable mode, slipping clutch, is also frequently visited.

4.2 Observer Selection and Precautions

Since the system is observable an EKF can be used to observe the states. Two main reasons exist for choosing the EKF. First the implementation is straight forward and the EKF has been successful in many applications, especially if the non-linearity is mild. Second it is easy to adjust the number of measurements according to system mode with the EKF. When in an unobservable mode the EKF will simply do an open loop simulation of the model, with the addition of a growing covariance matrix. In addition to the different modes discussed in Section 4.1 there are driving scenarios where M_e, and thereby y_2, is not available or reliable.

When the system is in a mode that makes one or more states unobservable the respective covariances will naturally grow, this helps the estimate to converge quickly when the state(s) become observable again, see e.g. Höckerdal et al. (2011). If the system stays in an unobservable mode for a prolonged time the covariance can grow too large and cause numerical issues in the observer. Nevertheless there exists a simple remedy to this problem; limit the covariance with its initial value, only the diagonal elements need to be limited, (Höckerdal et al., 2011). This needs to be considered in an online application.

Another practical issue is that the torque estimate from the engine control unit is slightly biased. Even if just by a few Newton meters the bias has a

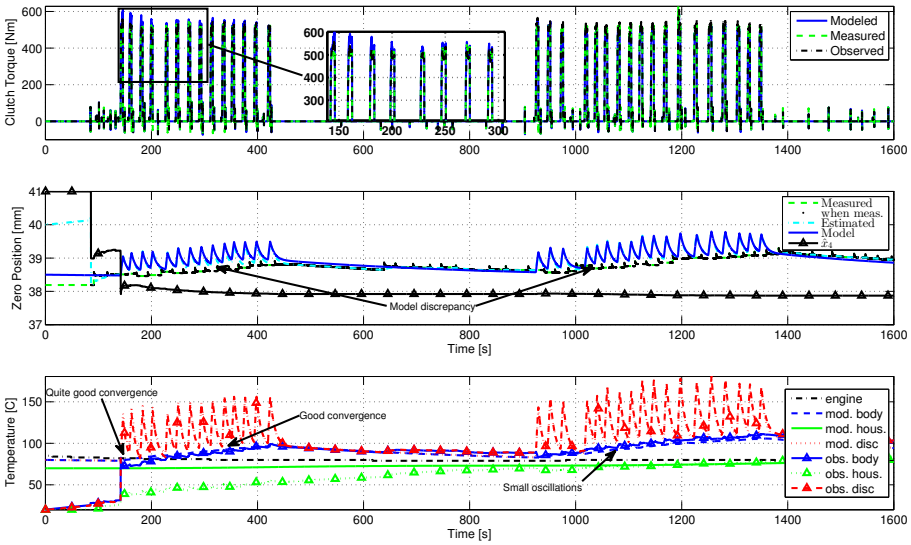

Figure 12: The model simulates the torque and zero position well given good initial values. The observer states are able to approach the model states although the initial states for the observer are far off. There is some oscillation in T_b due to a model discrepancy that is present in the x_0 signal but not the torque signal.

profound effect on the estimate during longer periods of open clutch. When the clutch is fully open the temperature would have to increase immensely in order to explain a non zero torque output. This can be remedied in many ways and a simple method is to set the torque to zero, when it is under a threshold governed by the accuracy. Here the threshold on measured torque was set to 20 Nm.

4.3 Selection of EKF Covariance Matrices

The Q and R matrices in an EKF has a physical interpretation as the process noise and the measurement noise, respectively. However in practice they are used to tune the trade-off between convergence rate and noise sensitivity. In order to get a good starting point the covariance matrix for the measurement noise was made to roughly match data using the following procedure: Both measurements have been manually examined at arbitrary time points and the standard deviations for the assumed white noise were set to approximately match the amplitudes of the noise. Then the variances are put on the diagonal elements of the covariance matrix:

$$R = \begin{bmatrix} 10^{-2} & 0 \\ 0 & 10^{2} \end{bmatrix} \tag{38}$$

The covariance matrix for the process noise is also given a diagonal structure as this gives one parameter to tune for each equation. Manual tuning of the observer resulted in the following matrix:

$$Q = \begin{bmatrix} 10^{-1} & 0 & 0 & 0 \\ 0 & 10^{-1} & 0 & 0 \\ 0 & 0 & 10^{-1} & 0 \\ 0 & 0 & 0 & 10^{-8} \end{bmatrix} \tag{39}$$

where $Q(4,4)$ has a very low value since $x_{0,\text{ref}}$ varies very slowly.

5 Observer Evaluation

The observer has been validated using the same measurement data as in Figure 10. Since no temperature measurements are available the model has been simulated using manually tuned initial values, $\begin{bmatrix} T_b, & T_h, & T_d, & x_{0,\text{ref}} \end{bmatrix} = \begin{bmatrix} 80, & 70, & 80, & 38 \end{bmatrix}$. Given these initial values the model predicts the torque and zero position well, see Figure 12 (or Figure 10), and therefore these trajectories of the temperature states are those sought by the observer. To test the convergence of the observer the states are given worst-case initial values, $\begin{bmatrix} T_b, & T_h, & T_d, & x_{0,\text{ref}} \end{bmatrix} = \begin{bmatrix} 20, & 20, & 20, & 41 \end{bmatrix}$, see Figure 12. The estimation-error covariance matrix is initially set to,

$$P_0 = \begin{bmatrix} 15 & 0 & 0 & 0 \\ 0 & 15 & 0 & 0 \\ 0 & 0 & 15 & 0 \\ 0 & 0 & 0 & 15 \end{bmatrix} \tag{40}$$

Note that the value of $P_0(4,4)$ is larger than the other diagonal elements in relative measures. During the first 85 s almost nothing happens since the clutch is open which makes the system unobservable. Only a slight increase in temperature is present since the observed states are below their equilibrium points. At 85 s when the clutch is closed (neutral gear) the sum of $\hat{x}_{0,\text{ref}}$ and the expansion should equal the measured x_0. As a consequence $\hat{x}_{0,\text{ref}}$ is drastically improved due to the large value in $P_0(4,4)$, while the temperature estimates are not. $\hat{x}_{0,\text{ref}}$ follows when the temperature estimates continue to rise slowly towards equilibrium. At 142 s when the clutch is slipping for the first time the temperature states, T_b and T_d, converge quite quickly, consequently $\hat{x}_{0,\text{ref}}$ is drastically improved. Between slipping phases in the data the clutch is fully closed and $\hat{x}_{0,\text{ref}}$ is given time to converge and subsequently the temperature states do so as well. The convergence of T_h is slow since its dynamics are slow and its effect on the measurements is indirect. Around 400 s $\hat{x}_{0,\text{ref}}$ converges to a value slightly lower than the models value. At 638 s there is a step disturbance in the zero position measurement. This leads to a small change in the temperature estimates due to a (too) high confidence in $\hat{x}_{0,\text{ref}}$. The small oscillations seen in

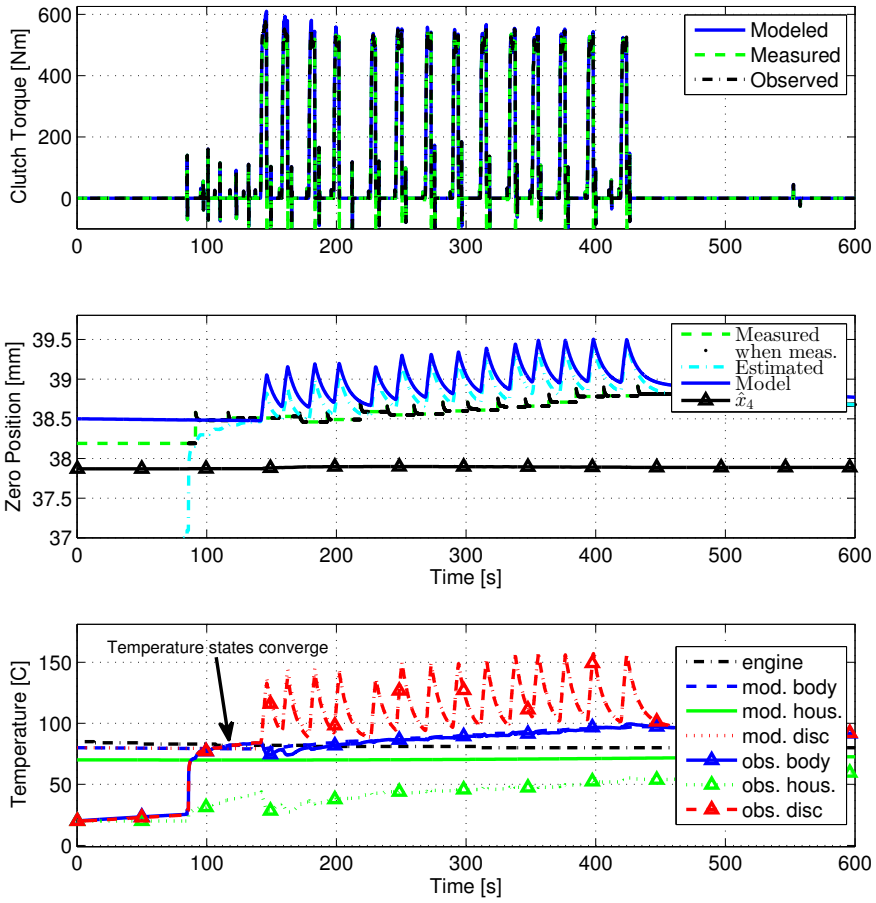

Figure 13: When $\hat{x}_{0,\text{ref}}$ has a good initial value and low covariance the temperature states converge quickly, compared to the case in Figure 12. The estimated states converge to the modeled states around 115 s. Between 140 s and 190 s the estimated torque is closer to the measured torque than the modeled torque is, which is accomplished by a slightly lower temperature and $x_{0,\text{ref}}$.

$\hat{T}_b$ are a consequence of that the observer is compensating for the discrepancy between modeled and measured zero position without loosing accuracy in the torque estimate.

The observer is working, although it takes some time to converge. However this is an extreme case, the temperature states could be given better initial guesses using the engine temperature and in particular, $x_{0,\text{ref}}$ does not change while the truck is powered off. Therefore $\hat{x}_{0,\text{ref}}$ can be given its final value from the last run as an initial guess, and $P_0(4,4)$ can be given the end value of $P(4,4)$

from the last run. For the case in Figure 12 the end values are $\hat{x}_{0,\text{ref}} = 37.9$ mm (38 mm in the model) and $P_0(4,4) = 5.5 \cdot 10^{-6}$ mm^2. Rerunning the observer on the same data, with $\hat{x}_{0,\text{ref}}$ initialized from data in the last run, yields the result in Figure 13. Now the temperature states can be seen to converge quicker, even before the clutch starts slipping at 142 s. For the first three torque pulses, between 140 s and 190 s, the estimated temperature states are a bit low compared to the modeled states. Nevertheless this is actually desirable since the modeled torque is a bit high for these three pulses, whereas the estimated torque is correct. This fast convergence is possible due to the use of the measurement of the zero position. Using the zero position the proposed observer can estimate the clutch temperature, and hence the torque transmissibility curve, without slipping the clutch. This is very useful since the clutch is closed for extended time periods during long haulage and during that time, the clutch temperature can change due to the engine and ambient temperature. This gives the possibility to track and know the torque transmissibility curve before the clutch starts to slip which is of great value for clutch and torque control, (Myklebust and Eriksson, 2013).

In Figure 12 and Figure 13 the observer has been running in 10 Hz. In order to investigate the effect of the sampling time on the observer, simulations have been carried out with sampling frequencies between 0.1-100 Hz. There is a slight decrease in accuracy with decreasing frequency and around 0.5 Hz the shapes of the state trajectories start to deviate from the shapes of the modeled state trajectories. In the data used here the torque pulses have a duration of about 4-5 s and at 0.5 Hz that means a few samples per pulse. More dynamic torque trajectories require higher sample frequencies for the observer. No difference was seen in convergence rate for different frequencies since the convergence rate is controlled by the Q and R matrices.

6 Conclusion

The transmitted torque in an HDT dry clutch at slipping conditions has been studied. Experiments show no direct slip-speed dependency at the levels of slip investigated here, instead dynamic effects are clearly visible. In particular the measurements show that the transmitted torque can vary up to 900 Nm for a given position. The dynamic behavior has two vastly different time constants, approximately a factor 30 apart, where both parts affect the transmitted torque through thermal expansion of clutch parts. A third-order state-space model with an output nonlinearity captures the behavior of the clutch.

In validations, on driving sequences with intense use of the clutch, the open-loop simulation error was kept under 100 Nm, which is less than 3 % of maximum engine torque and comparable to the accuracy of the engine torque estimate. The dynamic model that includes temperature states is a significant improvement compared to a static model. The model was developed, fitted and validated on a production HDT using production sensors only.

The model was then augmented with a wear parameter corresponding to

thinning of the clutch disc. In this augmented model the temperature states are observable both during slipping of the clutch and when the clutch is fully closed, the latter is due to the utilization of the zero-position measurement. The clutch disc wear on the other hand is only observable when the clutch is fully closed.

The implemented EKF can, using real data, converge from poor initial values, enabling prediction of the translation of the torque transmissibility curve. If, as often is the case, given good initial knowledge about the disc wear but poor initial temperatures the observer can converge within half a minute without slipping the clutch. The EKF is simple and suitable for real-time applications.

All modeling, design and validation steps have been performed using production sensors only, efficiently demonstrating that the EKF can be implemented in a production truck.

References

Marius Bataus, Andrei Maciac, Mircea Oprean, and Nicolae Vasiliu. Automotive clutch models for real time simulation. *Proceedings of the Romanian Academy, Series A*, 12(2):109–116, 2011.

Nicola Cappetti, Mario Pisaturo, and Adolfo Senatore. Modelling the cushion spring characteristic to enhance the automated dry-clutch performance: The temperature effect. *Proc IMechE, Part D: Journal of Automobile Engineering*, 226(11):1472–1482, 2012a.

Nicola Cappetti, Mario Pisaturo, and Adolfo Senatore. Cushion spring sensitivity to the temperature rise in automotive dry clutch and effects on the frictional torque characteristic. *Mechanical Testing and Diagnosis*, 3(2):28–38, 2012b.

Josko Deur, Vladmir Ivanovic, Zvonko Herold, and Milan Kostelac. Dry clutch control based on electromechanical actuator position feedback loop. *International Journal of Vehicle Design*, 60(3-4):305–326, 2012.

Pietro Dolcini, Hubert Béchart, and Carlos Canudas de Wit. Observer-based optimal control of dry clutch engagement. In *44th IEEE Conference on Decision and Control, and the European Control Conference*, pages 440–445, December 2005a.

Pietro Dolcini, Carlos Canudas de Wit, and Hubert Béchart. Improved optimal control of dry clutch engagement. *Proceedings of the 16th IFAC World Congress*, 16(1):1891–1891, 2005b.

Pietro Dolcini, Carlos Canudas de Wit, and Hubert Béchart. Lurch avoidance strategy and its implementation in AMT vehicles. *Mechatronics*, 18(1):289–300, May 2008.

Pietro J. Dolcini, Carlos Canudas de Wit, and Hubert Béchart. *Dry Clutch Control for Automotive Applications*. Advances in Industrial Control. Springer-Verlag London, 2010.

G. Ercole, G. Mattiazzo, S. Mauro, M. Velardocchia, F. Amisano, and G. Serra. Experimental methodologies to determine diaphragm spring clutch characteristics. In *SAE Technical Paper: 2000-01-1151*, March 2000.

Bingzhao Gao, Hong Chenc, Jun Li, and Lu Tian. Observer-based feedback control during torque phase of clutch-to-clutch shift process. *International Journal of Vehicle Design*, 58(1):93–108, 2012.

Franco Garofalo, Luigi Glielmo, Luigi Iannelli, and Francesco Vasca. Optimal tracking for automotive dry clutch engagement. In *2002 IFAC, 15th Triennial World Congress*, pages 1527–1527, 2002.

Luigi Glielmo and Francesco Vasca. Optimal control of dry clutch engagement. In *SAE Technical Paper: 2000-01-0837*, March 2000.

R Hermann and A Krener. Nonlinear controlability and observability. *IEEE Trans. on Automatic Control*, 22(5):728–740, 1977.

Erik Höckerdal, Erik Frisk, and Lars Eriksson. EKF-based adaptation of look-up tables with an air mass-flow sensor application. *Control Engineering Practice*, 19(5):442–453, 2011.

Matija Hoic, Zvonko Herold, Nenad Kranjcevic, Josko Deur, and Vladimir Ivanovic. Experimental characterization and modeling of dry dual clutch thermal expansion effects. In *SAE Technical Paper: 2013-01-0818*, April 2013.

Sungwha Hong, Sunghyun Ahn, Beakyou Kim, Heera Lee, and Hyunsoo Kim. Shift control of a 2-speed dual clutch transmission for electric vehicle. In *2012 IEEE Vehicle Power and Propulsion Conference*, pages 1205–1205, October 2012.

Jinsung Kim and Seibum B. Choi. Control of dry clutch engagement for vehicle launches via a shaft torque observer. In *2010 American Control Conference*, pages 676–681, June 2010.

Behrooz Mashadi and David Crolla. *Vehicle Powertrain Systems*. John Wiley & Sons Ltd, first edition, 2012.

G. Mattiazzo, S. Mauro, M. Velardocchia, F. Amisano, G. Serra, and G. Ercole. Measurement of torque transmissibility in diaphragm spring clutch. In *SAE Technical Paper: 2002-01-0934*, March 2002.

S.E. Moon, M.S. Kim, H. Yeo, H.S Kim, and S.H Hwang. Design and implementation of clutch-by-wire system for automated manual transmissions. *International Journal Vehicle Design*, 36(1):83–100, 2004.

Andreas Myklebust and Lars Eriksson. Torque model with fast and slow temperature dynamics of a slipping dry clutch. In *2012 IEEE Vehicle Power and Propulsion Conference*, pages 851–856, October 2012.

Andreas Myklebust and Lars Eriksson. The effect of thermal expansion in a dry clutch on launch control. In *7th IFAC Symposium on Advances in Automotive Control*, pages 458–463, September 2013.

Carl Nording and Jonny Österman. *Physics Handbook*. Studentlitteratur, 1999.

Wilson J. Rugh. *Linear System Theory*. Prentice-Hall, Inc., second edition, 1996.

Barna Szimandl and Huba Németh. Dynamic hybrid model of an electro-pneumatic clutch system. *Mechatronics*, 23(1):21–36, 2012.

Francesco Vasca, Luigi Iannelli, Adolfo Senatore, and Gabriella Reale. Torque transmissibility assessment for automotive dry-clutch engagement. *IEEE/ASME transactions on Mechatronics*, 16(3):564–573, June 2011.

M. Velardocchia, G. Ercole, G. Mattiazzo, S. Mauro, and F. Amisano. Diaphragm spring clutch dynamic characteristic test bench. In *SAE Technical Paper: 1999-01-0737*, March 1999.

M. Velardocchia, F. Amisano, and R. Flora. A linear thermal model for an automotive clutch. In *SAE Technical Paper: 2000-01-0834*, March 2000.

Anna Wikdahl and Åsa Ågren. Temperature distribution in a clutch. Master's thesis, Linköping University, 1999. Dept. of Mechanical Engineering.

Paper D

Thermal Clutch Model Observability and Observer Effects of a Torque Sensor in the Powertrain*

D

*Submitted to *IEEE/ASME Transactions on Mechatronics*.

Thermal Clutch Model Observability and Observer Effects of a Torque Sensor in the Powertrain

Andreas Myklebust and Lars Eriksson

Vehicular Systems, Department of Electrical Engineering, Linköping University, SE-581 83 Linköping, Sweden

Abstract

Torque sensors for automotive powertrains are becoming cheaper and a viable option for production vehicles. It is investigated how a torque sensor located on the input shaft of an Automated Manual Transmission (AMT) in a Heavy Duty Truck (HDT) affects the observability of a clutch model for torque transmission that includes thermal effects and aging. In order to handle an offset that is introduced with the new sensor the model is augmented with a random walk and an equation for the engine inertia dynamics. The sensor offset is observable regardless of mode of operation of the clutch and observability of the states in the original model is unchanged. Furthermore the design of an Extended Kalman Filter (EKF) built upon the augmented model requires a new mode of operation compared to an EKF built upon the original model. In addition a mode dependent process noise covariance matrix is used. The new EKF is evaluated using measurement data from an HDT equipped with a magnetoelastic torque sensor. The EKF is demonstrated to work and the estimates converge rapidly, even from poor initial values. It is also computationally simple and therefore suitable for real-time applications.

1 Introduction

Increasing demands on comfort, performance, and fuel efficiency in vehicles lead to more complex transmission solutions. Historically high efficiency was best accomplished with a classical Manual Transmission and comfort with a classical Automatic Transmission (AT). The Automated Manual Transmission (AMT) is one way to combine the best from two worlds. An important part in an AMT is clutch control that has a profound effect on vehicle performance. In clutch control it is of importance to know the torque transmitted in the clutch. Models have come to play an important role in estimation and control of the transmitted torque, (Myklebust and Eriksson, 2014), since torque sensors traditionally have been too expensive. According to Turner (1988) a sensor should cost less than 2 £ in order to be a feasible production solution within the automotive industry. However their cost is decreasing. In fact hydromechanic torque sensors have been used in production, (Audi of America, 2001). Torque sensors can be built in different ways, in Li et al. (2012) a torque sensor is constructed using two rotation speed sensors on a shaft with known stiffness. The sensors are equipped with a unique tooth each in order to get an unbiased estimate. Instead of measuring the torsion in a shaft, the torsion in the clutch damper springs is measured in Jung et al. (2001). This method was reported to have accuracy problems in Bohn et al. (2007), where instead a flywheel that sense torque through strain gauge spokes is developed. It was used to collect data from existing hybrid-electric vehicles with a minimum change of hardware. Marciszko (2004) includes a brief survey of different torque sensors and the magnetoelastic sensor is concluded to be the best type for automotive applications. The magnetoelastic sensor has been developed with automotive use in mind since the 80s, (Ribbens, 1981; Nonomura et al., 1987), and (Turner, 1988), and is the most common torque sensor within automotive research.

There are a number of torque sensors on the market but the control applications that utilize them is still a new research topic. Combustion phasing has been investigated in Larsson and Andersson (2005) and Andersson et al. (2008). The separation of a measured crankshaft torque into cylinder individual torque is studied in Thor et al. (2009). Driveline applications of torque measurement are found in Oral (2010) that studies how traction control is improved by the use of a torque sensor and in Marciszko (2004) and Cowan (2006) the output torque of an AT is controlled towards a reference torque using a magnetoelastic torque sensor on the output shaft. As the demands on powertrains keep increasing the precision in control systems will have to improve. Many possible control applications regarding powertrain comfort and performance could benefit from a torque sensor.

1.1 Outline and Contributions

This paper builds upon Myklebust and Eriksson (2014), where the observability of thermal dynamics and wear was investigated for a control oriented clutch

model as well as the design of an Extended Kalman Filter (EKF). The main novelty in this paper is the addition of a torque sensor to the driveline and the investigation of what implications there are on the observability and observer design when the sensor is added. The sensor comes with an offset that has to be compensated for, i.e. estimated. To see if an estimate is even possible the observability has to be investigated. The change in observability from Myklebust and Eriksson (2014) is non-trivial as the model contains several variables that produce an offset. In order to obtain observability in all operating modes the model has to augmented.

In Section 2 a brief description of the experimental platform is given. The platform is used to estimate the parameters of the thermal clutch model for the new test vehicle equipped with the torque sensor, contributing with further validation of the clutch model from Myklebust and Eriksson (2014). The clutch model is, in Section 3, augmented to include the addition of a torque sensor with unknown offset. The main contributions are that the observability of the new system is analyzed in Section 4 and an observer is designed and evaluated on experimental data in Section 5, effectively increasing the use of a torque sensor for clutch control purposes.

Figure 1: A photograph of the test vehicle Fronda. It is unloaded in the picture but during the experiments it has been loaded to total weight of 21 metric tonnes.

2 Experimental Setup

A rear-wheel drive Heavy Duty Truck (HDT), called Fronda, has been used for experiments, see Figure 1 for a picture. Fronda is equipped with a 14-speed AMT and a 12.7 liter L6 capable of producing 2550 Nm. In the experiments Fronda is loaded to 21.5 tonnes. The clutch, that is in focus here, is a dry single-plate pull-type normally closed clutch. A schematic is seen in Figure 2. The clutch is actuated by an electric motor that through a worm gear moves a hydraulic master cylinder that in turn moves a slave piston and via a lever pulls the throwout bearing. Both motor position, x_m, and slave piston position, x_p, are measured. In order to bring x_p to the same range as x_m and make data sets with different amount of wear comparable to each other the signal $x = x_p - x_{0,\text{ref}}$ is used for the slave position, see Figure 2.

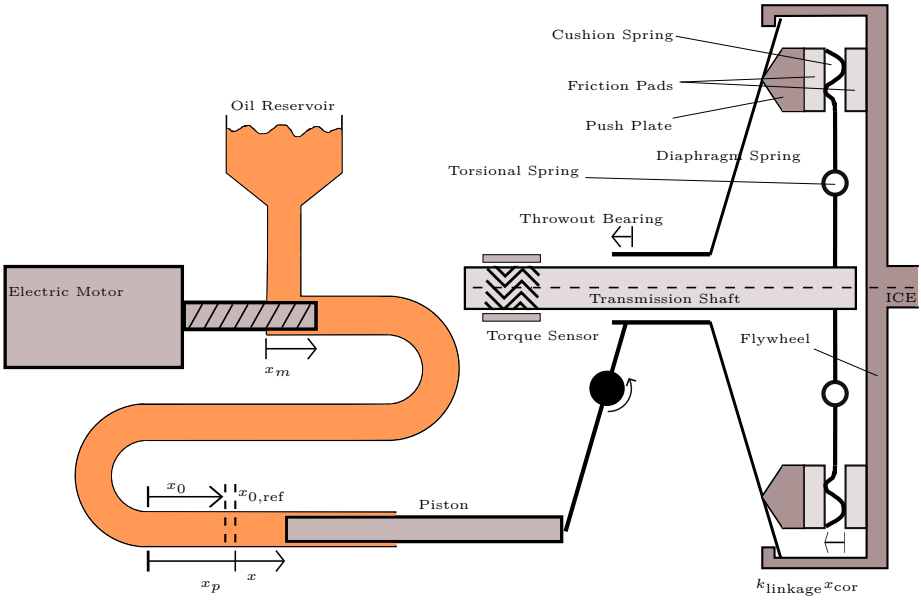

Figure 2: A schematic over the actuator and the dry single-plate pull-type clutch studied here. k_{linkage} is the combined ratio of all levers between the piston and the push plate.

Available (and relevant to this paper) production sensors are: engine speed, input shaft speed, coolant temperature, motor position and slave position. The engine speed and coolant temperature is measured by the Engine Control Unit (ECU) and sent via CAN to the Transmission Control Unit (TCU) that samples the other sensors. The TCU is capable of receiving CAN messages, sampling and actuating at 100 Hz. In addition to the production sensors a torque sensor, the Torductor (Sobel et al., 1996) a magnetoelastic sensor made by ABB, is equipped on the input shaft of the transmission. The torque sensor is sampled

at 10 kHz and has an accuracy of 2 %, if an unknown offset is compensated for. This offset is not constant, see Figure 3. In addition to the torque sensor the reported engine torque is available on CAN. The accuracy of this signal is around 100 Nm when the engine is warm. The exact properties when cold is not known. The engine torque signal is also known to be less exact during transients.

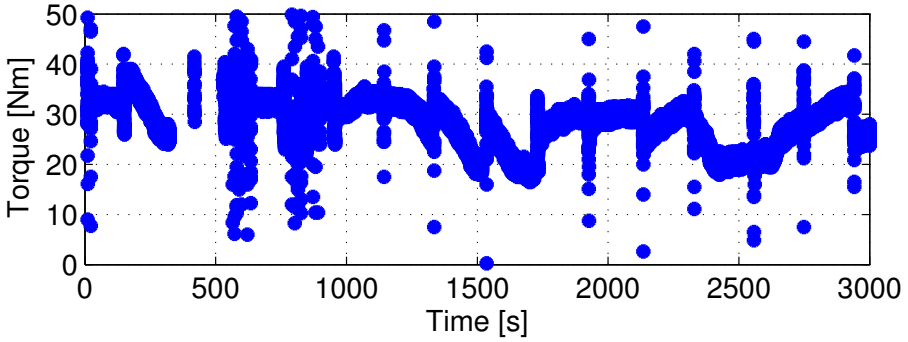

Figure 3: Torque-sensor measurement when the clutch is open ($x > 19$ mm). The sensor offset can be seen to vary with time. The outliers are due to driveline torsion acting on the input shaft after quick clutch disengagement.

3 Clutch Model

The modeled clutch is a single-plate dry clutch with two contact surfaces, see Figure 2 for an overview. The model presented here is based upon Myklebust and Eriksson (2014) but extended with a state equations for the torque sensor offset and a clutch-torque state. A measurement equation is also added for the engine speed.

Torque is transferred between the flywheel and the clutch disc through friction. The friction is modeled as coulomb friction with stick-slip behavior. This is simply modeled with two friction coefficients, one static, μ_s, and one dynamic, μ_k. By defining the ratio of the friction coefficients, $k_\mu = \frac{\mu_s}{\mu_k}$ the equation for the transmittable torque during sticking (the stiction torque) becomes:

$$M_{\text{trans},s} = k_\mu M_{\text{trans},k} \tag{1}$$

where $M_{\text{trans},k}$ is given by (21). The modeling of the two modes, slipping and locked-up, is done by a state machine, described in Section 3.1. All equations regarding the mode switching will not be used by the observer. Nevertheless they are useful for discussing some aspects of the mode switching that will give better understanding of the different modes introduced in Section 4.1.

3.1 Lock-Up/Break-Apart Logic

The clutch model has two modes, locked and slipping mode. While in locked mode, the clutch behaves as one rigid body, whereas during slipping the clutch consists of two bodies where each one has an angular velocity and position. Torque from the ICE, M_e, and transmission, M_t, are inputs and angular velocity on both sides, ω_e and ω_t, respectively, are states. The equations are:

Conditions for switching from slipping to locked mode:

$$\omega_e = \omega_t \tag{2}$$
$$|M_{\text{trans}}| \leq M_{\text{trans,s}} \tag{3}$$

Equations for the clutch in locked mode:

$$M_e - M_t = (J_e + J_{\text{fw}} + J_c)\,\dot{\omega}_e \tag{4}$$
$$\omega_c = \omega_e \tag{5}$$
$$M_{\text{trans}} = \frac{M_e J_c + M_t\,(J_e + J_{\text{fw}})}{J_e + J_{\text{fw}} + J_c} \tag{6}$$

Conditions for switching from locked to slipping mode:

$$|M_{\text{trans}}| \geq M_{\text{trans,s}} \tag{7}$$

Equations specific to the clutch in slipping mode:

$$M_{\text{trans}} = \text{sgn}(\underbrace{\omega_e - \omega_t}_{\Delta\omega})\,M_{\text{trans,k}} \tag{8}$$
$$M_e - M_{\text{trans}} = (J_e + J_{\text{fw}})\,\dot{\omega}_e \tag{9}$$
$$M_{\text{trans}} - M_t = J_c\dot{\omega}_t \tag{10}$$

The state machine is validated in Myklebust and Eriksson (2013). If J_c is considered neglectable $M_{\text{trans}} = M_t$ that is the measurement of the torque sensor. Also note that (9) holds in the locked mode as well. For the purpose of the observer the transmitted torque will be modeled as random walk, i.e.

$$\dot{M}_{\text{trans}} = e(t) \tag{11}$$

where $e(t)$ is white noise. How to model M_{trans} when the clutch is slipping will be discussed next.

3.2 Slipping Torque Model Structure

The rest of Section 3 discusses how to model the clutch during slipping, or more precise, how to model $M_{\text{trans,k}}$. $M_{\text{trans,k}}$ depends on several factors such as, actuator position, temperatures, rotational speeds and wear, where the

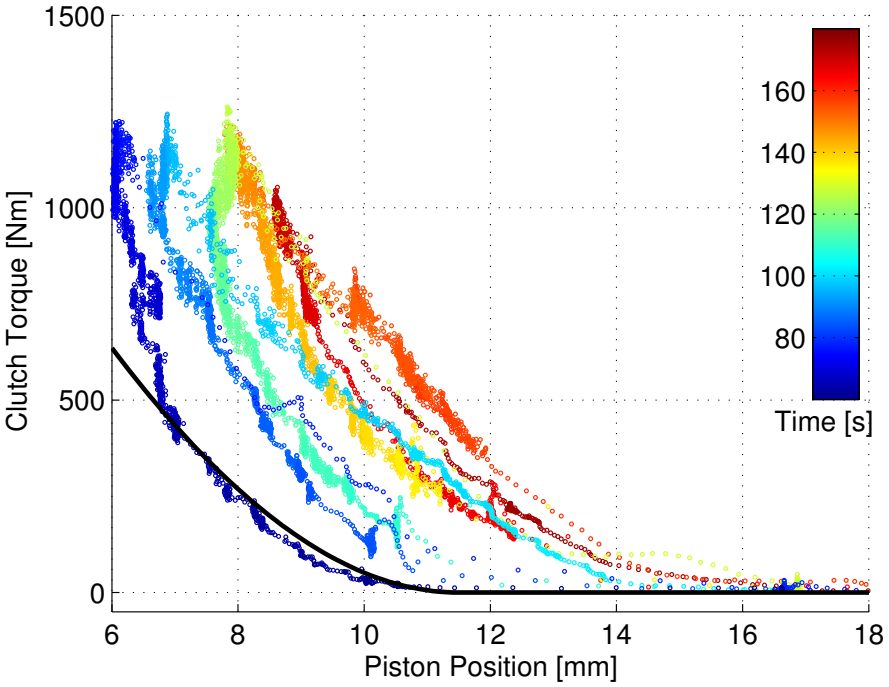

Figure 4: The clutch position, x, has been ramped back and forth while the clutch torque has been measured. During this experiment the truck was held stationary using the parking brake in order to avoid lock-up of the clutch. The transmitted torque clearly depends on something more than the clutch position, in particular there is a drift with time. The torque difference for a given position is up to 940 Nm. The black line is a parameterization of (12).

temperature is the most significant effect. In Figure 4 it is seen how the transmitted torque varies up to 940 Nm for a given position.

The shape of the torque transmissibility curve is mainly due to the cushion spring characteristics. In Dolcini et al. (2010) it is mentioned that this curve can be described by a third order polynomial,

$$M_{\text{ref}}(x_{\text{ref}}) = \begin{cases} a(x_{\text{ref}} - x_{\text{ref,ISP}})^3 \\ +b(x_{\text{ref}} - x_{\text{ref,ISP}})^2 & \text{if } x_{\text{ref}} < x_{\text{ref,ISP}} \\ 0 & \text{if } x_{\text{ref}} \geq x_{\text{ref,ISP}} \end{cases} \tag{12}$$

where x_{ISP} (Incipient Sliding Point) is the kiss point, where the push plate and clutch disc first meet and torque can start to transfer. When the actuator motor is fully retracted (position=0) the expansion can be measured through the position sensor on the slave. This slave position is called the zero position,

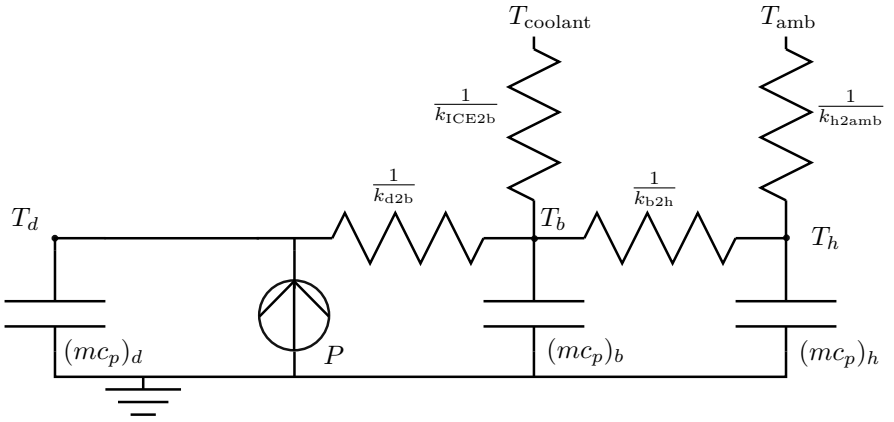

Figure 5: An electrical analogy of the temperature model (14)-(16).

x_0, see Figure 2, and can be modeled as,

$$x_0 = k_{\text{exp},1}\,(T_b - T_{\text{ref}}) + x_{0,\text{ref}} \tag{13}$$

The $x_{0,\text{ref}}$ parameter corresponds to x_0 when the temperature is T_{ref}. The temperature of the clutch body, T_b, is modeled according to the electrical analogy in Figure 5 expressed in equations below.

$$\begin{aligned}(mc_p)_b\dot{T}_b = {} & k_{\text{ICE2b}}(T_{\text{coolant}} - T_b) + k_{\text{b2h}}(T_h - T_b) \\ & + k_{\text{d2b}}(T_d - T_b)\end{aligned} \tag{14}$$

$$(mc_p)_h\dot{T}_h = k_{\text{b2h}}(T_b - T_h) + k_{\text{h2amb}}(T_{\text{amb}} - T_h) \tag{15}$$

$$(mc_p)_d\dot{T}_d = k_{\text{d2b}}(T_b - T_d) + P \tag{16}$$

where,

$$P = M_{\text{trans,k}}\,\Delta\omega \tag{17}$$

$x_{0,\text{ref}}$ will naturally decrease with wear as the friction pads get thinner, see Figure 2. However the thinning of the pads is a slow process and is modeled as

$$\dot{x}_{0,\text{ref}} = 0 \tag{18}$$

This part of the model is simulated in Figure 6. The two integrations in the open-loop simulation give a slow drift. In online applications, this drift can be compensated for using an observer, as in Section 4. In order to model the change in torque the piston position is corrected for the expansion effect of the clutch body and clutch disc to correspond to the actual compression of the flat spring; see Figure 1.

$$x_{\text{cor}} = x - \Delta x_0 \tag{19}$$

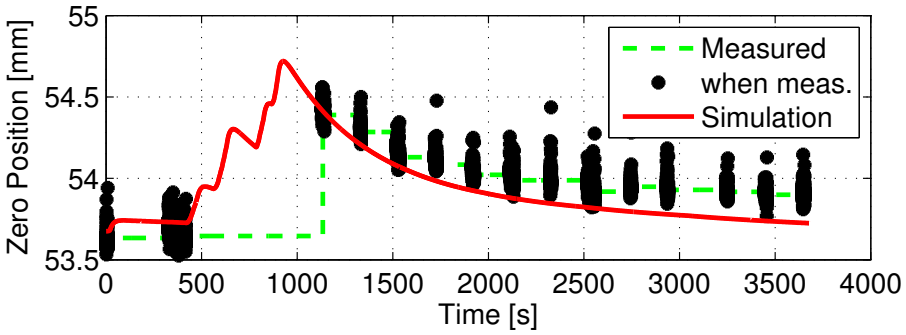

Figure 6: The clutch has been heated through slipping and then left to cool down. The zero position has been recorded as a measure of the expansion. The black dots in the data indicate when the clutch has been closed. The temperature model (13)-(15)- shows good agreement with the measurement.

The expansion of the clutch disc is modeled by extending (13) with an extra term

$$\begin{aligned}\Delta x_0 &= k_{\text{exp}}\left(T_b - T_{\text{ref}}\right) + k_{\text{exp},2}\left(T_d - T_{\text{ref}}\right) = \\ &= k_{\text{exp}}\left(T_b - T_{\text{ref}}\right) + k_{\text{exp},2}\left(\left(T_d - T_b\right) + \left(T_b - T_{\text{ref}}\right)\right) = \\ &= \underbrace{\left(k_{\text{exp}} + k_{\text{exp},2}\right)}_{k_{\text{exp},1}}\left(T_b - T_{\text{ref}}\right) + k_{\text{exp},2}\left(T_d - T_b\right) \end{aligned} \tag{20}$$

where the second term was practically zero during the zero-position measurements due to the fast dynamics of T_d. After applying (19) to the data in Figure 4 the result in Figure 7 is obtained.

The transmitted torque can now be calculated as,

$$M_{\text{trans,k}} = M_{\text{ref}}(x_{\text{cor}}) \tag{21}$$

Note that x_{cor} increases with temperature which in turn makes $M_{\text{trans,k}}$ increase with temperature.

3.3 Torque Sensor

The torque sensor is modeled as,

$$M_{\text{sensor}} = M_{\text{trans}} + M_0 \tag{22}$$

where the offset is slowly varying,

$$\dot{M}_0 = 0 \tag{23}$$

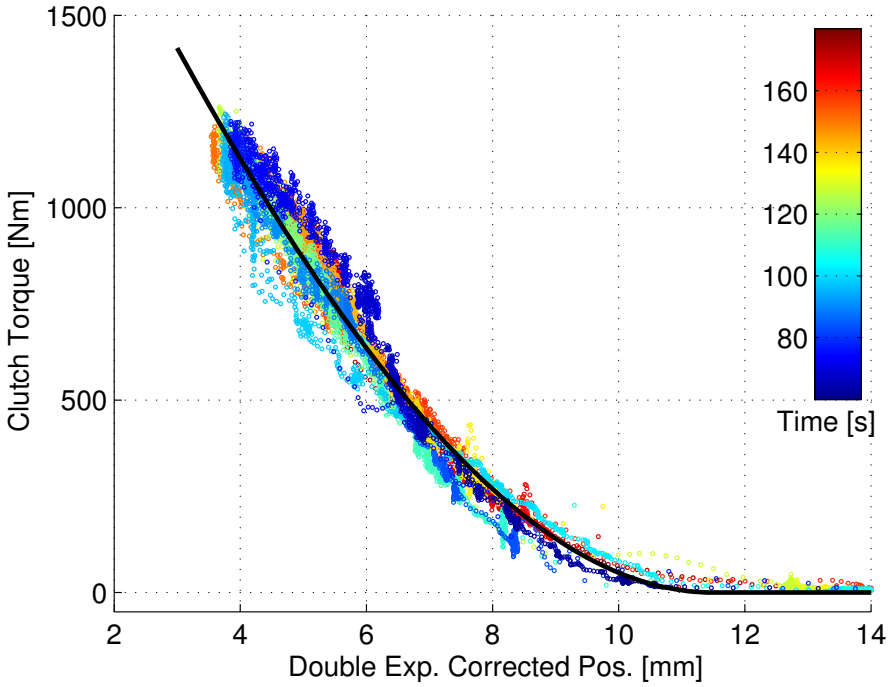

Figure 7: The data from Figure 4 has been corrected for expansion of the clutch body and disc using (19) and (20). The temperature based correction explains the torque drift.

3.4 Clutch Model Validation

The baseline model has been validated in Myklebust and Eriksson (2014, 2013) and Myklebust (2013) and a validation of the parameter estimation for Fronda is shown in Figure 8. That figure contains data similar to that of Figure 6. The modeled torque is usually within 100 Nm of the measured torque (sensor torque with an offline compensation for the sensor offset). All experiments presented here have been performed on a clutch from a different manufacturer than the clutch used in Myklebust and Eriksson (2014) and confirm the previous results on clutch thermal effects.

The clutch temperatures can not be quantitatively validated as no temperature measurements are available. Therefore only a qualitative validation is performed, showing that the magnitudes of the temperature states are reasonable for an HDT clutch, see Figure 8.

4 Observer

As shown in Myklebust and Eriksson (2013) the thermal effects in a dry clutch can have a significant effect on launch control of a vehicle. Controllers that assume the clutch torque to be an controllable input signal, e.g. Dolcini et al. (2008) and Garofalo et al. (2002), would need an underlying compensation of the thermal effect. This could be done like in Deur et al. (2012), although there measurements of the temperature is used. Due to the difficulties involved in measuring the temperatures of rotating bodies, this is not a feasible solution for production vehicles. Instead the model of Section 3 can be used to estimate the temperatures. With the help of an observer the model can be made insensitive to poor initial values and wear (here only considered as a change in $x_{0,\mathrm{ref}}$). The following definitions are made: state vector $X = \left[T_b,\, T_h,\, T_d,\, x_{0,\mathrm{ref}},\, \omega_e,\, M_{\mathrm{trans}},\, M_0\right]^T$, input vector $U = \left[x_p,\, P,\, T_{\mathrm{coolant}},\, T_{\mathrm{amb}}, M_e, \dot{x}\right]^T$ and intermediate output variable $\tilde{y} = \left[x_{\mathrm{cor}},\, M_{\mathrm{sensor}},\, x_0,\, \omega_e\right]^T$. In contrast to Myklebust and Eriksson (2012), x_p is used as input instead of x. This has a positive effect on the observability in Section 4.1. Now, with (20), (19), (21) and (12) the model can be expressed as:

$$\dot{X} = AX + BU \tag{24}$$

$$\tilde{y} = CX + DU + \begin{bmatrix} 1 \\ 0 \\ -1 \\ 0 \end{bmatrix} k_{\mathrm{exp},1} T_{\mathrm{ref}} \tag{25}$$

where,

$$A = \begin{pmatrix} -\frac{k_{\mathrm{b2h}}+k_{\mathrm{ICE2b}}+k_{\mathrm{d2b}}}{(mc_p)_b} & \frac{k_{\mathrm{b2h}}}{(mc_p)_b} & \frac{k_{\mathrm{d2b}}}{(mc_p)_b} & 0\ 0\ 0 & 0 \\ \frac{k_{\mathrm{b2h}}}{(mc_p)_h} & -\frac{k_{\mathrm{b2h}}+k_{\mathrm{h2amb}}}{(mc_p)_h} & 0 & 0\ 0\ 0 & 0 \\ \frac{k_{\mathrm{d2b}}}{(mc_p)_d} & 0 & -\frac{k_{\mathrm{d2b}}}{(mc_p)_d} & 0\ 0\ 0 & 0 \\ 0 & 0 & 0 & 0\ 0\ 0 & 0 \\ 0 & 0 & 0 & 0\ 0\ 0 & \frac{-1}{J_e+J_{\mathrm{flywheel}}} \\ 0 & 0 & 0 & 0\ 0\ 0 & 0 \\ 0 & 0 & 0 & 0\ 0\ 0 & 0 \end{pmatrix} \tag{26}$$

$$B = \begin{pmatrix} 0 & 0 & \frac{k_{\mathrm{ICE2b}}}{(mc_p)_b} & 0 & 0 & 0 \\ 0 & 0 & 0 & \frac{k_{\mathrm{h2amb}}}{(mc_p)_h} & 0 & 0 \\ 0 & \frac{1}{(mc_p)_d} & 0 & 0 & 0 & 0 \\ 0 & 0 & 0 & 0 & 0 & 0 \\ 0 & 0 & 0 & 0 & \frac{1}{J_e+J_{\mathrm{flywheel}}} & 0 \\ 0 & 0 & 0 & 0 & 0 & 0 \\ 0 & 0 & 0 & 0 & 0 & 0 \end{pmatrix} \tag{27}$$

$$C = \left(C_1^T, C_2^T, C_3^T, C_4^T\right)^T = \\ = \begin{pmatrix} -k_{\text{exp},1} + k_{\text{exp},2} & 0 & -k_{\text{exp},2} & -1 & 0 & 0 & 0 \\ 0 & 0 & 0 & 0 & 0 & 1 & 1 \\ k_{\text{exp},1} - k_{\text{exp},2} & 0 & k_{\text{exp},2} & 1 & 0 & 0 & 0 \\ 0 & 0 & 0 & 0 & \frac{30}{\pi} & 0 & 0 \end{pmatrix} \tag{28}$$

$$D = \begin{pmatrix} D_1 \\ D_2 \\ D_3 \\ D_4 \end{pmatrix} = \begin{pmatrix} 1 & 0 & 0 & 0 & 0 & 0 \\ 0 & 0 & 0 & 0 & 0 & 0 \\ 0 & 0 & 0 & 0 & 0 & 0 \\ 0 & 0 & 0 & 0 & 0 & 0 \end{pmatrix} \tag{29}$$

and the measurable model outputs are depending on the mode of operation. E.g. the zero position can only be measured when the clutch is fully closed. There are also some changes of the equations depending on the mode of operation. All this naturally affects observability and observer design, and is therefore analyzed below.

4.1 Observability

When studying the observability of a system the structure is important. Due to the varying nature of the system in this application it is natural to break down the problem into different cases: fully closed, engaged and locked-up, engaged and slipping, and open clutch.

Fully Closed Clutch

When the clutch is fully closed it is not restrictive to assume that the clutch is locked up. Then the clutch torque is a direct response of the engine torque and neither temperature nor clamp load dependent. Therefore the transmitted torque does not contribute with information regarding the temperature states, but the zero position does and can be measured so in this mode the output is:

$$y = \begin{bmatrix} M_{\text{sensor}} \\ x_0 \\ \omega_e \end{bmatrix} = \begin{bmatrix} C_2 \\ C_3 \\ C_4 \end{bmatrix} X + \begin{bmatrix} 0 \\ -1 \\ 0 \end{bmatrix} k_{\text{exp},1} T_{\text{ref}} \tag{30}$$

This subsystem, (24) together with (30), is locally observable according to linear theory, (Rugh, 1996). Note that M_0 is observable due to the inclusion of (9) and (11).

Engaged and Locked-Up Clutch

The clutch does not need to be fully closed in order to be locked-up. If the clutch is not fully closed the piston position does not contain any information about the thermal expansion since an expansion does not alter the piston position, instead it compresses the cushion spring. Furthermore the transmitted torque only gives a lower bound of the stiction torque and therefore the temperature states can be bounded, but not observed. The available measurements are,

$$y = \begin{bmatrix} M_{\text{sensor}} \\ \omega_e \end{bmatrix} = \begin{bmatrix} C_2 \\ C_4 \end{bmatrix} X \tag{31}$$

Rows five to seven of (24) and (31) creates a separate linear subsystem that is observable. So in summary $X_5 - X_7$ are observable but $X_1 - X_4$ are not in this mode.

Engaged and Slipping Clutch

In order to make (21) a state equation for the clutch-torque state (X_6) (21) has to be differentiated with respect to time. The following equation will replace the sixth row of (24) when in the slipping mode.

$$\dot{M}_{\text{trans}} = \dot{M}_{\text{trans,k}} = \frac{\partial M_{\text{ref}}(x_{\text{cor}})}{\partial x_{\text{cor}}} \left(\frac{\partial x_{\text{cor}}}{\partial T} \dot{T} + u_6 \right) \tag{32}$$

where $T = \left[T_b, T_h, T_d \right]^T$. When the clutch is slipping the output is given by:

$$y = h\left(X, U\right) = \begin{bmatrix} M_{\text{sensor}} \\ \omega_e \end{bmatrix} = \begin{bmatrix} C_2 \\ C_4 \end{bmatrix} X + \begin{bmatrix} M_{\text{ref}}(\tilde{y}_1) - X_6 \\ 0 \end{bmatrix} \tag{33}$$

This subsystem is non-linear and observability cannot be examined the same way as the previous modes. Instead a technique for non-linear systems is used, (Hermann and Krener, 1977). Let $\dot{X} = f(X)$ then the following matrix of Lie derivatives,

$$\begin{bmatrix} h_X \\ (L_f h)_X \\ (L_f^2 h)_X \end{bmatrix} \tag{34}$$

has rank seven and thus this subsystem have local weak observability with respect to all states.

Open Clutch

When the clutch is open the transmitted torque is simply zero. This gives a bound on the kiss point and thereby a bound on the temperature states but no observability. As in the case of the engaged and locked clutch $X_5 - X_7$ creates a separate subsystem. However here the equations can be simplified into

$$M_{\text{trans}} = 0 \tag{35}$$

$$\dot{M}_0 = 0 \tag{36}$$

$$y = M_{\text{sensor}} = M_0 \tag{37}$$

where observability is trivial.

Complete System

The complete system with all four different modes is a non-linear system. With non-linear systems the observability can depend on the input signal, (Hermann and Krener, 1977). There exists input-signal trajectories that control the system into the observable mode and therefore the complete system is observable. To obtain observability in practice the system needs to visit the observable mode, i.e. fully closed clutch and slipping clutch. Conveniently enough these modes are frequently visited during normal operation. The sensor offset can always be estimated.

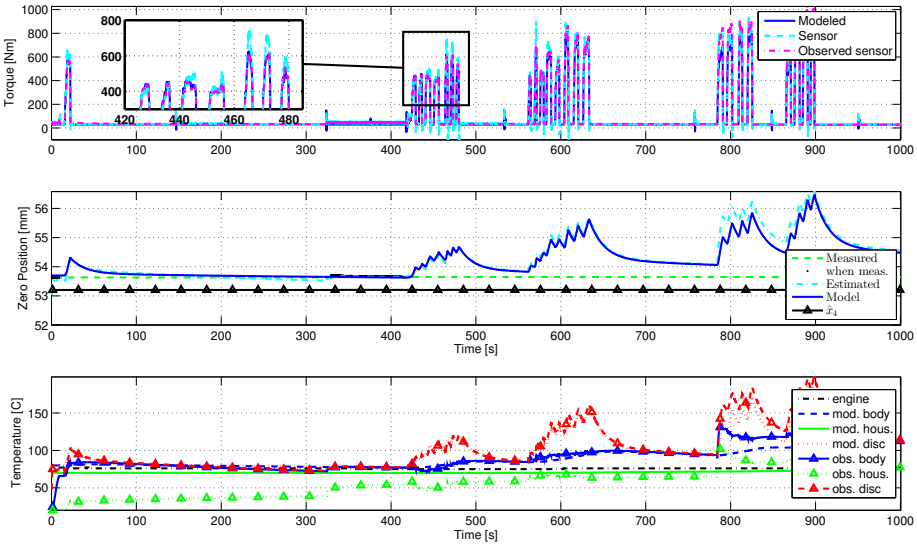

Figure 8: The model simulates the torque and zero position well, given good initial values. The observer states are able to approach the model states although the initial states for the observer are off. The observer states differ somewhat from the modeled states due to better torque estimation.

4.2 Observer Selection and Precautions

The observer is based on the same principles as the one in Myklebust and Eriksson (2014). It is thus an EKF that has limited covariance growth for the states and the main additions are the new measurement and a sensor offset. The differences mean that some modifications are necessary. The model equations and gradients are of course updated, other updates is a Q-matrix with varying elements, see Section 4.3, and the use of an open mode in the observer. In the previous EKF the open mode could be handled by the slipping mode due to the case switching in (12). However in order to avoid state drift during prolonged periods of an open clutch the torque measurement had to be set to zero when below a certain threshold. That is not possible here as the sensor offset has to be estimated, the solution is to let the observer enter an open mode where the equations of Section 4.1 are used. The switching condition to this mode, $x_{\text{cor}}\left(\hat{X}, U\right) > c$, is dependent on the current state estimate. If the observer believes that the clutch is open while it is actually engaged and slipping the EKF will work with the wrong set of model equations. A practical solution to this problem is to change the switching condition to $x_{\text{cor}}\left(\hat{X}, U\right) > c + 2$. Switching conditions for the other modes are $x_m = 0$ for fully closed and $\Delta\omega < \Delta\omega_{\text{threshold}}$ for transition from slipping to locked. Here $\Delta\omega_{\text{threshold}}$ has been given the conservative value of 100 RPM.

4.3 Selection of EKF Covariance Matrices

The Q and R matrices in an EKF has interpretations as the process noise and the measurement noise, respectively. However in practice they are used to tune the trade-off between convergence rate and noise sensitivity. In order to get a good starting point the covariance matrix for the measurement noise was made to roughly match data using the following procedure: All measurements have been manually examined at arbitrary time points and the standard deviations for the assumed white noise were set to approximately match the amplitudes of the noise. Then the variances are put on the diagonal elements of the covariance matrix:

$$R = \begin{bmatrix} 10^{1} & 0 & 0 \\ 0 & 10^{-2} & 0 \\ 0 & 0 & 1.1 \cdot 10^{-3} \end{bmatrix} \tag{38}$$

The covariance matrix for the process noise is also given a diagonal structure as this gives one parameter to tune for each equation. Manual tuning of the observer resulted in the following matrix:

$$Q = \begin{bmatrix} 10^{-1} & 0 & 0 & 0 & 0 & 0 & 0 \\ 0 & 10^{-1} & 0 & 0 & 0 & 0 & 0 \\ 0 & 0 & 10^{-1} & 0 & 0 & 0 & 0 \\ 0 & 0 & 0 & 10^{-8} & 0 & 0 & 0 \\ 0 & 0 & 0 & 0 & 10^{0} & 0 & 0 \\ 0 & 0 & 0 & 0 & 0 & q_{66} & 0 \\ 0 & 0 & 0 & 0 & 0 & 0 & 10^{-4} \end{bmatrix} \tag{39}$$

where q_{66} is 10^3 when the clutch torque is modeled as random walk, 10^2 when the clutch is slipping and 0 when the clutch is open and the clutch torque is zero. $x_{0,\mathrm{ref}}$ and M_0 are varying slowly, therefore the low values of $Q(4,4)$ and $Q(7,7)$.

5 Observer Evaluation

The observer has been validated using measurement data similar to that in Figure 6. Since no temperature measurements are available the model has been simulated using manually tuned initial values, $\begin{bmatrix} T_b,\ T_h,\ T_d,\ x_{0,\mathrm{ref}},\ M_0 \end{bmatrix} = \begin{bmatrix} 80,\ 70,\ 80,\ 53.2,\ 29 \end{bmatrix}$. Given these initial values the model predicts the torque and zero position well, see Figure 8, and therefore these trajectories of the temperature states are those sought by the observer. To test the convergence of the observer the states are given poor initial values, $\begin{bmatrix} T_b,\ T_h,\ T_d,\ x_{0,\mathrm{ref}},\ \omega_e,\ M_{\mathrm{trans}},\ M_0 \end{bmatrix} = \begin{bmatrix} 20,\ 20,\ 20,\ 53.2,\ \frac{500\pi}{30},\ 0,\ 0 \end{bmatrix}$, see Figure 8. The estimate-error covariance matrix is initially set to,

$$P_0 = \begin{bmatrix} 15 & 0 & 0 & 0 & 0 & 0 & 0 \\ 0 & 15 & 0 & 0 & 0 & 0 & 0 \\ 0 & 0 & 15 & 0 & 0 & 0 & 0 \\ 0 & 0 & 0 & 10^{-5} & 0 & 0 & 0 \\ 0 & 0 & 0 & 0 & 0.1 & 0 & 0 \\ 0 & 0 & 0 & 0 & 0 & 15 & 0 \\ 0 & 0 & 0 & 0 & 0 & 0 & 15 \end{bmatrix} \tag{40}$$

$P_0(4,4)$ is given a small value hence $x_{0,\mathrm{ref}}$ is usually well known since the last driving mission. $P_0(5,5)$ is also small because ω_e is directly measured. In the beginning the

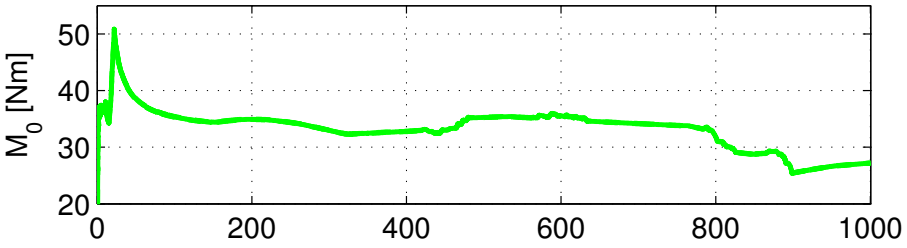

Figure 9: The estimated sensor offset during the simulation shown in Figure 8. The estimated offset quickly recovers from a poor initial value of 0 Nm and after an initial transient there are only slight variations in the estimated offset.

clutch is closed and the zero position can be measured. Therefore the temperature estimates improve quickly, but halts a while when the clutch opens at 9 s. When the clutch starts to slip at 15 s the temperatures converge. For the rest of the simulation the estimated temperatures only have small differences compared to the simulated temperatures. However these differences are actually a result of the fact that the estimated torque is closer to the measured torque than the simulated torque. The estimated sensor offset can be seen in Figure 9. As the test run starts it quickly recovers to a descent value from the poor initial value. After an initial transient there are only slight variations in the estimated offset. This test demonstrates that the observer is able to converge from poor initial values and is therefore a successful augmentation of the observer proposed in Myklebust and Eriksson (2014).

6 Conclusions

A transmission of a heavy duty truck equipped with a torque sensor in the driveline has been studied. The clutch model from Myklebust and Eriksson (2014) is fitted to the clutch of this truck, which is of a different manufacturer compared to the clutch in Myklebust and Eriksson (2014). This provides further validation of the general applicability of the proposed clutch model. The states of the model are estimated with an EKF providing information about both the torque and its transmissibility curve. The main difference compared to Myklebust and Eriksson (2014) is the addition of a torque sensor, which brings additional problems to the state estimation in the form of an additional state for a small but unknown sensor offset as well as new modes in the observer. An observability analysis shows that the system is observable, provided that the system trajectory passes all modes, in particular the sensor offset is always observable if an equation for the engine inertia dynamics is augmented to the model whereas the observability of the temperatures and $x_{0,\mathrm{ref}}$ are unchanged.

An EKF is designed that estimates the states, including the unknown offsets. An evaluation on experimental data shows that the observer converges and estimates temperatures, offsets, and transmitted torque. It is shown to converge from poor initial values, enabling prediction of the translation of the torque transmissibility curve and the current clutch torque, through the combination of the raw sensor output and the estimated offset. The EKF is simple and suitable for real-time applications.

References

Ingemar Andersson, Tomas McKelvey, and Mikael Thor. Evaluation of a vehicle installed closed loop spark advance controller based on a torque sensor. In *SAE Technical Paper: 2008-01-0987*, 2008.

Inc. Audi of America. Variable automatic transmission multitronic 01j, August 2001. Self-Study Program Course Number 951103.

Theodore Bohn, Michael Duoba, and Richard Carlson. In-situ torque measurements in hybrid electric vehicle powertrains. In *23rd International Electric Vehicle Symposium and Exposition 2007*, December 2007.

R. Cowan. Control of powertrain smoothness using output torque sensing and input torque control, January 31 2006. URL `http://www.google.com.br/patents/US6991584`. US Patent 6,991,584.

Josko Deur, Vladmir Ivanovic, Zvonko Herold, and Milan Kostelac. Dry clutch control based on electromechanical actuator position feedback loop. *International Journal of Vehicle Design*, 60(3-4):305–326, 2012.

Pietro Dolcini, Carlos Canudas de Wit, and Hubert Béchart. Lurch avoidance strategy and its implementation in AMT vehicles. *Mechatronics*, 18(1):289–300, May 2008.

Pietro J. Dolcini, Carlos Canudas de Wit, and Hubert Béchart. *Dry Clutch Control for Automotive Applications*. Advances in Industrial Control. Springer-Verlag London, 2010.

Franco Garofalo, Luigi Glielmo, Luigi Iannelli, and Francesco Vasca. Optimal tracking for automotive dry clutch engagement. In *2002 IFAC, 15th Triennial World Congress*, 2002.

R. Hermann and A. Krener. Nonlinear controlability and observability. *IEEE Trans. on Automatic Control*, 22(5):728–740, 1977.

Jongdae Jung, Do Jeong Ryu, Kyung-Seok Jeong, and Keun-Ho Chang. Development of a clutch disk torque sensor for an automobile. In *SAE Technical Paper: 2001-01-0869*, March 2001.

Stefan Larsson and Ingemar Andersson. An experimental evaluation of torque sensor based feedback control of combustion phasing in an SI-engine. In *SAE Technical Paper: 2005-01-0060*, April 2005.

Dongxu Li, Farzad Samie, Kumaraswamy Hebbale, Chunhao Lee, and Chi-Kuan Kao. Transmission virtual torque sensor - absolute torque estimation. In *SAE Technical Paper: 2012-01-0111*, April 2012.

Fredrik Marciszko. Torque sensor based powertrain control. Master's thesis, Linköpings Universitet, SE-581 83 Linköping, 2004.

Andreas Myklebust. Modeling and estimation for dry clutch control. Technical report, Linköping University, 2013. LiU-TEK-LIC-2013:50, Thesis No. 1616.

Andreas Myklebust and Lars Eriksson. Torque model with fast and slow temperature dynamics of a slipping dry clutch. In *2012 IEEE Vehicle Power and Propulsion Conference*, October 2012.

Andreas Myklebust and Lars Eriksson. The effect of thermal expansion in a dry clutch on launch control. In *7th IFAC Symposium on Advances in Automotive Control*, September 2013.

Andreas Myklebust and Lars Eriksson. Modeling, observability, and estimation of thermal effects and aging on transmitted torque in a heavy duty truck with a dry clutch. *IEEE/ASME Transactions on Mechatronics*, PP(99):1–12, 2014.

Yutaka Nonomura, Jun Sugiyama, Koji Tsukada, Masaharu Takeuchi, Koji Itoh, and Toshiaki Konomi. Measurements of engine torque with the intra-bearing torque sensor. In *SAE Technical Paper: 870472*, February 1987.

Hamid Oral. Traction control system using a torque sensor for adaptive engine throttle control. In *SAE Technical Paper: 2010-01-0629*, April 2010.

W. B. Ribbens. A non-contacting torque sensor for the internal combustion engine. In *SAE Technical Paper: 810155*, February 1981.

Wilson J. Rugh. *Linear System Theory*. Prentice-Hall, Inc., second edition, 1996.

Jarl R. Sobel, Jan Jeremiasson, and Christer Wallin. Instantaneous crankshaft torque measurement in cars. In *SAE Technical Paper: 960040*, February 1996.

Mikael Thor, Ingemar Andersson, and Tomas McKelvey. Modeling, identification, and separation of crankshaft dynamics in a light-duty diesel engine. In *SAE Technical Paper: 2009-01-1798*, June 2009.

J.D. Turner. Development of a rotating-shaft torque sensor for automotive applications. *IEE PROCEEDINGS Pt. D*, 135(5):334–338, September 1988.

Paper E

Dry Clutch Micro-Slip Control and Temperature Considerations*

E

*Submitted to *IEEE/ASME Transactions on Mechatronics*.

Dry Clutch Micro-Slip Control and Temperature Considerations

Andreas Myklebust, Lars Eriksson

Vehicular Systems, Department of Electrical Engineering, Linköping University, SE-581 83 Linköping, Sweden

Abstract

With an automatic clutch in the powertrain it is possible to micro-slip the clutch. Micro-slip is a continuous small slip in the clutch used to isolate the driveline from the oscillations in the torque produced by a combustion engine. A control structure has been designed for a micro-slip controller. The basic components are a Linear Quadratic (LQ) controller based on a linearized driveline model and an Extended Kalman Filter (EKF) that can compensate the torque request from the LQ controller for the thermal dynamics of the clutch. To remove some stationary errors, integral action has been added to the LQ controller by adding an extra state. An anti-windup scheme is used, and the additional parameters depend on clutch conditions. The reference slip value is set according to a derived formula for the flywheel-speed-oscillation amplitude together with a dynamic safety margin that can increase during transients. Altogether the controller has a simple structure and there should be no technical problems to implement it in a production vehicle. In simulations with transient torque, unknown road grades, and a mass parameter that has been varied by a factor of 2, the controller is able to follow the slip reference without locking up. The simulations are performed on a non-linear driveline model, previously validated with data, that has been augmented with a model for the oscillative torque produced by the engine in order to more accurately describe micro-slip conditions. The torque model is a sinusoidal model and has been fitted to high resolution data. The oscillation amplitude and frequency agree well with the data. The thermal behavior of a clutch with micro slip is analyzed and the EKF should be used for temperature surveillance together with some suggested counter measures although there were no excessive temperatures during simulations of recorded driving missions. However, the simulations show that the fuel consumption increase might be too large for a heavy-duty-truck application if micro-slip control is to be used at all operating conditions. Further analysis of costs versus benefits are required on a vehicle level but the feasibility of a micro-slip control system for a dry clutch truck has been proven.

1 Introduction

Increasing demands on comfort, performance, and fuel efficiency in vehicles lead to more complex transmission solutions. Historically high efficiency was best accomplished with a classical Manual Transmission and comfort with a hydraulic Automatic Transmission (AT). The Automated Manual Transmission (AMT) is one way to combine the best from two worlds. An important part in an AMT is clutch control that has a profound effect on vehicle performance. One new way to utilize an automatic clutch is micro-slip control. The thought behind micro-slip is to isolate the driveline from the oscillations in the torque produced by the Internal Combustion Engine (ICE) by slipping the clutch. When torque is transmitted to the driveline through a slipping clutch the torque is a result of friction, not combustion events, and is therefore smooth. A measurement showing this effect can be seen in Figure 1. However, when slipping the clutch it will wear and energy is dissipated into the clutch, increasing the fuel consumption and possibly leading to failure due to overheating. Therefore it is of great importance to keep the slipping speed as low as possible, hence the name micro-slip. The idea of micro-slip control in AMTs has been around for over 20 years (Albers, 1990), but the amount of literature on the subject is limited. In Albers (1990) a slip control system and its capability of isolating the driveline from engine oscillations are demonstrated. It is also concluded that the increase in clutch wear is not a problem as long as excessive temperatures are avoided. Furthermore it is seen that above a certain engine speed the vibration isolation is sufficient without micro-slip and slip control can therefore be turned off at high engine speeds. This functionality is confirmed to exist in a production solution in Audi of America (2001). Further confirmation is found in Fischer and Berger (1998) where excitation and resonance frequencies are studied. A remark is that locking the clutch is not only sufficient for vibration oscillation at higher engine speeds, it is also necessary. Moreover it is concluded that the hardware in the driveline's torsion damper can be simplified without sacrifice of comfort if micro-slip is used. Tests in passenger vehicles have been performed in Küpper et al. (2002) and the vibration isolation performance of a single-mass-flywheel slip-controlled vehicle is equal to that of a dual-mass flywheel equipped vehicle without slip control. Only a slight increase in wear was detected and fuel consumption was unchanged. The latter was possible since the smaller inertia of the single-mass flywheel contributed to a lower fuel consumption.

Slip control is also of interest for ATs. To improve the efficiencies of ATs a lock-up clutch (or Torque Converter Clutch (TCC)) is employed inside the Torque Converter (TC) that is capable of locking the pump to the turbine and thereby reducing the slip losses. Although the micro-slip thought is used for the TCC as well to allow a greater lock-up range and thereby improved fuel efficiency (Hiramatsu et al., 1985; Otanez et al., 2008). Both advanced control strategies, e.g. Higashimata et al. (2004), and more straight forward strategies, e.g. Hebbale et al. (2011), have been implemented and tested in passenger vehicles. In Higashimata et al. (2004) the TC is modeled as a linear parameter varying system, and a feedforward link together with a μ-synthesis feedback link is used to control the slip speed of the TCC. The controller is further developed using gain scheduling in Kaneko et al. (2009) and coasting capabilities are introduced in Katsumata et al. (2008). In Hebbale et al. (2011) model based feedforward and slip-references-signal smoothing are used in order to get smooth slip control. Although there are similarities between slip control in an AT and an AMT the two are quite different. In an AT there is a second path for the torque, through the nonlinear TC, which is not present in an AMT. Moreover the actuators are different and AMTs have less heat capacity.

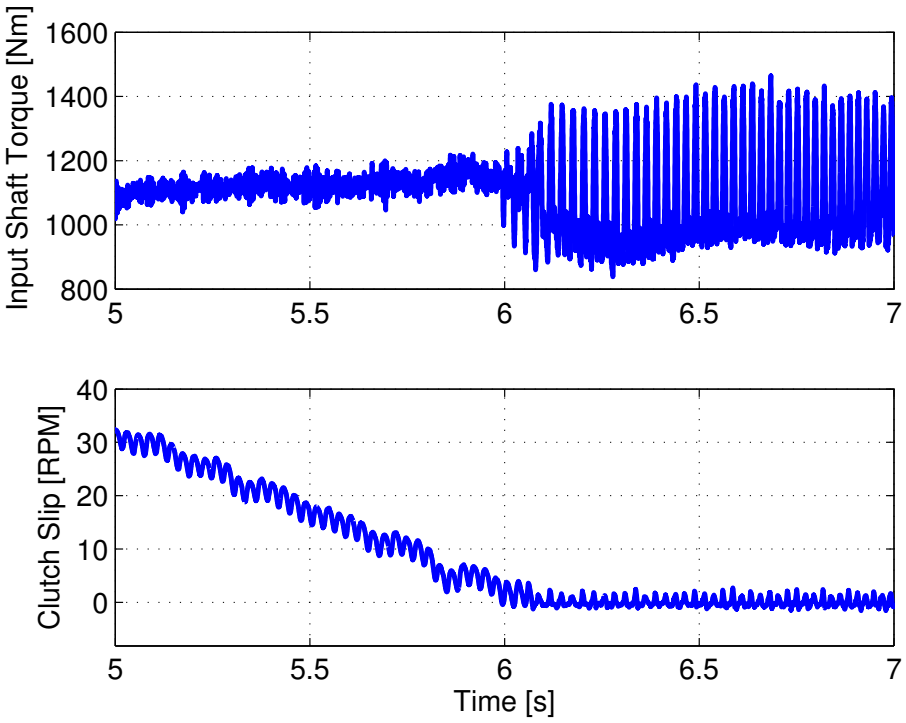

Figure 1: High resolution measurement of the clutch slip and a transmission input shaft torque sensor. The oscillations in the input shaft torque becomes significantly higher when the clutch locks up (zero slip speed) right after 6 s.

1.1 Contributions

Here a slip control system is developed for a Heavy Duty Truck (HDT) together with a physics-based slip-speed-reference framework. The control system consists of a Linear-Quadratic (LQ) optimal controller with integral effect, feedforward and some additional tweaks to increase the control performance. This results in a controller that is computationally simple and therefore suitable for online implementation. The integral part is complemented with conditional integration that is used both when the control signal is saturated (anti-windup) and when it is not. The slip-speed reference is calculated from a derived formula for the flywheel-speed-oscillation amplitude together with a dynamic safety margin. The entire control structure is evaluated using simulations on an earlier validated driveline model that here is augmented with a sinusoidal model for torque fluctuations in the ICE. The oscillation model has been validated using high resolution measurements from a driveline equipped with a torque sensor. Additional contributions are an analysis of the clutch heating and the fuel consumption increase caused by the micro slip through simulation of real-world driving missions.

2 Model

In order to test the performance of the proposed controller a model for vehicle simulation is used. The simulation model is taken from Myklebust and Eriksson (2013). This model contains three flexibilities in the driveline, see Figure 2, driving resistance, locked/slipping-mode transitions for the clutch and a thermal clutch model, see Figure 3. An overview of the complete model is found in Figure 4.

All parts of the model have been thoroughly validated against data with respect to vehicle speed trajectory, vehicle shuffle and the thermal behavior of the clutch. The simulation model is augmented with a model for the oscillative torque produced by the ICE in order to more accurately describe micro-slip conditions in Section 2.2. Moreover,

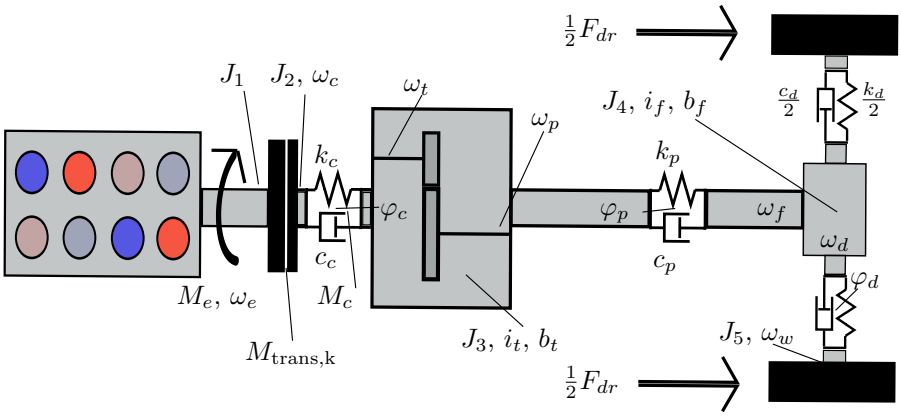

Figure 2: Sketch of the driveline model. Modeled parts and locations of flexibilities, parameters and states are visible. J=inertia, k=stiffness, c=damping, b=friction, i=gear ratio, ω=rotational speed, φ=torsion, M=torque, F=force.

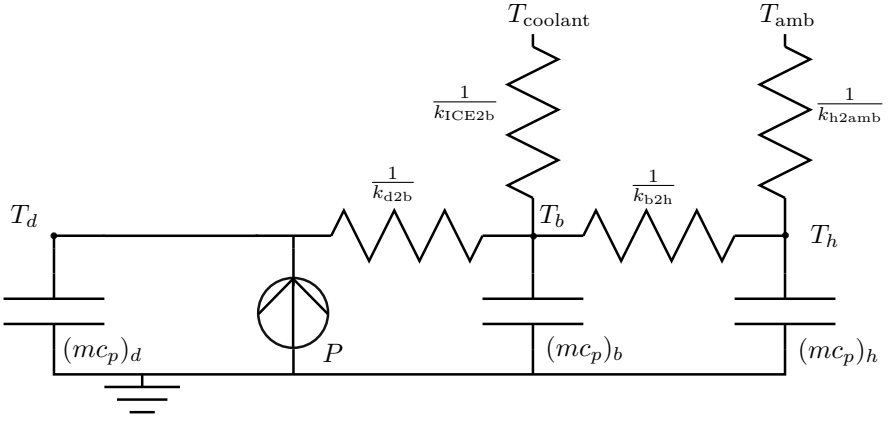

Figure 3: An electrical analogy of the clutch temperature model (1).

in Section 2.1 a simplified driveline model has been derived from the simulation model for controller synthesis. The simplified model contains only one driveline flexibility and considers the clutch torque to be the input signal and the engine torque a measurable disturbance. In addition the aerodynamic resistance is linearized.

When the clutch is slipping with positive slip and positive vehicle speed the simulation model equations can, with the following notation: temperature vector $T = \left[T_b,\, T_h,\, T_d\right]^T$, input vector $U_T = \left[x_p,\, P,\, T_{\text{coolant}},\, T_{\text{amb}}\right]^T$, $P = M_{\text{trans,k}}\,\Delta\omega = M_{\text{trans,k}}\,(\omega_e - \omega_c)$, and x_p is the clutch actuator position, be written as:

$$\dot{T} = A_T\,T + B_T\,U_T \tag{1}$$

$$x_{\text{cor}} = C_T\,T + D_T\,U_T + k_{\text{exp},1}T_{\text{ref}} - x_{0,\text{ref}} \tag{2}$$

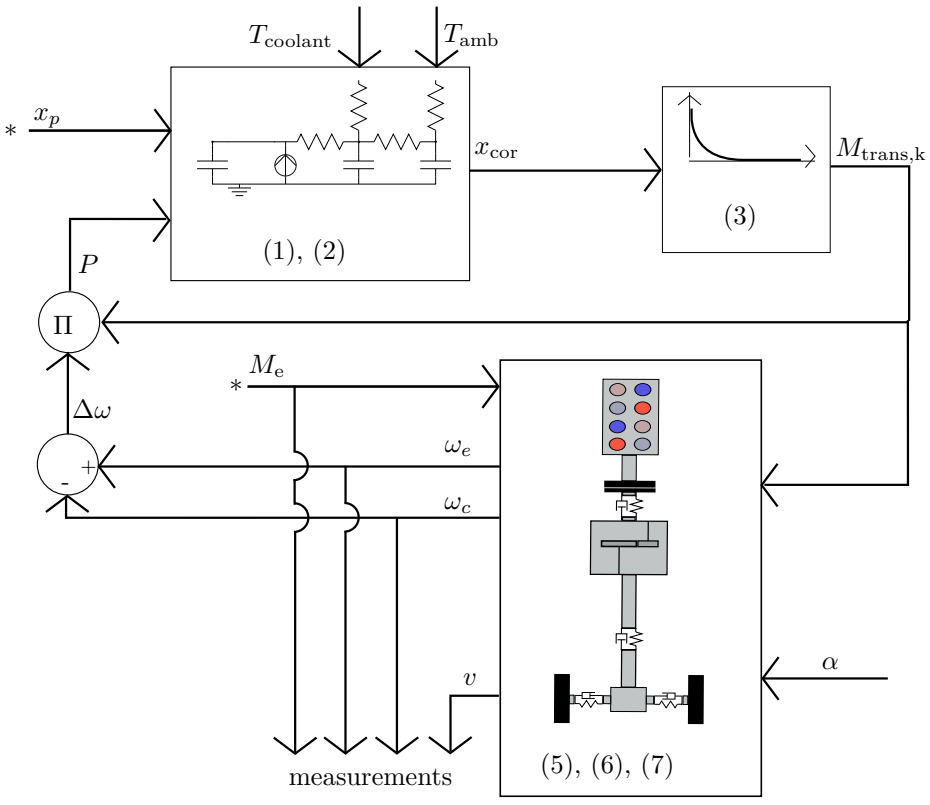

Figure 4: Schematic of how the different submodels are connected and which equations that belong to each submodel. Control signals are marked with a *.

where,

$$A_T = \begin{pmatrix} -\frac{k_{\mathrm{b2h}}+k_{\mathrm{ICE2b}}+k_{\mathrm{d2b}}}{(mc_p)_b} & \frac{k_{\mathrm{b2h}}}{(mc_p)_b} & \frac{k_{\mathrm{d2b}}}{(mc_p)_b} \\ \frac{k_{\mathrm{b2h}}}{(mc_p)_h} & -\frac{k_{\mathrm{b2h}}+k_{\mathrm{h2amb}}}{(mc_p)_h} & 0 \\ \frac{k_{\mathrm{d2b}}}{(mc_p)_d} & 0 & -\frac{k_{\mathrm{d2b}}}{(mc_p)_d} \end{pmatrix}$$

$$B_T = \begin{pmatrix} 0 & 0 & \frac{k_{\mathrm{ICE2b}}}{(mc_p)_b} & 0 \\ 0 & 0 & 0 & \frac{k_{\mathrm{h2amb}}}{(mc_p)_h} \\ 0 & \frac{1}{(mc_p)_d} & 0 & 0 \end{pmatrix}$$

$$C_T = \begin{pmatrix} -k_{\mathrm{exp},1} + k_{\mathrm{exp},2} & 0 & -k_{\mathrm{exp},2} \end{pmatrix}$$

$$D_T = \begin{pmatrix} 1 & 0 & 0 & 0 \end{pmatrix}$$

Equation (2) gives the compression of the non-linear flat spring, x_{cor}, located inside the clutch disc. The spring compression corresponds to a clamping force that in turn corresponds to a transmitted clutch torque,

$$M_{\mathrm{trans,k}} = \begin{cases} a(x_{\mathrm{cor}} - x_{\mathrm{kiss}})^3 & \\ +b(x_{\mathrm{cor}} - x_{\mathrm{kiss}})^2 & \text{if } x_{\mathrm{cor}} < x_{\mathrm{kiss}} \\ 0 & \text{if } x_{\mathrm{cor}} \geq x_{\mathrm{kiss}} \end{cases} \tag{3}$$

where x_{kiss} is the clutch kiss point, i.e. where disc and push plate make contact. For the driveline part of the model the state vector X_d that consists of rotational speeds and torsions,

$$X_d = \begin{bmatrix} \omega_e, \, \omega_c, \, \varphi_c, \, \omega_p, \, \varphi_p, \, \omega_d, \, \varphi_d, \, \omega_w \end{bmatrix}^T \tag{4}$$

F_{dr}, the driving resistance (sum of aerodynamic, rolling, and gravitational resistance), Y, the available measurements, and $U_d = \begin{bmatrix} M_e, \, M_{\mathrm{trans,k}} \end{bmatrix}^T$, the input vector, are defined. Now the driveline dynamics can be expressed as,

$$\dot{X}_d = A_d \, X_d + B_d \, U_d + \begin{bmatrix} 0, 0, 0, 0, 0, 0, 0, \frac{-r_w F_{\mathrm{dr}}}{J_5} \end{bmatrix}^T \tag{5}$$

$$Y = C_d \, X_d \tag{6}$$

with,

$$A_d = \begin{pmatrix} 0 & 0 & 0 & 0 & 0 & 0 & 0 & 0 \\ 0 & \frac{-c_c}{J_2} & \frac{-k_c}{J_2} & \frac{c_c i_t}{J_2} & 0 & 0 & 0 & 0 \\ 0 & 1 & 0 & -i_t & 0 & 0 & 0 & 0 \\ 0 & \frac{c_c i_t}{J_3} & \frac{k_c i_t}{J_3} & \frac{-c_1}{J_3} & \frac{-k_p}{J_3} & \frac{c_p i_f}{J_3} & 0 & 0 \\ 0 & 0 & 0 & 1 & 0 & -i_f & 0 & 0 \\ 0 & 0 & 0 & \frac{c_p i_f}{J_4} & \frac{k_p i_f}{J_4} & \frac{-c_2}{J_4} & \frac{-k_d}{J_4} & \frac{c_d}{J_4} \\ 0 & 0 & 0 & 0 & 0 & 1 & 0 & -1 \\ 0 & 0 & 0 & 0 & 0 & \frac{c_d}{J_5} & \frac{k_d}{J_5} & \frac{-c_d}{J_5} \end{pmatrix}$$

$$c_1 = c_c i_t^2 + b_t + c_p, \quad c_2 = c_p i_f^2 + b_f + c_d$$

$$B_d^T = \begin{pmatrix} \frac{1}{J_1} & 0 & 0 & 0 & 0 & 0 & 0 & 0 \\ -\frac{1}{J_1} & \frac{1}{J_2} & 0 & 0 & 0 & 0 & 0 & 0 \end{pmatrix}$$

$$C_d = \begin{pmatrix} 1 & 0 & 0 & 0 & 0 & 0 & 0 & 0 \\ 0 & 1 & 0 & 0 & 0 & 0 & 0 & 0 \\ 0 & 0 & 0 & 0 & 0 & 0 & 0 & r_w \end{pmatrix}$$

$$F_{\mathrm{dr}} = f_a v^2 + (f_r + \sin(\alpha))\, mg \tag{7}$$

where $v = r_w x_{d,8}$ is the vehicle speed and α is the road inclination angle. The only controllable inputs of the model (1)-(7) are M_e and x_p. Although M_e is actually controlled via a request to the engine control unit, M_{req}, M_e follows M_{req} in this model. During simulations limitations in the transient performance of the ICE has been considered through the choice of M_{req}.

2.1 Control Model

The driveline model has been simplified for purposes of control synthesis. This is important for keeping the control system complexity down. Only the case of a slipping clutch with positive slip speed has been considered in the simplified model in order to avoid non-linearities. Furthermore the driveshafts are the only flexibility in the driveline that is modeled, because it is the most significant flexibility. This simplification reduces the number of states and parameters. Moreover it is not limiting to assume that the vehicle speed, v, is positive since the clutch disc needs to approach the engine idle speed before micro-slip is possible. Due to the cascade control structure chosen in Section 3 $M_{\mathrm{trans,k}}$ is considered as an input. In the simulation model the clutch actuator dynamics,

$$x_p(t) = f\left(x_{\mathrm{p,req}}(t - \tau_d)\right) \tag{8}$$

is modeled as a time delay, τ_d, and a rate limitation. Unhandled time delays can give rise to oscillatory behavior in controlled systems. Therefore the time delay in the actuator is modeled as a time delay in the clutch torque. In order to get a simple and linear system the time delay is modeled using a first-order system with time constant equal to the time delay. A control model is obtained by simplifying the model (5)-(8) according to the above assumptions,

$$\dot{X} = A_c\, X + B_c\, U + \left[0, 0, 0, \tfrac{-r_w F_{\mathrm{dr}}}{J_5}, 0\right]^T \tag{9}$$

$$Y = C_c\, X \tag{10}$$

with,

$$A_c = \begin{pmatrix} 0 & 0 & 0 & 0 & -\frac{1}{J_1} \\ 0 & \frac{-c}{i_{\mathrm{tot}}^2 J_2'} & \frac{-k}{i_{\mathrm{tot}} J_2'} & \frac{c}{i_{\mathrm{tot}} J_2'} & \frac{1}{J_2'} \\ 0 & \frac{1}{i_{\mathrm{tot}}} & 0 & -1 & 0 \\ 0 & \frac{c}{i_{\mathrm{tot}} J_5} & \frac{k}{J_5} & \frac{-c}{J_5} & 0 \\ 0 & 0 & 0 & 0 & \frac{-1}{\tau_d} \end{pmatrix}$$

$$B_c^T = \begin{pmatrix} \frac{1}{J_1} & 0 & 0 & 0 & 0 \\ 0 & 0 & 0 & 0 & \frac{1}{\tau_d} \end{pmatrix}$$

$$C_c = \begin{pmatrix} 1 & 0 & 0 & 0 & 0 \\ 0 & 1 & 0 & 0 & 0 \\ 0 & 0 & 0 & r_w & 0 \end{pmatrix}$$

Note that (9) is non-linear as F_{dr} depends on v^2. The state vector X consists of the engine speed, the friction pad speed, the driveshaft torsion, wheel rotational

speed, and the clutch torque, $X = \left[\omega_e,\, \omega_c,\, \varphi_d,\, \omega_w,\, M_{\text{trans,k}}\right]^T$, the input vector is $U = \left[M_e,\, M_{\text{trans,k,req}}\right]^T$, and $i_{\text{tot}} = i_t i_f$. The parameters k, c, and J_2' can be estimated so that the control model fits data or calculated as lumped parameters from the simulation model.

$$\frac{1}{k} = \frac{1}{k_d} + \frac{1}{k_p i_f^2} + \frac{1}{k_c i_{\text{tot}}^2} \tag{11}$$

$$\frac{1}{c} = \frac{1}{c_d} + \frac{1}{c_p i_f^2} + \frac{1}{c_c i_{\text{tot}}^2} \tag{12}$$

$$J_2' = J_2 + \frac{J_3}{i_t^2} + \frac{J_4}{i_{\text{tot}}^2} \tag{13}$$

Linearization

In order to facilitate the use of linear model-based techniques for the controller synthesis the system is linearized. Since the system parameter i_t already is gear dependent it is natural to make (at least) one linearization point per gear. The most natural point to linearize around is the middle of the speed range for the ICE (1500 RPM) and slightly lower for the clutch speed since it is micro slipping, i.e.,

$$x_{1,\text{lin}} = 1500\pi/30 \tag{14}$$

$$x_{2,\text{lin}} = 1475\pi/30 \tag{15}$$

$$x_{4,\text{lin}} = x_{2,\text{lin}}/i_{\text{tot}} \tag{16}$$

$$x_{3,\text{lin}} = r_w F_{\text{dr}}\left(x_{4,\text{lin}}\right)/k \tag{17}$$

$$x_{5,\text{lin}} = r_w F_{\text{dr}}\left(x_{4,\text{lin}}\right)/i_{\text{tot}} \tag{18}$$

$$u_{1,\text{lin}} = u_{2,\text{lin}} = x_{5,\text{lin}} \tag{19}$$

The only non-linearity in the control model is the aerodynamic drag in the driving resistance force. The first-order Taylor expansion around $x_{4,\text{lin}}$, assuming flat road, $\alpha = 0$, is

$$F_{\text{dr}} = f_a r_w^2 x_4^2 + f_r mg = \tag{20}$$

$$= F_{\text{dr}}(x_{4,\text{lin}}) + 2 f_a r_w^2 x_{4,\text{lin}}(x_4 - x_{4,\text{lin}}) + \mathcal{O}\left((x_4 - x_{4,\text{lin}})^2\right) \tag{21}$$

This gives the addition

$$\Delta a_{c,4,4} = \frac{-2 f_a r_w^3 x_{4,\text{lin}}}{J_5} \tag{22}$$

to element $a_{c,4,4}$ in A_c. By using $A_{\text{c,lin}} = A_c|_{a_{c,4,4}=\frac{-c}{J_5}+\Delta a_{c,4,4}}$, $X_\Delta = X - X_{\text{lin}}$, $U_\Delta = U - U_{\text{lin}}$, and $Y_\Delta = Y - C_c X_{\text{lin}}$ the control model can be written as a linear system.

$$\dot{X}_\Delta = A_{\text{c,lin}}\, X_\Delta + B_c\, U_\Delta \tag{23}$$

$$Y_\Delta = C_c\, X_\Delta \tag{24}$$

2.2 Oscillating Torque Model

When micro-slipping, the lower limit of the slip is set by the amplitude of the speed oscillations of the flywheel, (Hiramatsu et al., 1985) and (Albers, 1990). Therefore it is

useful to extend the simulation model with a model for the engines torque fluctuations. Data has been collected using an HDT equipped with a precise torque sensor on the input shaft of the transmission. Both the torque sensor and the standard speed sensors have been sampled at 10 kHz so the torque and speed oscillations are clearly visible, see Figure 1 or Figure 5. For details about the experimental setup see Myklebust and Eriksson (2014b).

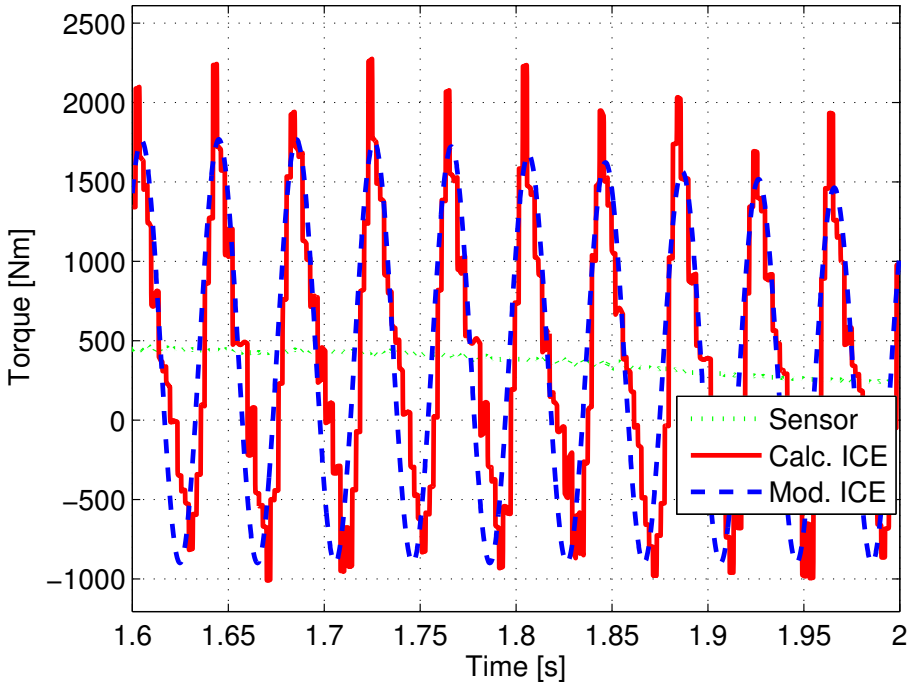

Figure 5: The calculated engine torque oscillations are compare to those modeled with (26)-(27). The fit is good and can handle that the measured mean torque is changing. The value of the peak torque has been sacrificed for better fit during the rest of the oscillation. The parameter estimation was performed on a different data set from that shown in the figure.

First the ICE net torque oscillations must be calculated since the torque sensor is located on the input shaft, i.e. it measures M_c, see Figure 2. To calculate the net torque, M_e, data when the clutch is slipping has been chosen. The benefit of using slipping data is that the smooth torque will keep the clutch torsion (fairly) constant and it can be assumed that $M_{\text{trans,k}} = M_c$. Then the net torque can be calculated as,

$$M_e = M_c + J_1 \dot{\omega}_e \tag{25}$$

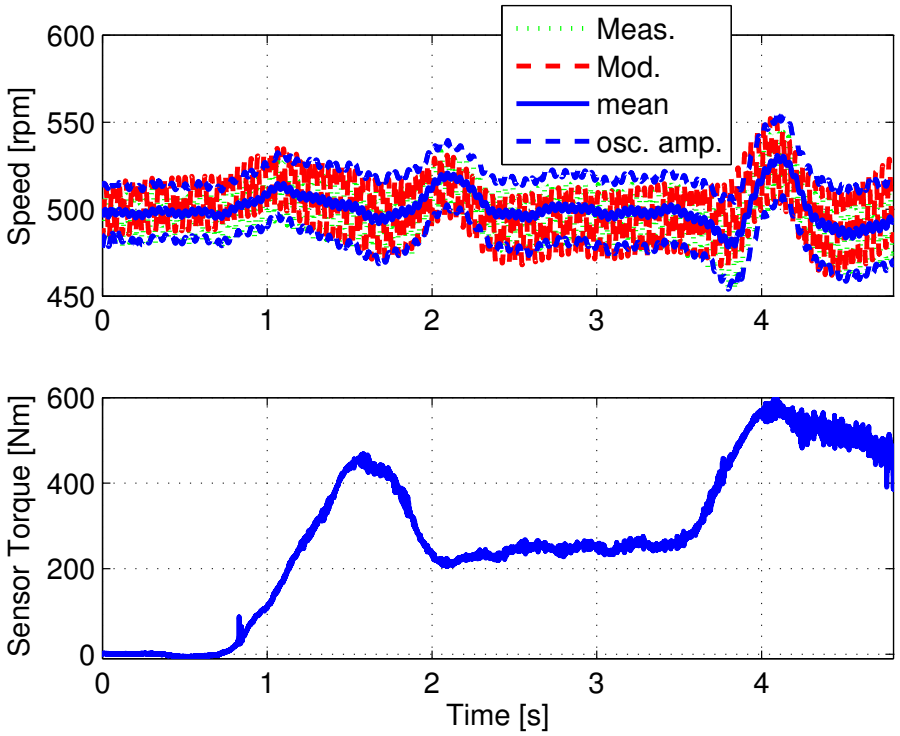

Figure 6: Simulated engine speed using (25)-(27). The fit is good with respect to oscillation amplitude and frequency during varying mean torque. Also seen in the figure is the mean speed and the oscillation amplitude calculated with (29). The formula agrees well with the data. The parameter estimation was performed on a different data set from that shown in the figure.

Second a sinusoidal model can be fitted to the calculated M_e. The model is

$$M_e = \overline{M}_e + k_{\text{osc}} \left(\overline{M}_e + M_{\text{idle}} \right) \sin \left(\frac{n_{\text{cyl}} \theta_e}{2} \right) \tag{26}$$

$$\theta_e = \int_0^t \omega_e \, \mathrm{d}t + \theta_{e,0} \tag{27}$$

where $\overline{M}_e$ is the mean ICE net torque and can be calculated as a rolling average of ± 1000 samples of M_e from (25). In the simulation model $\overline{M}_e$ is taken as M_{req}. First, $k_{\text{osc}} M_{\text{idle}}$ is tuned to data when the truck is idling. Second k_{osc} is tuned to data when the truck is not idling. A validation of the model with a separate data set can be seen in Figure 5.

The torque model has also been confirmed to give correct speed oscillations by plugging (26) into (25) and simulating the engine speed. The result is seen in Figure 6. The important knowledge for the control system is the oscillation amplitude, and it can be calculated from the torque model. Plug the torque model (26)-(27) into (25)

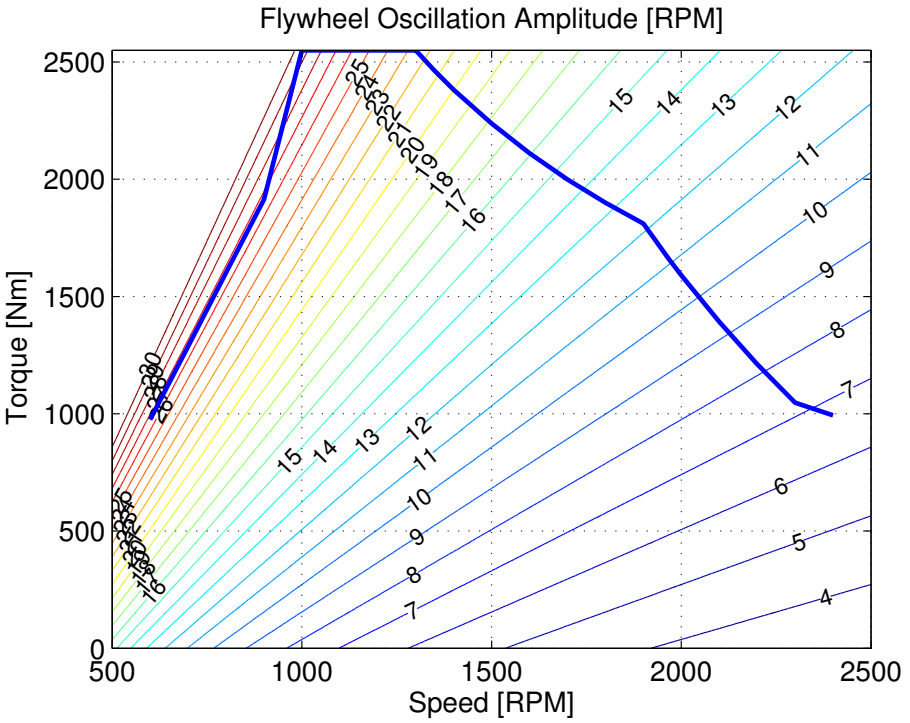

Figure 7: Calculated amplitude of engine speed oscillations at the flywheel. The blue thick line is the maximum torque for the inline six cylinder engine and the contour lines shows the amplitude. The peak value of the oscillations is almost 30 RPM, significantly more than in Figure 8.

and assume steady state conditions, i.e. $\overline{M}_e = M_c$ and a constant mean speed $\bar{\omega}_e$, and $\theta_{e,0}$ can be set to zero with out loss of generality. Then

$$\begin{aligned} J_1\dot{\omega}_e &= k_{\text{osc}}\left(\overline{M}_e + M_{\text{idle}}\right)\sin\left(\frac{n_{\text{cyl}}\bar{\omega}_e}{2}t\right) \Leftrightarrow \\ \omega_e &= \int_0^t \frac{k_{\text{osc}}}{J_1}\left(\overline{M}_e + M_{\text{idle}}\right)\sin\left(\frac{n_{\text{cyl}}\bar{\omega}_e}{2}\tau\right)\mathrm{d}\tau = \\ &= \frac{k_{\text{osc}}}{J_1}\left(\overline{M}_e + M_{\text{idle}}\right)\frac{2}{\bar{\omega}_e n_{\text{cyl}}}\left[-\cos\left(\frac{n_{\text{cyl}}\bar{\omega}_e}{2}\tau\right)\right]_0^t \end{aligned} \tag{28}$$

and it is clear that the oscillation amplitude will be

$$A_\omega\left(\overline{M}_e, \bar{\omega}_e\right) = \frac{2k_{\text{osc}}\left(\overline{M}_e + M_{\text{idle}}\right)}{J_1\bar{\omega}_e n_{\text{cyl}}} \tag{29}$$

This formula has been validated against data in Figure 6.

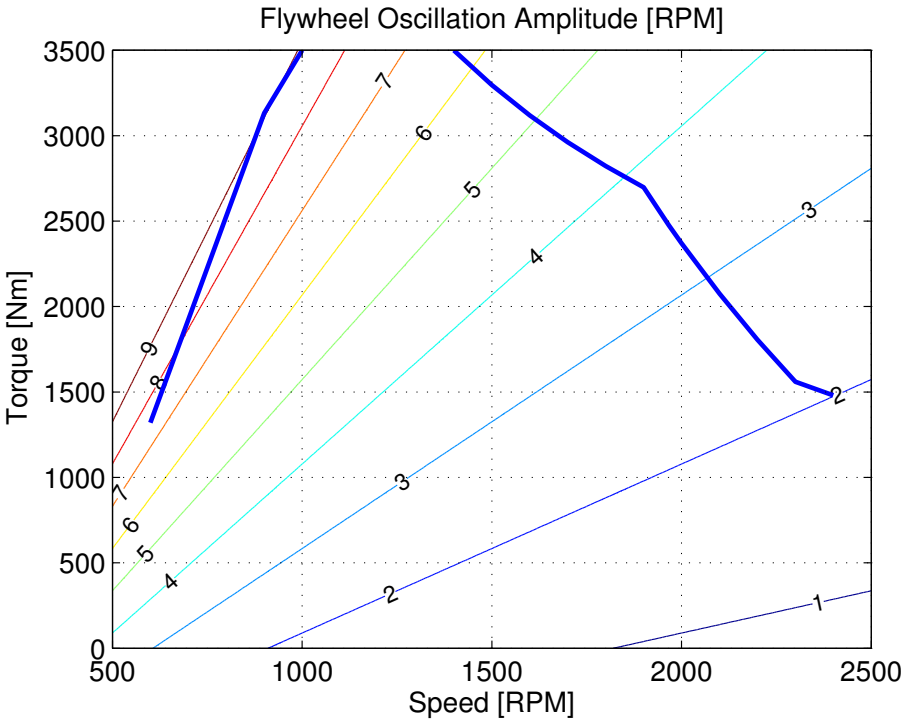

Figure 8: Calculated amplitude of engine speed oscillations at the flywheel. The blue thick line is the maximum torque for the V8 engine and the contour lines shows the amplitude. The peak value of the oscillations is 9 RPM, significantly less than in Figure 7.

Number of Cylinders

The experimental data presented here is for a Scania inline six cylinder engine. Therefore a six cylinder engine was simulated using a complex engine model that models individual cylinder pressures and piston masses as well as crankshaft flexibilities, (Eriksson et al., 2013). It was not tuned to data, it was only used to check that the shape of the calculated M_e trajectory is feasible. Nevertheless two more cylinders were added in the complex model without changing any other parameters except for the ignition sequence. The oscillations were seen to have reduction corresponding to a factor of $1/2$ in k_{osc}. If a Scania V8 engine is to be simulated the decrease in k_{osc} together with an increase in J_1 and n_{cyl} will result in a large reduction in A_ω, see Figure 7 for an engine map that shows A_ω for the L6 engine and Figure 8 for a map of the V8. Since the L6 engine causes a more difficult control problem it will be the primary target here.

Sensor Dynamics

The speed sensors signals available to the transmission control unit are not fast enough to capture the firing sequence oscillations in the powertrain. Therefore the simulation model needs to be augmented with some sensor dynamics in order to simulate realistic control performance. The sensors have been modeled as second-order low-pass filters.

$$\Omega_{\text{sensor}} = \frac{\omega_n^2}{s^2 + 2\zeta\omega_n s + \omega_n^2}\Omega_{\text{true}} \tag{30}$$

where ω_n is the natural frequency of the filter and ζ is the damping.

3 Controller

A micro-slip controller has been designed and tested on the simulation model. A natural control structure would be to use the M_e to control the slip speed and $M_{\text{trans,k}}$ to control the vehicle motion (v, φ_d or some other variable) as requested by the driver since a powertrain with a slipping clutch has a triangular structure.

$$\begin{pmatrix} \Delta\omega \\ v \end{pmatrix} = \begin{pmatrix} G_{11} & G_{12} \\ 0 & G_{22} \end{pmatrix} \begin{pmatrix} M_e \\ M_{\text{trans,k}} \end{pmatrix} \tag{31}$$

Nonetheless the driver request is interpreted as a requested engine torque, M_{req} and M_e is therefore not considered a controllable variable in the micro-slip controller. It is instead handled as a measurable disturbance. A motivation for this is stringent requirements on functional safety within the automotive industry, specifically the requirements regarding unintended torque, (Eriksson and Nielsen, 2014). This design choice also avoids some problems regarding the higher maximum actuation rate of the clutch compared to the ICE as well as coordinated control of two control units. The controller structure is shown in Figure 9.

In similar control problems, like Pettersson and Nielsen (2003) where vehicle speed control with active damping by engine control is studied or Dolcini et al. (2010) where slip control during a launch is studied, it has been successful to use a driveshaft model of the driveline in order to design an LQ-controller. In Pettersson and Nielsen (2003) the clutch was assumed locked and in Dolcini et al. (2010) the clutch torque has been assumed directly controllable and the aerodynamic drag has been neglected instead of linearized since it is small during launch. Due to the previous success of the LQ-controller, the simple implementation and its (often) good robustness properties this is the choice of controller. To avoid stationary errors during accelerations integral action is added to the LQ-scheme. The LQ-controller will due to the structure of the control model, (23) have the clutch torque as control variable. The clutch torque is only controllable through the clutch actuator position x_p and therefore the clutch torque is converted into a position using a look-up table of (3). However, this position needs to be adjusted for the temperature effects in the clutch. That is done by utilizing the implementation of the Extended Kalman Filter (EKF) done in Myklebust and Eriksson (2014a). A feedback link could be added here to ensure that the correct clutch torque is actuated but that is not necessary here since the clutch torque already is part of a supervisory control loop.

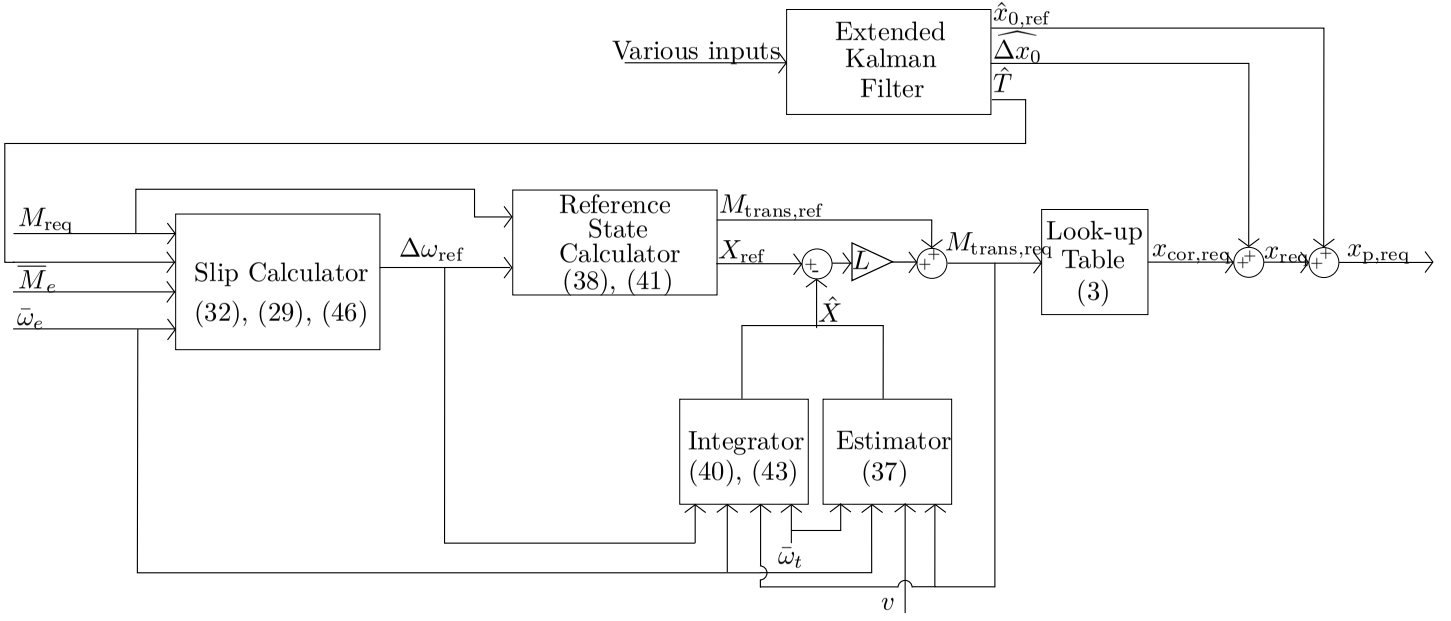

Figure 9: Schematic over the controller. The various subsystem, their interactions and respective equations can be seen. Equations (40) and (41) are made obsolete in Section 3.3 but are included in the schematic since they are more intuitive than (43).

3.1 Reference Slip

A reference value needs to be set for the slip-speed controller. The absolute minimum value for the slip is A_ω calculated with (29). Some error margin should be given to the controller so $A_{\text{margin}} = 1$ rad/s is added to A_ω. During evaluation of the controller it was found useful to give the controller some extra margin of error when there is a sudden torque drop in the driveline. This has been implemented by using a factor that is proportional to the derivative of the requested torque with a lower (unit) limit and a rate limiter when the factor is decreasing. The former so that the margin is never lowered and the latter to avoid sharp transients after the torque drop. In summary,

$$\Delta\omega_{\text{ref}} = f\left(-2 \cdot 10^{-4} \frac{\mathrm{d}M_{\text{req}}}{\mathrm{d}t}\right)(A_\omega + A_{\text{margin}}) \tag{32}$$

where $f(\cdot)$ is the lower saturation limit and negative-rate limiter. In the simulations M_{req} has been smooth and thereby easy to differentiate but in a production vehicle some filtering might be necessary as M_{req} corresponds to the driver request.

3.2 Observer

When controlling a clutch it is of importance to compensate for the thermal dynamics of the clutch, (Myklebust and Eriksson, 2013). In order to do that the temperatures are needed. They also have a direct use in the controller for overheat protection, see Section 5. The temperatures can not be measured and a simulation will have problems with initial values and drift. Therefore an observer is used. The observer used here is developed in Myklebust and Eriksson (2014a) and the details are given in the reference. The observer is an EKF that estimates the clutch temperatures and thereby the shift of the torque transmissibility curve, Δx_0. In addition it estimates a wear parameter, $x_{0,\text{ref}}$, that corresponds to the thinning of the clutch friction pads. These two estimates are used to compensate the output of the look-up table for the thermal effects inside the clutch.

$$x_{\text{p,req}} = x_{\text{cor,req}} + \widehat{\Delta x_0} + \hat{x}_{0,\text{ref}} \tag{33}$$

where $x_{\text{cor,req}}$ is the output of the look-up table.

3.3 LQ-Design

The heart in the micro-slip controller is the LQ or Linear Quadratic controller. The basic theory about the LQ technique can be read about in Glad and Ljung (2003) or Skogestad and Postlethwaite (2007). The principle is to minimize a quadratic cost function,

$$J = \int ||Z - R||^2_{Q_1} + ||U - U_{\text{ref}}(R)||^2_{Q_2}\ \mathrm{d}t \tag{34}$$

where Z is the vector of performance variables,

$$Z = MX_\Delta \tag{35}$$

and $U_{\text{ref}}(R)$ is chosen to give $Z = R$ in steady state. The resulting controller will be on the form

$$U = U_{\text{ref}}(R) + L\left(X_{\text{ref}}(R) - \hat{X}\right) \tag{36}$$

where $X_{\text{ref}}(R)$ is the stationary values when $Z = R$ and L is the state feedback gain given by the minimization of (34) while X_Δ is constrained by the model (23). During the minimization the first column of B_c was omitted since u_1 is considered a disturbance. Here the performance variable is the slip speed so that $R = \Delta\omega_{\text{ref}}$ and $M = \begin{bmatrix}1, -1, 0, 0, 0\end{bmatrix}$. The tuning of the Q_1 and Q_2 matrices will be discussed in Section 3.3 but first some other considerations.

State Feedback

An LQ controller requires full state feedback but only three out of five states are measured. The unmeasured states have simply been simulated using the control model.

$$\hat{X} = \begin{pmatrix} \bar{\omega}_e \\ \bar{\omega}_t \\ \int \left(\frac{\bar{\omega}_t}{i_{\text{tot}}} - \frac{v}{r_w} \right) \mathrm{d}t \\ v/r_w \\ \frac{1}{\tau_d s + 1} M_{\text{trans,req}} \end{pmatrix} \tag{37}$$

$\hat{x}_5$ is a stable system but $\hat{x}_3$ will probably suffer from drift and poor initial values in a production solution. This could be solved using an observer or $\hat{x}_3$ could simply be calculated from the shaft torque during steady-state operation. The latter approach keeps the complexity of the controller low. This simple approach to the estimation problem is the reason that control problem is considered as an LQ formulation and not an LQG.

Feedforward and Reference State Calculation

For target tracking to work in the LQ scheme reference states, X_{ref}, and a reference (feedforward) control signal, U_{ref}, are needed in the control law, (36). If the reference signal, R, is assumed constant the reference values are those that give $Z = R$ when (9) is in steady state. The reference values are therefore a function of $\Delta\omega$ as well as the measurable disturbance M_{req}

$$\begin{aligned} U_{\text{ref}} &= M_{\text{req}} \\ X_{\text{ref}} &= \begin{pmatrix} x_{2,\text{ref}} + \Delta\omega_{\text{ref}} \\ i_{\text{tot}} x_{4,\text{ref}} \\ \frac{i_{\text{tot}} M_{\text{req}}}{k} \\ \sqrt{\frac{i_{\text{tot}} M_{\text{req}} - r_w f_r m g}{f_a r_w^3}} \\ M_{\text{req}} \end{pmatrix} \end{aligned} \tag{38}$$

with the addition that $x_{4,\text{ref}}$ is zero if the tractive force is less than the rolling resistances.

Integral Action

During accelerations or constant disturbances, e.g. road slopes, the controller suffers from a stationary error, see Figure 10. One way to get integral action in an LQ-controller is to add an extra state for the integral of Z and then include this state in the cost function, (Skogestad and Postlethwaite, 2007).

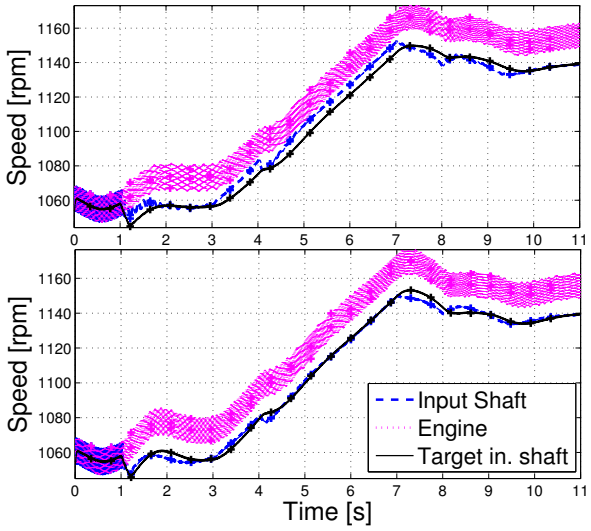

Figure 10: A simulation of a driving sequence in low crawler gear on flat road. In the top figure the controller has a steady error during 3 s to 7 s. In the lower plot the error has been removed by addition of integral action to the controller. The "Target input shaft" line is $\bar{\omega}_e - \Delta\omega_{\text{ref}}$. The controller is activated at 1 s.

$$\dot{x}_6 = x_1 - x_2 \tag{39}$$

$$\hat{x}_6 = \int \bar{\omega_e} - \bar{\omega_t}\,\mathrm{d}t \tag{40}$$

$$x_{6,\text{ref}} = \int \Delta\omega_{\text{ref}}\,\mathrm{d}t \tag{41}$$

$$M = \begin{bmatrix} 1 & -1 & 0 & 0 & 0 \\ 0 & 0 & 0 & 0 & 1 \end{bmatrix} \tag{42}$$

Since $\Delta\omega_{\text{ref}}$ is (almost) constant $x_{6,\text{ref}}$ will be constantly growing, likewise for $\hat{x}_6$. Although not mathematically a problem, in a controller this will soon lead to overflow. The solution is to only integrate the error, $e(t) = \Delta\omega_{\text{ref}} - \Delta\bar{\omega}$.

Conditional Integration When incorporating integrators in a controller it is always necessary to have anti-windup functionality. Here it is implemented as conditional integration, i.e. if the control signal saturates the updating of the integral part is stopped. Moreover with conditional integration the integration can be stopped when the control error is too large in order to make the system less oscillative without

changing the behavior at small errors. The drawback with this is that if there is a large stationary error the controller will not recover. To avoid this the integrator has not been completely shut off, instead the integrand is multiplied by a factor I_{low} when the error is lower than -3 rad/s. A peculiarity with the micro-slip-control problem is that negative errors are less dangerous than positive errors, since positive errors might cause lock-up of the clutch, which leads to a deteriorated driving experience. Therefore positive errors have been given more weight by a factor I_{pos} in the integrand. Both I_{low} and I_{pos} are considered to be tuning variables. The integrator can be summarized as,

$$I_{\text{part}} = x_{6,\text{ref}} - \hat{x}_6 = \int I_{\text{gain}} e(t)\,\mathrm{d}t \tag{43}$$

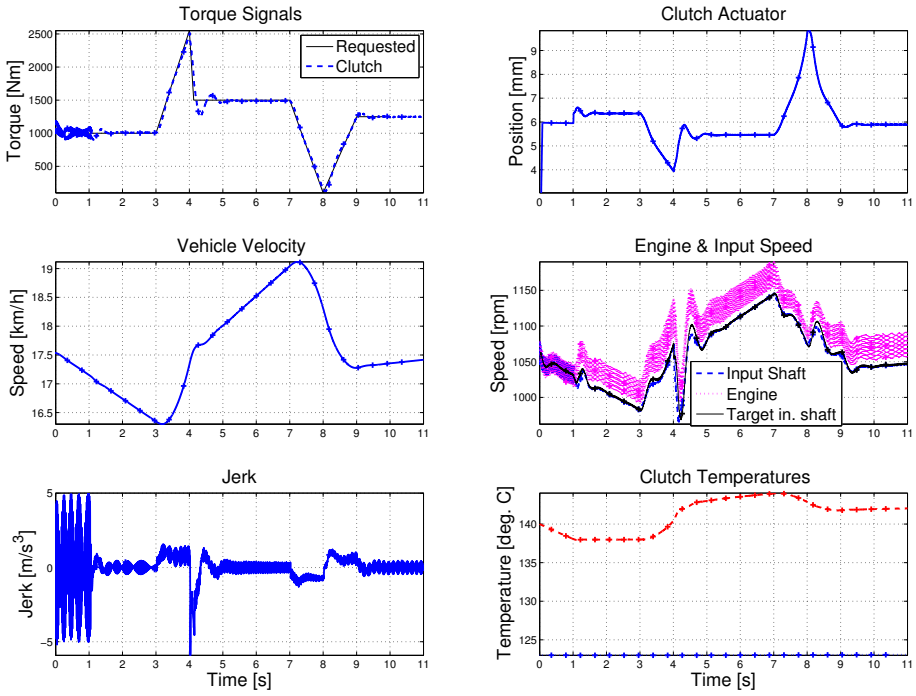

Figure 11: A simulation of a driving sequence in 5th gear in a 6 % uphill. Oscillations are attenuated when the controller is activated at 1 s and the reference slip is achieved even during transient ICE torque and unknown road slope. For a more detailed view of the slip see Figure 12. In the middle-right plot the "Target input shaft" line is $\bar{\omega}_e - \Delta\omega_{\text{ref}}$.

where,

$$I_{\text{gain}} = \begin{cases} 0 & \text{if } M_{\text{trans,req}} > M_{\text{trans,max}} \\ 0 & \text{if } M_{\text{trans,req}} < 0 \text{ Nm} \\ I_{\text{pos}} & \text{if } e(t) > 0 \\ I_{\text{low}} & \text{if } e(t) < -3 \text{ rad/s} \\ 1 & \text{otherwise} \end{cases} \tag{44}$$

To fit (43) into the structure presented in Figure 9 the integrator block needs to produce $-I_{\text{part}}$ that the reference-state-calculator block matches with a zero so that the contribution to the control signal will be $L_6 I_{\text{part}}$.

Tuning

Tuning variables for the controller are Q_1, Q_2, I_{low}, and I_{pos}. The Q_1 has been given a diagonal structure for ease of tuning.

$$Q_1 = \begin{pmatrix} q_1 & 0 \\ 0 & q_2 \end{pmatrix} \tag{45}$$

Furthermore $Q_2 = 1$ because it is only the ratio between the elements in Q_1 and Q_2 that matters for the result. Since the system parameters depend on the gear ratio and separate linearization points are used for each gear it is natural to tune the system separately for each gear. The tuning for some example gears are seen in Table 1. It is interesting to note that $I_{\text{low}} > 1$ for the 10th gear.

Table 1: Tuning of control parameters for three different gear ratios. Clear variations can be seen between the gears.

Gear	q_1	q_2	I_{low}	I_{pos}
low crawler	10^2	$5 \cdot 10^2$	0.1	1
5	10^2	10^5	0.1	4
10	10^2	10^5	2	1

4 Controller Evaluation

Simulations have been performed on the simulation model in order to evaluate the performance of the micro-slip controller. In Figure 11 a simulation in 5th gear and 6 % slope is seen.

At 1 s the controller is activated and it can be seen both in the clutch torque and the vehicle jerk that the ICE-torque oscillations are attenuated. Jerk is the time derivative of the acceleration and a common comfort measure, (Sorniotti et al., 2007) or (Zeng et al., 2013). At 3 s the ICE torque increases at maximum rate until 4 s where it drops at maximum rate. At 4 s the ICE torque is at its maximum value and the ICE speed is at its minimum that allows maximum torque. This corresponds to the operating point that has the largest oscillations in Figure 7. During these conditions the controller is able to keep the control error small with the exception for a peak in the rapid torque decrease at 4 s, see Figure 12. However, the peak is short in duration

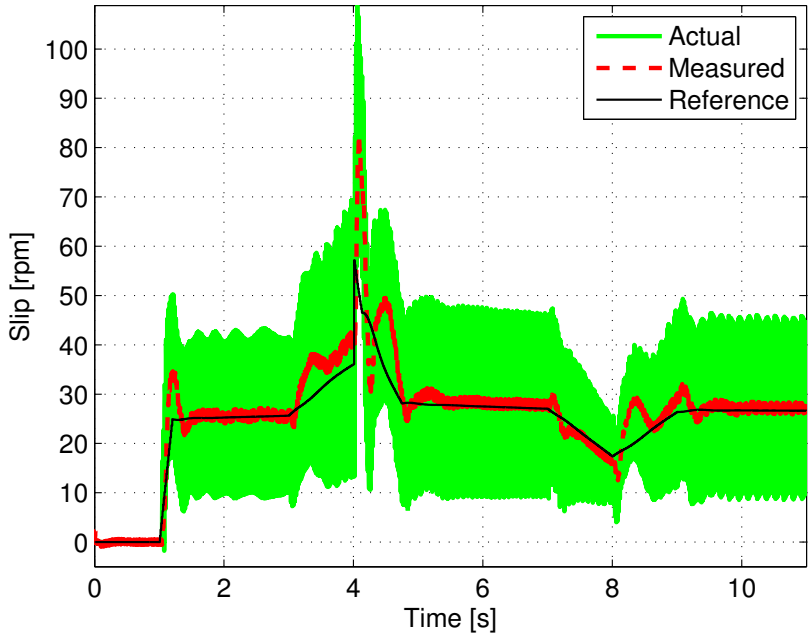

Figure 12: The actual slip speed between the flywheel and clutch disc as well as the slip speed measured by the controller in the case of Figure 11. The measured slip speed follows the reference well and the actual speed is not (too) close to zero.

and in the negative error direction so it is acceptable. The extra safety margin in (32) is seen active between 4 s and 4.75 s.

A second scenario can be seen in Figure 13. There in 10th gear, with a 1 %-uphill, a higher vehicle speed, and a similar torque trajectory to that of Figure 11. The controller takes longer time to unlock the clutch at activation in 10th gear than in 5th gear, due to the lower value of I_{pos}. The truck has a clearly different response to the torque trajectory but the controller still keeps the slip at reference value.

The model parameter that varies the most for an HDT is the mass. An unloaded truck weighs about 10 metric tonnes and a fully loaded truck can weigh up to 60 tonnes in Sweden. The nominal mass of 40 tonnes has therefore been altered a factor of 2 in both directions in the controller and control model. The simulation results can be seen in Figure 14. The changes in slip speed trajectory are insignificant and the robustness of the controller is demonstrated.

5 Temperature Considerations

An important aspect of micro slip control is thermal management since heat is continuously dissipated into the clutch. The amount of heat that is dissipated and thereby

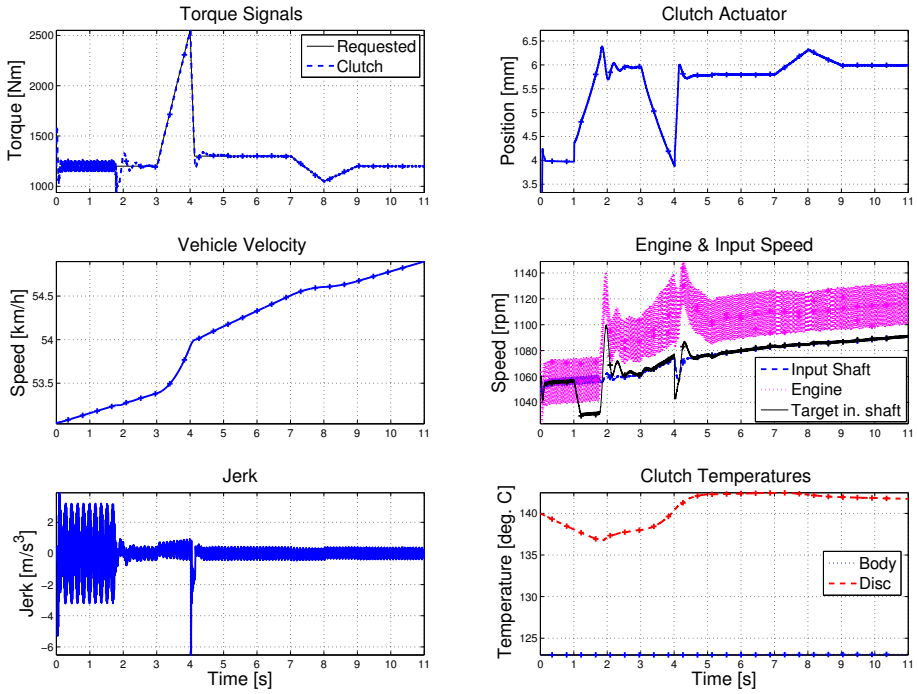

Figure 13: A simulation of a driving sequence in 10th gear in a 1 % uphill. The controller is activated at 1 s but the clutch does not unlock until 1.8 s since the integrator needs time to achieve a low enough torque. After an initial transient the reference slip is achieved even during transient ICE torque and unknown road slope. The "Target input shaft" line is $\bar{\omega}_e - \Delta\omega_{\text{ref}}$.

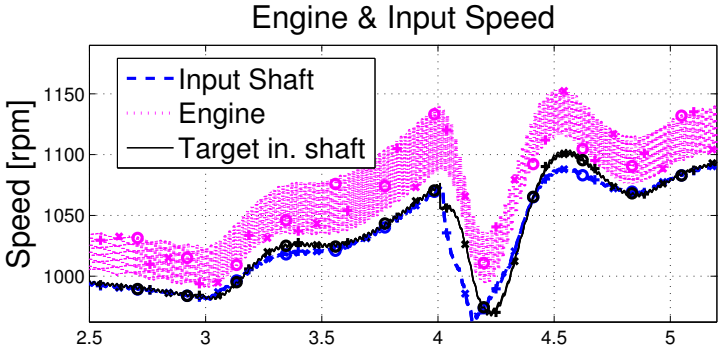

Figure 14: Same simulation as in Figure 11 but with three different values for the mass parameter in the controller and control model. '+' is 20 metric tonnes, 'x' is 40 tonnes (correct value), and 'o' is 80 tonnes. It is hard to tell any difference with the eye. The controller is very robust against mass changes.

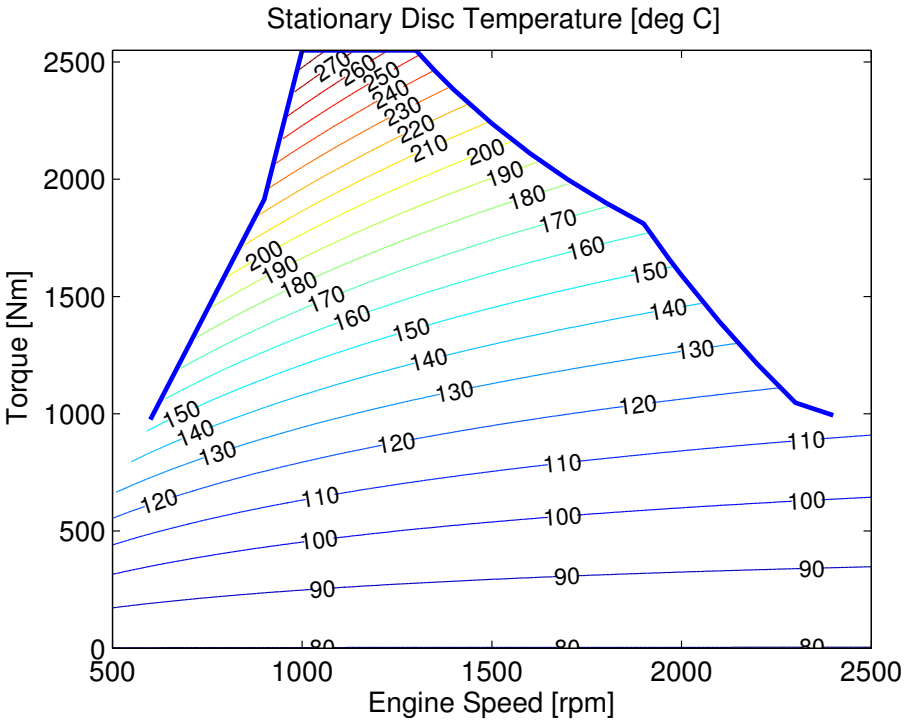

Figure 15: The steady-state value of the clutch disc temperature, T_d, across the L6 engine map when $\Delta\omega = \Delta\omega_{\text{ref}}$, $T_{\text{coolant}} = 90$ °C, and $T_{\text{amb}} = 10$ °C. Due to durability reasons it is preferable to keep the temperature below 200 °C, which could be problematic for high torques.

the steady-state value of the clutch disc temperature is dependent on the operating point of the engine and can be calculated using (1) and (32). The results are found in Figure 15. It is desirable to keep the clutch disc temperature below 200 °C to avoid premature failure of the clutch. For high clutch torques the temperature will eventually increase beyond 200 °C. Although that will take some time and high torques are seldomly sustained over a longer time period. To investigate if the temperature increase is a problem some driving missions have been simulated. Torque profiles from recordings of real-world driving missions have been used together with the assumptions that $\Delta\omega = \Delta\omega_{\text{ref}}$ at all time, $M_{\text{trans,k}} = \overline{M}_e$, and $T_{\text{amb}} = 10$ °C. With these assumptions no road profile, head wind, or similar information is required and the simulation is of low computational complexity since only (1) needs to be simulated. The initial temperatures have been tuned to roughly match the final temperatures. A highway driving mission is seen in Figure 16 and an urban driving mission is seen in Figure 17. In both cases the temperatures are kept well below 200 °C. Nevertheless extreme driving cycles might still overheat the clutch and measures must be taken. Küpper et al. (2006) suggests that gearshift control can be used to dissipate less heat

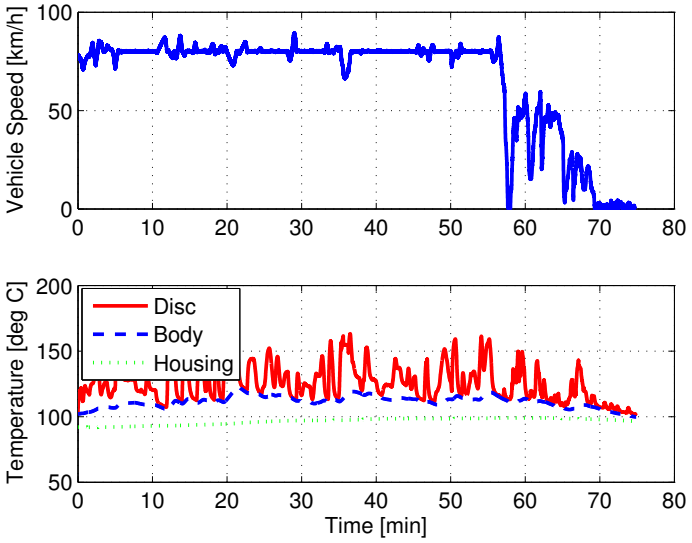

Figure 16: A highway driving mission has been simulated using recorded engine torque, engine speed and engine temperature under the assumptions $\Delta\omega = \Delta\omega_{\text{ref}}$, $M_{\text{trans,k}} = \overline{M}_e$, and $T_{\text{amb}} = 10$ °C. The temperatures stay around 130 °C so the clutch does not overheat.

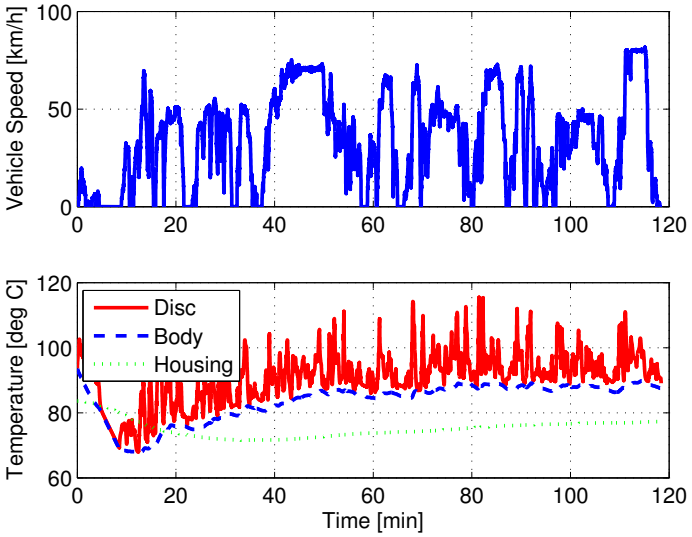

Figure 17: An urban driving mission has been simulated using recorded engine torque, engine speed and engine temperature under the assumptions $\Delta\omega = \Delta\omega_{\text{ref}}$, $M_{\text{trans,k}} = \overline{M}_e$, and $T_{\text{amb}} = 10$ °C. The temperatures stay around 90 °C so the clutch does not overheat.

or alternatively the direct approach, lowering the slip speed at a cost of increased vibrations. One implementation of the latter is to linearly lower the slip safety margin when the temperature starts to get high,

$$A_{\text{margin}} = \begin{cases} 1 & \text{if } T_d < 150 \text{ °C} \\ \dfrac{T_d - 150}{200 - 150} & \text{if } 150 \leq T_d \leq 200 \text{ °C} \\ 0 & \text{if } T_d > 200 \text{ °C} \end{cases} \tag{46}$$

The risk of transmitting oscillations will increase but less heat will be dissipated. Even with no safety margin at all the clutch is still at risk of overheating, see Figure 18. If the clutch overheats a design choice has to be made. Should the clutch open and the car stop, should the clutch lock-up and allow oscillations to be transmitted, should the slip be maintained hoping that nothing breaks, should the driver be alerted in any way? The answer lies outside the scope of this paper. It is worth mentioning that

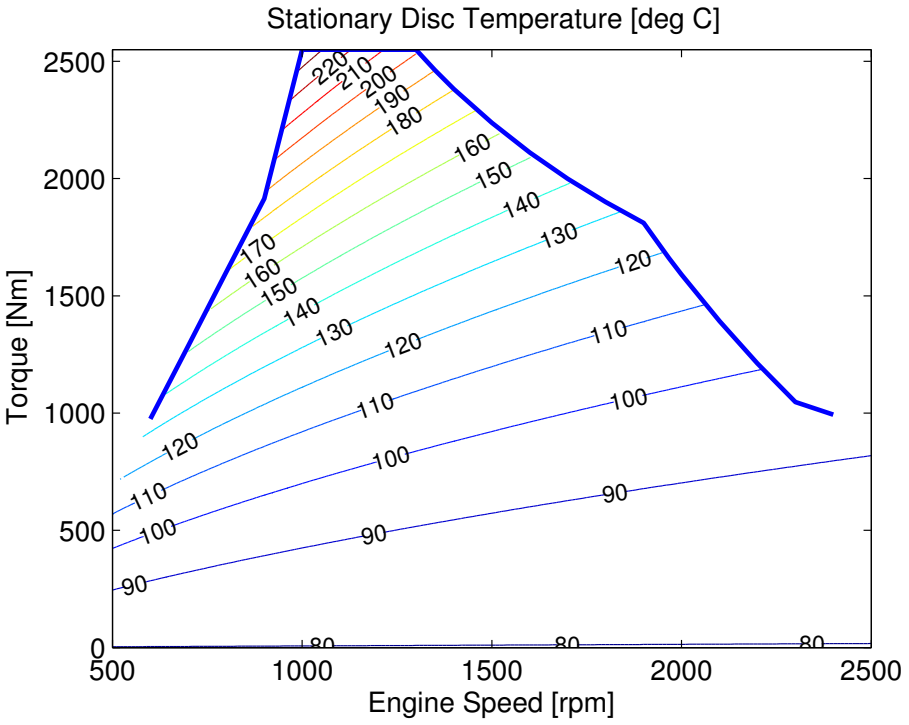

Figure 18: The steady-state value of the clutch disc temperature, T_d, across the L6 engine map when $\Delta\omega = A_\omega$, $T_{\text{coolant}} = 90$ °C, and $T_{\text{amb}} = 10$ °C. Due to durability reasons it is preferable to keep the temperature below 200 °C. This is less problematic when no safety margin is used for the slip compared to the nominal case in Figure 15 but could still be problematic for high torques.

the thermal problems are greatly reduced if the engine produces less oscillations, see Figure 19 for the stationary temperatures when using the V8 engine.

6 Fuel Consumption

The heat dissipated in the clutch during micro slipping is taken from the kinetic energy of the engine that in turn comes from the chemical energy in the fuel. Therefore micro-slipping will increase the fuel consumption. The simulations made in Section 5 are used for a fuel consumption analysis. With the assumptions made in Section 5 the energy put into the clutch is,

$$E_{\text{in}} = \int M_e \omega_e \mathrm{d}t \tag{47}$$

the useful energy is,

$$E_{\text{out}} = \int M_e(\omega_e - \Delta\omega)\mathrm{d}t \tag{48}$$

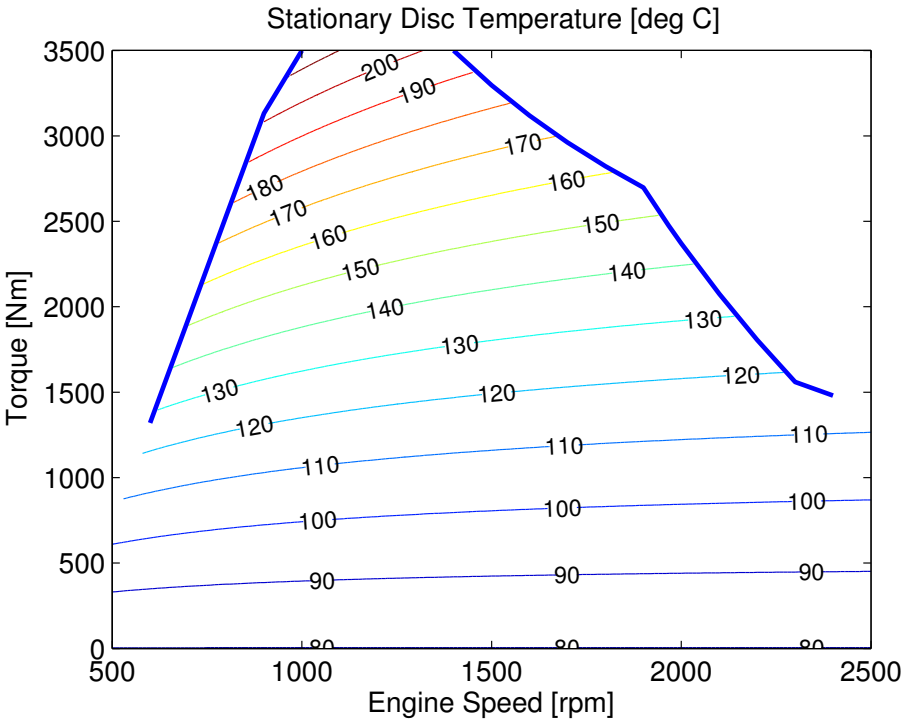

Figure 19: The steady-state value of the clutch disc temperature, T_d, across the V8 engine map when $\Delta\omega = \Delta\omega_{\text{ref}}$, $T_{\text{coolant}} = 90$ °C, and $T_{\text{amb}} = 10$ °C. Due to durability reasons it is preferable to keep the temperature below 200 °C. This is almost not a problem for the V8 engine.

Table 2: Calculated efficiencies for a micro-slipping clutch for different cases. The efficiency loss is large for an HDT if the clutch is always slipping.

Driving mission	Slipping	Engine	Efficiency [%]
urban	always	L6	98.1
highway	always	L6	97.5
urban	always	V8	98.9
highway	always	V8	98.7
urban	$\omega_e < 1100$ rpm	L6	99.3
highway	$\omega_e < 1100$ rpm	L6	99.7

and the clutch efficiency is

$$\eta = \frac{E_{\text{out}}}{E_{\text{in}}} \tag{49}$$

The efficiency has been calculated for both driving cycles and the result is presented in Table 2. The fuel consumption increases with about 2 % which is a lot for an HDT. Even for the V8 that has significantly smaller oscillations the fuel consumption increase is roughly 1 %. However, if the slip control only is active below a certain engine speed, as suggested in Albers (1990); Audi of America (2001) and Fischer and Berger (1998) fuel consumption can be improved. Lets say that sufficient vibration isolation is achieved with a locked clutch above 1100 rpm so that the highway cruising is done with a locked clutch, then the fuel consumption increase is only around 0.5 % and perhaps micro-slip control is a feasible solution for HDTs. When looking at Figure 7 it seems more intuitive to put the micro-slip limit along one of the contour lines instead of at a fixed engine speed. Nevertheless the vibration dynamics of the complete powertrain has to be analyzed to be conclusive on that matter.

7 Conclusions

A control structure has been made for a micro-slip controller. The basic components are an LQ controller based on the simplified model and an EKF that can compensate the torque request from the LQ controller for the thermal dynamics of the clutch. The temperature compensation is important for the assumption that the clutch torque is directly controllable. To remove some stationary errors integral action has been added to the LQ controller by adding an extra state. A sinusoidal model over the ICE-torque fluctuations has been fitted to high resolution data. The oscillation amplitude and frequency agrees well with the data. The reference slip value is set according to a formula for the flywheel-speed-oscillation amplitude derived from the torque model together with a dynamic safety margin that can increase during transients. The controller is able to follow the slip reference without risk of locking up in simulations with transient torque, unknown road grades and a mass parameter that has been varied. The thermal behavior of a clutch with micro slip is analyzed and the EKF should be used for temperature surveillance although there were no temperature problems during simulations of recorded driving missions. The controller has a simple structure and there should be no technical problems to implement it in a production vehicle. However, the fuel consumption increase might be too large for an HDT application.

Nonetheless the real benefits of micro-slip control will only be evident when combined with other changes in the powertrain. For example a simplified torsion damper, lowered specification for gears, or a lowered idle speed. Weather the benefits are worth the cost and in which operating points to use micro-slip control is left for another study. However, the feasibility of a micro-slip control system for a dry clutch HDT has been proven.

References

Albert Albers. Torque control isolation (TCI) the smart clutch. In *4th LuK Symposium*, 1990.

Inc. Audi of America. Variable automatic transmission multitronic 01j, August 2001. Self-Study Program Course Number 951103.

Pietro J. Dolcini, Carlos Canudas de Wit, and Hubert Béchart. *Dry Clutch Control for Automotive Applications.* Advances in Industrial Control. Springer-Verlag London, 2010.

Daniel Eriksson, Lars Eriksson, Erik Frisk, and Mattias Krysander. Flywheel angular velocity model for misfire and driveline disturbance simulation. In *7th IFAC Symposium on Advances in Automotive Control*, Tokyo, Japan, 2013.

Lars Eriksson and Lars Nielsen. *Modeling and Control of Engines and Drivelines.* John Wiley & Sons, 2014.

Robert Fischer and Reinhard Berger. Automation of manual transmissions. In *6th LuK Symposium*, 1998.

Torkel Glad and Lennart Ljung. *Reglerteori - Flervariabla och olinjära metoder.* Studentlitteratur, 2nd edition, 2003.

Kumaraswamy Hebbale, Chunhao Lee, Farzad Samie, Chi-Kuan Kao, Xu Chen, Jeremy Horgan, and Scott Hearld. Model based torque converter clutch slip control. In *SAE Technical Paper: 2011-01-0396*, April 2011.

Akira Higashimata, Kazutaka Adachi, Satoshi Segawa, Nobuo Kurogo, and Hironobu Waki. Development of a slip control system for a lock-up clutch. In *SAE Technical Paper: 2004-01-1227*, April 2004.

Takeo Hiramatsu, Takao Akagi, and Haruaki Voneda. Control technology of minimal slip-type torque converter clutch. In *SAE Technical Paper: 850460*, February 1985.

Yutaka Kaneko, Kazutaka Adachi, Fumiyo Iino, and Mitsuo Hirata. Development of a slip speed control system for a lock-up clutch (part iii). In *SAE Technical Paper: 2009-01-0955*, April 2009.

Yuji Katsumata, Satoshi Segawa, Kazutaka Adachi, and Akira Higashimata. Development of a slip speed control system for a lock-up clutch (part ii). In *SAE Technical Paper: 2008-01-0001*, April 2008.

Klas Küpper, Roland Seebacher, and Olaf Werner. Think systems - software by LuK. In *7th LuK Symposium*, 2002.

Klas Küpper, Boris Serebrennikov, and Georg Göppert. Software for automized transmissions - intelligent driving. In *8th LuK Symposium*, 2006.

Andreas Myklebust and Lars Eriksson. The effect of thermal expansion in a dry clutch on launch control. In *7th IFAC Symposium on Advances in Automotive Control*, September 2013.

Andreas Myklebust and Lars Eriksson. Modeling, observability, and estimation of thermal effects and aging on transmitted torque in a heavy duty truck with a dry clutch. *IEEE/ASME Transactions on Mechatronics*, PP(99):1–12, 2014a.

Andreas Myklebust and Lars Eriksson. Thermal clutch model observability and observer effects of a torque sensor in the powertrain. Submitted to IEEE/ASME Transactions on Mechatronics, 2014b.

Paul Otanez, Farzad Samie, Chunhao Joseph Lee, and Chi-Kuan Kao. Aggressive torque converter clutch slip control and driveline torsional velocity measurements. In *SAE Technical Paper: 2008-01-1584*, April 2008.

Magnus Pettersson and Lars Nielsen. Diesel engine speed control with handling of driveline resonances. *Control Engineering Practice*, 11(3):319–328, March 2003.

Sigurd Skogestad and Ian Postlethwaite. *Multivariable Feedback Control - Analysis and Design*. John Wiley & Sons Ltd, 2nd edition, 2007.

Aldo Sorniotti, Enrico Galvagno, Andrea Morgando, Mauro Velardocchia, and Fabrizio Amisano. An objective evaluation of the comfort during the gear change process. In *SAE Technical Paper: 2007-01-1584*, April 2007.

Huabing Zeng, Yulong Lei, Yao Fu, Yongfa Li, and Wanhua Ye. Analysis of a shift quality metric for a dual clutch transmission. In *SAE Technical Paper: 2013-01-0825*, April 2013.

Paper F

Road Slope Analysis and Filtering for Driveline Shuffle Simulation*

F

*Published in *2012 IFAC Workshop on Engine and Powertrain Control, Simulation and Modeling.*

Road Slope Analysis and Filtering for Driveline Shuffle Simulation

Andreas Myklebust and Lars Eriksson

Vehicular Systems, Department of Electrical Engineering, Linköping University, SE-581 83 Linköping, Sweden

Abstract

In powertrain analysis, simulation of driveline models are standard tools, where efficient and accurate simulations are important features of the models. One input signal with high impact on the accuracy is the road slope. Here it is found that the amplitude discretization in production road-slope sensors can excite vehicle shuffle dynamics in the model, which is not present in the real vehicle. To overcome this problem road-slope information is analyzed with the aid of both measured and synthetic road profiles, where the latter are generated from regulatory road specifications. The analysis shows that it is possible to separate vehicle shuffle resonances and road-slope information, and designs are proposed for on- and off-line filtering of the road-slope-sensor signal in spatial coordinates. Applying the filter to measured data shows that vehicle shuffle is significantly attenuated, while the shape of the road slope profile is maintained. As a byproduct the use of smoothing the rolling resistance is shown.

1 Introduction

When analyzing powertrains and their controls, the results will of course depend on the model but also on the input signals. The quality of the input signals have a big impact on simulation results, e.g. noise components in the inputs can have a profound effect on the outputs. A motivating example is given in Figure 3 where powertrain oscillations are induced due to sensor discretization levels, of integer percentage points, in road slope.

This example of discretization noise in the road-slope signal and how it influences simulated dynamics of a driveline is in focus here. Attention is also given to how a measured road-slope-sensor signal can be filtered so that the high frequency content, that can excite driveline dynamics and might result in vehicle shuffle, is removed while the relevant information is maintained. This is of importance when powertrains are simulated for control applications where vehicle shuffle has to be avoided. Examples of such control applications are vehicle-speed control, (Pettersson and Nielsen, 2002), driver-filter design, (Gerhardt et al., 1998), gear-shift control, (Fredriksson and Egardt, 2003), (Pettersson and Nielsen, 2000), and launch control, (Garofalo et al., 2002), (Dolcini et al., 2008).

Little work exists in the area of analyzing and filtering road slope data, even though road-grade information is used in different applications. For example Gao et al. (2011) studies road slope estimation and also how an incorrect estimation of the constant road slope effects the control of clutch disengagement. Estimation of the road slope for various applications is also treated in e.g. Lingman and Schmidtbauer (2002), Sebsadji et al. (2008) and Bae et al. (2001). In Sahlholm (2011), where a road slope estimator is developed, low frequency errors are introduced to study the effect on look-ahead control and motivate the need of a good road grade estimator. Sahlholm (2011) filtered the road data using a third-order Butterworth low-pass filter with spatial cut-off frequency of $9 \cdot 10^{-3}$ m^{-1} before being used. In the related literature there is no quantitative analysis of the frequency content in the road-slope data.

A driveline model is developed for analysis of the interaction between road-slope data and vehicle shuffle. Measurement data is collected from a heavy duty truck, in order to both validate the model and to get realistic signals for the study. In addition the frequency content of different roads is analyzed, both theoretically and through measured road-slope data.

2 Powertrain model

In order to investigate how the quality of the road-slope signal affects simulation, a simulation model is required. A longitudinal model of a heavy-duty truck has therefore been developed. The model has to capture important dynamics in the driveline and how they make the truck shuffle. The model is an extension of the model in Pettersson (1997) that was used for evaluation of oscillation damping by engine control during tip-in maneuvers. Pettersson (1997) identified the important flexibilities in the driveline that cause vehicle shuffle and therefore the same model structure is used here. The model is built in a modular way and then condensed into a state space model.

An overview of the different modules and their information exchange is given in Figure 1, which also defines the nomenclature used in this paper. Each module corresponds to a part in the powertrain, Internal Combustion Engine (ICE), clutch, gearbox, propeller shaft, final drive, drive shafts and vehicle dynamics.

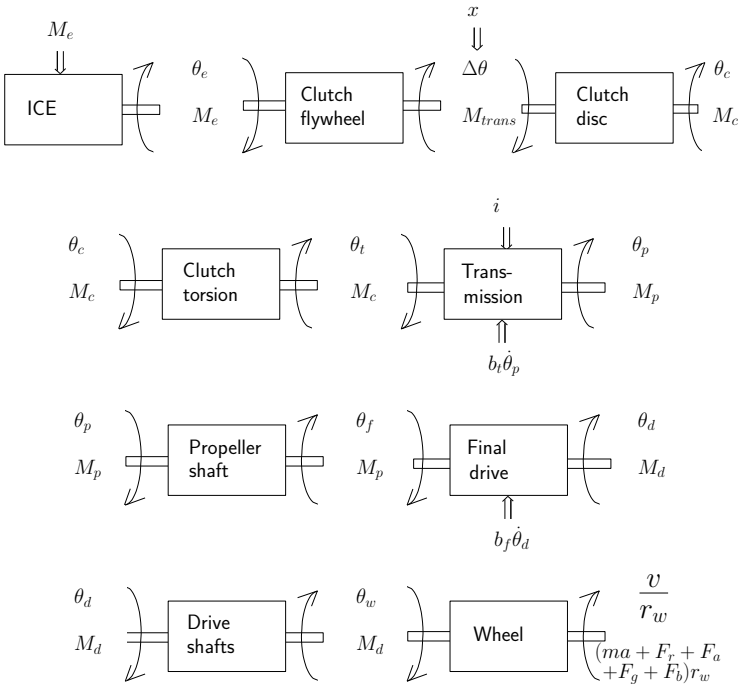

Figure 1: Sketch of the subsystems and their information exchange in the truck model.

2.1 Internal Combustion Engine

The ICE produces the engine torque, M_e, that is given as model input. Note that this is the net (brake) torque of the ICE, e.g. $M_e = 0$ with open clutch will keep the engine speed constant.

2.2 Clutch

The clutch is modeled in three separate parts. The actuator, the clutch disc where slip might occur, and a torsional part that is flexible.

Clutch Actuator

The clutch position, x, is normalized by its maximum stroke, $x_{\max}$ to get a relative position. The relative position is assumed to have an effective range, x_{eff} where the resulting normal force between the clutch plates are unsaturated. This effective range is transformed so that 0 corresponds to zero normal force and 1 corresponds to maximum normal force. This transformed signal is assumed to be proportional to the applied normal force.

The natural output from the actuator is the clamping force, F_N. Nevertheless the clamping force is directly recalculated into a transmittable torque, $M_{\text{trans}} = k\mu F_N$,

that is used as actuator output. There are two friction coefficients, one static, μ_s, and one dynamic, μ_k. Let μ_k be part of k_{clutch} and define the ratio of the friction coefficients, $k_\mu = \frac{\mu_s}{\mu_k}$. Then the equations for the clutch actuator become:

$$x_{\text{eff}} = \begin{cases} L_l, & \frac{x}{x_{\max}} < L_l \\ \frac{x}{x_{\max}}, & L_l \leq \frac{x}{x_{\max}} \leq L_u \\ L_u, & L_u < \frac{x}{x_{\max}} \end{cases} \tag{1}$$

$$M_{\text{trans},k} = k_{\text{clutch}} \frac{L_u - x_{\text{eff}}}{L_u - L_l} \tag{2}$$

$$M_{\text{trans},s} = k_\mu M_{\text{trans},k} \tag{3}$$

Note that (2) is a simple model of the slipping clutch compared to Myklebust and Eriksson (2012).

Clutch Disc

The modeled clutch is a single-plate dry clutch with two contact surfaces. Torque is transferred between the clutch disc and flywheel through friction. The friction is modeled as coulomb friction with stick-slip behavior. Torque from the ICE, M_e, and driveline, M_c, are inputs and angular velocity & angle on both sides, $\dot{\theta}_e$ & θ_e and $\dot{\theta}_c$ & θ_c, respectively, are outputs.

The clutch model has two modes, locked and slipping mode. While in locked mode, the clutch behaves as one rigid body, whereas during slipping the clutch consists of two bodies where each one has an angular velocity and position. The condition for the transition from slipping to locked mode is that the speed difference is zero and the transmitted torque, M_{trans} is less than the static transmittable torque, $M_{\text{trans,s}}$. The condition for transition from locked to slipping mode is when M_{trans} rises above $M_{\text{trans,s}}$.

Using θ_e, $\dot{\theta}_e$, θ_c, and $\dot{\theta}_c$ as states gives the following equations for the clutch disc:
Conditions for switching from slipping to locked mode:

$$\dot{\theta}_e = \dot{\theta}_c \tag{4}$$

$$M_{\text{trans}} \leq M_{\text{trans,s}} \tag{5}$$

Equations for the clutch in locked mode:

$$M_e - M_c = (J_{\text{ICE}} + J_{\text{fw}} + J_c)\,\ddot{\theta}_e \tag{6}$$

$$\dot{\theta}_c = \dot{\theta}_e \tag{7}$$

$$M_{\text{trans}} = \frac{M_e J_c + M_c\,(J_e + J_{\text{fw}})}{J_e + J_{\text{fw}} + J_c} \tag{8}$$

Conditions for switching from locked to slipping mode:

$$M_{\text{trans}} \geq M_{\text{trans,s}} \tag{9}$$

Equations specific to the clutch in slipping mode:

$$M_{\text{trans}} = \text{sgn}\left(\dot{\theta}_e - \dot{\theta}_c\right) M_{\text{trans,k}} \tag{10}$$

$$M_e - M_{\text{trans}} = \left(J_e + J_{\text{fw}}\right) \ddot{\theta}_e \tag{11}$$

$$M_{\text{trans}} - M_c = J_c \ddot{\theta}_c \tag{12}$$

Torsional Part

The main flexibility of the clutch is in the torsion springs in the clutch disc. They are located on the vehicle side of the friction surfaces. Therefore the flexibility of the clutch is modeled as a separate part of the clutch, located on the transmission side of the clutch disc, like in Moon et al. (2004).

The clutch torsional part is modeled as a torsional spring and damper. It takes speed & angle from the clutch disc, $\dot{\theta}_c$ & θ_c, and the input shaft of the transmission, $\dot{\theta}_t$ & θ_t, as input and returns a torque, M_c. The equation for the torsional part is:

$$M_c = c_c(\dot{\theta}_c - \dot{\theta}_t) + k_c(\theta_c - \theta_t) \tag{13}$$

2.3 Transmission

The gear number (input) is converted to a gear ratio, $i_{t,i}$, and gearbox inertia, $J_{t,i}$. The gear ratio scales the input-side torque, M_c, & inertia into output-side torque, M_t, & inertia, J_t. The speed is calculated from the output side to the input side and then integrated to an angle, θ_t. There is also a speed proportional (viscous) friction in the transmission. On the output side the outputs torque & inertia are summed with the propeller shaft torque, M_p, & inertia, J_p, to produce the outputs speed, $\dot{\theta}_p$, & angle, θ_p using Newton's second law.

Note that no synchronizers are modeled and the model can not engage neutral gear. Therefore gear shifting will be instantaneous. This is an acceptable approximation when the clutch is disengaged, since the transmission input side has low inertia compared to the rest of the vehicle.

With the states $\dot{\theta}_p$, θ_p, and θ_t the equations become:

$$M_t = M_c \, i_{t,i} \tag{14}$$

$$\left(J_{t,i} + J_p\right) \ddot{\theta}_p = M_t - b_t \dot{\theta}_p - M_p \tag{15}$$

$$\dot{\theta}_t = \dot{\theta}_p i_{t,i} \tag{16}$$

2.4 Propeller Shaft

The flexible propeller shaft is modeled in the same way as the clutch flexibility, (13). The equation for the propeller shaft is:

$$M_p = c_p(\dot{\theta}_p - \dot{\theta}_f) + k_p(\theta_p - \theta_f) \tag{17}$$

2.5 Final Drive

The final drive with differential is assumed to act symmetrically on the drive shafts. Therefore it can be modeled as the transmission but with fixed gear ratio, i_f, and

inertia, J_f. With the states $\dot{\theta}_d$, θ_d the equations become:

$$\left(J_p i_f^2 + J_f + J_d\right)\ddot{\theta}_d = M_p i_f - b_f \dot{\theta}_d - M_d \tag{18}$$

$$\dot{\theta}_f = \dot{\theta}_d i_f \tag{19}$$

2.6 Drive Shafts

The flexible drive shafts can, with the symmetrical differential, be lumped into one and modeled in the same way as the clutch flexibility, (13). The equation is:

$$M_d = c_d(\dot{\theta}_f - \dot{\theta}_w) + k_d(\theta_f - \theta_w) \tag{20}$$

This is the main flexibility in the driveline.

2.7 Vehicle Dynamics

The non-driveline parts that affect the longitudinal dynamics are modeled in this block. That is, the wheels and vehicle. Tire dynamics are neglected and rolling condition is assumed. The wheels simply consists of a radius, r_w, an inertia, J_w and a rolling resistance force, F_r.

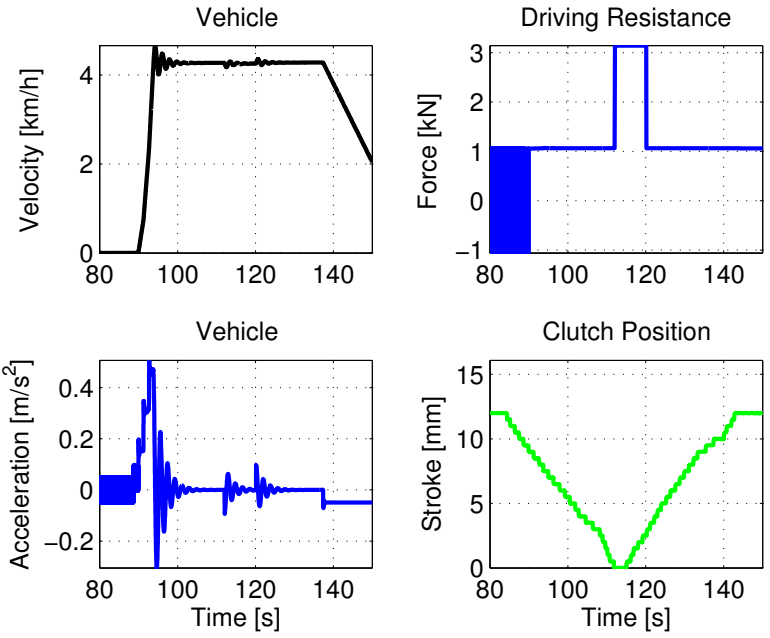

Figure 2: In the upper right plot it is seen how the rolling resistance is constantly switching sign during the first ten seconds of the simulation. In the lower left plot it is seen in addition how the acceleration is switching, while the speed is practically zero, upper left plot.

Model inputs that directly affect the vehicle dynamics are braking force and road-slope angle, α (in radians). The road-slope angle is used to calculate the gradient force that is added with the braking force, rolling resistance and aerodynamic drag. The sign of the vehicle velocity is used so that rolling resistance, braking force and air resistance will oppose the vehicle movement.

The drag forces are subtracted from the drive shaft torque and divided by the vehicle mass, m, in order to calculate the vehicle acceleration, a, which is integrated to velocity and fed back to the drive shafts as angular velocity.

Discontinuity of Rolling Resistance

The rolling resistance has a static component that changes sign with the velocity of the vehicle. Around zero velocity this leads to a large discontinuity in the rolling resistance. If this is not properly handled there can be significant oscillations in the vehicle velocity and loading torque. See Figure 2 for a simulation example of this. One possibility is to use a state machine to control the states and transition between rolling and stand still. Another simpler cure to this problem is to smooth the rolling resistance using e.g. the following smoothing function

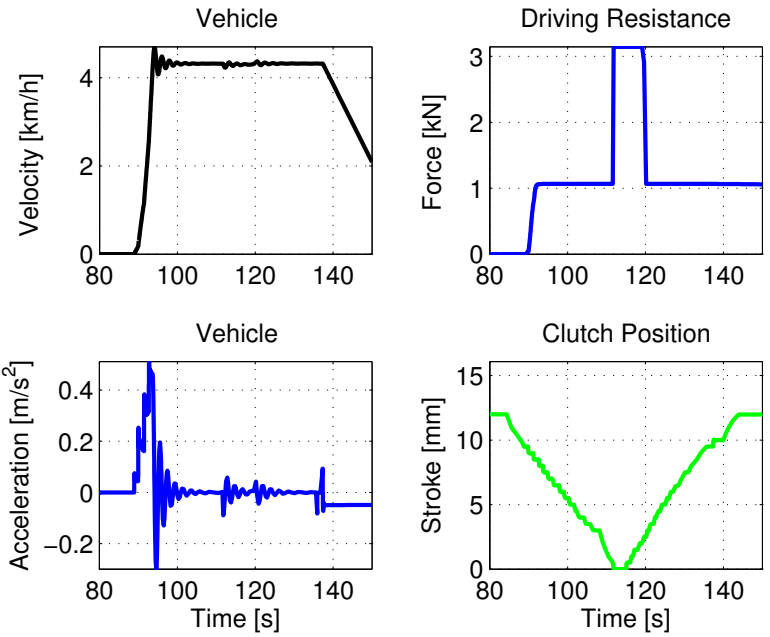

Figure 3: Simulation with the smoothed rolling resistance model. In the upper right plot it is seen that the rolling resistance does not increase until the velocity starts to increase (upper left plot). Moreover the acceleration can be seen to be zero until movement starts. Moreover it can clearly be seen that when the driving resistance, due to discretization levels of road slope signal, makes steps, at 110 s and 120 s, there are longitudinal oscillations.

$$f(v) = 1 - e^{-c_{sr}v^2} \tag{21}$$

where v is the vehicle speed (in m/s) and c_{sr} is a tuning parameter. A smaller c_{sr} gives more smoothing, which speeds up the simulation more but affects the rolling resistance higher up in the speed range. Here $c_{sr} = 16$ is selected as an empirical value that gives large reductions in simulation time without a significant effect on the rolling resistance at speeds above 0.5 km/h, see Figure 3. The simulation time was reduced with up to 85% when the smoothing function was used in cases similar to that in Figure 3. With the states v ($\dot{v} = a$) and θ_w the equations become:

$$F_a = \frac{1}{2}\rho_a c_w A_f v^2, \quad F_g = mg\sin(\alpha) \tag{22}$$

$$F_r = f(v)(c_{r1} + c_{r2}|v|)mg, \quad \dot{\theta}_w = v/r_w \tag{23}$$

$$\begin{aligned}\frac{M_d}{r_w} - \mathrm{sgn}(v)(F_r + F_a + F_b) - F_g = \\ = \left(m + \frac{J_w + J_d}{r_w^2}\right) a\end{aligned} \tag{24}$$

2.8 State-Space Model

The vehicle speed, $y = v$, is the output and the velocities and torsions are chosen as state variables

$$\begin{aligned}x &= \left(x_1,\ x_2,\ x_3,\ x_4,\ x_5,\ x_6,\ x_7\right)^T = \\ &= \left(\omega_e,\ \theta_e - \theta_t,\ \omega_p,\ \theta_p - \theta_f,\ \omega_d,\ \theta_d - \theta_w,\ \omega_w\right)^T\end{aligned} \tag{25}$$

In order to get a compact representation of the model, the engine torque, $g_1 = u_1 = M_e$, and driving resistance, $g_2 = F_{\mathrm{dr}} = F_r + F_a + F_g + F_b = F_r + F_a + u_2$, are collected into two separate signals. In the analysis in Section 3 the clutch is closed, gear is fixed, and velocity is positive. Then the system can be conveniently written as:

$$\begin{aligned}\dot{x} &= A\,x + B\,g(x,u) \\ y &= C\,x\end{aligned} \tag{26}$$

with,

$$\begin{aligned}g(x,u) &= \left[u_1,\ \frac{\rho_a c_w A_f r_w^2 x_7^2}{2} + (c_{r1} + c_{r2} r_w x_7)mg + u_2\right]^T, \\ A &= \begin{pmatrix} \frac{-c_c}{J_1} & \frac{-k_c}{J_1} & \frac{c_c i_t}{J_1} & 0 & 0 & 0 & 0 \\ 1 & 0 & -i_t & 0 & 0 & 0 & 0 \\ \frac{c_c i_t}{J_2} & \frac{k_c i_t}{J_2} & \frac{-c_1}{J_2} & \frac{-k_p}{J_2} & \frac{c_p i_f}{J_2} & 0 & 0 \\ 0 & 0 & 1 & 0 & -i_f & 0 & 0 \\ 0 & 0 & \frac{c_p i_f}{J_3} & \frac{k_p i_f}{J_3} & \frac{-c_2}{J_3} & \frac{-k_d}{J_3} & \frac{c_d}{J_3} \\ 0 & 0 & 0 & 0 & 1 & 0 & -1 \\ 0 & 0 & 0 & 0 & \frac{c_d}{J_4} & \frac{k_d}{J_4} & \frac{-c_d}{J_4} \end{pmatrix}, \\ J_1 &= J_e + J_c, \quad J_2 = J_t + J_p, \\ J_3 &= J_p i_f^2 + J_f + J_d, \quad J_4 = m_v r_w^2 + J_w + J_d, \\ c_1 &= c_c i_t^2 + b_t + c_p, \quad c_2 = c_p i_f^2 + b_f + c_d,\end{aligned} \tag{27}$$

$$B^T = \begin{pmatrix} \frac{1}{J_1} & 0 & 0 & 0 & 0 & 0 & 0 \\ 0 & 0 & 0 & 0 & 0 & 0 & \frac{-r_w}{J_4} \end{pmatrix}$$

$$C = \begin{pmatrix} 0 & 0 & 0 & 0 & 0 & 0 & r_w \end{pmatrix}$$

Note that (26) is a non-linear system as g_2 depends on x_7^2.

2.9 Linearization

The Bode diagram is used to analyze the gain and resonances in the system, and to facilitate this the system is linearized. Noting that the only non-linearity in the state-space model is in g_2 we can easily do the linearization by augmenting the A-matrix. This is done by doing the first-order Taylor expansion around v_0 of the aerodynamic drag

$$F_a = \frac{1}{2}\rho_a c_w A_f (2v_0 v - v_0^2) + \mathcal{O}\left((v - v_0)^2\right) \tag{28}$$

giving the addition

$$\Delta a_{7,7} = \frac{-r_w^2 (c_{r2} mg - \rho_a c_w A_f v_0) v}{J_4} \tag{29}$$

to element $a_{7,7}$ in A. The constant terms in the linearization are taken care of by the torque and torsions that correspond to steady state at v_0.

$$\begin{aligned} \dot{x}_\Delta &= A_{\text{aug}}\, x_\Delta + B\, u_\Delta \\ y_\Delta &= C\, x_\Delta \end{aligned} \tag{30}$$

were A_{aug} is the A-matrix augmented with $\Delta a_{7,7}$.

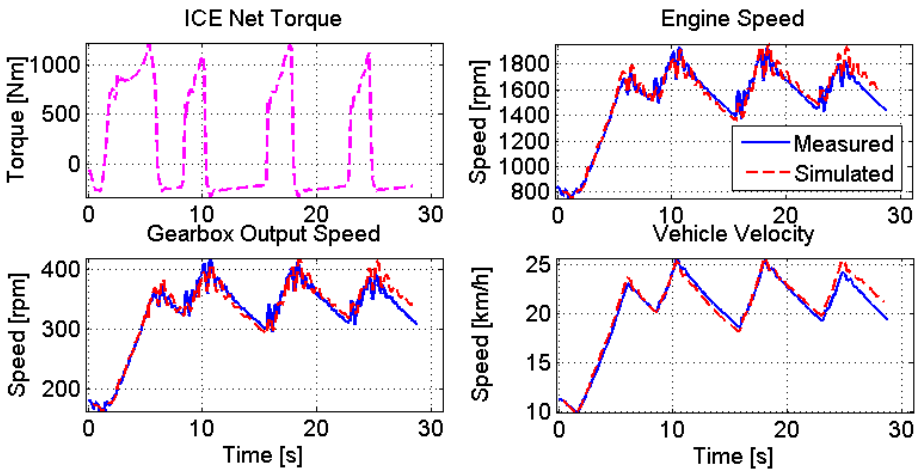

Figure 4: Model validation using tip-in/tip-out maneuvers for fifth gear. The model is run in open loop and it agrees well with data.

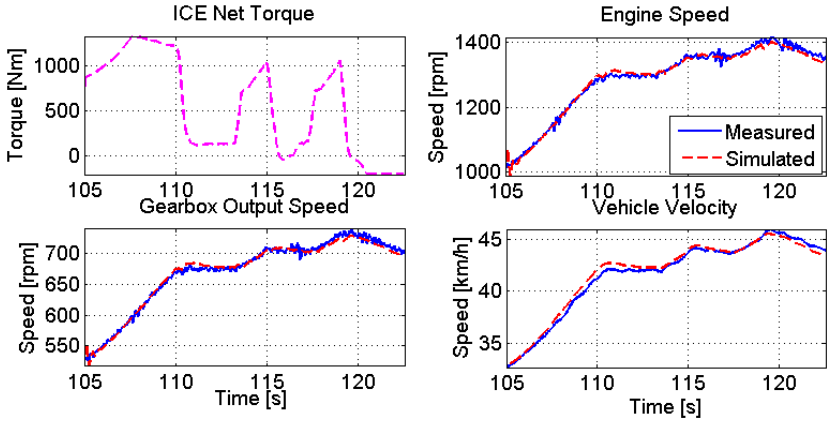

Figure 5: Model validation using tip-in/tip-out maneuvers for ninth gear. The model is run in open loop and it captures the trends in speed variations as well as the shuffle oscillations well. There are some quick oscillations that are missed.

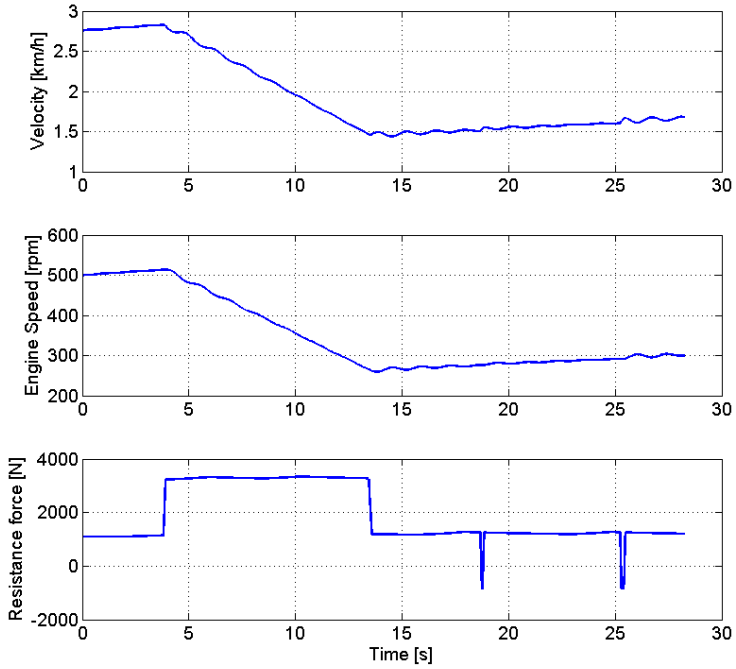

Figure 6: Showing how a one percentage point step in road slope affects truck behavior in 1st gear when engine torque is constant. A change in vehicle velocity with an oscillation superimposed can be seen.

2.10 Model Validation

The modular truck model has been validated using measurements from tip-in and tip-out maneuvers. Measurements of engine torque and road grade have been used as input for open-loop simulation of the model. Note that it is of great importance to have accurate road-grade information, when simulating the system. Otherwise the vehicle speed would have a large drift compared to the measurement. The model agrees well with measurement data for low gears, see Figure 4, and quite well for high gears, see Figure 5. In the latter case there were some small high frequency oscillations that were not captured in the model. Nonetheless the main vehicle shuffle frequency and amplitude have been captured in both cases. Therefore the model is suitable for simulations of cases where vehicle shuffle is a concern.

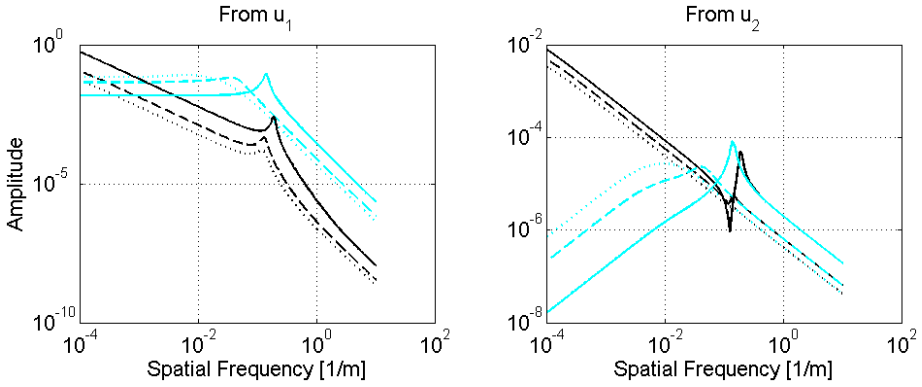

Figure 7: Bode plot of the open-loop system (black) and the closed-loop system (cyan), both systems in first (solid), sixth (dashed), and eighth (dotted) gear. Spatial frequency is used in order to enable comparisons with the road spectra in Section 4. The spatial frequency has been calculated using the maximum speed of each gear. For the open loop system $u = [M_e \; F_{\text{dr}}]^T$ and for the closed loop system $u = [w_{\text{e,ref}} \; F_{\text{dr}}]^T$. For both cases $y = v$. It can be seen that the resonance peaks vanishes at eighth gear. For the closed loop case, in the right plot, the peak moves towards lower frequencies as the gear number is increased.

3 Slope Signal Effect on Simulation

The linearized state-space model (30) is used to investigate the effect of a discretized slope signal on vehicle shuffle. First, no braking is assumed. Second, for slopes less than 20%, $\sin(\alpha)$ can, with great accuracy, be considered equal to the road slope in percent ($= \tan\alpha$). Since roads made for heavy duty trucks in Sweden have a maximum slope of 12% (highways have a maximum of 8% slope), (Swedish Road Administration, 2004), this is a very sound simplification. These two assumptions make $u_{\Delta,2}$ proportional to the road slope, and therefore suitable as input signal for this study.

The truck has been simulated, in first gear with constant engine torque, using a measured driving resistance as input. The measured driving resistance contains three

pulses, one long and two short, see Figure 6. The changes in driving resistance are due to that the road-slope signal is discretized in amplitude. This kind of signal contains a very wide frequency range. Therefore it induces oscillations in the driveline that are visible alongside the ramp changes in velocity. This can be explained by viewing the Bode plot of the system found in Figure 7. In the bode plot, there is a resonance peak in the transfer function from F_{dr} to v. This peak is the reason for the oscillations, however the peak has a low amplitude compared to the low frequency gain. Therefore the ramp changes in velocity are much greater than the oscillations. Note that also the transfer function from M_e to v has a resonance peak that can result in driveline oscillations. Consequently if the system is under feedback, e.g. speed control, then both resonance peaks can be excited by a slope step, leading to even more driveline oscillations.

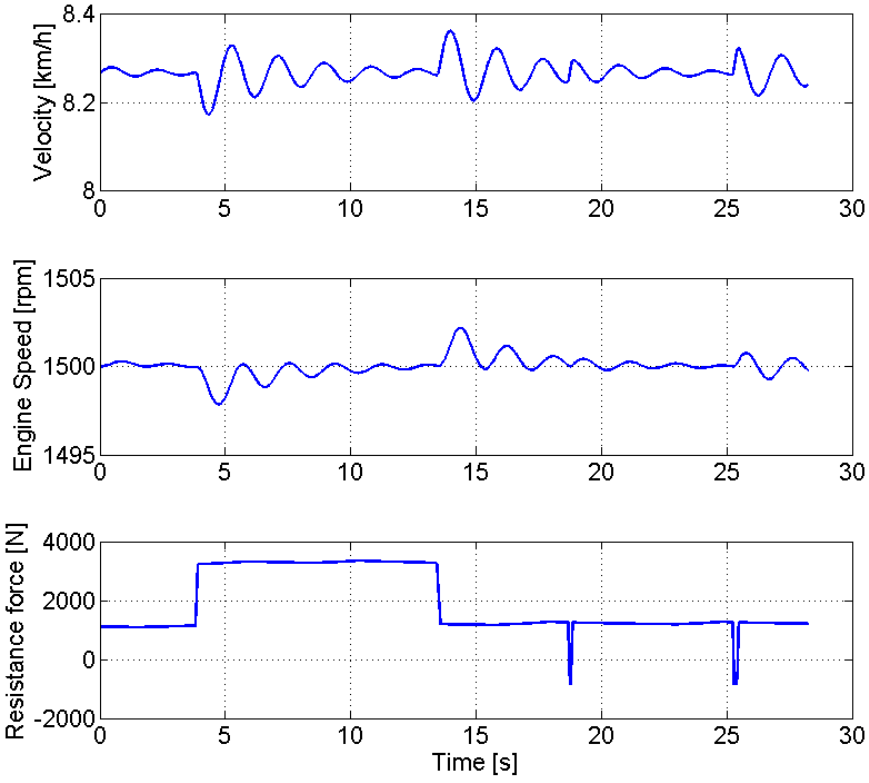

Figure 8: Oscillations in vehicle speed (longitudinal shuffle) can be seen when one-percentage-point pulses in road slope are present. Engine speed is kept constant by a PI-controller.

To highlight this a PI-controller for engine speed control is introduced

$$e = \dot{\theta}_{\mathrm{e,ref}} - \dot{\theta}_e \tag{31}$$

$$\dot{x}_8 = e \tag{32}$$

$$M_e = K_P e + K_I x_8 \tag{33}$$

where K_P and K_I are the controller parameters. With the speed controller the results in Figure 7 and Figure 8 are obtained. The driveline oscillations are now more clearly seen as well as the resonance peak in the transfer function from F_{dr} to v, which now also attains its maximum at the resonance. A better tuning or a more advanced controller could perhaps avoid the oscillations in the closed loop case, but this would only cure the symptoms and not the cause, which is the high frequency content in the input. It can thus be concluded that some kind of filtering should be applied to the road slope signal.

It should however be noted that the occurrence of the sharp resonance peak, and therefore the need for filtering, is dependent on the selected gear. In the closed loop case, higher gear means that the peak in the transfer function moves towards lower frequencies, while in the open loop case it moves slightly towards higher frequencies. The peak also becomes less pronounced with higher gear numbers and vanishes at gear eight. So no filtering is needed for gears higher than seven.

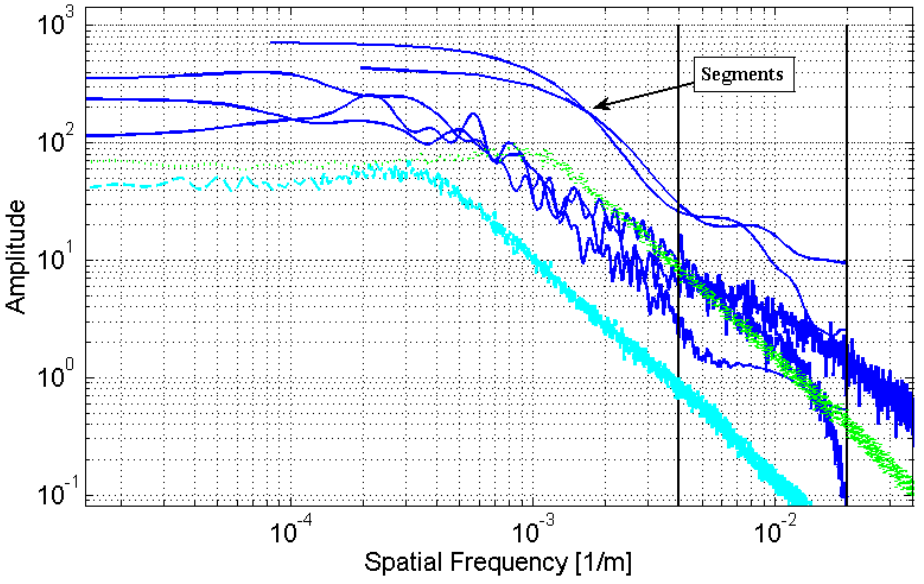

Figure 9: Frequency spectra for five measured highways (blue solid), one synthetic highway (cyan dashed), and one synthetic city road (green dotted). They all have similar shapes and most of their energy in frequencies below $1 \cdot 10^{-3}$ 1/m. The two shorter curves correspond to segments of the longer roads. The two black vertical lines mark the cut-off frequency and the -30 dB frequency of the filter.

4 Road Frequency

When filtering the road-slope signal, it is of great interest to keep the important information in the signal. In order to achieve this it must be understood how a road-slope profile typically looks like.

According to official road-design policies (see Swedish Road Administration (2004) for Swedish and AASHTO (2004) for US), the road segments between constant slopes have a parabolic shape,

$$z = \frac{x^2}{2R} \tag{34}$$

where z is the elevation, x the longitudinal position and R the curve parameter. The parabola works as an approximation of a circle with radius R. For Swedish highways (89 km/h for heavy duty trucks) R can be as low as 1250 m and in cities (50 km/h) R

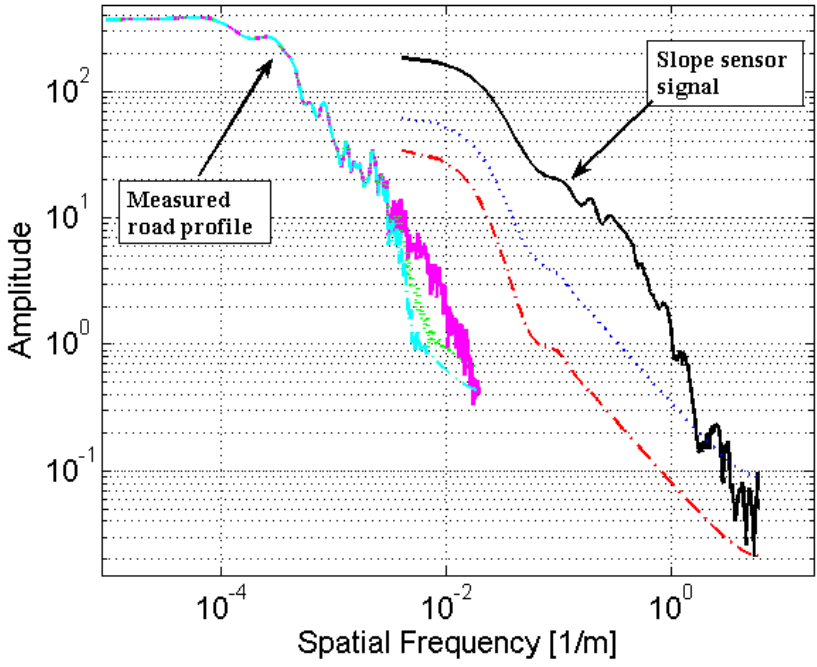

Figure 10: A real road profile in solid. With its filtered ditos in dashed-doted (non-causal) and dotted (causal) slightly below (hard to tell apart). The short measured slope signal is also found in solid. It too has its filtered dito in dashed-doted (non-causal) and dotted (causal) below. The measured signal has lost a lot of its high frequency content whereas the road profile has kept its low frequency content. Just as intended.

can be as low as 300 m. The slope can be calculated as,

$$\tan\alpha = \lim_{x_2\to x_1}\left(\frac{z_2-z_1}{x_2-x_1}\right) = \lim_{x_2\to x_1}\left(\frac{x_2^2-x_1^2}{2R(x_2-x_1)}\right) = \\ = \lim_{x_2\to x_1}\left(\frac{x_2+x_1}{2R}\right) = \frac{x}{R} \quad (35)$$

As stated earlier, slopes can be considered small and together with $x \approx vt$ it yields,

$$\alpha = \frac{v}{R}t \quad (36)$$

This means that the slope varies as a piece-wise linear and continuous function. A piece-wise linear function contains sharp knees and has an infinite frequency content but the amplitude decreases with frequency. To get an idea of the spectrum a synthetic road is constructed by picking a number of random inclinations with random lengths, then connecting these slopes with vertical curves of random radii. For simplicity reasons uniform distributions are assumed for all variables. The inclinations have been selected from the range dictated by Swedish Road Administration (2004). The radii have been selected from a narrow range above the minimum value. The range of the slope-length distributions are set exponentially with respect to the inclination, with flat ground giving the widest range. This is to mimic that in reality flat segments usually are longer then steep slopes. These assumptions are used to construct an approximation of a worst-case road. The resulting frequency spectrum is seen in Figure 9. Most of the power is in spatial frequencies below $3 \cdot 10^{-4}$ 1/m.

This theoretical "worst-case road" has been complemented with frequency spectra of different measured road segments[1]that indicate similar cut-off frequencies and roll-off rates, Figure 9. This indicates that the synthetisation method is sound and therefore it has been used for making a city road (50 km/h speed limit). The different limitations on maximum slope and R results in a road with higher frequency content. The main power is below $1 \cdot 10^{-3}$ 1/m.

Looking at the data for the road slope frequency content, Figure 9, and the Bode diagram for the model, Figure 7, one sees that the road data starts to fall off for frequencies below the resonance frequency of the driveline. This provides an opportunity to reduce the problem of oscillations by filtering the road slope signal. Especially since the Bode diagram represents the case with lowest spatial frequency (highest speed for each gear), which represents the worst case with minimum separation between frequencies.

5 Filter Design

The design rules for the filter are that it should have little impact on the naturally occurring road frequencies and damp those that could excite driveline oscillations.

According to the investigation in the previous section the important road frequencies lie below $1 \cdot 10^{-3}$ 1/m, the location of the knee of the synthetic city road. However note that the two shorter segments in Figure 9 have a later roll off than the long roads because these particular segments are rich on high frequency content. Likewise

[1]The road segments are the Järna segment, Jönköping-Linköping, Koblenz-Trier, Norrköping-Södertälje and the Olstorp segment

choosing the filter cut-off frequency at the knee of the city road profile might lead to filtering of naturally occurring frequencies on a segment of this profile. Therefore the cut-off frequency is taken with one decade of margin compared to the knee, i.e $f_{\text{co}} = 4 \cdot 10^{-3}$ 1/m. However there is never any guarantee that no real frequencies will be filtered as the theory have shown an infinite frequency content.

Frequencies that need to be damped are those around the resonance peak, see Figure 7, that exists for gear seven or lower. Maximum speed in seventh gear is about 50 km/h so it makes sense to choose f_{co} from the city road. The lowest frequency for any resonance peak is $f_{\text{lo}} = 2 \cdot 10^{-2}$ 1/m, which is that of gear seven in closed loop. As the resonance peak is quite low in seventh gear, -30 dB of attenuation is chosen at f_{lo}. The filter will naturally attenuate more at the peaks for lower gears.

These requirements can be fulfilled by, for example a third or higher order low pass Butterworth filter with a cut-off frequency of $4 \cdot 10^{-3}$ 1/m (-40 dB at f_{lo}). Note that while on one hand higher order gives a steeper gain curve and more margin to the requirements, on the other it gives more phase lag, i.e. time delay. In addition a higher filter order is more complex so computation time will increase. Therefore the lowest possible order is desirable in an on-line application. It might also be desirable to filter in the time domain, in that case the filter will be speed dependent. In an off-line application computational time is of less importance and the signal can be filtered both in the forward and reverse direction in order to get a zero phase filter.

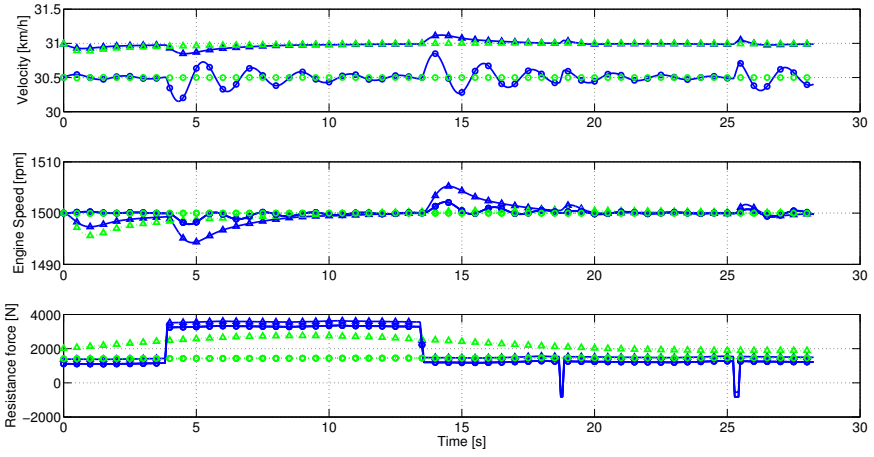

Figure 11: Original slope signal with its simulation response in solid blue. The acausally filtered signal and its response are shown in dashed green. Triangles are seventh gear and circles are first gear. The velocity response in first gear has been scaled. The oscillations are successfully filtered. Note that in first gear the slope signal is filtered more since the pulses are shorter in spatial coordinates.

6 Results

Figure 11 shows that third order filtering of driving resistance effectively eliminates the oscillations in both first and seventh gear. In Figure 10 it can be seen that the high frequency content in the road slope sensor is significantly reduced whereas the real road profile is essentially the same. A road profile together with causally and non-causally filtered versions are displayed in Figure 12, showing that the general behavior of the road profile is preserved. It can thus be concluded that the filter design works as intended. Furthermore a third order filter is sufficient even in the off-line application, where it would be trouble free to increase the order.

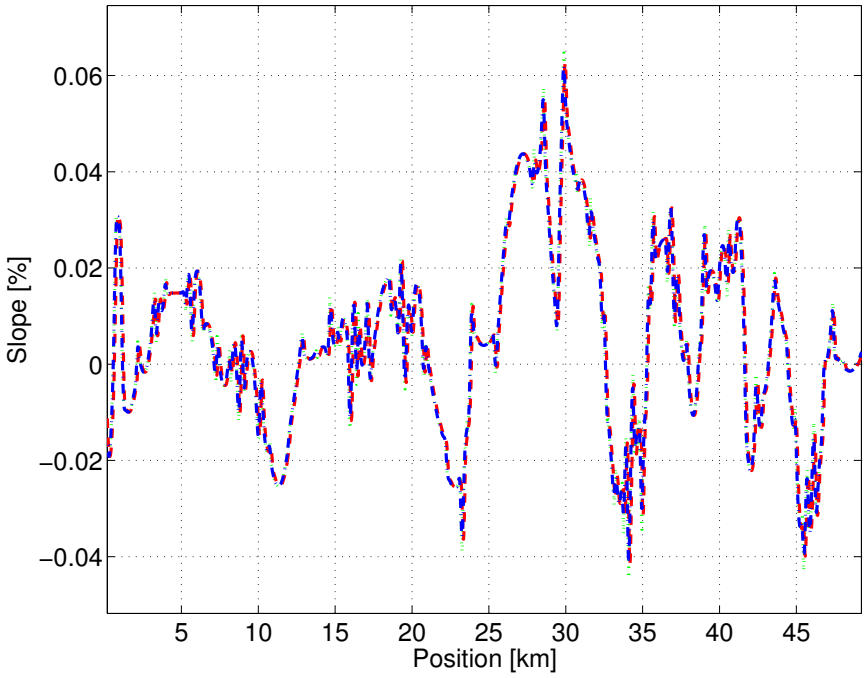

Figure 12: The road profile as function of position. Unfiltered in dotted green, causally filtered in dashed red and non-causally filtered in dash-dotted blue. The three signals are practically the same.

7 Conclusions

In this paper a model that describes vehicle shuffle of a heavy duty truck has been summarized and validated. Special emphasis was given to the interaction between driveline and road. In particular it was shown that smoothing the rolling resistance around zero speed gives a significant reduction in simulation time for driving with start and stop scenarios.

Furthermore, experimental data from a production road slope sensor was shown to have a big impact on the simulation of the vehicle. In particular the high frequency content, introduced by amplitude discretization in the sensor, was shown to excite driveline oscillations. The oscillations also become more pronounced when the driveline had a feedback speed controller.

The frequency content in a theoretical worst-case road and measured roads, have been investigated and found to be below the resonance frequency of the model in every gear. It was also shown that the frequency separation was large enough to make a low-pass-filter design possible for the road-slope sensor.

Finally a design is proposed for a filtering method consisting of a low pass Butterworth filter in the spatial domain that eliminates erroneous behavior caused by high frequency disturbances in the slope signal, e.g. discretization. Applying the filter to measured data shows that the driveline oscillations are significantly attenuated, while the shape of the road-slope profile is maintained.

References

AASHTO (2004). *A policy on geometric design of highways and streets: 2004*. American Association of State Highway and Transportation Officials.

Bae, H.S., Ryu, J., and Gerdes, J.C. (2001). Road grade and vehicle parameter estimation for longitudinal control using gps. In *2001 IEEE Intelligent Transportation Systems*.

Dolcini, P., de Wit, C.C., and Béchart, H. (2008). Lurch avoidance strategy and its implementation in AMT vehicles. *Mechatronics*, 18(1), 289–300.

Fredriksson, J. and Egardt, B. (2003). Active engine control for gear shifting in automated manual transmissions. *International Journal of Vehicle Design*, 32(3-4), 216–230.

Gao, B., Lei, Y., Ge, A., Chen, H., and Sanada, K. (2011). Observer-based clutch disengagement control during gear shift process of automated manual transmission. *Vehicle System Dynamics*, 49(5), 685–701.

Garofalo, F., Glielmo, L., Iannelli, L., and Vasca, F. (2002). Optimal tracking for automotive dry clutch engagement. In *2002 IFAC, 15th Triennial World Congress*.

Gerhardt, J., Hönninger, H., and Bischof, H. (1998). A new approach to functional and software structure for engine management systems - bosch me7. In *SAE Technical Paper: 980801*.

Lingman, P. and Schmidtbauer, B. (2002). Road slope and vehicle mass estimation using kalman filtering. *Supplement to Vehicle System Dynamics*, 37(1), 12–23.

Moon, S., Kim, M., Yeo, H., Kim, H., and Hwang, S. (2004). Design and implementation of clutch-by-wire system for automated manual transmissions. *International Journal Vehicle Design*, 36(1), 83–100.

Myklebust, A. and Eriksson, L. (2012). Torque model with fast and slow temperature dynamics of a slipping dry clutch. In *2012 IEEE Vehicle Power and Propulsion Conference*.

Pettersson, M. (1997). *Driveline Modeling and Control*. Ph.D. thesis, Linköpings Universitet.

Pettersson, M. and Nielsen, L. (2000). Gear shifting by engine control. *IEEE Transactions Control Systems Technology*, 8(3), 495–507.

Pettersson, M. and Nielsen, L. (2002). Diesel engine speed control with handling of driveline resonances. *Control Engineering Practice, Advances in Automotive Control*, 11(3), 319–328.

Sahlholm, P. (2011). *Distributed road grade estimation for heavy duty vehicles*. Ph.D. thesis, KTH School of Electrical Engineering.

Sebsadji, Y., Glaser, S., Mammar, S., and Dakhlallah, J. (2008). Road slope and vehicle dynamics estimation. In *2008 American Control Conference*.

Swedish Road Administration (2004). Vägar och gators utformning - linjeföring. Technical report, Vägverket Publikation 2004:80.

Linköping studies in science and technology, Dissertations
Division of Vehicular Systems
Department of Electrical Engineering
Linköping University

No 1 Magnus Pettersson, *Driveline Modeling and Control*, 1997.

No 2 Lars Eriksson, *Spark Advance Modeling and Control*, 1999.

No 3 Mattias Nyberg, *Model Based Fault Diagnosis: Methods, Theory, and Automotive Engine Applications*, 1999.

No 4 Erik Frisk, *Residual Generation for Fault Diagnosis*, 2001.

No 5 Per Andersson, *Air Charge Estimation in Turbocharged Spark Ignition Engines*, 2005.

No 6 Mattias Krysander, *Design and Analysis of Diagnosis Systems Using Structural Methods*, 2006.

No 7 Jonas Biteus, *Fault Isolation in Distributed Embedded Systems*, 2007.

No 8 Ylva Nilsson, *Modelling for Fuel Optimal Control of a Variable Compression Engine*, 2007.

No 9 Markus Klein, *Single-Zone Cylinder Pressure Modeling and Estimation for Heat Release Analysis of SI Engines*, 2007.

No 10 Anders Fröberg, *Efficient Simulation and Optimal Control for Vehicle Propulsion*, 2008.

No 11 Per Öberg, *A DAE Formulation for Multi-Zone Thermodynamic Models and its Application to CVCP Engines*, 2009.

No 12 Johan Wahlström, *Control of EGR and VGT for Emission Control and Pumping Work Minimization in Diesel Engines*, 2009.

No 13 Anna Pernestål, *Probabilistic Fault Diagnosis with Automotive Applications*, 2009.

No 14 Erik Hellström, *Look-ahead Control of Heavy Vehicles*, 2010.

No 15 Erik Höckerdal, *Model Error Compensation in ODE and DAE Estimators with Automotive Engine Applications*, 2011.

No 16 Carl Svärd, *Methods for Automated Design of Fault Detection and Isolation Systems with Automotive Applications*, 2012.

No 17 Oskar Leufvén, *Modeling for control of centrifugal compressors*, 2013.

No 18 Christofer Sundström, *Model Based Vehicle Level Diagnosis for Hybrid Electric Vehicles*, 2014.

No 19 Andreas Thomasson, *Modeling and control of actuators and co-surge in turbocharged engines*, 2014.

No 20 Emil Larsson, *Model Based Diagnosis and Supervision of Industrial Gas Turbines*, 2014.